New Methodology for Probing Catalytic Reactions by ESI-MS

by

Krista Lynn Vikse
B. Sc., University of British Columbia Okanagan, 2006

A Dissertation Submitted in Partial Fulfillment
of the Requirements for the Degree of

DOCTOR OF PHILOSOPHY

in the Department of Chemistry

Supervisory Committee

New Methodology for Probing Catalytic Reactions by ESI-MS

by

Krista Lynn Vikse
B. Sc., University of British Columbia Okanagan, 2006

Supervisory Committee

Dr. J. Scott McIndoe, Department of Chemistry
Supervisor

Dr. Lisa Rosenberg, Department of Chemistry
Departmental Member

Dr. Cornelia Bohne, Department of Chemistry
Departmental Member

Dr. Christoph Borchers, Department of Biochemistry and Microbiology
Outside Member

Abstract

Supervisory Committee

Dr. J. Scott McIndoe, Department of Chemistry
Supervisor

Dr. Lisa Rosenberg, Department of Chemistry
Departmental Member

Dr. Cornelia Bohne, Department of Chemistry
Departmental Member

Dr. Christoph Borchers, Department of Biochemistry and Microbiology
Outside Member

Bis(dimethylamino)-2-(4-methoxyphenyl)naphthalene (**3**) and 1,8-bis(dimethylamino)-4-diphenylphosphonaphthalene (**5b**) were synthesized as ESI-active analogues of the common organometallic ligands η^6-anisole and triphenylphosphine. The water-soluble phosphine, sodium triphenylphosphine monosulfonate (Na^+**7**$^-$), was re-purposed as an ESI-active ligand. Its solubility in organic solvents and amenability to electrospray ionization was improved by replacing Na^+ with the non-coordinating bis(triphenylphosphine)iminium cation.

A new sample introduction method named PSI (pressurized sample infusion) was developed for the continuous infusion of air/moisture-sensitive samples into the mass spectrometer. The flow rate can be determined using a modified version of the Hagen-Poiseuille equation, and the ability of PSI (coupled with an ESI tag) to give quantitative kinetic data is demonstrated. A method for maintaining a dry, air-free ESI source is described for the analysis of highly reactive samples.

The above developments were applied to the study of the copper-free Sonogashira (Heck alkynylation) reaction. The proposed active catalyst ($Pd(0)L_2$, where L = PPh_3 or **7**) was observed, and its reactivity with iodomethane in the gas phase was determined to be less than that of Pd(0)L. Nevertheless, $Pd(0)L_2$ is extremely reactive and even oxidatively adds dichloromethane ($t_{1/2}$ = 10.7 min at 40 °C). Under standard reaction

conditions intermediates corresponding to oxidative addition and transmetallation were detected, and coordination of base to palladium was observed for secondary amines but not triethylamine. Reductive elimination was achieved in the gas phase for a series of *para*-substituted aryl iodides with phenylacetylene, and the slope of the resulting Hammett plot (ρ) was -0.5. No evidence for the previously hypothesized anionic mechanism was observed.

Simultaneous kinetic analysis of charged substrate, products and intermediates in the copper-free Sonogashira reaction was conducted using PSI-ESI-MS and high quality, information rich data for each species over time was obtained. In the absence of protons, reductive elimination is rate-limiting and the rate of reaction is relatively high. In the presence of protons (a byproduct of the reaction), transmetallation is rate-limiting and the rate of reaction is much slower. The use of a strong base was shown to improve the efficiency of the reaction, and an experimentally-derived catalytic cycle for the copper-free Sonogashira reaction is proposed.

Table of Contents

List of Abbreviations

acac	acetylacetate
Ar	aryl
BF_4^-	tetrafluoroborate
Bn	benzyl
b.p.	boiling point
CI	chemical ionization
CID	collision induced dissociation
COD	cyclooctadiene
Col V	collision voltage
cP	centipoise
Cp	cyclopentadienyl ligand
Cp*	pentamethylcyclopentadienyl ligand
CV	cone voltage
Cy	cyclohexyl
Da	Dalton
dba	dibenzylideneacetone
DBSQ	3,5-di-tert-butylsemiquinone
DBU	1,8-diazabicyclo[5.4.0]undec-7-ene
DC	direct current
dmbp	6,6'-dimethyl-2,2'-bipyridyl
DMSO	dimethylsulfoxide
DTBC	3,5-di-tert-butylcatecholate
EDESI	energy-dependent electrospray ionization
EI	electron ionization
EPR	electron paramagnetic resonance
ESI	electrospray ionization
ESI(+)-MS	positive-ion electrospray ionization mass spectrometry
ESI(-)-MS	negative-ion electrospray ionization mass spectrometry
FT-ICR	Fourier transform ion cyclotron resonance

FTMS	Fourier transform mass spectrometry
HPLC	high pressure liquid chromatography
ID	inner diameter
IR	infrared
KE	kinetic energy
LIFDI	liquid introduction field desorption ionization
m	*meta*
$[M]^+$	positive molecular ion peak
$[M]^-$	negative molecular ion peak
MALDI	matrix-assisted laser desorption ionization
MAO	methylaluminoxane
MCP	microchannel plate
Me	methyl
MeTACN	1,4,7-trimethyl-1,4,7-triazacyclononane
m.p.	melting point
MS	mass spectrometry/ mass spectrometer/ mass spectrum
MS/MS	tandem mass spectrometry
m/z	mass-to-charge ratio
NBS	*N*-bromosuccinimide
NEt_3	triethylamine
NHC	*N*-heterocyclic carbene
NMR	nuclear magnetic resonance
OA	oxidative addition
OAc	acetate
OTf	trifluoromethanesulfonate
p	*para*
PEEK	polyetheretherketone
PF_6^-	hexafluorophosphate
Ph	phenyl
ppm	parts per million
PPN	bis(triphenylphosphoranylidene)ammonium

^{i}Pr	isopropyl
PSI	pressurized sample infusion
psi	pound per square inch
^{t}Bu	tert-butyl
Pyr	pyridine
Q-TOF	quadrupole-time-of-flight
RE	reductive elimination
RF	radio frequency
RSD	relative standard deviation
SSI	sonic spray ionization
TDC	time-to-digital converter
terpy	terpyridine
THF	tetrahydrofuran
TIC	total ion current
TM	transmetallation
TOF	time-of-flight
TPA	tris(2-pyridyl-methyl)amine
TPPMS	triphenylphosphine monosulfonate
UV	ultraviolet
UV/Vis	ultraviolet/visible
VEASI	Venturi easy ambient sonic spray ionization
XAFS	X-ray absorption fine structure
XAS	X-ray absorption spectroscopy

List of Figures

List of Schemes

List of Structures

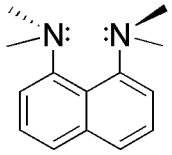

(**1**)

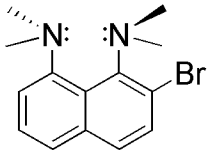

(**2a**)

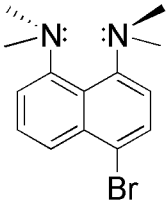

(**2b**)

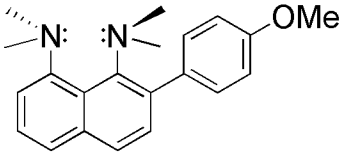

(**3**)

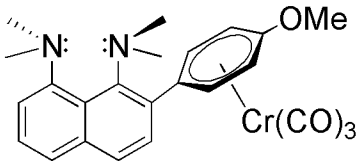

(**4**)

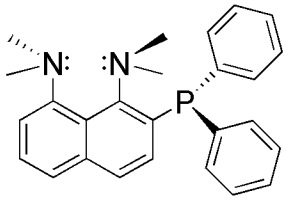

(**5a**)

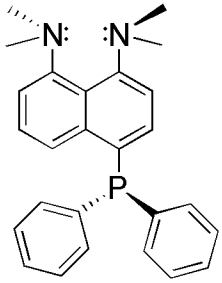

(**5b**)

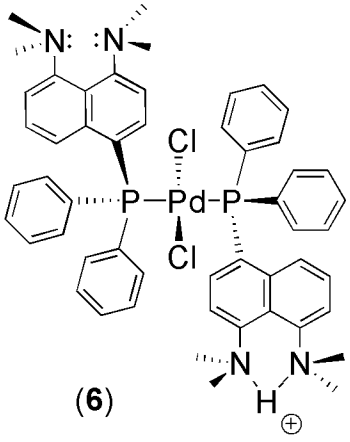

(**6**)

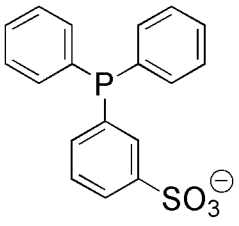

(**7**)

Acknowledgments

First I would like to thank Scott for sharing his wisdom about all things chemistry and academic, and for putting up with my dogged scepticism. I hope that his passion for new ideas and immaculate figures has worn off on me, and that someday I learn to mentor as he does: with seemingly infinite patience and enthusiasm.

Nichole Taylor has been an exceptional TA supervisor and graciously agreed to hand over an enthusiastic bunch of Chem361 students from the Spring 2010 and 2011 terms to assist with the collection of flow rate data. The UVic chemistry staff and Ori Granot in particular have been indispensible, and always eager to help when I come running with a problem. Dr. Allen Oliver and Dr. Robert MacDonald provided X-ray crystallography services, and the University of Victoria provided financial support for this work.

My fellow lab mates Danielle, Keri, Matt, Nicky, Jen, Tyler, Zohrab, Jingwei and Cara all deserve credit for keeping me sane from day-to-day by sharing despair over failed experiments, and by making me smile each in their own way. Danielle and Keri have become lifelong friends, and as such I expect yearly Christmas letters and the occasional unannounced visit. I am very grateful to Zohrab and Cara for their contributions to the PSI project, specifically to Zohrab for continuing and improving upon this work.

I am blessed to have two loving families who support me in everything I do, and for that I can never thank them enough. My mother is wholly responsible for my inordinate fondness for a clean lab bench, and my father turned me into a scientist long before I ever took a science class.

Finally, I could not have completed this work without my wonderful husband Jason who has endured five years of a mind-numbing retail job to keep us solvent while I studied, and who proof-read this entire dissertation; if you asked him I’m not sure which he would claim was worse. He threatens to refer to me only as Dr. Vikse if I ever graduate...

Dedication

To Jason, Mom and Dad

Overview

The goal of this work was to develop general methodology for the simple analysis of air- or moisture-sensitive organometallic catalytic reactions by electrospray ionization mass spectrometry (ESI-MS). In this way we hoped to harness the speed, sensitivity and simplicity of ESI-MS analysis to probe the mechanistic details of important organometallic processes, so that the rational development of more effective catalysts and reaction conditions for these processes was possible.

A number of research groups specialize in performing these types of analyses and some highlights are discussed in Chapter 1; however, ESI-MS is still not a technique that is commonly employed by organometallic chemists, and the reasons for this are discussed in Chapter 2 along with a brief overview of the theory of ESI-MS.

To overcome the barriers associated with using ESI-MS for the study of organometallic systems charged substituents were employed to "tag" ESI-silent catalysts or reactants, and a new sample introduction technique named PSI (pressurized sample infusion) was developed for the continuous introduction of air- and moisture-sensitive reaction mixtures into a mass spectrometer. The details of these two approaches are discussed in Chapters 3 and 4 respectively.

Finally, to demonstrate the usefulness of these techniques they were applied to the study of the copper-free Sonogashira (Heck alkynylation) reaction. Chapter 5 shows how the identification and gas-phase reactivity of key intermediates was made possible using a negatively-charged ESI-active ligand, and Chapter 6 demonstrates the future potential of using PSI-ESI-MS along with an ESI-active substrate to obtain kinetic data simultaneously from reactants, products and intermediates.

Chapter 1. Literature Review

1.1 A brief history of mass spectrometry

In 1913 the field of mass spectrometry was born when J. J. Thomson, inspired by the work of Goldstein and Wien,[1] used magnetic and electric fields to separate the two isotopes of neon (^{20}Ne and ^{22}Ne) in the gas phase and image them on a photographic plate.[2] Shortly after this experiment, in 1918, A. J. Dempster laid the groundwork for the development of modern mass spectrometers by designing an instrument capable of resolving all of the known elements while maintaining sufficient signal intensity using electric and magnetic fields.[3] He was also the first to use electron ionization (EI) as an ionization method for mass spectrometry.[4, 5] EI, a method in which electrons produced from a heated filament collide with and ionize gaseous analytes, quickly became the most common ionization method for mass spectrometry. However, as the technique was applied to larger, more complex molecules a significant drawback became apparent. The high-energy collisions between energized electrons and analyte molecules resulted in fragmentation and loss of valuable molecular weight information. For this reason a complementary group of ionization methods called "soft" ionization methods was developed in the latter half of the 1900s.

The first soft ionization method to be developed was chemical ionization (CI). A close relative to EI, it uses the electrons generated from a negatively-charged, heated metal filament to ionize a reagent gas such as methane. The ionized gas reacts with itself to create a mixture of reactive species including CH_5^+ which can ionize analyte molecules through proton transfer.[6] This ionization process was much lower in energy than EI and $[M+H]^+$ molecular ions could be generated for small organic molecules, but CI was still not capable of handling larger molecules (> 600 Da).

Today the two most popular soft ionization methods are electrospray ionization (ESI) and matrix-assisted laser desorption ionization (MALDI). Both were developed in the late 1980s, and

the 2002 Nobel Prize in Chemistry was awarded to Fenn[7,8] and Tanaka[9] for the development of ESI and MALDI, respectively.

Although ESI was actually invented by Dole in 1968[10] it was not until the 1980s that Fenn demonstrated its use as an ionization method for large molecules. It then became an immediate success for the analysis of biomolecules, proteins and peptides in solution.[1] This was in part because of its ability for soft ionization and in part because it is the only ionization method capable of stabilizing multiply-charged analytes. The ability to transfer multiply charged molecules into the gas phase meant that very large analyte molecules could achieve a mass-to-charge ratio (*m/z*) small enough for analysis by a standard mass spectrometer. ESI is the ionization technique used in our research group and the details of the ionization process will be discussed further in Chapter 2.

MALDI was introduced shortly after ESI, and as the name suggests, it relies on the use of an organic matrix with a UV chromophore. The analyte is co-crystallized on a plate with a large excess of the appropriate matrix (usually an aromatic acid).[11,12] A UV laser is focused on the matrix and causes excitation of the matrix molecules. This leads to the formation of a plume of vaporized matrix and analyte. Within the plume protonation of the analyte by the matrix results in charged analyte molecules in the gas phase. The matrix absorbs almost all the energy from the laser leaving the analyte molecules unfragmented. Because of its gentleness and potential for easy automation MALDI was also quickly adopted by the biological community. The process results almost exclusively in singly-charged ions, and is nearly always used in conjunction with time-of-flight mass analyzers (*vide infra*).

As new ionization methods were being reported, a variety of mass analyzers with different specialties were developed as well: the quadrupole mass spectrometer,[13, 14] a robust and relatively small and inexpensive analyzer; the time-of-flight (TOF) mass spectrometer conceived by Stephens[15] and ideally suited for the analysis of very large analytes; Wolfgang Paul's ion trap[16] with the ability to perform multiple stages of ion selection and fragmentation; and the high resolution Fourier Transform Ion Cyclotron Resonance (FT-ICR) mass spectrometer developed

by Comisarow and Mashall[17] are among the most popular. Combinations of these analysers led to tandem mass spectrometry which allowed for the study of ion/molecule reactions.[18]

Now over 100 years old, mass spectrometry is used ubiquitously in the analysis of small molecules, biomolecules and proteins.[19] It is used for detecting environmental contaminants and drug metabolites, analyzing the atmosphere of the earth and other planets, peptide and gene sequencing, forensic analysis, disease screening, and measuring isotope ratios.[1] But there are still a number of areas that have remained relatively untouched by the development of mass spectrometry. One that is of particular interest to us is the study of organometallic catalysis.

1.2 Applying ESI-MS to organometallic catalysis

There are a number of things that make mass spectrometry, and especially ESI-MS, well suited to the study of organometallic catalysis. (1) ESI-MS is a soft technique that operates on solutions and can leave weak bonding interactions intact. (2) Only species that are already charged in solution or contain an easily charged site are detected. Because of this most common solvents are "invisible" and very low detection limits are acessible.[20, 21] (3) Analysis is fast (on the order of seconds), and (4) intermediates at nanomolar concentrations can be detected with ease. Finally, (5) since each species in solution is usually represented by a single peak in the mass spectrum it is simple to extract information from complex mixtures.

A growing body of literature exists in which investigators have taken advantage of these attributes of ESI-MS to study organometallic systems. The first was Berman who used ESI-MS to detect a number of environmentally important organoarsenic ions.[22] Another notable early example comes from Canty in 1993 who reported the positive ESI-MS and tandem MS studies of various palladium and platinum organometallic complexes.[23] Since then, the primary use of ESI-MS in this area has been in the identification of short-lived, low concentration intermediates. It has been used in the study of catalytic oxidation,[24-27] hydrogenation,[28-30] hydrosilylation[31] and carbon-carbon bond-forming[32-34] reactions. A large amount of the attention has been given to palladium-catalyzed carbon-carbon bond-forming reactions.[33, 35-40]

A number of book chapters have been written on the subject of ESI-MS analysis of organometallic reaction intermediates.[41-43] Here, an up-to-date review of works that are particularly relevant to this dissertation, and focusing on the use of ESI-MS to study organometallic catalysis, is provided.

In order to investigate any catalytic system by ESI-MS all species of interest must be charged; either inherently, adventitiously (e.g. by protonation or loss of a halide) or intentionally by installing a charged or chargeable tag: the studies discussed here will be organized accordingly.

1.2.1 Inherently-charged systems

Reactions with inherently charged intermediates allow for straightforward analysis – the standard reaction mixture can simply be sampled and infused directly into the mass spectrometer. Oxidation reactions lend themselves particularly well to this method of analysis since the reaction intermediates are often inherently charged. A range of manganese-containing intermediates for a variety of reactions have been observed and the groups of Bortolini[24, 44-46] and Smith[26, 47, 48] have been strong contributors to research in this area.

Among the first reports was the investigation of an iron-catalyzed oxidation system in 1997. ESI-MS was used to characterize the intermediate $[Fe^{III}\text{-TPA(OOH)}]^{2+}$ in the stereospecific hydroxylation of alkanes by H_2O_2 (TPA= tris(2-pyridyl-methyl)amine).[49] It is unique among oxidation reactions studied by ESI-MS in that all other reports address manganese- or vanadium-catalyzed systems.

Manganese-catalyzed reactions

In 1998 the existence of a commonly invoked intermediate for a variety of oxygen transfer reactions of the form $\{O=Mn^{V}\}$ was supported by interception of an $[O=Mn^{V}(salen)(OIPh)]^{+}$ complex (Figure 1.1 A) and a binuclear $[\mu\text{-}O(Mn^{IV}(salen)(OIPh))_2]^{2+}$complex (Figure 1.1 B).[50]

Later, an ESI-MS study on the Mn-catalyzed oxidative kinetic resolution of secondary alcohols by $PhI(OAc)_2$ reported the observation of a similar manganese salen intermediate $[Mn^{V}(salen)(PhIO)(OCH(CH_3)Ph]^{+}$(Figure 1.1 C).[25] This, along with the observation of $[Mn^{III}(salen)(PhI(OAc)_2)]^{+}$(Figure 1.1 D), allowed the proposal of a possible catalytic cycle for the kinetic resolution of secondary alcohols by this system.

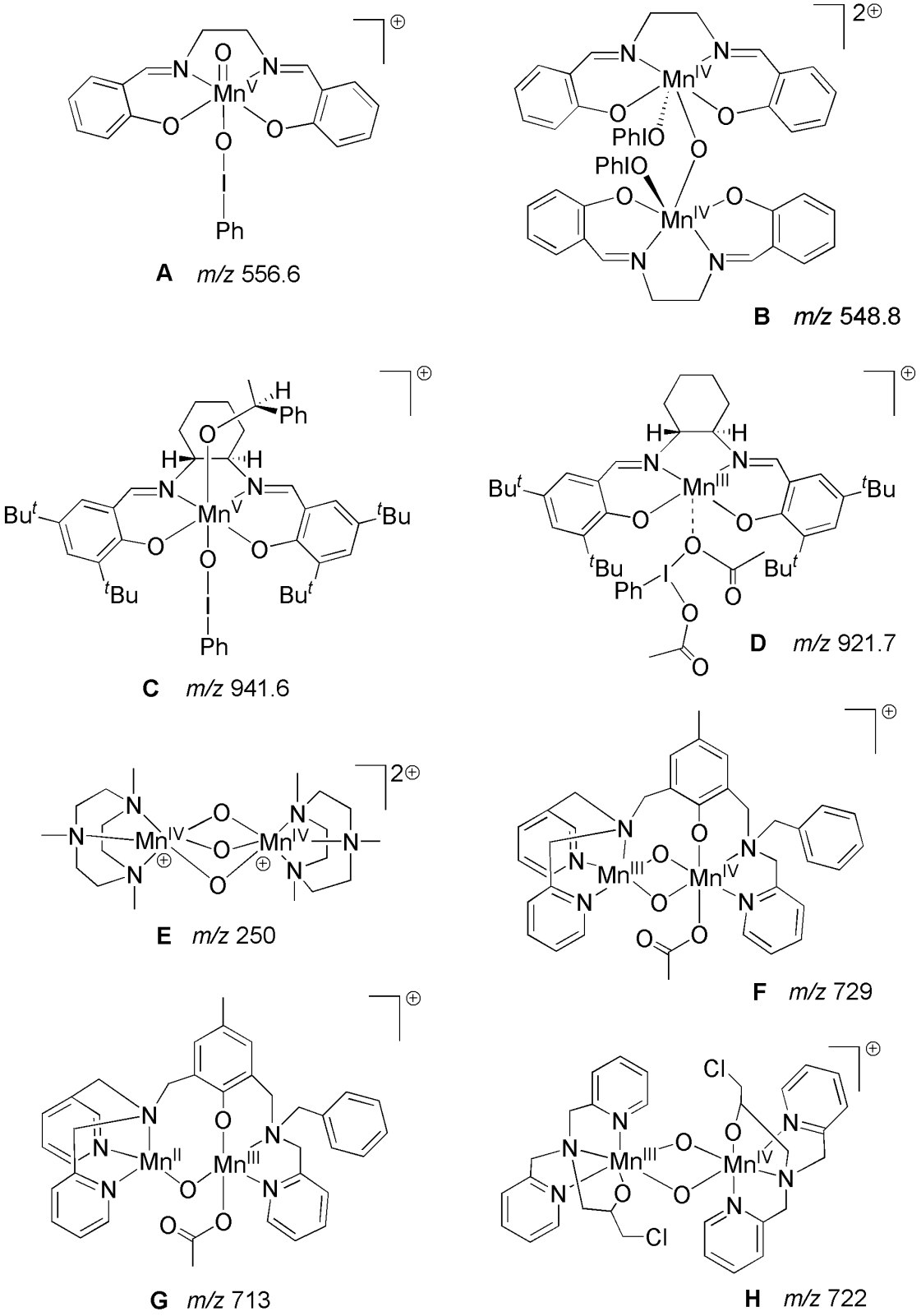

Figure 1.1: Manganese-containing species observed by ESI(+)-MS.

Mn-MeTACN complexes have been studied extensively by ESI-MS in the oxidation of a variety of organic substrates using hydrogen peroxide (MeTACN = 1,4,7-trimethyl-1,4,7-triazacyclononane). An assortment of binuclear and mononuclear species has been observed.[47,26,48] One interesting example focused on the use of these complexes for the oxidative drying of alkyd paints. The binuclear complex, $[Mn_2^{IV}(\mu\text{-}O)_3MeTACN)_2]^{2+}$ (Figure 1.1 E), was shown to be an effective catalyst; in this case for oxidation of ethyl linoleate (a model complex for alkyd resins).[51] From a solution of $[Mn_2^{IV}(\mu\text{-}O)_3MeTACN_2](PF_6)_2$ and hydroperoxide, peaks corresponding to $[Mn_2^{IV}(\mu\text{-}O)_3MeTACN_2]^{2+}$ were initially dominant and small peaks corresponding to $[Mn^{IV}Mn^{III}(\mu\text{-}O)_3MeTACN_2]^{+}$ were present. After 24 hours peaks corresponding to $[Mn_2^{III}(\mu\text{-}O)_2MeTACN_2]^{2+}$ dominated the spectrum, consistent with the catalyst acting to decompose hydroperoxides via a reversible equilibrium between $Mn(IV)_2$/Mn(IV)Mn(III) /$Mn(III)_2$ (Scheme 1.1). In alkyd paints this decomposition of hydroperoxides leads to the formation of volatile aldehyde products which aid in the drying of the oil paint.

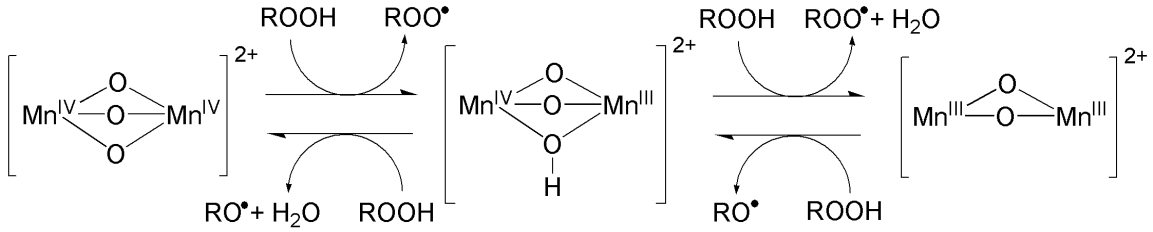

Scheme 1.1: Proposed catalytic cycle for the decomposition of hydroperoxide by Mn-MeTACN based on ESI-MS studies. Modified from reference 51.

The mechanism of peroxide disproportionation by various dimanganese complexes was investigated by Dubois et al. using ESI-MS. Proposed active species of the forms bis(μ-oxo)dimanganese(III/IV) (Figure 1.1 F, *m/z* 729) and (μ-oxo)dimanganese(II/III) (Figure 1.1 G, *m/z* 713) were observed in each case and confirmed by isotope labelling ESI-MS studies. For the intermediate containing two oxygen atoms, it was determined that both oxygen atoms come from the same hydrogen peroxide molecule. An overall mechanism was proposed.[52,53]

Finally in 2009, based on ESI-MS experiments and supported by UV-Vis and EPR experiments, the binuclear manganese complex $[(PClNOL)Mn^{III}\text{-}(\mu\text{-}O)_2\text{-}Mn^{IV}(PClNOL)]^{+}$

(Figure 1.1 H, *m/z* 722) was proposed to be responsible for the catalase-like activity of the manganese(II) compound $[Mn^{II}(HPClNOL)(\eta_1\text{-}NO_3)(\eta_2\text{-}NO_3)]$ HPClNOL = $N((CH_2)C_5H_4N)_2(CH_2(CH)OH(CH_2)Cl)$.[54]

Vanadium-catalyzed reactions

The few vanadium-based studies present in the literature are listed here and once again focus on the identification of key intermediates in vanadium-catalyzed oxidations.

In 2001, negative ion ESI-MS studies suggested that monoperoxovanadium species are responsible for the vanadium-catalyzed oxidation of isopropyl alcohol to acetone.[44] Fragmentation studies conducted in the gas phase showed loss of acetone from the species $[OV(O_2)(O^iPr)_2]^-$ (Figure 1.2 A, *m/z* 217), confirming that the reaction occurs within the inner sphere of the metal.

In 2003, the intermediate $[VO(OH_2)(OH)(OBr)]^+$ (Figure 1.2 B, *m/z* 197/199) was observed by ESI-MS and implicated as a potential intermediate in the vanadium-catalyzed oxidation of bromide by hydrogen peroxide.[46] This reaction provides a source of Br^+ for halogenation reactions, or on further addition of hydrogen peroxide leads to a source of singlet oxygen.

In 2005, a selection of pre-catalysts used in the vanadium-catalyzed oxygenation of 3,5-ditert-butylcatechol was studied by ESI-MS. Experiments were conducted on numerous post-reaction solutions for which the use of various vanadium pre-catalysts led to the detection of two common negative ions: $[VO(DTBC)_2]^-$ (Figure 1.2 C) and $[V(DTBC)_3]^-$ (DTBC = 3,5-di-tert-butylcatecholate dianion).[55] Through kinetic experiments the species corresponding to $[V(DTBC)_3]^-$ was ruled out as the catalytically active species and the neutral species that was shown to correspond to $[VO(DTBC)_2]^-$, namely $(VO(DBSQ)(DTBC))_2$ (DBSQ = 3,5-di-tert-butylsemiquinone anion), was reported as a common catalyst for this reaction. While this study is perhaps more suited to the section on adventitiously-charged systems since the proposed active catalyst is in fact neutral, it is described here along with the other vanadium-catalyzed systems for cohesion.

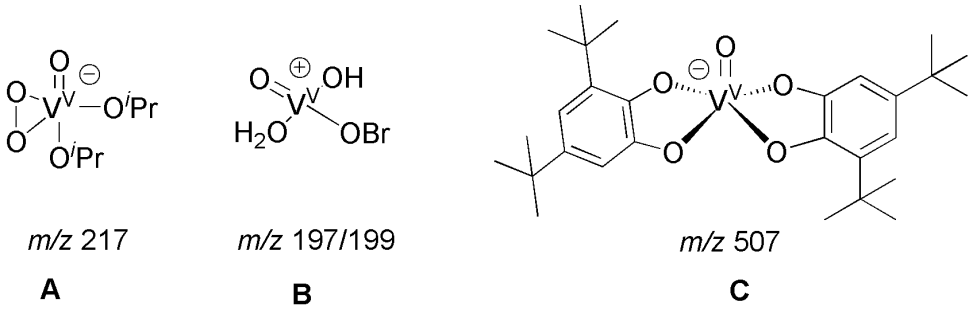

Figure 1.2: Vanadium-containing species observed by ESI(-)-MS and ESI(+)-MS.

Palladium-catalyzed reactions

As opposed to most oxidation reactions, palladium-catalyzed carbon-carbon bond-forming reactions generally proceed through neutral intermediates, but there are some exceptions.

An early example of this is the detection of the unique binuclear sandwich Pd complex (Figure 1.3 A) identified by ESI-MS in 1999 and proposed in the enantioselective Manich-type reaction of enol silyl ethers with N-aryl-iminoacetic acid esters. A potentially active mononuclear species (Figure 1.3 B) with a vacant coordination site was also observed and a mechanism for the reaction was outlined based on these two species.[56] A similar but more current example is a Michael-type Friedel-Crafts reaction of indoles with chalcones to which $FeCl_3$ and $PdCl_2$ were added. The addition of these two metals at 5 mol% was found to improve the efficiency and lower the cost of the reaction. ESI-MS investigation led to the identification of the potentially responsible species: a bimetallic iron-palladium catalyst of the form $[FePd(chalcone)Cl_5]^+$.[57]

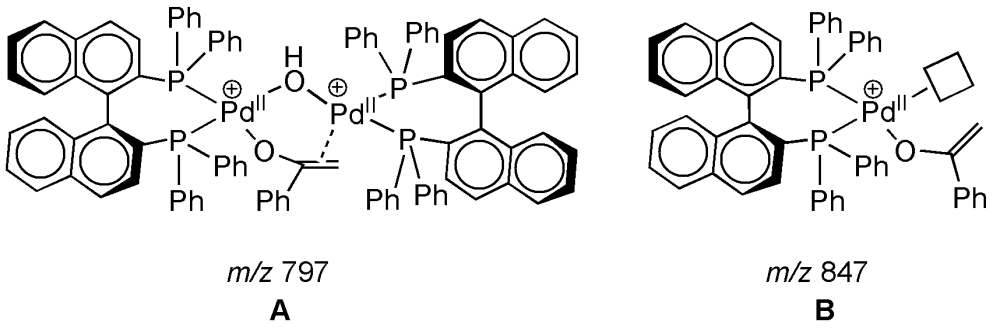

m/z 797
A

m/z 847
B

Figure 1.3: Bi- and mono-nuclear palladium ions observed by ESI(+)-MS and proposed as catalytic intermediates in the enantioselective Manich-type reaction of enol silyl ethers with N-aryl-iminoacetic acid esters.[56]

Certain aspects of the Heck and Suzuki reactions and one example of a palladium-catalyzed allylic substitution reaction have also lent themselves to study by this method.

In 2004, Matsuda developed a phosphane-free version of the Heck reaction involving arene diazonium salts with $[Pd_2(dba)_3]\cdot$dba as the palladium source.[58] Eberlin studied it by ESI-MS(/MS) to verify the proposed catalytic cycle.[36] Pd-containing species were observed which supported the proposed process involving oxidative nitrogen extrusion, ligand exchange, olefin insertion, and β-hydride elimination (Scheme 1.2). No species related to a Pd-bound arene diazonium cation were observed presumably because the intermediate is too short-lived. The species $[(4\text{-MeOPh})Pd(CH_3CN)(dba)]^+$ (*m/z* 488) becomes dominant in the mixture of palladium and diazonium salt after 90 minutes, and addition of various olefins demonstrates that this species is the most active towards olefin insertion.

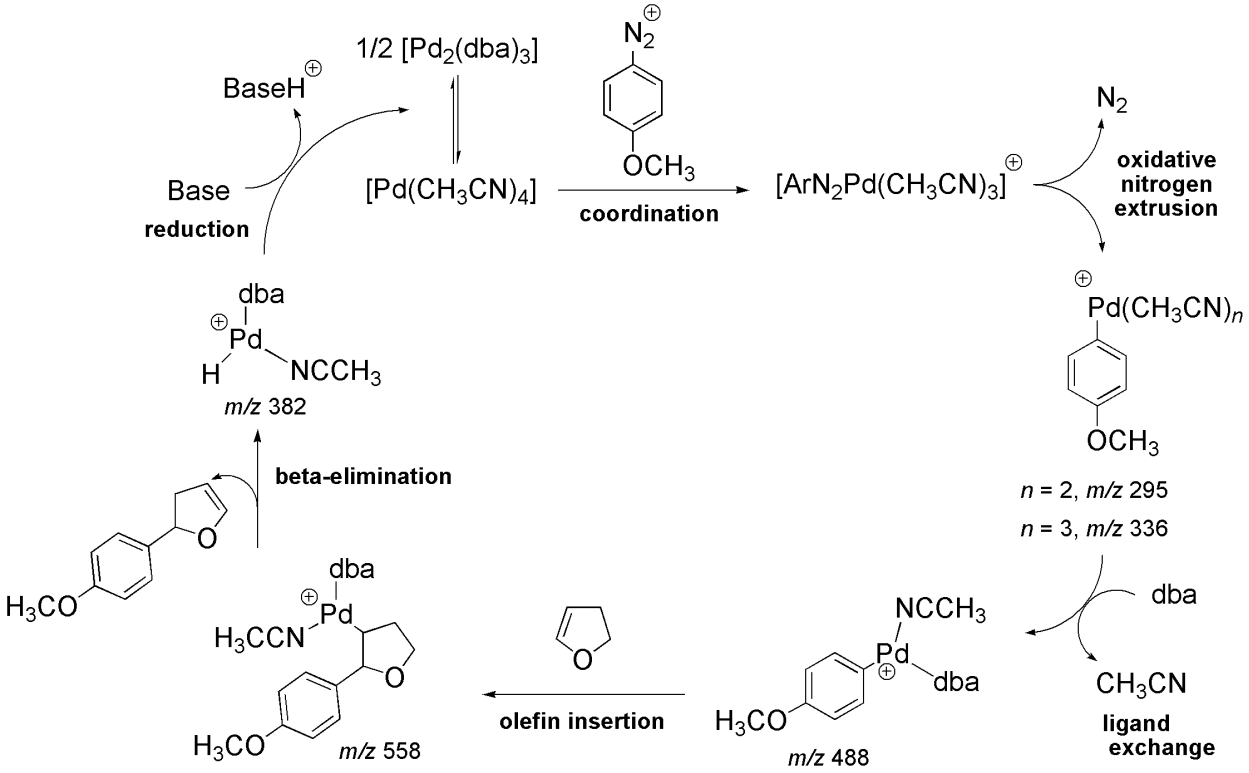

Scheme 1.2: Proposed mechanism for the Heck reaction with arene diazonium salts based on ESI(+)-MS data, *m/z* values are given for observed cationic species. Modified from reference 36.

More recently Stefani et al. studied the Heck reaction using tellurides[59] and Svennebring et al.[38] reported the identification of three types of cationic, catalytic intermediates (Figure 1.4 A-C) in the microwave-assisted, phosphane-containing Heck arylation of electron rich olefins. In the latter case the species observed support a Pd(0)/Pd(II)-based cycle. This provided direct evidence for reduction of the palladium precatalyst to Pd(0) by the ligand and confirmed oxidative addition of the aryl substrate, but no Pd-bound olefin intermediates were observed. This is often the case either because the olefin-bound species is neutral or because OA is the rate-limiting step and the subsequent steps occur too quickly to be observed by the sampling method (in this case sampling included quenching and dilution of samples from a reaction vessel).

In 2007, ESI-MS was used in the negative-ion mode to detect the boron species responsible for transmetallation in the Suzuki reaction: $[PhB(OCH_3)_3]^-$ (Figure 1.4 D).[60] And in 2009 it allowed the first *in situ* observation of small catalytically active palladium clusters during a Suzuki

reaction that could be precursors to catalytically active palladium nanoparticles. Specifically $[(IL)_5Pd_3(H_2O)]^+$, $[(IL)_3Pd_3(H_2O)_7]^+$ and transmetallation product $[(IL)_2PdAr]^+$ were observed where IL = an imidazolium cation or *N*-heterocyclic carbene.[61]

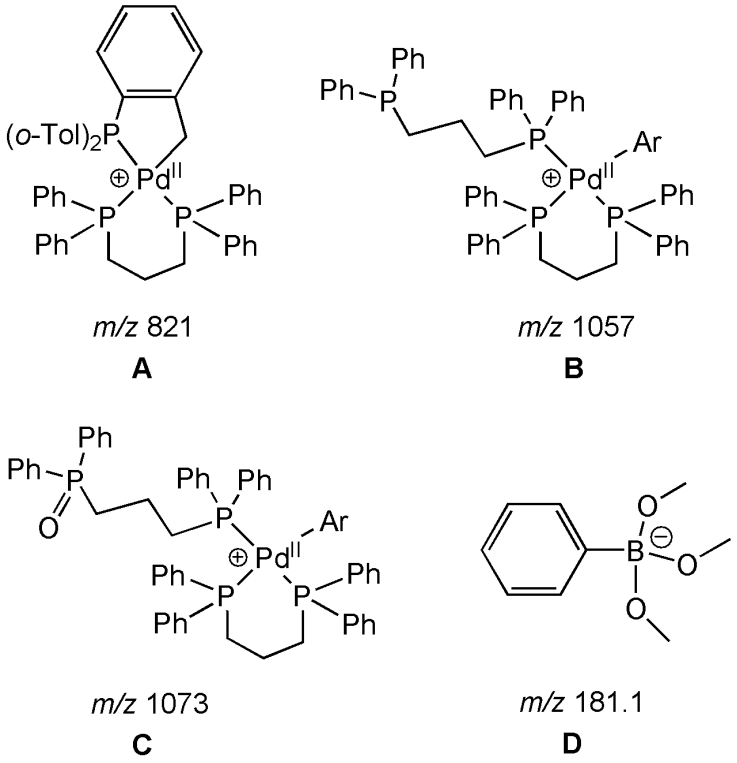

Figure 1.4: (A-C) Palladium-containing species observed by ESI-MS and implicated in the microwave-assisted Heck arylation of electron rich olefins.[38] (D) A boron-containing ion implicated in the transmetallation step of the palladium-catalyzed Suzuki cross-coupling reaction.[60]

Analysis of a simple Pd-catalyzed allylic substitution reaction lead to the discovery of two reversibly formed binuclear bridged Pd complexes (Figure 1.5) that are proposed to be formed by direct Pd-Pd bond formation and act as a reservoir for the active mononuclear catalyst.[40] The observation of dimers when using ESI-MS is common and it is important to confirm that they truly exist in solution and are not just formed during the ESI process. In this case it was supported by ^{31}P and ^{1}H NMR studies of stoichiometric reaction mixtures and *in situ* XAFS experiments.[62]

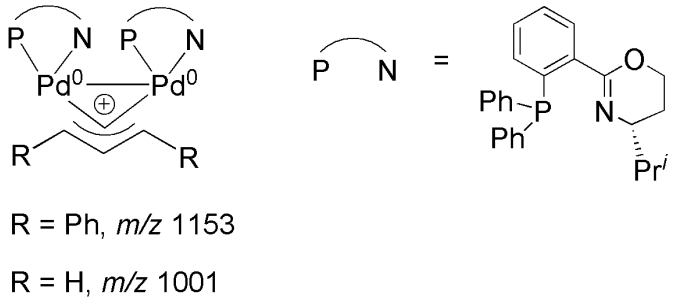

R = Ph, *m/z* 1153

R = H, *m/z* 1001

Figure 1.5: Two binuclear palladium-bridged allylic complexes discovered by ESI(+)-MS analysis. They are proposed to serve as reservoirs for the active catalyst in a palladium-catalyzed allylic substitution reaction.[40]

While ESI studies of systems catalyzed by other metals are rare, one report investigated a ruthenium-catalyzed reaction with naturally charged Ru-cluster intermediates. The cubane structure $[Ru_4(\eta^6\text{-}C_6H_6)_4(OH)_4]^{4+}$ was shown to exist in solution by direct observation of $[Ru_4(\eta^6\text{-}C_6H_6)_4(O)_3(OH)]^+$.[28] The corresponding dimer $[Ru_2(\eta^6\text{-}C_6H_6)_2(O)(OH)]^+$ was also observed and proposed as the active catalyst in the hydrogenation of benzene.

Finally, direct observation of seven intermediates involved in the hydrosilylation and dehydrogenative silylation of phenylacetylene by an Ir^{II}-NHC type catalyst allowed the elucidation of both the hydro- and dehydrogenative silylation mechanisms (Scheme 1.3).[31] Analysis of fragmentation patterns produced by MS/MS experiments lent insights into the connectivity of species $[I]^+$ and $[III]^+$ where the mass assignment itself was ambiguous. Use of the modified substrate 4-aminophenylacetylene, which is visible by ESI-MS, confirmed formation of the products and indicated the dominant mechanism under each set of reaction conditions.

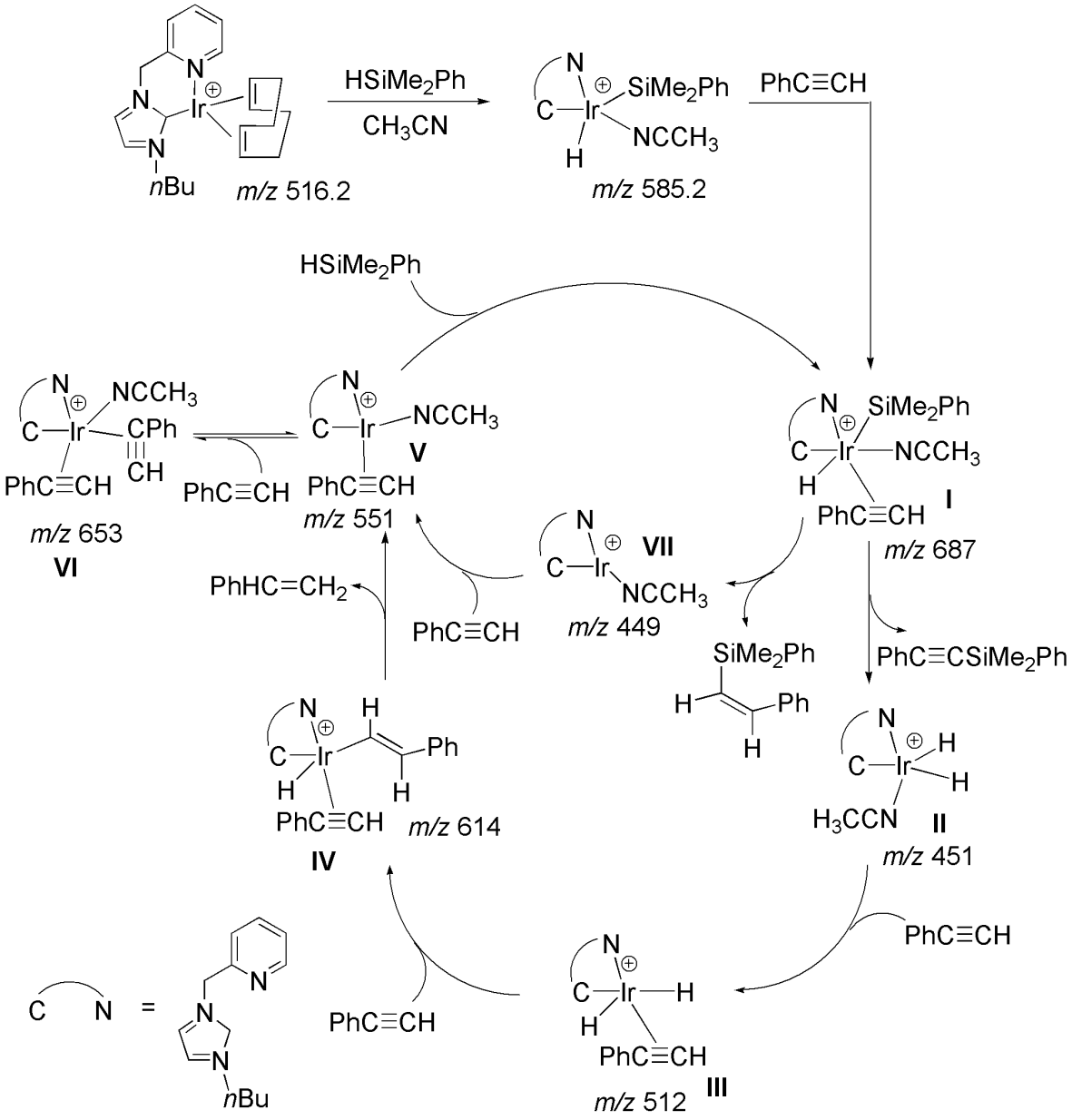

Scheme 1.3: Proposed mechanisms for the hydrosilylation and dehydrogenative silylation of phenylaceylene by an iridium catalyst, *m/z* values are given for cationic species observed by ESI(+)-MS. Modified from reference 31.

Peter Chen pioneered the mechanistic study of gas-phase reactions by ESI-MS.[63-67] A modified mass spectrometer (octupole / quadrupole / octupole / quadrupole) allows for introduction of gas-phase reagents and subsequent reaction with the analyte at the first octupole. The gas-phase products can then be analyzed directly in the first quadrupole, or studied in further detail by

collision-induced dissociation in the second octupole and analysis in the second quadrupole. This not only permits the detection of potential short-lived intermediates, but also allows a direct interrogation of their reactivity. The method is highlighted by a 1997 study of alkane C-H activation by $[CpIr^{III}(PMe_3)(CH_3)L]^+$ or $[Cp^*Ir^{III}(PMe_3)(CH_3)L]^+$, where L is dichloromethane, acetonitrile or triflate.[68, 69] Previously, the C-H activation of alkanes by these Ir(III) complexes was proposed to occur by one of two mechanisms: oxidative addition followed by reductive elimination, or concerted sigma-bond metathesis. However, in gas-phase reaction experiments, loss of CH_4 occurred readily after collisional removal of the weakly bound ligand, L, leading the investigators to propose a novel mechanism in which methane is lost by cyclometallation with the methyl groups on phosphine before any C-H activation of the alkane (Scheme 1.4). Deuterated studies allowed them to exclude the possibility of any participation by the methyl groups of Cp*.

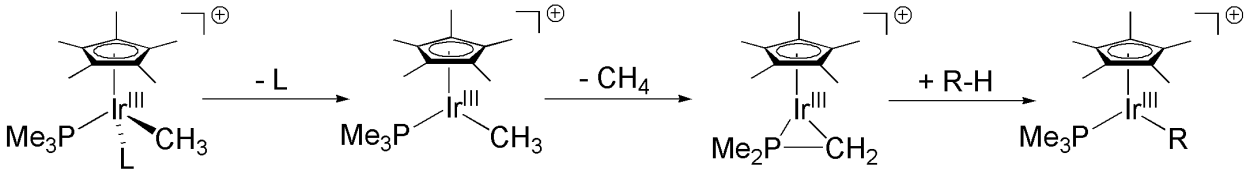

Scheme 1.4: Proposed mechanism for C-H activation of alkanes by Ir^{III} complexes, ions and reactivity shown here were observed in the gas phase. Modified from reference 68.

1.2.2 Adventitiously-charged systems

In adventitiously-charged systems intermediates are inherently neutral, but charged species occur without intervention through one or more ionization mechanisms. The most common ionization mechanisms are protonation of a basic site, reversible loss of an anionic ligand like I^- or Br^-, or association of an alkali metal like Na^+ or K^+ (alkali metals are often present as contaminants in mass spectrometers) (Figure 1.6). Like inherently charged systems, no modification to the reaction mixture is required. Loss of an anionic ligand is particularly common in organometallic complexes[70] and as a result adventitiously-charged systems were among the first to be investigated by ESI-MS.

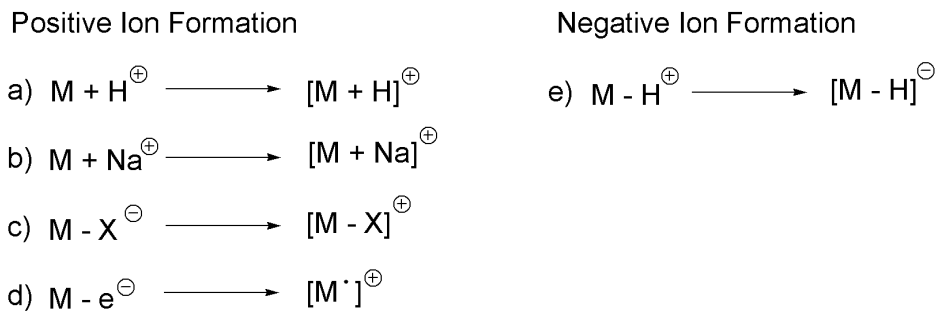

Figure 1.6: Common ionization pathways: a) protonation of a basic site b) association of a cation to a basic site c) halide loss d) oxidation e) deprotonation of an acidic site.

A 1993 study on the Raney nickel-catalyzed homo-coupling of 2-bromo-6-methylpyridine allowed for the observation of a number of potentially active catalyst species including the dimer $[(dmbp)Ni(\mu\text{-}Br)_2Ni(dmbp)Br]^+$ through loss of a bromide ligand,[32] and in the late 1990s the reactive intermediates in the Ti^{IV}-catalyzed enantioselective sulfoxidation of organic sulfides were extensively analyzed by ESI-MS through protonation of the ligands on titanium;[24, 71] however, most subsequent work has focused on palladium-catalyzed or ruthenium-catalyzed reactions.

Early investigations into the mechanism of palladium-catalyzed C-C bond-forming reactions supported the formation of oxidative addition intermediates in the following cases: when bis-phosphane chelating ligands were employed in the Heck arylation of methyl acrylate (loss of halide),[72] during the intramolecular cyclization of enamides to form spiro-compounds (loss of halide),[73] and in the self-coupling of arylboronic acids (loss of anionic boron ligand).[74] In the last case relevant species were also intercepted by protonation of intermediates when the reaction was quenched with trifluoroacetic acid. For example $[Pd(H)(PPh_3)_2(B(OH)(OH_2))]^+$ was detected which is a species implicated in the regeneration of the catalyst.

More recently, cationic intermediates have been observed in the Heck reactions of: arene diazonium salts catalyzed by triolefinic macrocycle Pd(0) complexes,[36, 75] o-iodophenols and ennoates to form new lactones,[76] and o-iodophenols with olefins (the *oxa*-Heck reaction).[77] In the first case ions were formed by oxidation of the analyte at the capillary, or by association of $[NH_4]^+$ or Na^+. In the two other cases ionization occurred through the more typical loss of a

halide ligand. The *oxa*-Heck reaction provides a good example of how these experiments are typically performed and the type of information that can be obtained. The oxyarylations of olefins were performed in acetone, catalyzed by palladium, and required the presence of sodium carbonate as base. Samples from the reaction mixtures were diluted with acetonitrile and analyzed by ESI(+)-MS. Loss of iodide after oxidative addition of *o*-iodophenol to palladium afforded positively-charged intermediates. Species consistent with oxidative addition, such as $[Pd(PPh_3)_2(C_6H_5O)]^+$, and the formation of palladacycles of the type seen in Scheme 1.5 were observed. Based on this a mechanism for the reaction was proposed (Scheme 1.5).

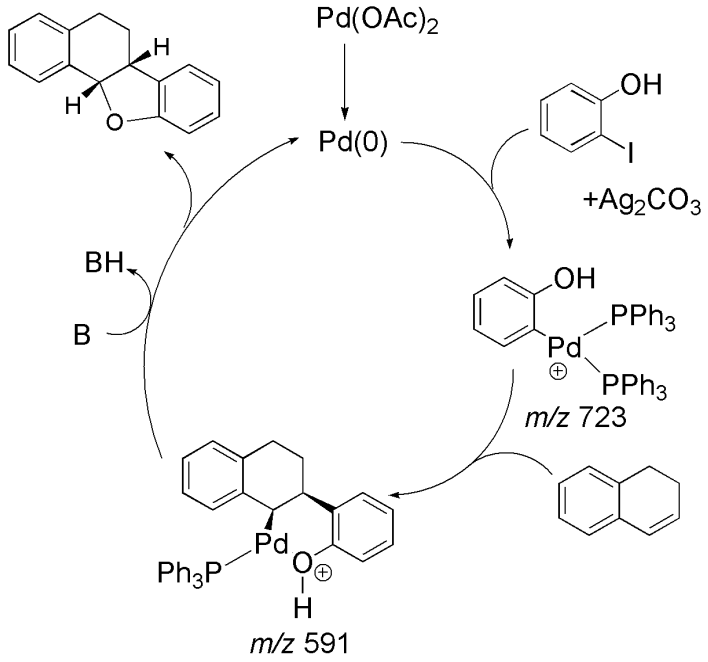

Scheme 1.5: Proposed mechanism for the oxyarylation of olefins, *m/z* values are given for cationic intermediates observed by ESI(+)-MS. B = base. Modified from reference 77.

A Suzuki cross-coupling reaction between arene diazonium salts and potassium trifluoroborates was studied by ESI-MS in 2007,[35] and used the same triolefinic macrocyclic Pd(0) complex that had been found to catalyze the phosphane-free Heck reaction.[36, 75] To further investigate the general mechanism of the reaction, ESI-MS was used to monitor the coupling of 4-$CH_3PhN_2BF_4$ and KBF_3Ph catalyzed by $Pd_2(dba)_3$ in H_2O/CH_3CN. An oxidative addition

intermediate was observed along with protonated transmetallation intermediates and homo-coupling intermediates (Scheme 1.6 I, II and III, respectively).

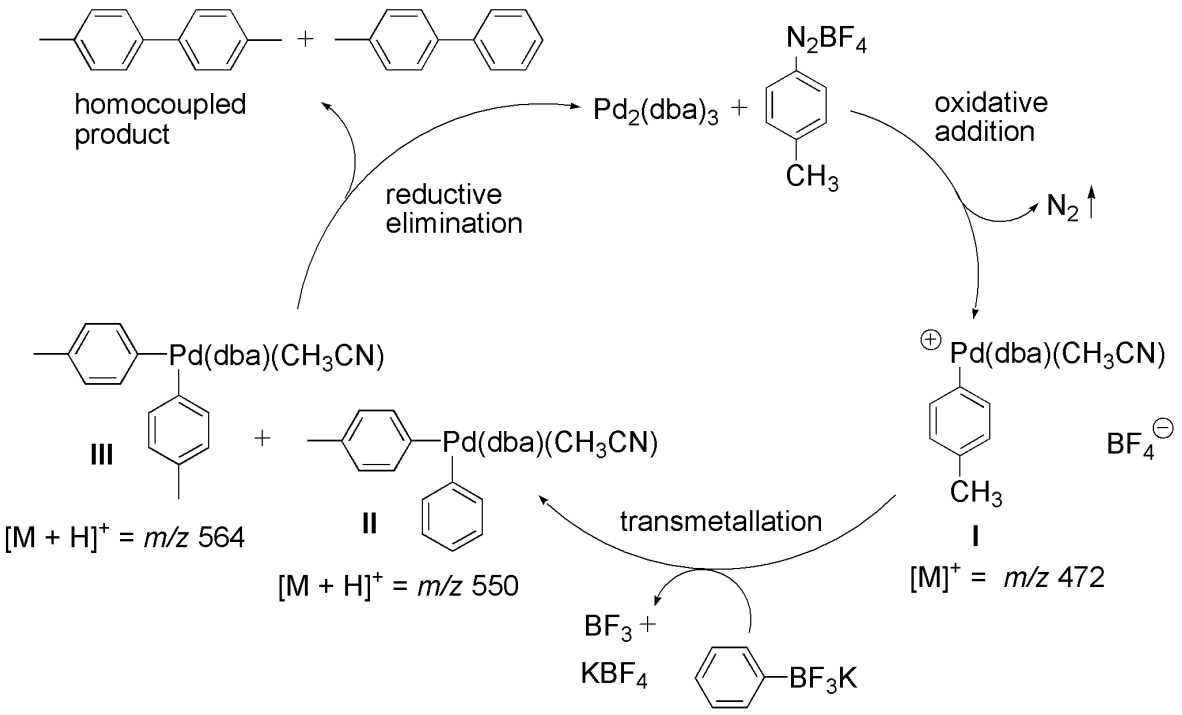

Scheme 1.6: Proposed mechanism for the Suzuki cross-coupling reaction of arene diazonium salts with potassium trifluoroborates based on ESI-MS investigation, *m/z* values are given for cationic intermediates observed by ESI(+)-MS. Modified from reference 35.

A 2007 paper by Santos and Eberlin provides an excellent example of a non-innocent ESI process that allows detection of otherwise neutral intermediates.[78] The expected Pd^0 active species for a typical Stille reaction was indirectly observed as its molecular ion $[Pd(PPh_3)_2]^{\bullet+}$. The molecular ion was formed by oxidation of the neutral species at the capillary during the ESI process.[78] The proposed oxidative addition and transmetallation intermediates were also observed, primarily as their molecular ions: $[M]^{\bullet+}$. Figure 1.7 below shows an intermediate undergoing transmetallation. Observation of these Pd-based radical cations provides support for the proposed Stille reaction mechanism. Care must be taken when examining the behaviour of these radical species in the gas phase since their reactivity is unknown and is unlikely to be the same as their neutral analogs.

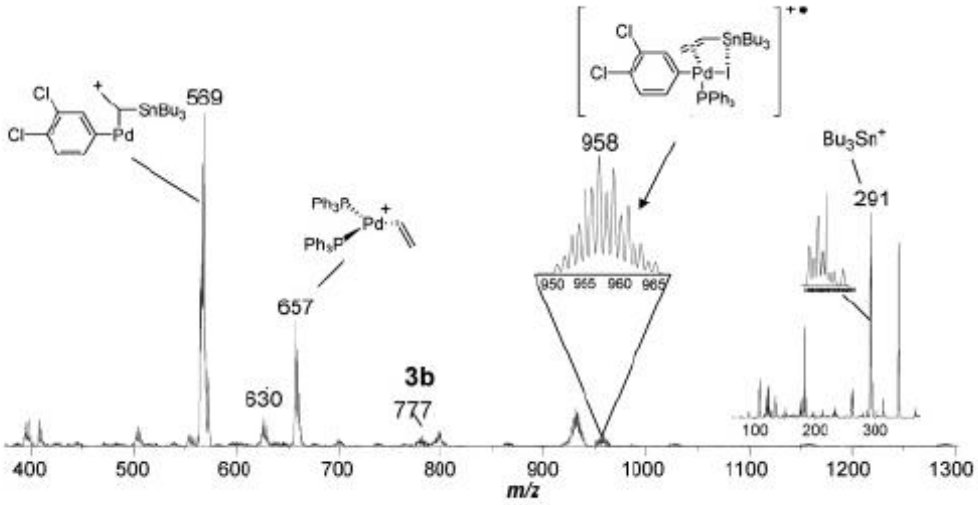

Figure 1.7: ESI(+)-MS of the Stille reaction of 3,4-dichloroiodobenzene and vinyltributyltin in acetonitrile mediated by $Pd(PPh_3)_4$. A radical cation intermediate undergoing transmetallation is observed at *m/z* 958. Reprinted with permission from "The Mechanism of the Stille Reaction Investigated by Electrospray Ionization Mass Spectrometry" Leonardo S. Santos, Giovanni B. Rosso, Ronaldo A. Pilli, and Marcos N. Eberlin *J. Org. Chem.* **2007** *72* (15), 5809-5812. Copyright ©2007 American Chemical Society.

The role of Pd(II) in improving the selectivity of carbon-carbon bond formation in the allylic substitution of 1-acetoxy-1,3-diphenylpropene by acetylacetone in an aqueous system was investigated by Muzart and Roglans (Scheme 1.7).[34]

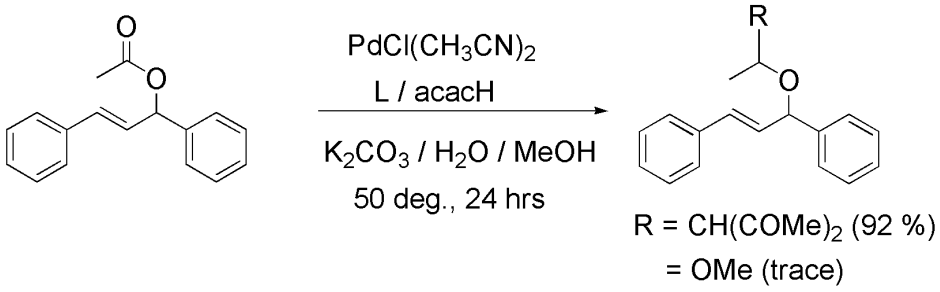

Scheme 1.7: Allylic substitution of 1-acetoxy-1,3-diphenylpropene by acetylacetone (acacH).[34]

The metal complex could be seen in both the positive- and negative-ion mode by loss of halide from the metal, or loss of proton from the ligand respectively. Peaks corresponding to the presence of a Pd-enolate complex of the form $[Pd^{II}(Cl)L(acac)]^+$

(L=[$(HOCH_2CH_2NHCOCH_2)_2NCH_2]_2$) (Figure 1.8 A) were observed in both positive and negative mode while no peaks corresponding to the traditionally proposed Pd-allyl intermediate were observed (a control was done to prove they could see these species using a Pd(0) source). These observations led to the conclusion that the role of palladium involved the selective nucleophilic attack of the central carbon of the Pd-enolate complex and not stabilization of a Pd-allyl intermediate.

The similar substitution of allylic acetates with sodium *para*-toluenesulfonate using the catalytic mixture $[(\eta^3\text{-allyl})PdCl]_2$ and L (same as above) in aqueous media was also studied by the same group, but with very different results.[39] Peaks were observed corresponding to allyl-type intermediates such as $[PdL(PhCH{=}CHC(OAc)HCH_3) - OAc]^+$ (Figure 1.8 B). Two possible mechanisms were proposed based on these observations, one of which involves a Pd(IV) intermediate.

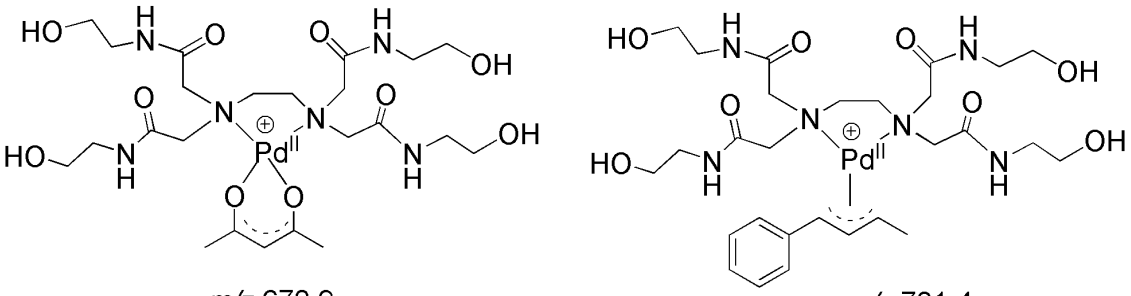

Figure 1.8: A) A Pd-enolate complex observed by ESI(+)-MS during the palladium-catalyzed allylic substitution of 1-acetoxy-1,3-diphenylpropene by acetylacetone.[34] B) A Pd-allyl complex observed by ESI(+)-MS during the palladium-catalyzed substitution of allylic acetates with sodium *para*-toluenesulfonate.[39]

Some less common Pd-catalyzed bond-forming reactions have been investigated as well, including tellurium-carbon bond formation (ionized by loss of halide),[33] intramolecular nitrogen-carbon bond formation (ionized by association of H^+ or Na^+),[79] and the formation of two new carbon-oxygen bonds in the hydroxyalkoxylation of 2-allylphenols (ionized by loss of H^+ in negative-ion mode, and loss of anionic ligand or association of Na^+ in positive-ion mode).[80] An

impressive study by Guo et al. determined the mechanism of a palladium-catalyzed three-component cyclization reaction (the formation of cis-pyrolidine derivatives from imine, iodobenzene and 2-(2,3-allenyl)malonate).[81] Three key cationic organopalladium species which had lost halide ligands were detected by ESI-FTMS. All ions were characterized by accurate mass determination and subjected to collision induced dissociation to aid in the structural assignment. A carbopalladation mechanism was proposed which takes into account all experimental data (Scheme 1.8). Oxidative addition of iodobenzene yields the first intermediate, carbopalladation of 2-(2,3-allenyl)malonate gives the second intermediate, and deprotonation and addition of imine leads to the final intermediate. The cycle is completed by intramolecular allylic animation to give the product and the regenerated catalyst. Potassium adducts of the products were also observed to appear as the reaction progressed.

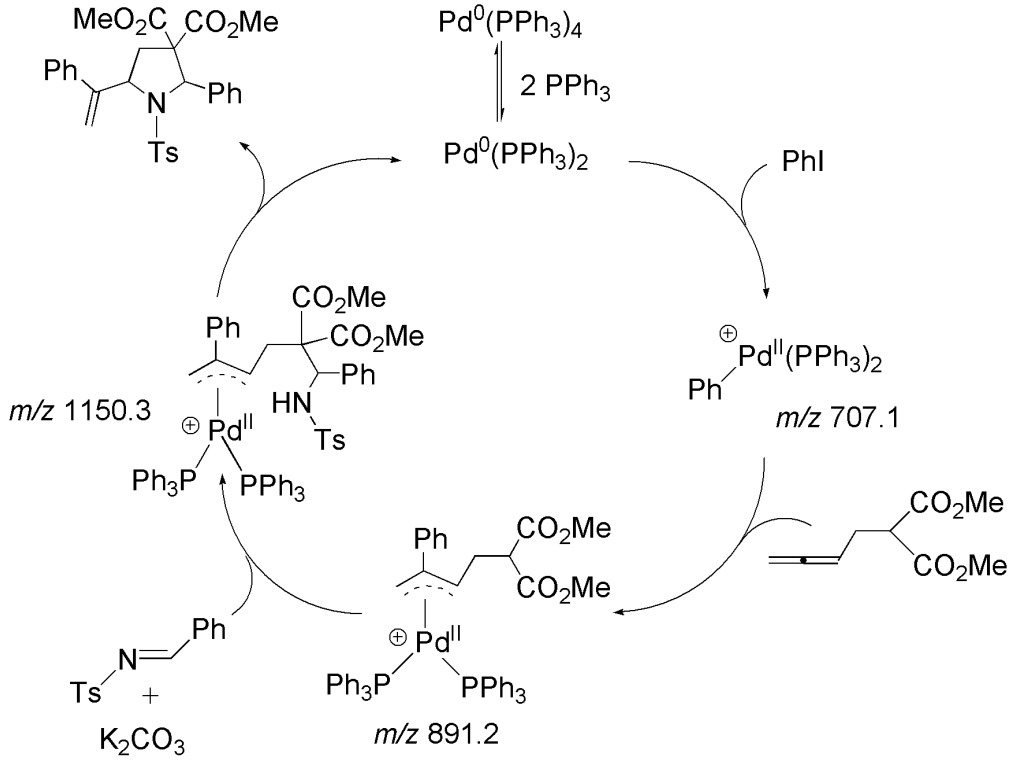

Scheme 1.8: Proposed mechanism for the formation of cis-pyrolidine derivatives from imine, iodobenzene and 2-(2,3-allenyl)malonate by ESI(+)-FTMS, *m/z* values are given for observed cationic intermediates. Modified from reference 81.

There has been some interest in the study of ruthenium-catalyzed systems. For example, hydrogenation reactions catalyzed by Ru(II)-arene complexes have been the focus of a few ESI-MS studies, the first of which appeared in 2000. In this report, three species (Figure 1.9 A, B and C) were detected in a mixture of the pre-catalyst $[Ru^{II}Cl(\eta^6\text{-cymene})]_2$ and *cis*-aminoindanol ($C_9H_{10}NO$) in isopropanol, in the absence of any substrate. Upon addition of acetophenone as a substrate no new peaks were observed.[82] The authors suggest that these results support the mechanism proposed by Noyori involving a six-centered transition state in which the substrate is not directly bound to the metal (Figure 1.9 D).[83]

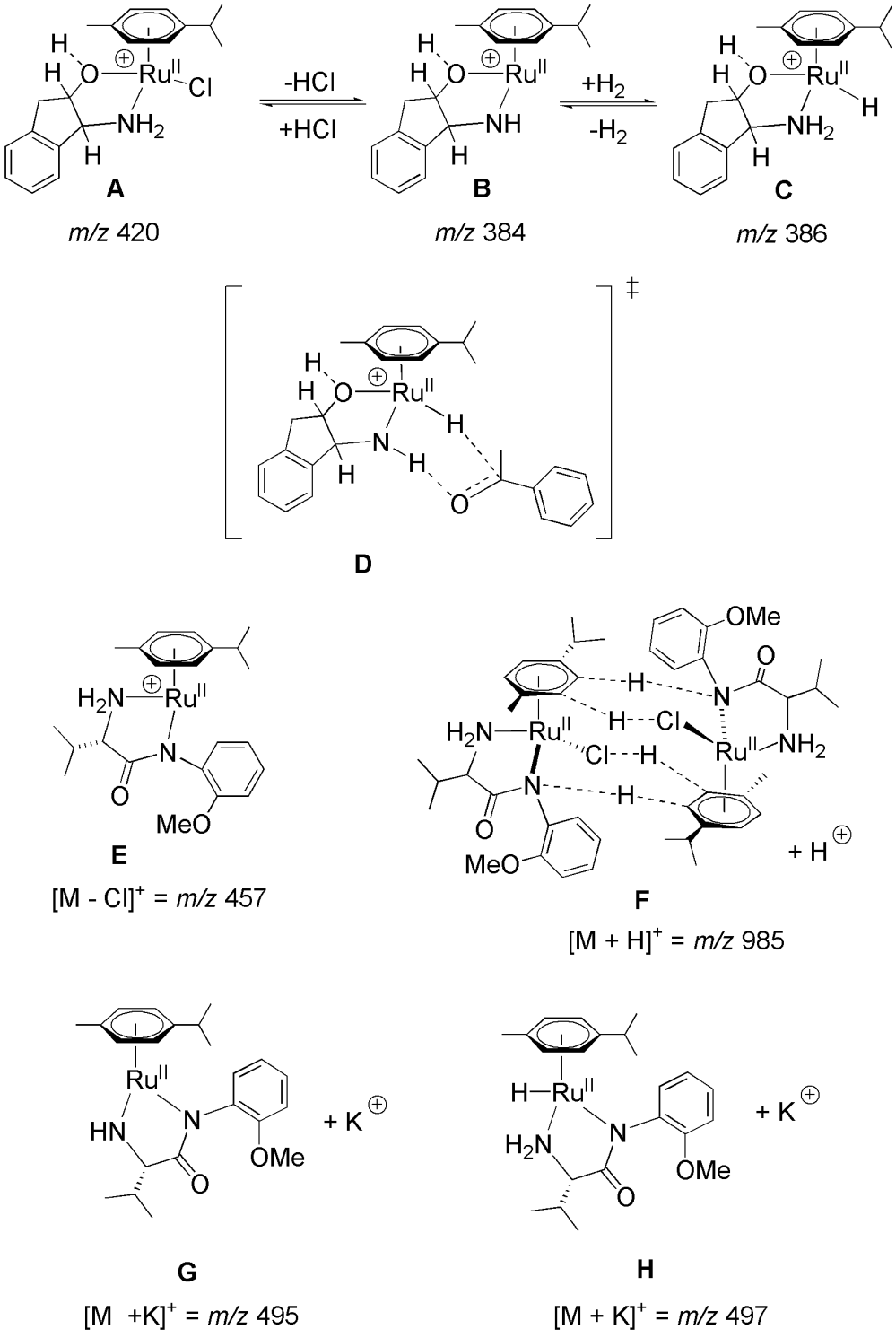

Figure 1.9: Ruthenium-containing complexes observed by ESI(+)-MS.

A similar study employing both ESI(+)-MS and ESI(-)-MS also studied the asymmetric hydrogenation of acetophenone, but with Ru(II)-arene catalysts containing amino amide ligands: Ru(cymene)Cl(N-N) where N-N = $H_2NCH(^{i}Pr)C(O)N(o\text{-}(MeO)Ph)$. Peaks were seen (by loss of Cl^- or gain of H^+ or K^+) corresponding to the monomer and piano-stool type dimers of the precatalyst, the $16e^-$ active catalyst, and a hydride-containing intermediate (Figure 1.9 E-H respectively). This provided further support for Noyori's mechanism and highlighted the potential involvement of dimers in the catalysis.[29]

1.2.3 Charged or chargeable tags

Monitoring catalytic reactions that have intrinsically- or adventitiously-charged intermediates is simple, and analyses of these types of systems constitute the bulk of the literature in this area, but many of the most important catalytic organometallic reactions proceed through neutral intermediates where there are no reliable ionization mechanisms for visualization by MS. In order to study these systems a charged or chargeable (usually having an acidic or basic site) tag is required. Importantly, the tag must not introduce steric or electronic effects that interfere with the catalysis in any significant way.

In 1994, Canary et al. purposefully used a substrate with an easily protonated site to study the palladium-catalyzed reactions of pyridyl bromide with three different phenylboronic acids by ESI-MS. Pyridyl bromide was selected as a chargeable tag due to the ability of the ring nitrogen to become protonated. Relying on this ionization mechanism, oxidative addition intermediates and transmetallation intermediates were observed (Figure 1.10).[84] A majority of the existing works are focused on the study of ruthenium-catalyzed systems, and they often make use of permanently-charged ligands that were designed for water solubility. The groups of Traeger,[85, 86] Dyson,[87] Nicholson[88] and Chen[65, 89, 90] have made significant contributions to this area; however, it is still a somewhat underappreciated approach.

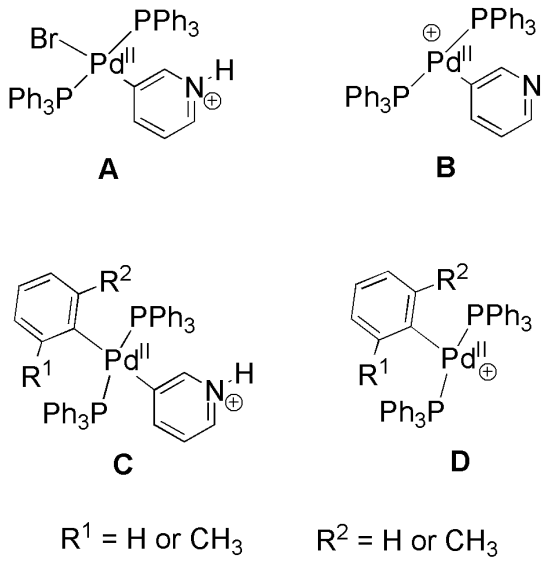

Figure 1.10: **(**A and B) Oxidative addition intermediates $[(pyrH)Pd(PPh_3)_2Br]^+$ and $[(pyr)Pd(PPh_3)_2]^+$, (C & D) Transmetallation intermediates $[(pyrH)(R_1R_2C_6H_3)Pd(PPh_3)_2]^+$ and $[(R_1R_2C_6H_3)Pd(PPh_3)_2]^+$ (R_1 = H or CH_3 and R_2 = H or CH_3).

An investigation of the hydrogenation of styrene by Ru(II)-arene type catalysts with negatively-charged, water soluble, diphosphine ligands (Figure 1.11 A) was reported in 2004. Analysis by ESI(-)-MS yielded peaks corresponding to the anions $[Ru(\eta^2\text{-P-P})(\eta^6\text{p-cymene})Cl]^{3-}$ (Figure 1.11 B), $[Ru(\eta^2\text{-P-P})(\eta^6\text{p-cymene})H]^{3-}$ (Figure 1.11 C), and $[Ru(\eta^2\text{-P-P})(\eta^6\text{-PhC}_2H_5)H]^{3-}$ (Figure 1.11 D) and reveal an arene exchange process that is active during catalysis.[30] Further experiments demonstrated that the arene exchange process is only active in the presence of both substrate and dihydrogen and is not active when starting with the pre-formed hydride complex, all of which suggests that the exchange takes place on a dihydrogen-containing complex. H/D exchange experiments were also performed by ESI-MS and NMR and they demonstrate the presence of a dynamic equilibrium between a dihydrogen and hydride complex.

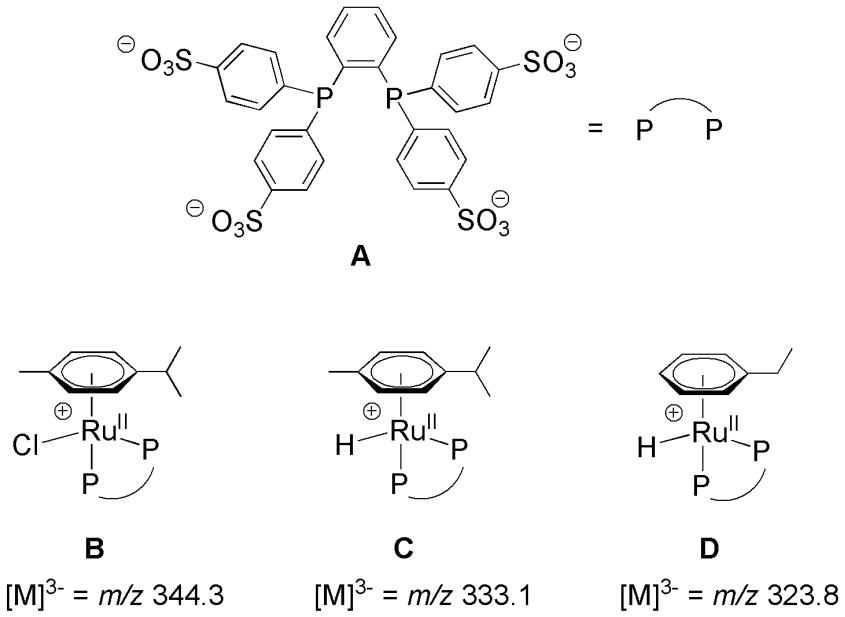

Figure 1.11: Ruthenium species bearing a multiply-charged bidentate phosphine ligand and involved in the catalytic hydrogenation of styrene. Ions were detected in the negative-ion mode.[30]

Two first generation ruthenium olefin metathesis catalysts were studied by Metzger[91] with the aid of the charged ligand $[P(Cy)_2(CH_2CH_2N(Me)_3)]^+Cl^-$, originally developed by Grubbs[92, 93] as a water-soluble ligand (Figure 1.12 A, B). Inclusion of the charged ligand allowed ESI-MS observation of the proposed 14-electron catalytically active Ru species (Figure 1.12 C) directly from solution, and confirmed many other aspects of the catalytic ring-closing metathesis cycle proposed by Grubbs.

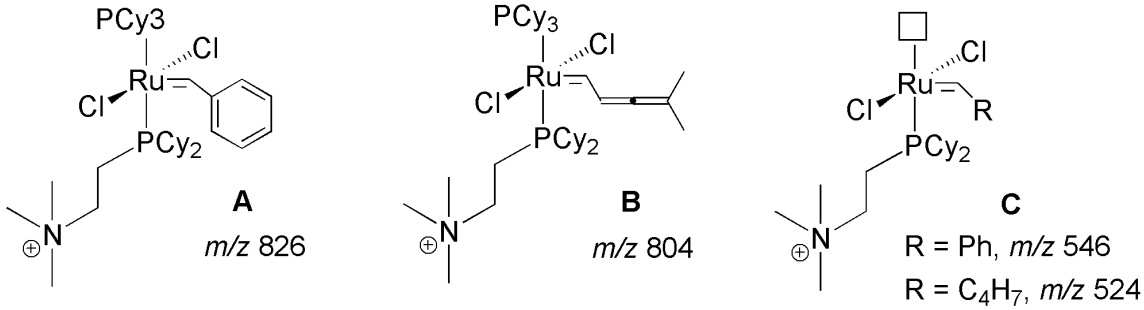

Figure 1.12: Two charge-tagged analogues of first generation ruthenium olefin metathesis catalysts (A & B), and the corresponding 14-electron active species observed by ESI(+)-MS (C).[91]

Ruthenium-catalyzed hydroformylation of alkenes was also studied using charged tags.[94] A unique permanently-charged version of a self-assembling bidentate ligand (Figure 1.13) was synthesized to study the catalytic mechanism.

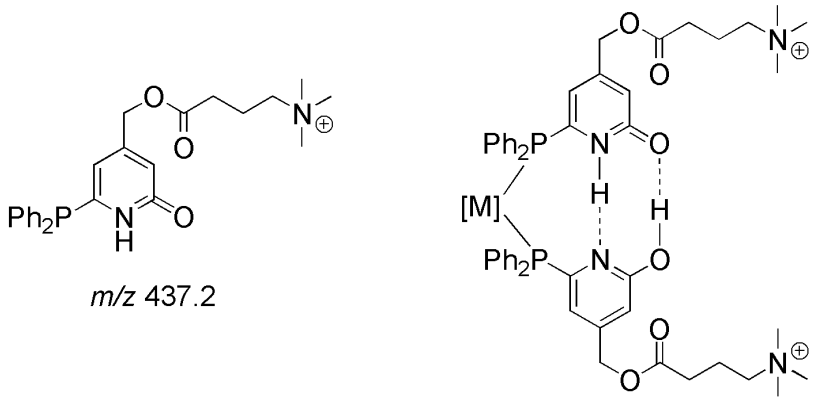

Figure 1.13: A permanently-charged, self-assembling bidentate ligand for observation of metal catalysts by ESI(+)-MS.[94]

Along with studies of the catalyst solution and stoichiometric reaction mixtures, the hydroformylation reaction was studied online under typical reaction conditions by connecting a pressurized autoclave (20 bar) directly to the mass spectrometer via a splitter. While this allowed them to identify new reaction intermediates they did not take advantage of their real-time sampling to extract any kinetic data from the observed intermediates over time. Nevertheless, a new hydroformylation reaction mechanism for self-assembling ligands was proposed based on ESI-MS studies including D_2-incorporation experiments (Scheme 1.9).

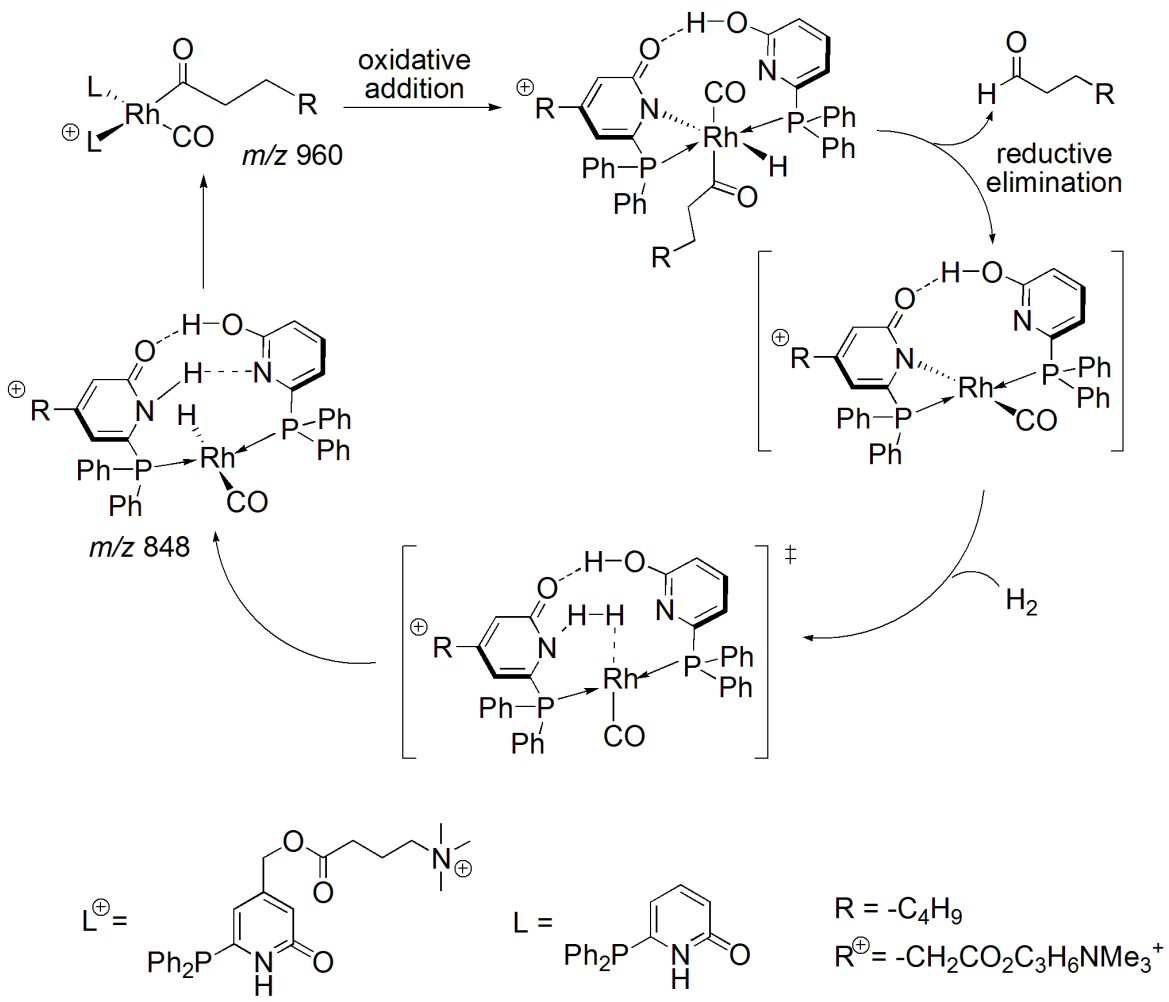

Scheme 1.9: A proposed ruthenium-catalyzed hydroformylation mechanism involving self-assembling ligands and informed by ESI(+)-MS analysis. Modified from reference 94.

A palladium-catalyzed system in which charged tags were used was very recently reported by Schade et al. in which they also monitor the relative concentrations of product and reactant over time (see Section 1.3 below).[95] This article also includes examples of the use of charged quaternary ammonium-tagged substrates for studying Zn, Mg and In systems by ESI-MS.

Our group's contributions to the area of developing and employing charged and chargeable ESI-MS tags include: the development of various chargeable or charged phosphine ligands analogous to commonly used mono- or bi-dentate neutral phosphine ligands;[96, 97, 98] using a tethered charged pyridinium group to study distannoxane speciation during esterification

catalysis;[99] and examining olefin hydrogenation and silane dehydrocoupling with a charged analogue of Wilkinson's catalyst.[97,98]

A key example of the usefulness of charged tags in probing reaction mechanisms is found in our study of the esterification of alcohols and carboxylic acids reportedly catalyzed by distannoxanes.[100] A permanently-charged pyridinium group was incorporated into the proposed distannoxane catalyst and the catalyst was then readily observed by ESI(+)-MS in solutions of methanol and acetonitrile (Figure 1.14a). However, on addition of the carboxylic acid all distannoxane species disappeared and mono-tin species dominated the spectra (Figure 1.14b). This led to the performance of a number of control experiments in which the reaction was repeated in the presence of only mono-tin species and in the absence of all tin species with only HBr present (a byproduct formed on reaction of the carboxylic acid with the distannoxane). Surprisingly, the reaction proceeded most efficiently when only HBr was present suggesting that distannoxanes are in fact not responsible for catalyzing the esterification reaction.

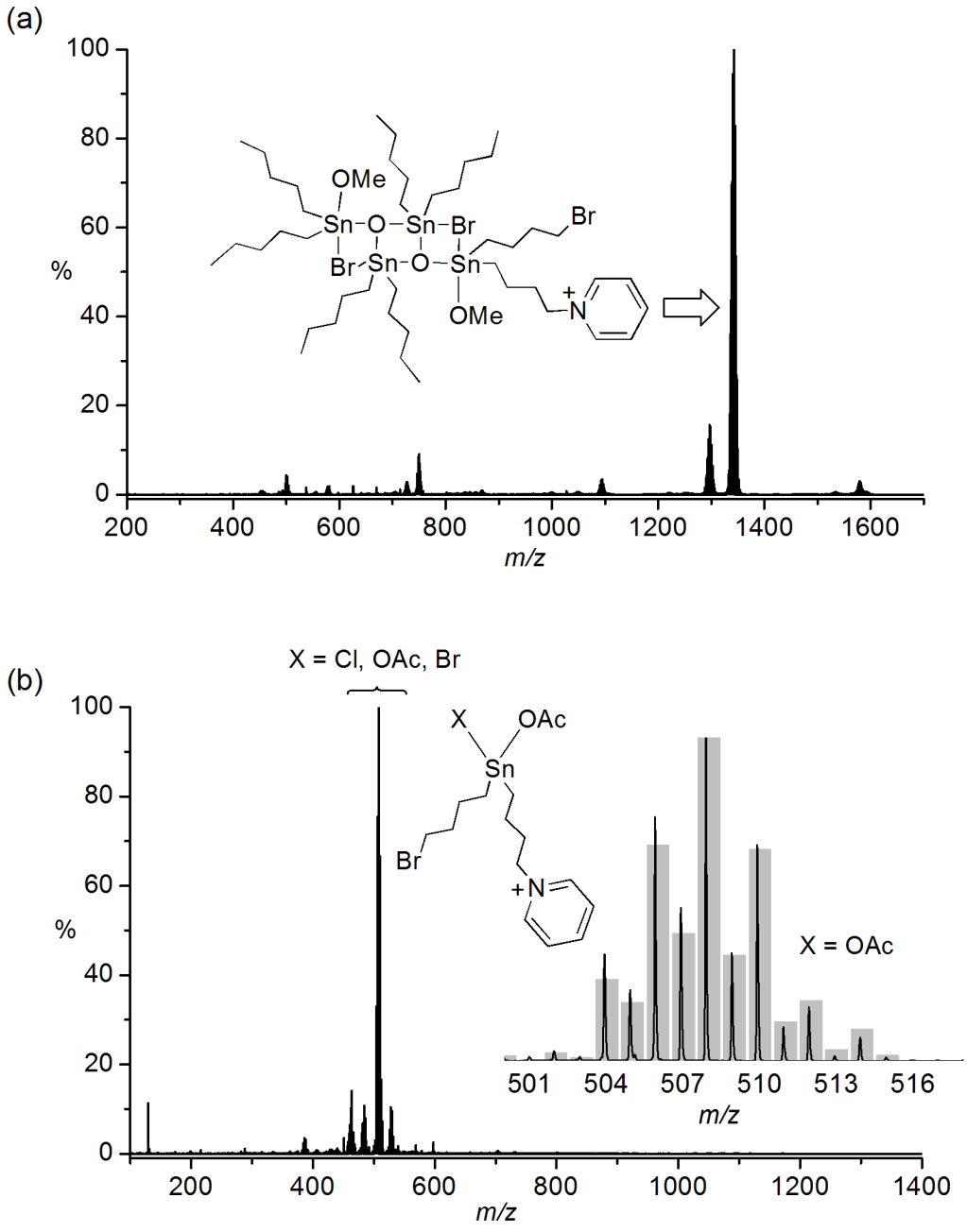

Figure 1.14: (a) ESI(+)-MS of $[SnBrX(C_4H_8Br)(C_4H_8NC_5H_5)]^+ Br^-$ (X = Cl or Br) with Bu_2SnO in methanol after 3 h reflux, (b) ESI(+)-MS of the reaction of $[SnBrX(C_4H_8Br)(C_4H_8NC_5H_5)]^+ Br^-$ (X = Cl or Br) with Bu_2SnO in methanol after addition of acetic acid. Note the absence of any higher mass species in the presence of acid. Modified figures from reference 99. Reproduced with permission.

1.3 Continuous reaction monitoring

Most of the experiments discussed above involve sampling of the organometallic reactions at discreet time intervals in order to better understand the composition of the reaction mixture as the reaction progresses. A few recent works have gone one step further and monitored the reaction profile of key species continuously over time in such a way that kinetic data can be obtained.[27, 37, 95, 98] A related micro-review[101] and book[102] by Santos discuss online ESI-MS investigations of primarily organo-catalyzed reactions but also include organometallic examples.

A precursor to these types of studies was reported in 2006 by Enquist in which an oxidative Heck-type reaction was sampled periodically and a graph of the intensities of all the observed intermediates was generated. In Figure 1.15 cationic palladium complexes corresponding to the active catalyst (A1 and A2), transmetallated intermediates (B1 – B3), and a palladium-bound olefin intermediate (C1) are shown, these were directly observed by ESI-MS.[37] By examining the intensity of these intermediates over time the investigators noticed that intermediates corresponding to the catalyst at the beginning of the cycle (Figure 1.15 A1 and A2) increased throughout the reaction while the intensity of intermediates related to transmetallation (Figure 1.15 B1 – B3) decreased. From this they postulated that the rate of the transmetallation step decreased over time as the transmetallation partner (an arylboronic acid) was consumed.

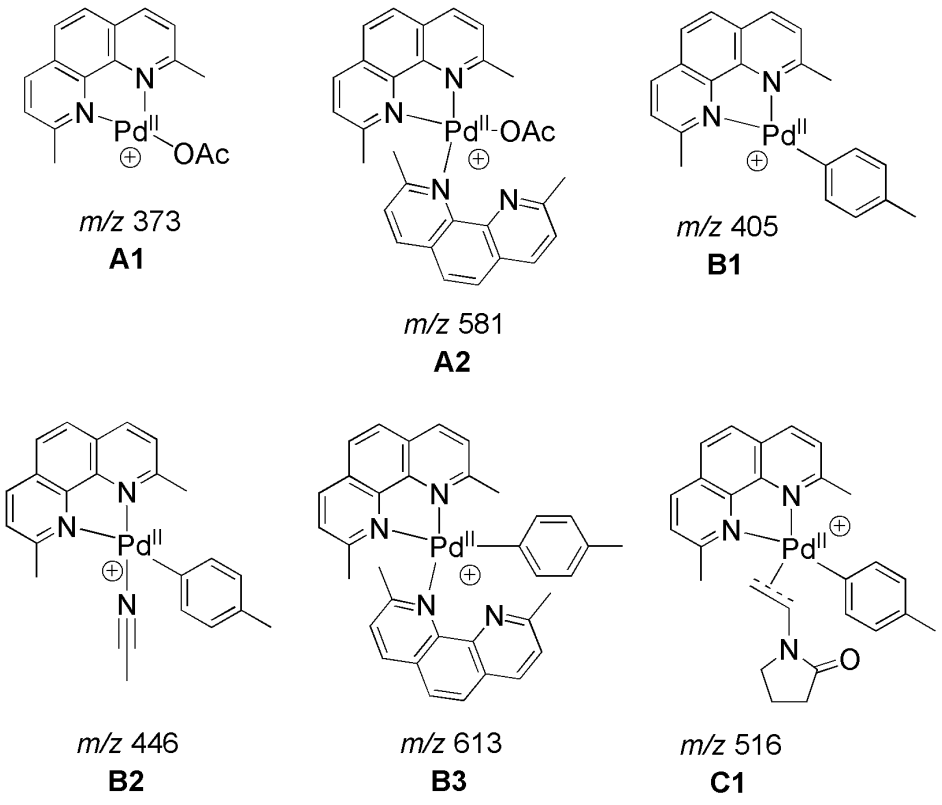

Figure 1.15: Cationic intermediates in the oxidative Heck arylation of 1-vinyl-2-pyrrolidinone by *p*-tolylboronic acid observed by ESI(+)-MS.[37]

In 2007, a manganese-catalyzed oxygen-evolving system that acts as a model for the oxygen-evolving complex of photosystem II was studied by ESI-MS (as well as EPR, UV/Vis, and XAS). $Mn^{IV/IV}{}_2O_2(terpy)_2(SO_4)_2$ was determined to be the dominant species in solution but an observed correlation in the ESI mass spectra between a signal representing $[Mn^{III/IV}{}_2O_2(terpy)_2(OAc)_2]^+$ (*m/z* 726) and the oxone signal $[KH_2SO_5]^+$ (*m/z* 153) over time led to the conclusion that the binuclear $Mn^{III/IV}$ species was in fact the active precatalyst (Figure 1.16).[27] The reaction solution was sampled by ESI-MS approximately every 2.5 min.

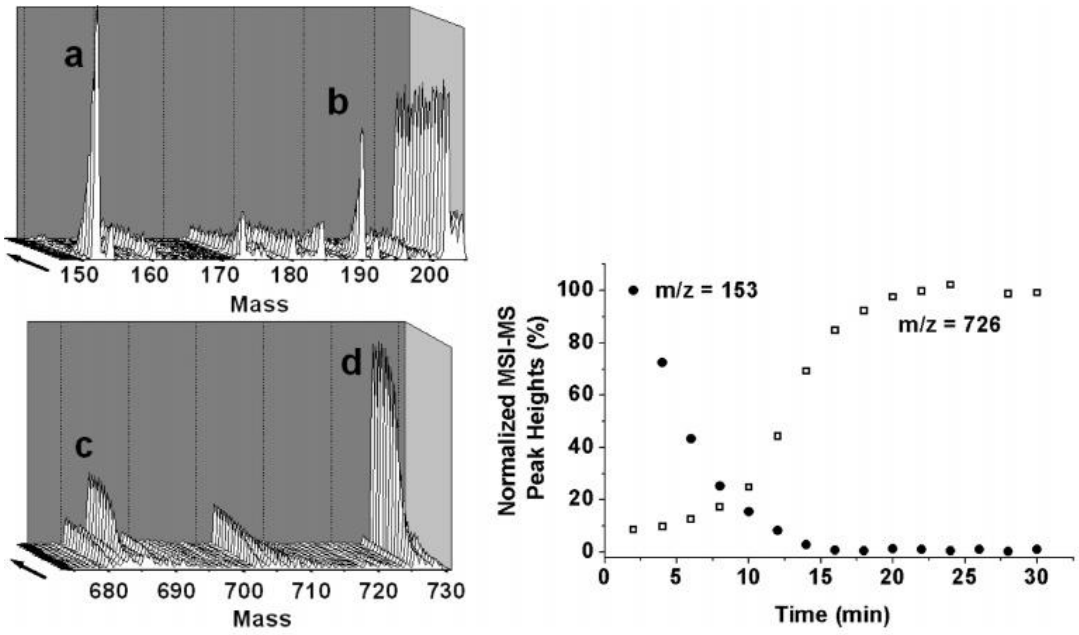

Figure 1.16: (left) ESI(+)-MS of the catalytic solution showing spectra of two separate runs from 2 to 30 min (arrows represent the increase of time), with 2-min intervals. Assigned peaks are (a) *m/z* 153, $KH_2SO_5^+$, (b) *m/z* 191, $K_2HSO_5^+$, (c) *m/z* 684, $[Mn^{III/IV}{}_2O_2(terpy)_2(OAc)(OH)]^+$, and (d) *m/z* 726, $[Mn^{III/IV}{}_2O_2(terpy)_2(OAc)_2]^+$. (right) Peak heights of *m/z* 153 and 726 over time. Reprinted with permission from "Speciation of the Catalytic Oxygen Evolution System: $[Mn^{III/IV}{}_2(\mu\text{-}O)_2(terpy)_2(H_2O)_2](NO_3)_3 + HSO_5^-$" Hongyu Chen, Ranitendranath Tagore, Gerard Olack, John S. Vrettos, Tsu-Chien Weng, James Penner-Hahn, Robert H. Crabtree and Gary W. Brudvig Inorganic Chemistry **2007** 46(1), 34-43. Copyright ©2007 American Chemical Society.

In 2010, a palladium-catalyzed Negishi cross-coupling reaction between the quaternary ammonium, charged substrate (*p*-iodophenyl)-trimethyl-ammonium iodide ($[ArI]^+I^-$) and benzylzincbromide to form (*p*-benzylphenyl)-trimethyl-ammonium iodide ($[ArBn]^+I^-$) was monitored.[95] Reaction mixtures were drawn into a syringe and injected continuously at room temperature into the mass spectrometer over 30 minutes beginning approximately 2 minutes after the start of the reaction (Figure 1.17). A plot of relative signal intensity versus time is obtained, and signals for the reactant and product are shown (the results for two different catalyst loadings are shown). The authors state that the high noise levels are a result of the inherently poor signal stability of the ESI process; however, we have not found this to be an issue in our work. Despite the high noise levels they were able to successfully observe the effects of catalyst loading and reagent concentration on the reaction, and they derived a rate constant for the oxidative addition

of (*p*-iodophenyl)-trimethyl-ammonium to palladium at room temperature (k_2 = 4 ± 2 L mol^{-1} s^{-1}).

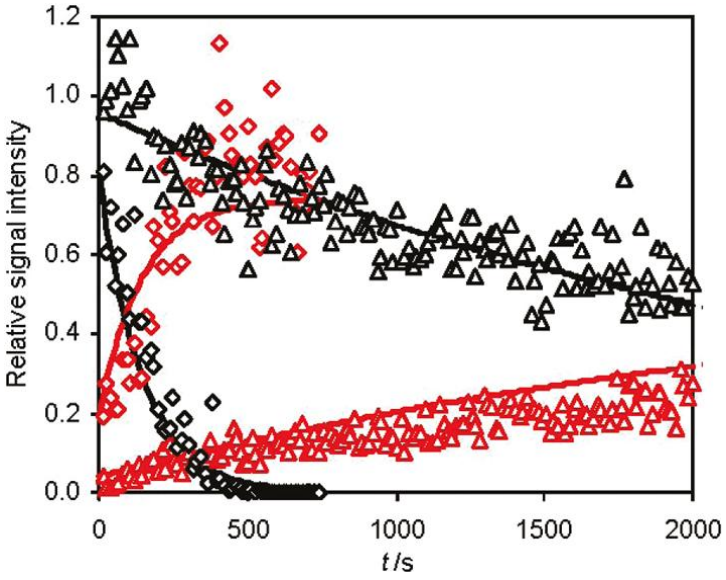

Figure 1.17: Time dependence of the normalized signal intensities of reactant [ArI]$^+$ (*m/z* 262, black) and product [ArBn]$^+$ (*m/z* 226, red) formed in the Pd-catalyzed cross-coupling reaction with BnZnBr in CH_3CN at room temperature as determined by ESI mass spectrometry. Results of two experiments with different catalyst loadings are shown (diamond = 100 mol %, triangle = 5 mol% relative to [ArI]$^+$). Reprinted with permission from "Charged Tags as Probes for Analyzing Organometallic Intermediates and Monitoring Cross-Coupling Reactions by Electrospray-Ionization Mass Spectrometry" Matthias A. Schade, Julia E. Fleckenstein, Paul Knochel, Konrad Koszinowski *The Journal of Organic Chemistry* **2010** *75* (20), 6848-6857. Copyright ©2010 American Chemical Society.

In collaboration with the Rosenberg group, our group has investigated the reaction of Wilkinson's catalyst with a dialkylsilane using time-resolved ESI-MS and the charged phosphine ligand $[Ph_2P(CH_2)_4PPh_2(CH_2Ph)]^+BF_4^-$ as an ESI handle.[98] In contrast to the previous example where only a reactant and product were monitored over time, these experiments examined only reaction intermediates which contained the charged phosphine tag. Stoichiometric solutions of $RhCl(PPh_3)_3$ and (*n*-hexyl)$_2SiH_2$ doped with the charged ligand were injected into the MS continuously directly from a syringe pump in an adjacent glovebox. The ESI-MS data confirmed the speciation of the reaction mixture that was observed by NMR experiments and a number of additional species were identified. Behaviour of the species over time allowed the proposal of a

reaction mechanism for the dehydrocoupling of silane including a competing catalyst decomposition pathway that is present due to trace amounts of water (Scheme 1.10).

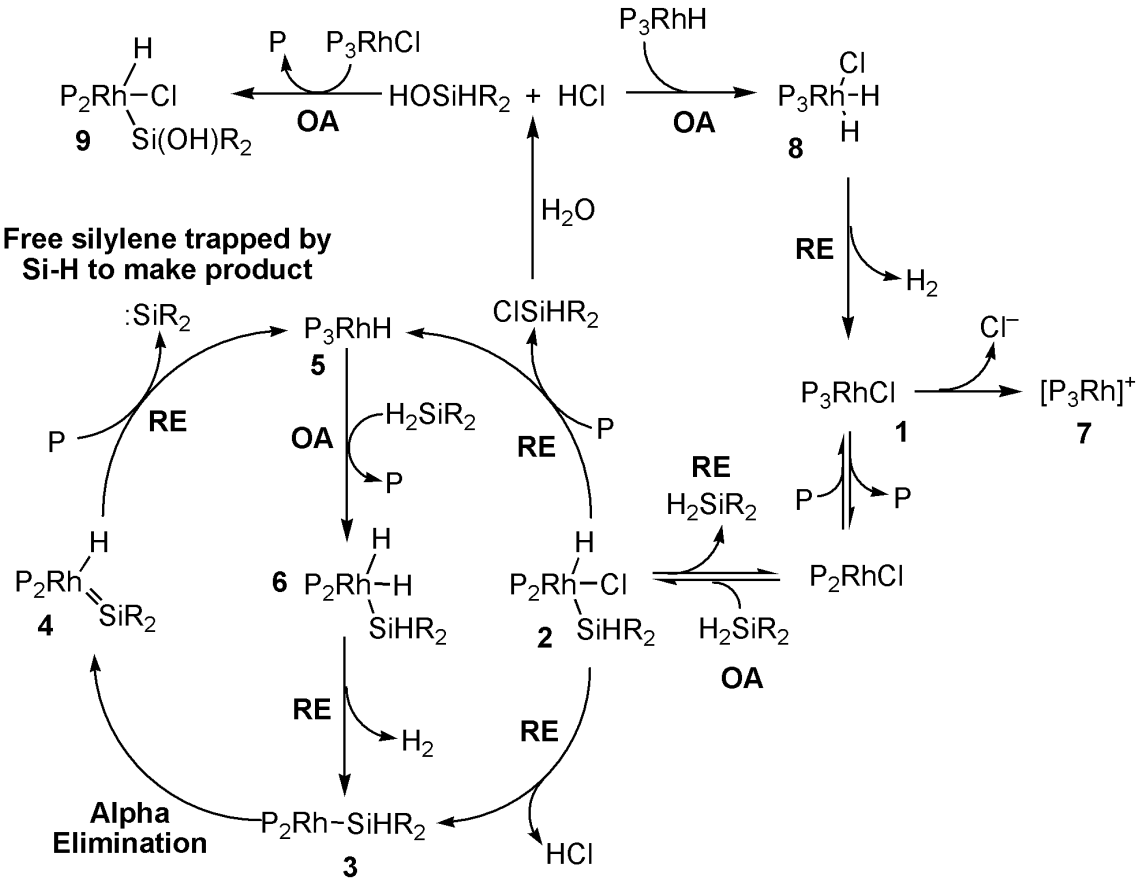

Scheme 1.10: Proposed reaction mechanism for silane dehydrocoupling catalyzed by Wilkinson's catalyst as elucidated by NMR and ESI(+)-MS.[98] Numbered complexes were observed by ESI-MS through the coordination of a charged phosphine ligand $[Ph_2P(CH_2)_4PPh_2(CH_2Ph)]^+$. P = PPh_3 or $[Ph_2P(CH_2)_4PPh_2(CH_2Ph)]^+$, R = *n*-hexyl.

1.4 Conclusions

From the above examples it is apparent that mass spectrometric studies can provide detailed mechanistic information about catalytic organometallic reactions. This field has experienced rapid growth primarily due to the introduction of ESI-MS as an ionization method which can gently transfer solution-phase ions into the gas phase. In some cases the species of interest are

already charged in solution (or can easily become charged), and the use of charged tags allows investigation of otherwise neutral systems. Over the past decade increasingly comprehensive investigations of catalytic organometallic reactions by ESI-MS have appeared in the literature, yet there is still a long way to go in establishing this approach as a general tool for organometallic chemists. The fact that very little kinetic data has been obtained by ESI-MS for organometallic systems is primarily due to: (1) the absence of a simple continuous sampling technique that can easily accommodate air- and moisture-sensitive solutions, and (2) the perceived difficulty in quantifying ESI-MS data. The work presented in this dissertation aims to address these and other common problems associated with the application of ESI-MS to the study of catalytic organometallic reactions.

Chapter 2. Practical Considerations

2.1 Difficulties in applying ESI-MS to catalytic organometallic systems

Despite the benefits and successful applications discussed in Chapter 1, the number of papers published on the use of ESI-MS to study organometallic catalysis is quite small compared to the ones written on the use of NMR and other techniques to study the same systems. The low profile of ESI-MS is in part due to a number of practical difficulties in applying MS to catalytic organometallic reactions:

(1) **Only species that are already charged in solution are visible by ESI-MS**. At the very least they must have an energetically favourable ionization mechanism as presented in the previous chapter. This is due to the mechanism by which ESI produces ions in the gas phase (see section 2.2.1 below).

(2) **Air- and moisture-sensitive solutions are difficult to handle**. This again has to do with the ESI process. ESI operates under atmospheric conditions; practically this means that the solution being analyzed is sprayed into a source that contains air and moisture. Any compounds sensitive to air and moisture have the potential to react thus changing the observed speciation. The reacted species can also cause blockage of the charged capillary.

(3) **Quantification of ESI-MS data is not straightforward**. The exact details of the transformation from ions in solution to ions in the gas phase are still not fully understood, but we do know that different ions have different ionization efficiencies which depend on a number of factors including the structure and polarity of the analyte, the solvent used, and the presence of other ions in solution. The result is that if you do not have access to a reference sample for the species of interest quantitative information about relative concentrations of analytes in a solution is very difficult to obtain. It becomes even more problematic when considering reaction mixtures in which the reaction mixture composition is changing over time.

(4) **Sampling rate is limited**. While obtaining an ESI-MS spectrum takes on the order of a second, in most cases the number of data points that can be obtained over the course of a reaction is severely limited by the fact that a reaction mixture must typically be manually sampled and diluted before analysis. This inhibits the investigator's ability to obtain continuous real-time data and their ability to study the initial moments of a reaction.

There are two recent reviews that describe a number of specialized methods for online monitoring with ESI-MS that can, in some cases, address the problem of reaction sampling.[102, 103] These include the use of online mixing tees (or microreactors),[104, 105] electrochemical cells,[106] or photochemical[107-109] cells for analysis of reactions at very short time scales, in a time-resolved fashion, and/or during an electrochemical or photochemical reaction. A method has also been reported for the continuous monitoring of process-scale organic reactions,[110] and a publication appearing earlier this year described a new technique named VEASI (Venturi Easy Ambient Sonic-Spray Ionization).[111] VEASI combines the ionization method SSI (sonic-spray ionization) with the continuous introduction of liquid samples into a mass spectrometer in order to obtain real-time data from reaction mixtures. Despite this proliferation of online monitoring techniques, a method for the simple online monitoring of a heated and stirring air-sensitive reaction over time has not previously been reported.

This dissertation will provide practical solutions for each of the problems described above, and a model system will be presented in which our approach has been successfully applied to gain valuable mechanistic information for a catalytic system. To do this, a thorough understanding of instrument theory and MS experiment types is required and this chapter outlines the most relevant information.

2.2 Instrument theory

A Micromass Q-TOF *micro* mass spectrometer was used to carry out the work described herein. It is equipped with an electrospray ionization source and contains both a quadrupole and time-of-flight mass analyzer. An understanding of how these components function is imperative

in order to draw meaningful conclusions from data that is collected using new or unorthodox methods. Since this dissertation includes such methodology a detailed description of the theory and function for all of these components is provided here. An overview of the standard experiments performed using this technology is also included.

2.2.1 Electrospray ionization

Mass spectrometry operates on ions in the gas phase, so before it can be applied to the analysis of solutions a technique for transferring ions from solution into the gas phase is required. Electrospray ionization (ESI) is one of the most commonly used techniques for this purpose (Figure 2.1).

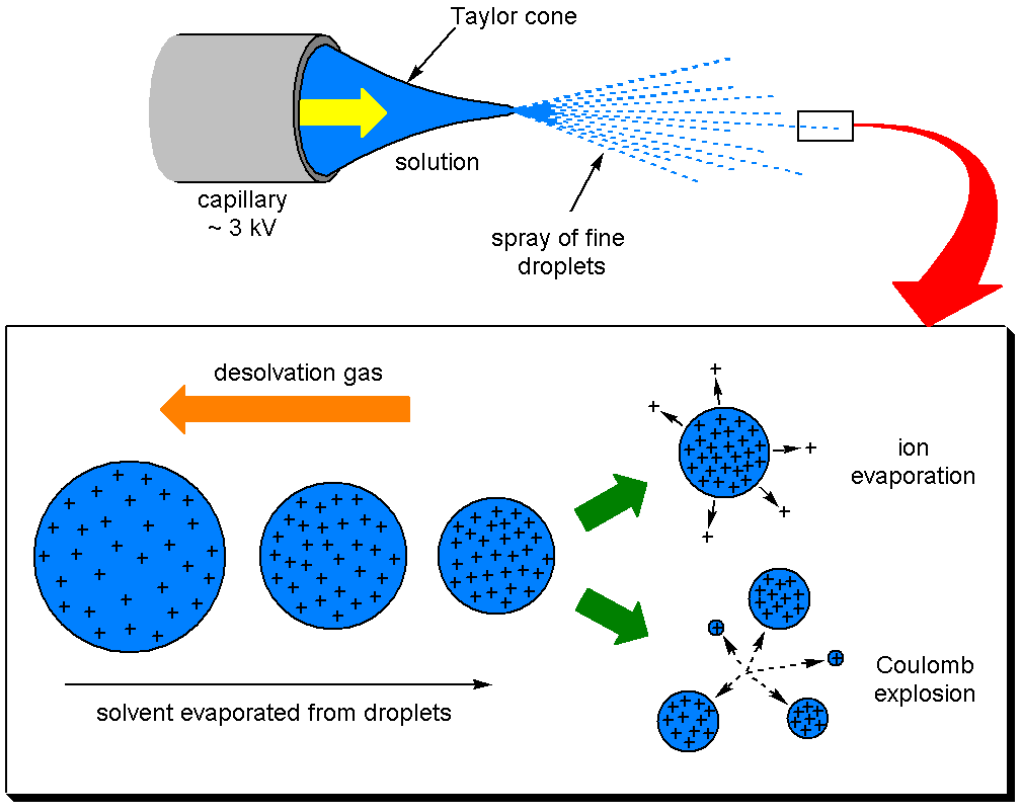

Figure 2.1: The desolvation process in electrospray ionization. Modified with permission of the author from Henderson, W., McIndoe J. S., *Mass Spectrometry of Inorganic and Organometallic Compounds*. John Wiley & Sons, Ltd. West Sussex: 2005, p. 92.

In electrospray ionization, a dilute solution containing the ion of interest is injected slowly (a few microliters per minute) into the source of the mass spectrometer usually by syringe pump or HPLC. The solution enters a charged metal capillary which, in positive-ion mode, acts to create an excess of positive ions in solution (in negative-ion mode, the potentials are reversed and so an excess of negative ions are produced).[112] The solution emerges from the capillary as a Taylor cone.[113] At the apex of the Taylor cone the solution breaks into a fine mist of positively-charged droplets which are bathed in a heated desolvation gas. If the ions are small they are thought to be transferred from the droplets into the gas phase by a combination of ion evaporation[114] and/or Coulombic explosion.[10] In Ion Evaporation Mode (IEM), single ions "evaporate" from the surface as the surface area of the droplet shrinks due to solvent evaporation. In Coulombic explosion, the repulsion of like charges within a droplet increases as the droplet shrinks until the forces of repulsion exceed the surface tension of the droplet and a number of similarly sized product droplets are formed. The process is then repeated for each of the product droplets until gas-phase ions result. The extent to which each of these processes contributes to the formation of small gas-phase ions is unclear and probably varies from case to case. Studies in our group favour ion evaporation in the case of protonated water clusters.[115] Large ions (> 5000 Da) are more likely transferred into the gas phase by droplet fission to produce droplets containing one ion each, and then evaporation of solvent until the bare ion is left (the Charged Residue Model).[116] Once in the gas phase, ions are drawn into the mass spectrometer to be analyzed. Little or no fragmentation of the ions from solution occurs during these transitions.[117]

Electrospray ionization can be thought of as an electrochemical process (Figure 2.2). In positive-ion mode the tip of the ESI probe is the anode. The cathode is comprised of the baffle (in some cases), the inner surfaces of the mass spectrometer, and the detector. In the negative-ion mode the reverse is true. There is typically a 2-5 kV potential difference between the anode and cathode.[118]

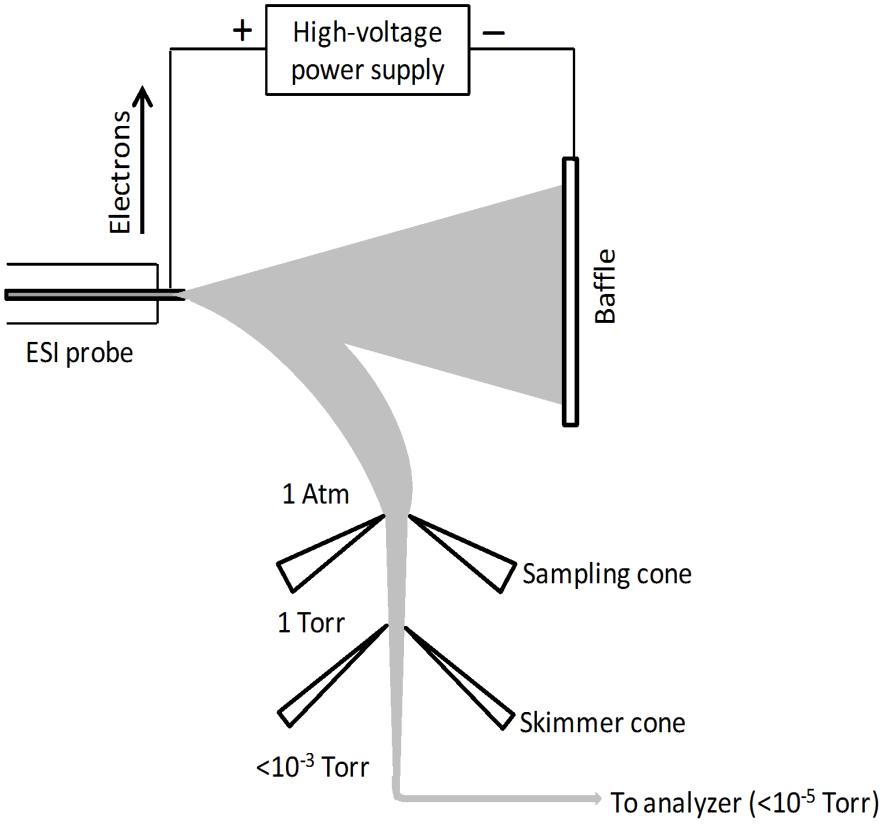

Figure 2.2: Schematic of a Z-spray™ source operating in positive-ion mode. The grey shaded region represents possible cation pathways. Electrons travel separately along a wire to the baffle and other metal surfaces in the source and within the MS. When a cation hits one of these surfaces it is neutralized and the circuit is completed.

In positive-ion mode either electrolytes in solution, or iron in the stainless steel capillary are oxidized to separate electrons from cations. The circuit is completed when a constant flow of positive ions move, via the electrospray process, from the tip of the capillary to the various metal surfaces in the source or the interior of the mass spectrometer (including the detector) where they are neutralized.[116] A small fraction of the ions produced reach the detector. Due to the electrochemical nature of this process, there is one caveat: if the solution being analyzed is dilute and an easily oxidized analyte such as Pd(0) is present, it can be oxidized in order to maintain sufficient ion flow. In this case radical cations are produced and unpredictable radical reactions can ensue which lead to complex spectra that are difficult to interpret. If this behaviour is observed the negative-ion mode may yield more reliable results.

Our particular instrument has a Z-spray™ source as seen in Figure 2.2. The name comes from the fact that ions follow a Z-shaped path into the instrument. This design minimizes the number of neutral molecules that make their way into the mass spectrometer and thus it reduces chemical background noise.[118]

2.2.2 Quadrupole mass analyzers

In a quadrupole mass analyzer, ions in the gas phase are accelerated through a space between four parallel, cylindrical metal rods as shown below (Figure 2.3). The two rods opposite each other form a pair between which rapidly alternating DC and RF potentials are applied. The effect of the resulting dynamic field on an ion entering the quadrupole is dependent on the ion's mass and charge and each ion with a unique *m/z* ratio will follow a different complex path through the quadrupole (most end up colliding with the rods). By selecting a set of DC and RF potentials (defined by the Mathieu equation) so that only one *m/z* ratio has a stable trajectory through the quadrupole, ions of that *m/z* ratio can be isolated and detected.[119] To perform a single scan over a range of *m/z* values, the field created by the DC and RF potentials must be altered hundreds or thousands of times, each time stabilizing the trajectory of a single *m/z* ratio. To scan a range from *m/z* 50 to *m/z* 2000 takes about a second, but slower scan rates can be used to improve resolution.

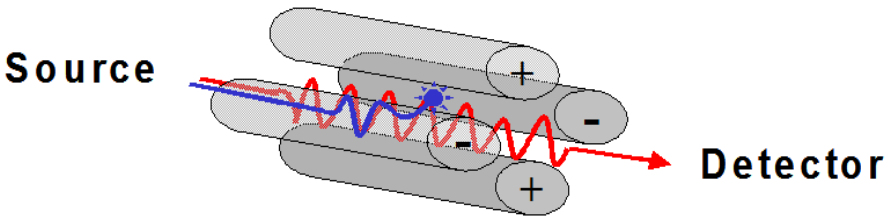

Figure 2.3: Schematic of a quadrupole mass analyzer showing the trajectory of two ions with different mass-to-charge ratios.

2.2.3 Orthogonal time-of-flight mass analyzers

In an orthogonal time-of-flight (TOF) mass analyzer (Figure 2.4), a momentary electric field gradient is applied perpendicular to an incoming gas-phase ion beam. This "pulse" causes the formation of a small packet of ions with kinetic energy proportional to their charge (Equation 1) moving in a direction orthogonal to the ion beam. Ions are then separated spatially as they travel down the flight tube with velocities proportional to their kinetic energy and mass (Equation 2).

$$KE = zeV \quad (1)$$

$$KE = \tfrac{1}{2} mv^2 \quad (2)$$

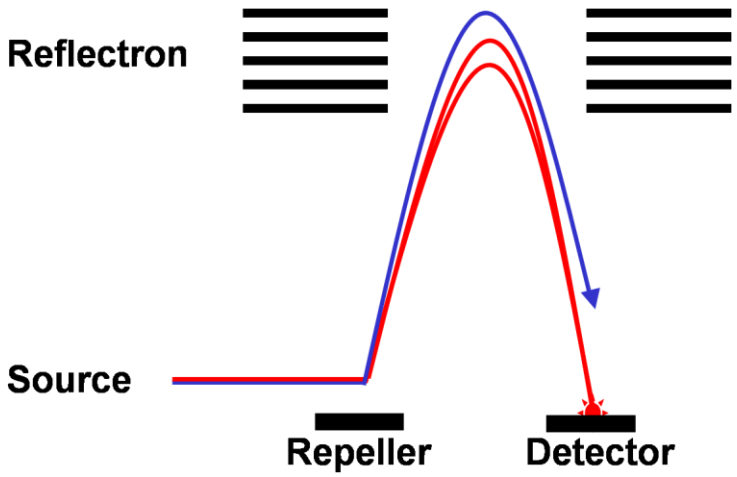

Figure 2.4: Schematic of an orthogonal TOF mass analyzer showing the flight path of two ions with the same *m/z* ratio (red) and one with a different *m/z* ratio (blue).

To account for small variations in start position and initial kinetic energy, ions are usually focused by a reflectron before reaching the detector. The reflectron is made up of a series of increasingly strong electric fields, which repel the ions as they approach the end of the flight tube, eventually causing the ions to reverse direction and head towards the detector. To understand how this focuses the ions, consider ions of only one *m/z* ratio. Those with a slightly higher kinetic energy will travel further into the reflectron before reversing direction, and will therefore take longer to reach the detector, whereas ions with low kinetic energy will penetrate

the reflectron to a lesser degree and take less time to reach the detector. The reflectron is tuned so that all ions of the same *m/z* ratio arrive at the detector simultaneously. Each initial pulse contains only a few ions, and on the order of 10,000 pulses can be performed in one second. Combined, they produce a single spectrum.[120] A major advantage of the TOF mass analyzer is that there is no inherent mass limit, so any ion that can be put into the gas phase can be manipulated and detected.

2.3 Common experiment types

There are four types of commonly performed MS experiments in our research group and each provides access to a different set of information. They are: standard MS experiments, collision induced dissociation experiments (CID), energy-dependent CID or energy-dependent ESI experiments (EDESI), and ion/molecule reaction experiments. A schematic drawing of the instrument is provided below to aid in the description of each of these processes (Figure 2.5).

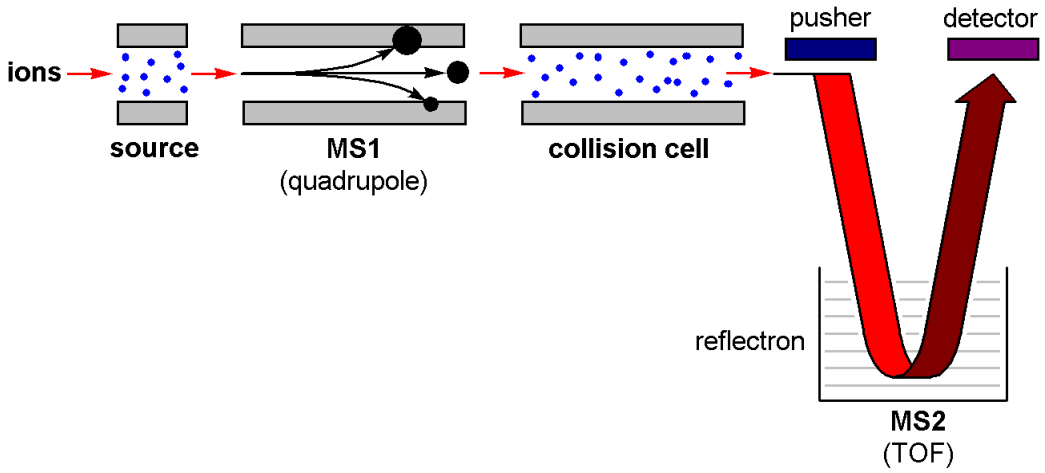

Figure 2.5: Schematic drawing of a quadrupole/time-of-flight (Q-TOF) mass spectrometer operating in MS/MS mode. In MS mode all ions are allowed to pass through MS1 and the collision cell. Modified from Henderson, W., McIndoe J. S., Eds. *Mass Spectrometry of Inorganic and Organometallic Compounds*. John Wiley & Sons, Ltd. West Sussex: 2005, p. 39.

2.3.1 MS experiments

In a standard MS experiment using a Q-TOF mass spectrometer, ions in solution are infused into the source of the instrument, subjected to the electrospray process and drawn through a sampling cone and a smaller skimmer cone. Nitrogen gas flows in the opposite direction of the ion flow at the entrance to the skimmer cone to further desolvate the ions (Figure 2.2). The ions enter a high vacuum area (~10^{-6} torr) and proceed to the quadrupole mass analyzer (MS1). In the case of a normal MS experiment all ions are simply allowed to pass through the quadrupole and the following collision cell into the TOF analyzer (MS2). The TOF analyzer then separates the ions in time based on their mass-to-charge ratio, they are detected on a microchannel plate (MCP) detector and a full mass spectrum is obtained.

2.3.2 CID experiments

The most common type of CID experiment is an MS/MS experiment. For MS/MS all ions are once again transferred into the gas phase and proceed to the quadrupole mass analyzer, but then only ions of a single *m/z* are allowed to exit the quadrupole. These ions are accelerated into the collision cell so that they undergo energetic collisions with argon gas (10^{-5} torr) in the cell which causes fragmentation of the selected ion. The fragments that emerge from the collision cell are separated by the TOF analyzer and detected thus providing structural information for the selected ion.

Alternatively, if the analyte solution is simple (i.e. contains only one or two types of ions), CID can be performed on the entire solution in the source of the instrument by using a high cone voltage. This is called in-source CID. In this case collisions with nitrogen cone gas in the source cause fragmentation and the quadrupole and collision cell act as simple ion guides. The TOF analyzer separates the resulting fragments.

2.3.3 EDESI experiments

Energy Dependant Electrospray Ionization (EDESI) is a technique developed by Dyson and coworkers in 2000[121] which allows further information to be collected from CID experiments. By performing a stepwise increase of the cone voltage (EDESI) or the collision energy (EDESI-MS/MS) over time, information about the relative energy required for different fragmentation processes or ion/molecule reactions can be obtained. To display this data effectively three-dimensional contour plots must be generated (Figure 2.6). Ions of different mass-to-charge ratios are plotted with respect to cone voltage (or collision energy) thus showing which species are stable at which cone voltages, and at what energy fragmentation begins for a given ion. For example: species that fragment easily will only be present at low cone or collision voltages. The contours provide information about the intensity of each peak throughout the experiment. It is common to display a summed mass spectrum above the EDESI plot as shown below to aid in interpretation.

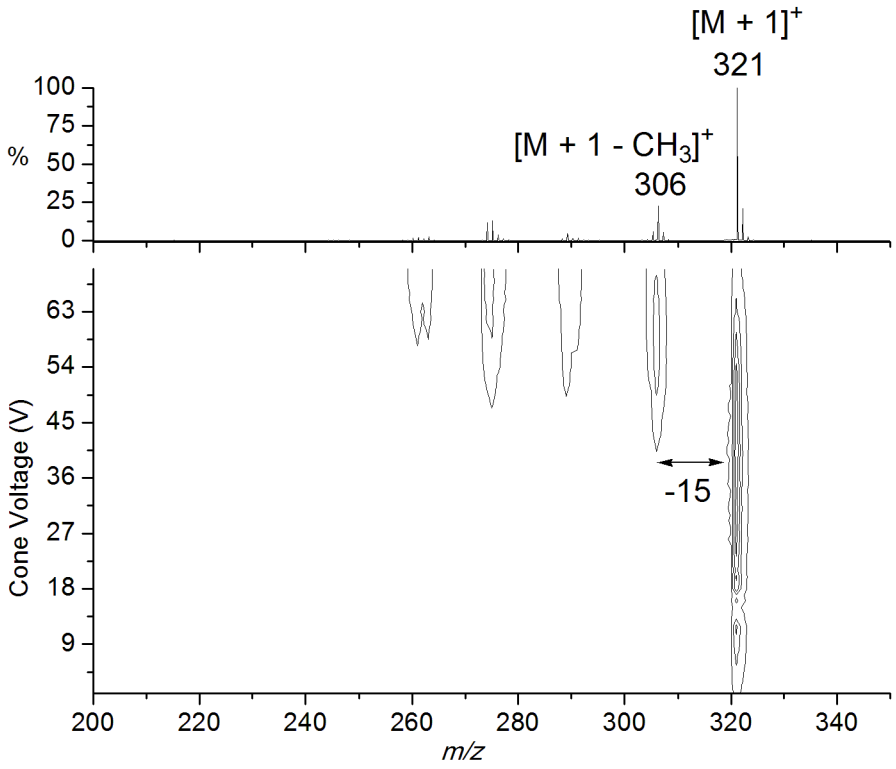

Figure 2.6: EDESI of chargeable ligand 1,8-bis(dimethylamino)-2-(4-methoxyphenyl)naphthalene in its protonated form (*m/z* 321). (see Chapter 3 for discussion of this data).

2.3.4 Ion/molecule reaction experiments

Conducting ion/molecule reactions in the gas phase within a mass spectrometer has become a well-used practice to gain information about the behaviour of organometallic ions that are too reactive to be easily studied in solution.[122] We have modified our Q-TOF so that we can perform ion/molecule reactions in the collision cell or in the source of the instrument.[123] To perform these reactions the gaseous or volatile, neutral substrate of interest is infused into source (or the collision cell). Then a solution containing the reactive ion is injected just as for a normal MS experiment. The ion will then interact with the neutral substrate in the source or collision cell and any resulting product ions can be detected.

If the neutral substrate is infused into the source, then any or all ions present in the sample solution may react with the substrate. After interaction with the substrate there is the potential to isolate a product with a specific *m/z* in the quadrupole and perform CID or EDESI experiments on it in the collision cell before detection.

Different and complementary data is obtained if the neutral substrate is infused into the collision cell. In this case a single ion can be isolated from the sample solution, using the quadrupole mass analyzer, so that only it has the opportunity to react with the neutral substrate. This experiment is ideal for confirming the reactivity of a specific ion; however, further CID or EDESI experiments cannot be performed on the resulting product ions since they are formed in the collision cell of the instrument.

2.4 Special precautions

In order to obtain meaningful data about the behaviour and abundance of various species in a catalytic system a number of special precautions must be implemented:

First, **low cone voltage settings must be used**. Many organometallic compounds contain weak bonds that fragment easily at high cone voltage settings. This was demonstrated in our research lab by analyzing a solution of $[RhCl(PPh_3)_2(PPh_2C_4H_8PPh_2CH_2Ph)]^+$ (Figure 2.7).[97] At low cone

voltages (< 10 V) the most intense peak in the mass spectrum corresponded to the species present in solution; however, at cone voltages typical for analysis of organic molecules (> 20 V) the major peak in the spectrum was no longer the ion in solution, but one of its fragments that has lost a phosphine ligand, $[RhCl(PPh_3)(PPh_2C_4H_8PPh_2CH_2Ph)]^+$. This fragmentation is caused by energetic collisions between the analyte and the atmosphere in the source. Obviously this misrepresentation of species in solution must be avoided if the goal is to identify species that are present in solution. Cone voltages lower than 5 V typically result in a detrimental loss in overall signal intensity, so cone voltages between 5 and 10 V are ideal.

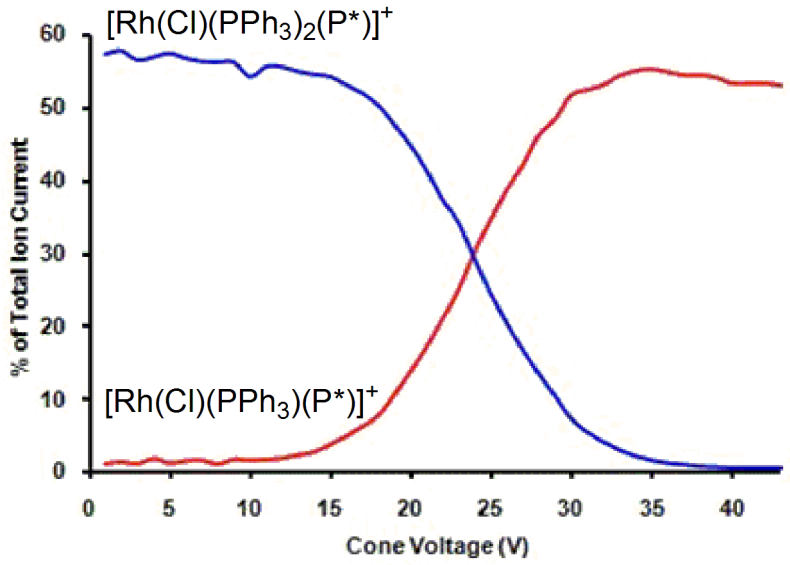

Figure 2.7: Intensity of $[RhCl(PPh_3)_2(P^*)]^+$ (precursor) and $[RhCl(PPh_3)(P^*)]^+$ (product) ions as a proportion of total ion current as cone voltage is increased. P* = $[PPh_2C_4H_8PPh_2CH_2Ph]^+$. As cone voltage is increased, in-source fragmentation causes loss of a phosphine ligand from $[RhCl(PPh_3)_2(P^*)]^+$. Modified from reference 97.

Second, **the concentration of the solution to be analyzed must fall within the linear range of the detector**. If there is any hope to obtain quantitative data by ESI-MS the total number of ions that enter the mass spectrometer must be limited. This is a counter-intuitive problem for most MS users who constantly strive for lower detection limits and higher ion transmission. It arises from the way in which ions are detected. After passing through the flight tube, ions hit a micro-channel plate (MCP) which consists of an array of electron multiplier tubes. The impact

produces a cascade of electrons which are then collected by a metal anode. A time-to-digital converter (TDC) registers an event every time the number of secondary electrons generated exceeds a certain threshold. So, whether one ion hits the MCP or two ions impact simultaneously the threshold will be exceeded and only one ion will be counted.[124] In order to ensure that each ion is counted, the number of ions that enter the mass spectrometer must be such that only one ion of a particular mass passes through the flight tube in a given pulse.

There is also the problem of counting dead time: for a short period of time after an ion is detected, no other ions can be detected, so again, if the number of ions in a given pulse is too high some of them may fall on the MCP during a period of dead time and not be counted. If the number of ions entering the MS is not regulated both of these phenomenon will make it impossible to get accurate quantitative data.

Third, **for MS/MS experiments in which the energy of fragmentation is being investigated, a constant collision pressure over all experiments is required**. The ion energy required for fragmentation in a collision cell depends on the number of molecules that are available for collision (i.e. the collision pressure), so the collision pressure must be kept constant in order allow comparison between different experiments. The ability to tune the collision pressure on most instruments is limited and only rough control is possible. The pressure in the collision cell also drifts on the timescale of days, so the easiest way to avoid inconsistent data is to perform all related experiments on the same day. While this may sound like a significant limitation, the reality is that most fragmentation experiments are short, and dozens can be performed in a day.

Chapter 3. ESI-Active Ligands

The first barrier that must be overcome to study a metal-catalyzed system by ESI-MS is that all species of interest in the reaction mixture must be charged or have easily chargeable sites. Charged or chargeable ligands or substrates provide a convenient way to address this problem, as described in Section 1.2.3 and the recent review by Chisholm and McIndoe.[125]

Our group is working to develop a library of charged or chargeable ligands and substrates for analysis of organometallic reactions by ESI-MS. These ESI-active molecules are based on common ligands and substrates in organometallic chemistry. A charged or chargeable group is installed on the periphery of the molecule so that once it binds to the metal, the charged group will not interfere with the electronic or steric nature of the active site. The addition of a charge renders any metal complexes of the ligand or substrate visible by ESI-MS so key species in a reaction may be observed and studied. Compounds synthesized or developed as ESI tags for this library during the course of this work are described here.

3.1 Chargeable ESI-active ligands

Chargeable ESI tags are neutral molecules that coordinate to a species of interest, and at a secondary site bind either an acid or a base to become charged. Chargeable tags (as opposed to permanently-charged tags) are appealing for a number of reasons: 1) Any effect that the charged group may have on reactivity is mitigated since the charged tag is in equilibrium with its neutral counterpart, 2) if the effect of the charged group is significant, it may be possible to allow the reaction to proceed primarily in the presence of the neutral version of the tag and only charge the tag immediately before analysis by adjusting the pH of the reaction mixture, 3) chargeable ligands have the potential to aid in catalyst recovery since their solubility in organic solvents can be manipulated by changing the pH of the reaction mixture.

We have developed a number of chargeable ligands derived from the strong base 1, 8-bis(dimethylamino)naphthalene also known as "Proton Sponge®" that serve as analogues for

commonly used organometallic ligands.[96] First studied by Alder and coworkers, Proton Sponge® (**1**) (Figure 3.1) is a very strong, non-nucleophilic base (pK_a = 12.34 in H_2O) with high thermodynamic basicity but relatively low kinetic bacisity.[126-128] Proton Sponge® acts to bind H^+ by forming intramolecular hydrogen bonds with both nitrogen centers in the molecule to give the charged $[N^{\cdots}H^{\cdots}N]^+$ moiety. Historically, Proton Sponge® has been used extensively as a non-nucleophilic proton abstractor in organic synthesis.[129, 130]

The high thermodynamic basicity of Proton Sponge® is attributed to a combination of factors.[126, 131, 132] The methyl groups bound to each nitrogen sterically clash with each other and force the nitrogen lone pairs to point toward each other adopting an "in-in" conformation.[133] This leads to a high degree of lone pair-lone pair repulsion and causes the naphthalene backbone to be twisted. By protonating the neutral molecule a more optimal geometry is attained, steric strain is relieved, and the naphthalene ring returns to planarity.[127] Additional stabilization is gained through the strong intramolecular hydrogen bonds formed between the proton and both nitrogen lone pairs.[131]

The low kinetic basicity of Proton Sponge® arises from the steric crowding of the basic site by the four nearby methyl groups. These methyl groups and the proximity of the two nitrogen centers to each other are also responsible for the high selectivity that Proton Sponge® has for H^+; All other cations are too large to fit in the resulting pocket.[126] The overall effect is that Proton Sponge® is approximately six orders of magnitude more basic than typical aromatic amines, and can selectively trap adventitious protons and become charged.

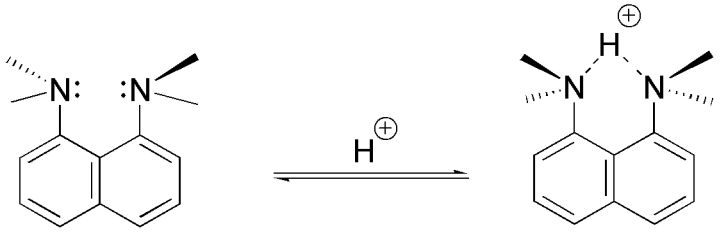

Figure 3.1: Proton Sponge® (1,8-bis(dimethylamino)naphthalene, 1) in its unprotonated and protonated forms.

We expected Proton Sponge® to be a well-behaved electrospray-active tag based on the properties discussed above. Other potentially interfering cations such as Na^+ or K^+ are too large to bind to Proton Sponge®, so the mass spectrum of Proton Sponge® displays only the $[M + H]^+$ peak. Its high ionization efficiency in solution leads to signal intensities approaching those of inherently-charged ions allowing for detection at very low concentrations and ensuring that all Proton Sponge®-containing species are represented in the spectrum. Di-protonation is extremely unfavorable[126] and the doubly-charged ion is never seen which should further simplify resulting spectra. By appending the Proton Sponge® moiety to common organometallic ligands we should be able to provide an efficient and selective means of remotely charging and investigating a variety of organometallic compounds and their reactivity.

3.1.1 Arene ligand analogue

Arenes are used extensively as η^6-ligands in organometallic chemistry. Their ability to change hapticity and expose an active metal center makes them excellent ligands for catalyst precursors.[134] They have been used in hydrogenation and hydration reactions, olefin metathesis, cycloaddition and polymerization reactions.[134, 135] For this reason the electrospray-active analogue of methoxybenzene was selected as a target compound. 1,8-bis(dimethylamino)-2-(4-methoxyphenyl)naphthalene (**3**) was synthesized, and its usefulness as an "electrospray-friendly" ligand was demonstrated by investigating the gas-phase reactivity of the chromium carbonyl complex $Cr(CO)_3$(**3**), (**4**).

3 was synthesized via bromination of Proton Sponge® at the two position as previously described by Farrer[96] to give{1,8-bis(dimethylamino)naphthalene-2-yl}bromide (**2a)**. Then, **2a** and 4-methoxyphenylboronic acid were coupled via a Suzuki cross-coupling reaction catalyzed by $Pd(OAc)_2/PPh_3$ in *n*-propanol and water to give **3** (Scheme 3.1).

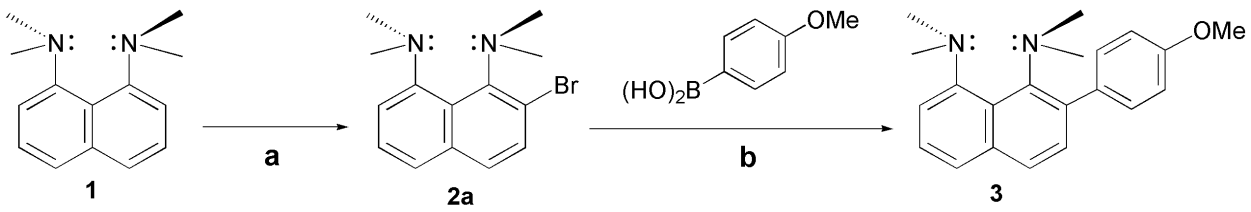

Scheme 3.1: Synthesis of **3**. a) NBS/ THF/ -78 °C. b) $Pd(OAc)_2$/ PPh_3/ $NaCO_3H$/ *n*-propanol/water. Reflux 12 h.

After aqueous workup, the white crystalline product was isolated in 41% yield, and a single crystal structure of **3** was obtained (Figure 3.2, see Appendix A for details). In its unprotonated form the Proton Sponge® moiety deviates from planarity as expected due to mutual repulsion of the lone pairs on each nitrogen atom. This can be seen in the torsion angles of -8.78° for N(1)-C(11)-C(20)-C(19) and -9.63° for N(2)-C(19)-C(20)-C(11). The anisole group lies slightly off perpendicular to the plane of the naphthalene ring (torsion angle: C(13)-C(12)-C(21)-C(22) = 107.50°) and we would expect metal coordination to occur on the side of the arene ring that is furthest from the methyl groups on Proton Sponge®.

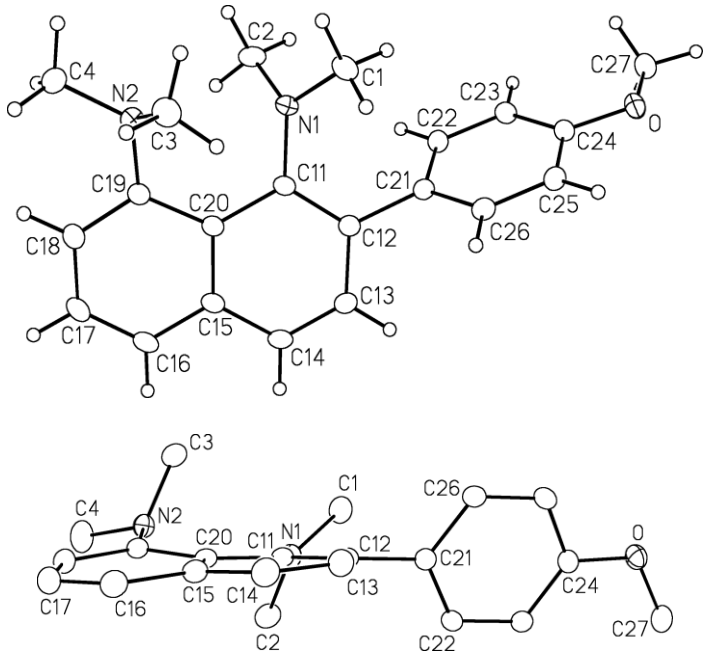

Figure 3.2: Single crystal structure of 1,8-bis(dimethylamino)-2-(4-methoxyphenyl)naphthalene (**3**). Side- (top) and edge-on (bottom) perspectives.

The approximate pK_a of 3 was determined by NMR transprotonation experiments.[136] A deuterated acetonitrile solution containing equimolar amounts of unprotonated **3** and protonated Proton Sponge® ([**1**H]$^+$, [BF_4]$^-$ counter ion) was allowed to come to equilibrium overnight and a ^{1}H NMR experiment was performed. The solubility of **3**, **1**, [**3**H]$^+$[BF_4]$^-$ and [**1**H]$^+$[BF_4]$^-$ in acetonitrile were all carefully tested beforehand since any insolubility would lead to inaccurate signal intensities and therefore an inaccurate pK_a value. The high chemical shift for the coordinated proton in both compounds appears at around 19 ppm where there are no interfering signals thus providing us with an ideal NMR handle. In the low-field region of the spectrum two peaks were seen: one at δ 19.49 ppm corresponding to [**3**H]$^+$ and the other at δ 18.67 ppm corresponding to [**1**H]$^+$. The size of the integrations for the NMR signals corresponding to [**3**H]$^+$ and [**1**H]$^+$ were averaged over 4 separate experiments. Using the average ratio of the integrations and the pK_a of **1** (18.18 in CH_3CN), the K_a of **3** was calculated to be (1.50 ± 0.06) x 10^{18}. The pK_a is approximately equal to that of Proton Sponge® (18.2 ± 0.7 at 297 K in CD_3CN). Figure 3.3 shows the relative intensities of the two signals for one of the NMR experiments.

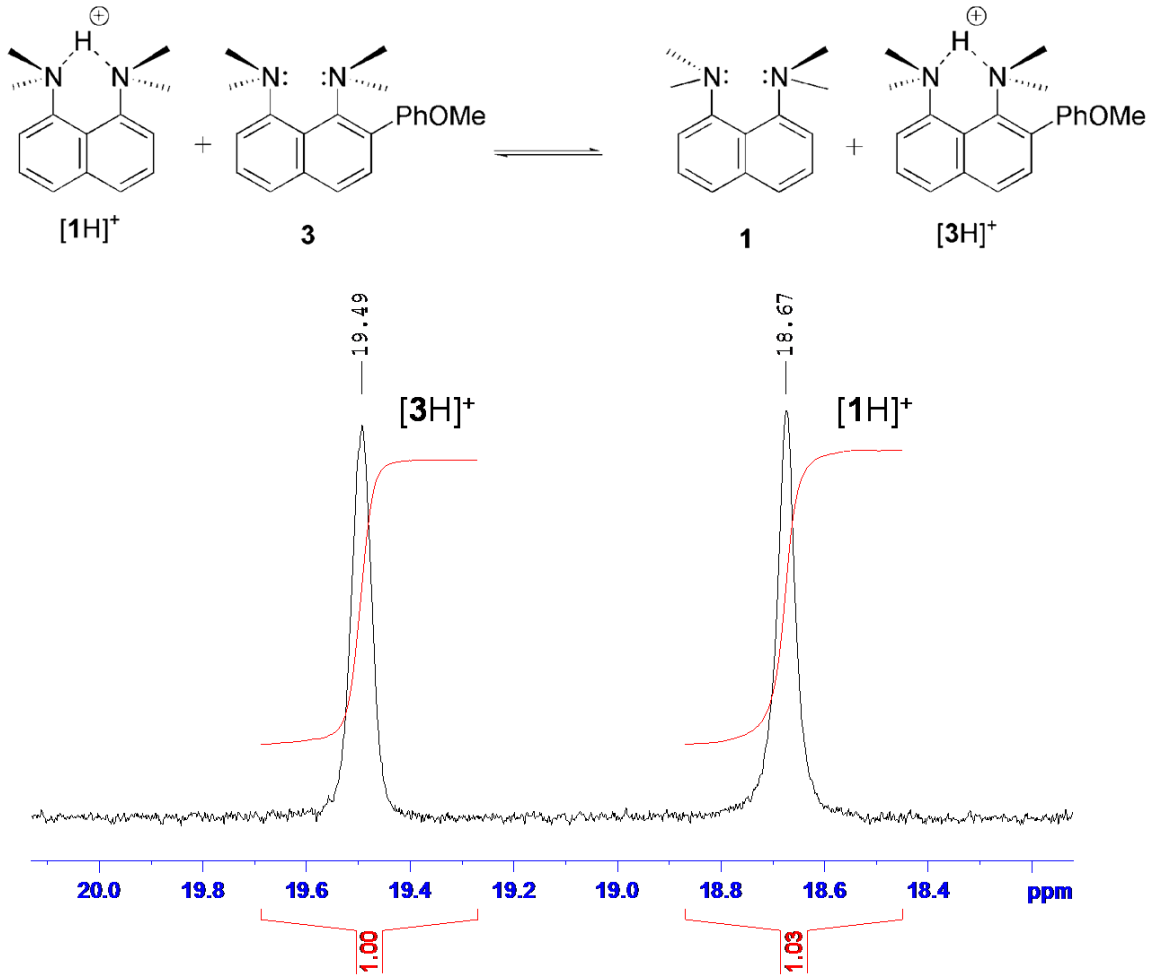

Figure 3.3: ^{1}H NMR spectrum (18 – 20 ppm) of an equimolar mixture of [**1**H]$^{+}$ and **3** in deuterated acetonitrile. Two singlets are observed corresponding to the acidic proton in [**1**H]$^{+}$ (18.67 ppm) and [**3**H]$^{+}$ (19.49 ppm).

The ESI mass spectrum of **3** in dichloromethane (and spiked with formic acid) is dominated by the [M + H]$^{+}$ peak as expected. There are no dimers, no coordination of sodium or potassium ions, and no doubly-charged species. The complete dominance of a single ionization pathway and the excellent signal intensity exhibited by **3** demonstrates its potential as a good ESI probe (Figure 3.4).

An EDESI experiment performed on **3** shows that the compound begins to fragment at a cone voltage of approximately 45 V with loss of a 15 Da fragment. This is consistent with loss of one

methyl group as a neutral radical (Figure 2.6), a fairly high-energy process consistent with the elevated cone voltage.

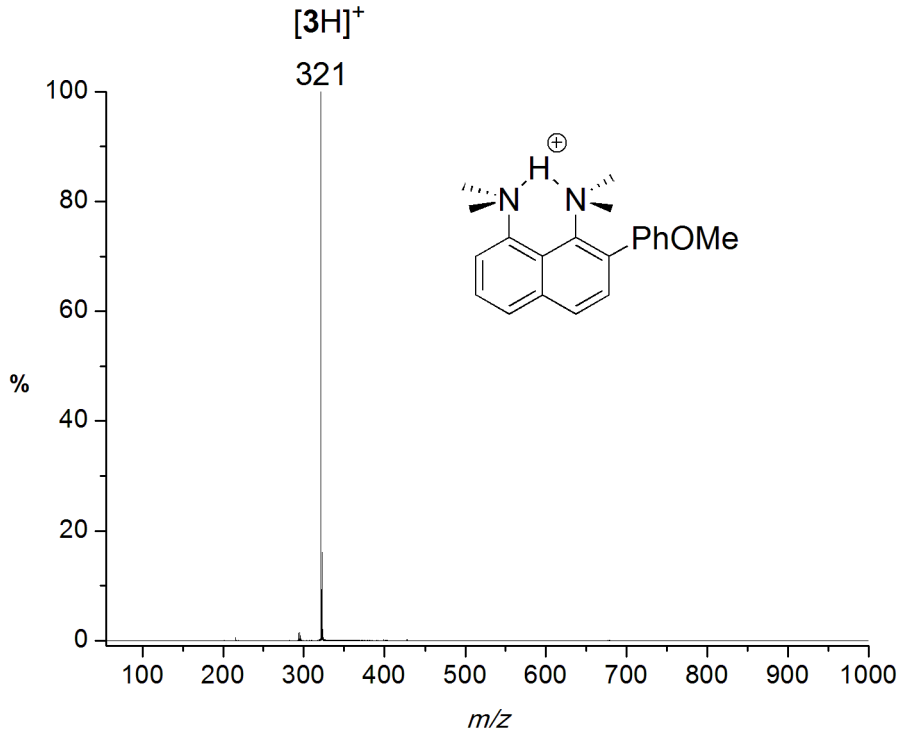

Figure 3.4: ESI(+)-MS of **3** ($[M + H]^+$ = *m/z* 321) in dichloromethane spiked with formic acid.

To further test the suitability of **3** as an ESI probe, the η^6-coordinated chromium tricarbonyl complex of **3** was synthesized. Chromium hexacarbonyl in THF and dibutyl ether was reacted with **3** under reflux for 24 hours.[137] After workup and recrystallization, yellow rod-like crystals were obtained and the crystal structure of chromium(**3**)tricarbonyl (**4**) was solved (Figure 3.5, see Appendix B for details).

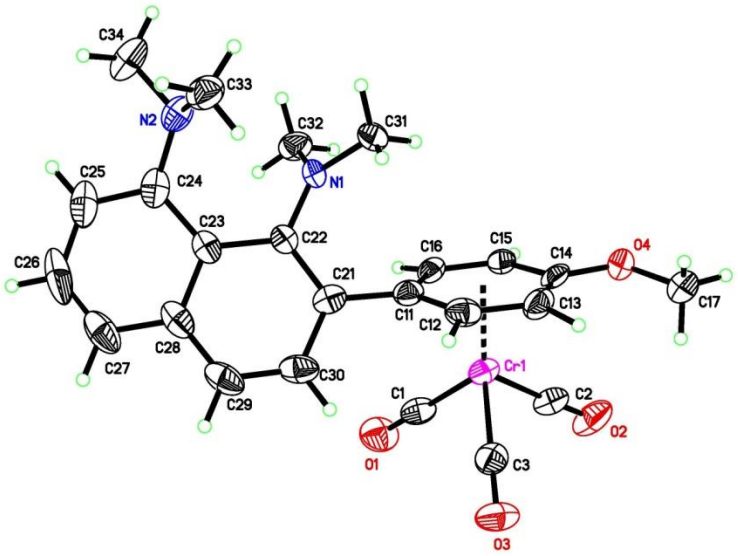

Figure 3.5: Single crystal structure of chromium(**3**)tricarbonyl (**4**).

The crystal structure shows the expected η^6-coordination of the arene ligand where the metal center binds to the face of the arene that is pointing away from the nitrogen groups of the proton sponge. This is ideal since the portion of the complex bearing the charge is far-removed from the reactive chromium center. The CO-Cr-CO angles of 88.1°, 88.7° and 90.3° are typical for a chromium tricarbonyl complex (87-92°)[138] indicating that steric perturbation of the complex due to addition of the chargeable group is minimal. Solution phase data is consistent with the crystal structure; the proton NMR spectrum displays signals consistent with η^6-coordination of the ligand. The IR spectrum of **4** displays CO stretches at 1964 cm^{-1} and 1890 cm^{-1}, compared to values for Cr(η^6-anisole)$(CO)_3$ of 1978 cm^{-1} and 1908 cm^{-1}).[139]

The ESI(+)-MS of $[\mathbf{4}H]^+$ shows that the proton sponge tag behaves as expected. The spectrum is clean and dominated by the $[M + H]^+$ signal (Figure 3.6). No competing ionization processes are active. Some uncoordinated ligand is observed (*m/z* 321) perhaps indicating that the anisole ligand is labile in solution or that the arene-Cr interaction is relatively weak and some fragmentation of the compound occurs during the ESI process.

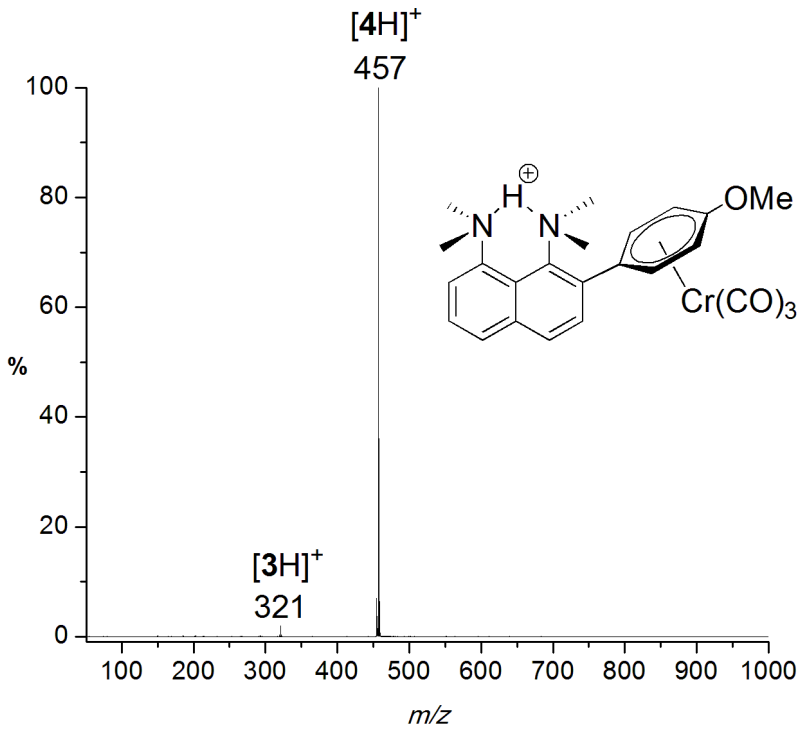

Figure 3.6: ESI(+)-MS of **4** in methanol ($[M + H]^+$ = *m/z* 457). A small amount of free ligand **3** is also observed ($[M + H]^+$ = *m/z* 321).

Further information regarding the structure and reactivity of **4** may be obtained through an EDESI experiment. In this case the experiment reveals that there is a threshold cone voltage of approximately 27 V at which all three CO groups are lost simultaneously (Figure 3.7). While perhaps unintuitive, these results are consistent with earlier studies of a number of similar chromium carbonyl complexes by Dyson and McGrady.[140] They found that the dominant fragmentation pathway by electron ionization mass spectrometry is loss of all three carbonyl groups. They also noted much smaller peaks corresponding to the di- and mono-carbonyl species and on closer examination these peaks are observable in our spectrum as well, $[Cr(\mathbf{3})(CO)_2 + H]^+$ = *m/z* 429 and $[Cr(\mathbf{3})(CO) + H]^+$ = *m/z* 401. Since the fragmentation we observed matches with that found in the literature, we are further convinced that **3** is a suitable ESI-active probe.

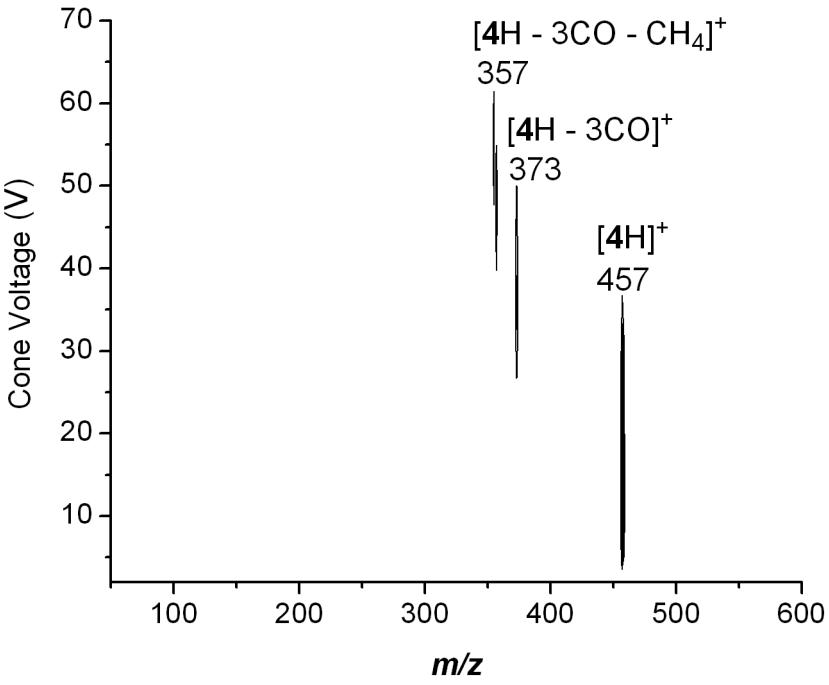

Figure 3.7: EDESI(+)-MS of **4** in dichloromethane spiked with formic acid. Scan time = 2 s. CO dissociation (*m/z* 373) and ligand fragmentation (*m/z 357*) pathways are observed.

At higher cone voltages (> 40 V) decomposition of the ligand occurs with loss of methane (16 Da). In an attempt to further understand this decomposition process MS/MS experiments were performed on [**4**H]$^+$ and deuterium labelled [**4**D]$^+$. Loss of 16 Da is observed as the major decomposition pathway (after CO dissociation) in the presence and in the absence of deuterons (Figure 3.8). This outcome suggests that the fragmentation process does not involve loss of the acidic proton, or a loss of 17 Da would be expected. It is unclear what the mechanism of this fragmentation might be, and at relatively high cone voltages (> 40 V) there is enough collisional energy present that chemically unintuitive processes can occur. What is important to note is that use of this ligand as an ESI tag is not advisable at cone voltages greater than 40 V.

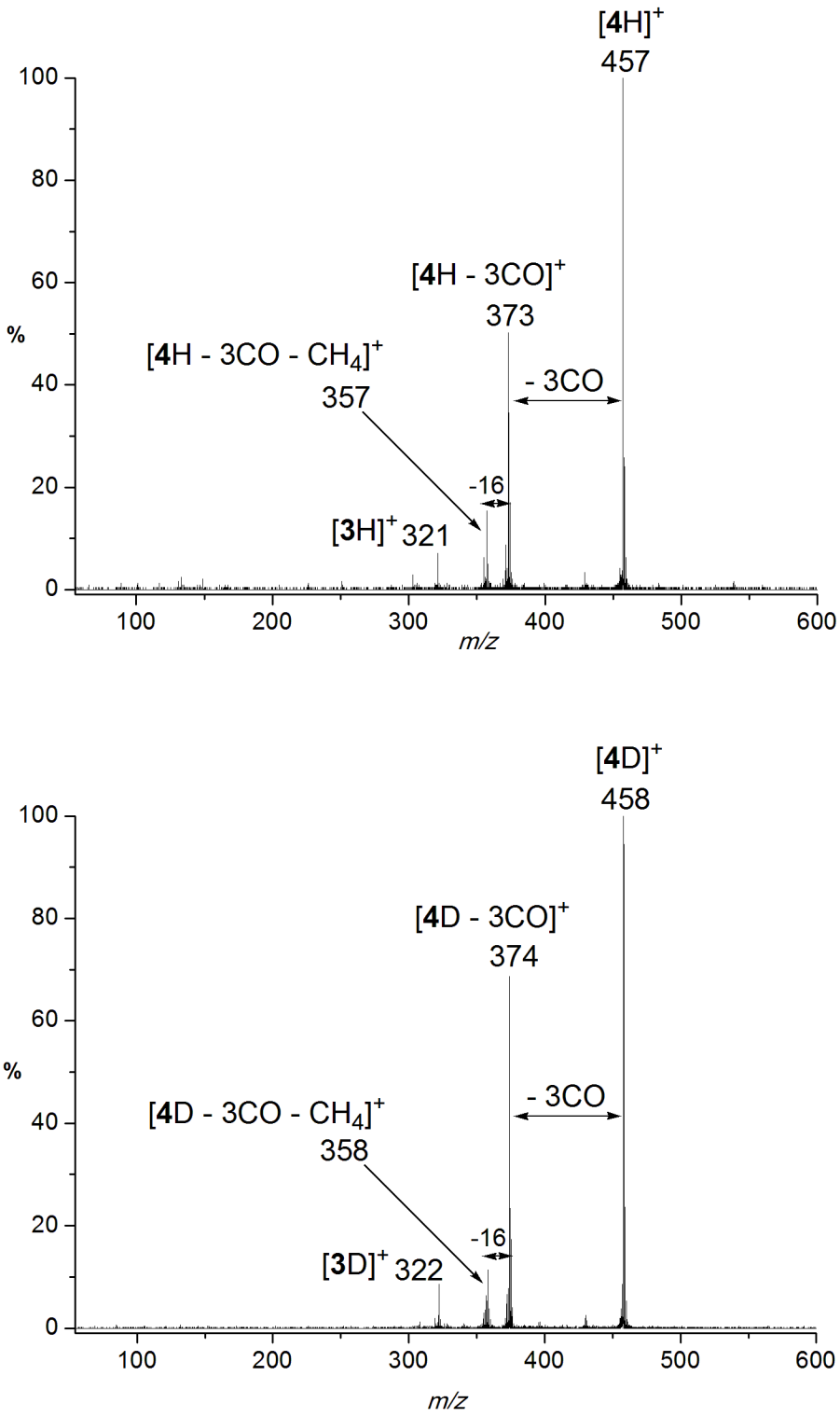

Figure 3.8: (top) ESI(+)-MS/MS of **4** in methanol spiked with formic acid. (bottom) ESI(+)-MS/MS of **4** in d_1-methanol spiked with formic acid.

3.1.2 Phosphine ligand analogue

Previously some work was done in our group by Nicky Farrer[96] to develop a suitable Proton Sponge®-containing ligand to act as an electrospray handle for organometallic complexes. Triphenylphosphine was selected as the parent ligand since it is inexpensive, readily available and is used routinely as a ligand in many catalytic reactions. Proton Sponge® can be substituted for one of the phenyl groups on phosphorus to give the *ortho*- or *para*- electrospray-active ligands 1,8-bis(dimethylamino)-2-diphenylphosphonaphthalene (**5a**) or 1,8-bis(dimethylamino)-4-diphenylphosphonaphthalene (**5b**) (Figure 3.9).

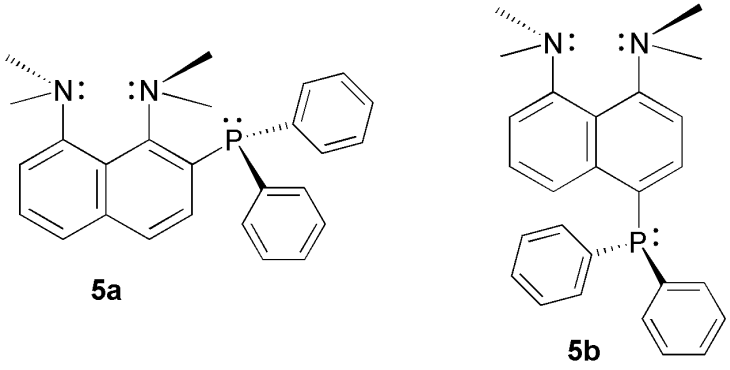

Figure 3.9: **5a**) 1,8-bis(dimethylamino)-2-diphenylphosphonaphthalene. **5b**) 1,8-bis(dimethylamino)-4-diphenylphosphonaphthalene.

Initial work by Farrer on the two isomers revealed that while synthesis of **5a** was trivial (Scheme 3.2 **a** and **c**), synthesis of **5b** was not. The problem lies in the first step of the reaction: bromination of Proton Sponge®. *Ortho*-bromination is effectively accomplished using brominating agent NBS which is selective for *ortho*-bromination at low temperatures;[141] however, despite attempting the reaction under a variety of brominating conditions that were reported in the literature,[131, 142-145] selective *para*-bromination at only one of the *para*-sites on Proton Sponge® was elusive. Product mixtures which included *ortho*-substituted and di-substituted compounds were obtained, purification of **5b** from these mixtures was difficult, and low yields were obtained.[146] Crystal structures of both **5a** and **5b** were obtained but further work focused on **5a**.

While working with the charged ligand **5a** (in which the parent ligand is attached to Proton Sponge® in the *ortho*-position) we observed reactivity that called into question the innocence of this ligand. Farrer synthesized a variety of **5a**-derivatized metal complexes including $PdCl_2$(**5a**)$_2$ and Ru(η^6-*p*-cymene)Cl_2(**5a**). The mass spectra of these complexes were dominated by the peak corresponding to $[M\text{-}Cl]^+$ peak with a less intense $[M+H]^+$ signal present.[146] The presence of two competing ionization pathways is undesirable since the complexes of interest are represented by multiple signals in the mass spectrum. The resulting spectra are more complicated and often difficult to interpret. The loss of chloride to form a positively-charged ion is a well documented ionization pathway for chlorine-containing metal complexes.[70] We hypothesize that for $PdCl_2$(**5a**)$_2$ and Ru(η^6-*p*-cymene)Cl_2(**5a**), crowding at the metal center from the methyl groups on the proton sponge functionality may be favouring this lower coordination state.

This less than ideal reactivity caused us to revisit the idea of using a *para*-substituted Proton Sponge® as a charged ligand. We hoped to inhibit any unwanted participation of the proton sponge functionality in our reactions by having the charged functionality further removed from the reactive center. When bound to a metal center, the dimethylamino groups of **5b** are further removed from the metal center than those of **5a** and are unable to interfere with reactivity at the metal centre. If **5b** is to be used as an electrospray probe, however; there must exist an efficient and inexpensive way to synthesize it.

Work by Farrer indicated that addition of bromine to a solution of Proton Sponge® in CCl_4 was the most promising approach, and optimization of the synthesis of **5b** was undertaken with that in mind. After a series of attempts, conditions were developed under which **5b** could be produced with an overall isolated yield of 19% in two steps (Scheme 3.2 **b** and **c**). There was no appreciable formation of ortho- or di-brominated byproducts at the bromination stage; therefore, purification of **2b** was not required.

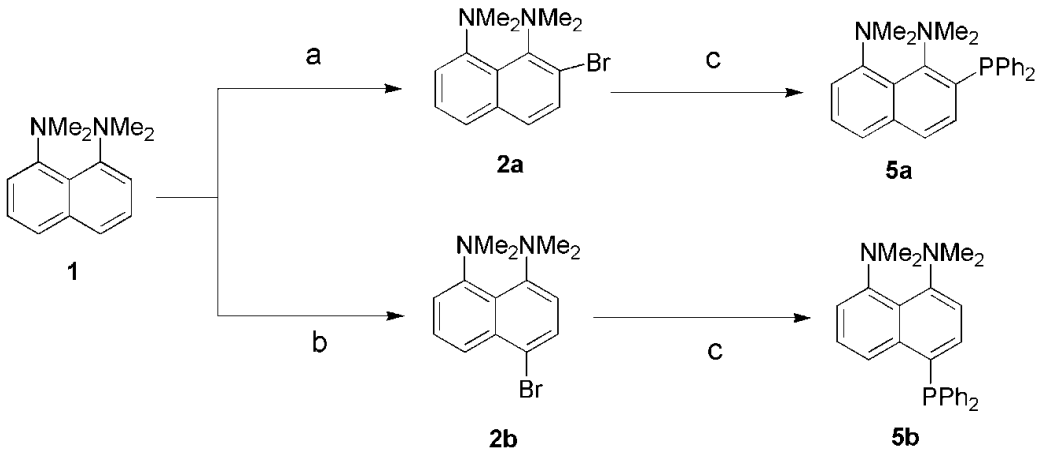

Scheme 3.2: Synthesis of **5a**[96] and **5b**. a) NBS/ THF/ -78 °C. 63% yield. b) Br_2/ CCl_4/ 22 °C. 52% yield. c) n-BuLi/ THF/ -78 °C, PPh_2Cl/ THF/ -78 °C.

2b was synthesized by dropwise addition of bromine (diluted in carbon tetrachloride) to a carbon tetrachloride solution of Proton Sponge® at room temperature. This addition must be performed slowly (~2.5 hours) to maintain selectivity for **5b**. After addition of aqueous solutions of sodium thiosulfate and sodium hydroxide a mass spectrum of the solution was acquired (Figure 3.10). It shows good selectivity for addition of only one bromine atom to Proton Sponge® (only small amounts of the starting material, *m/z* 215, and the di-brominated side product, *m/z* 457, are observed); however, MS is not able to distinguish between the *ortho*- and *para*-brominated isomers.

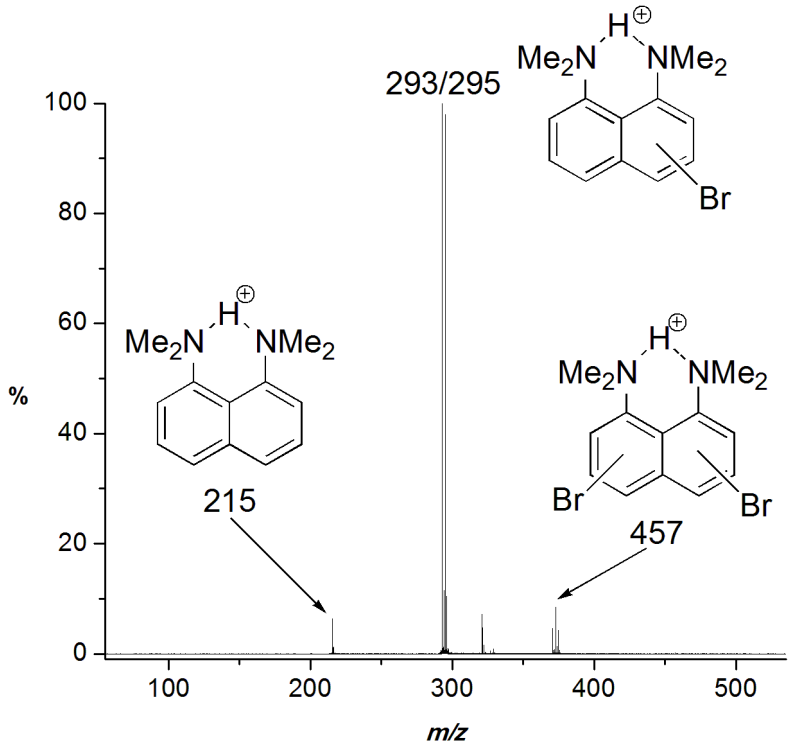

Figure 3.10: ESI(+)-MS of **2b** ($[M + H]^+$ = *m/z* 293/295) from a quenched and diluted reaction mixture of **1** and Br_2 dissolved in carbon tetrachloride. Small signals for unreacted **1** and the dibrominated byproduct are observed.

After workup, a ^1H NMR experiment was performed to confirm that the correct isomer was formed (Figure 3.11). We observed that the *para*-isomer is in fact formed in a ratio of 93:7 (*para*:*ortho*). This is a complete reverse of the ratio obtained in the synthesis of **2a** when NBS at -78 °C is used for bromination (9:91, *para*:*ortho*).

2b was used without further purification to form **5b** via lithiation and treatment with PPh_2Cl at low temperature in THF. The mixture was allowed to warm to room temperature with stirring and then allowed to settle. After filtration, deep orange crystals of **5b** were formed in the filtrate *via* solvent evaporation.

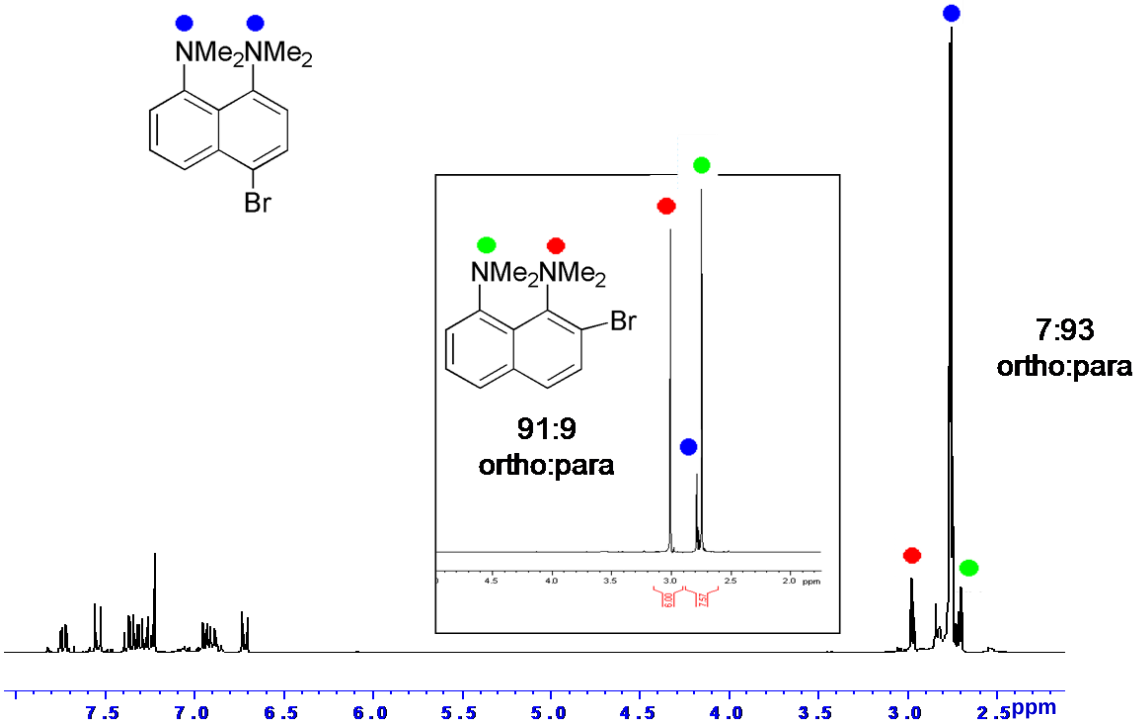

Figure 3.11: ^{1}H NMR (300 MHz, $CDCl_3$) of the *para*-brominated Proton Sponge®. Inset: High-field region of the ^{1}H NMR of the *ortho*-brominated Proton Sponge®. Signals due to the methyl groups in both the *ortho*- and *para*-brominated compounds are assigned.

The mass spectrum of **5b** gave the expected single, intense $[M+H]^+$ peak. To test the behaviour of the tag when coordinated to a metal center, a solution of $PdCl_2COD$ in dichloromethane was combined with a solution of **5b** in dichloromethane and an ESI-MS of the mixture was collected (Figure 3.12). The major signal in the spectrum (*m/z* 975) corresponds to $[PdCl_2(\mathbf{5b})_2H]^+$ (**6**) in which one of the chargeable ligands is protonated. In contrast to **5a**, no signal exists corresponding to ionization by loss of chloride (*m/z* 940) and very little of the free ligand is observed (*m/z* 399) suggesting that **5b** performs well as a ligand for palladium.

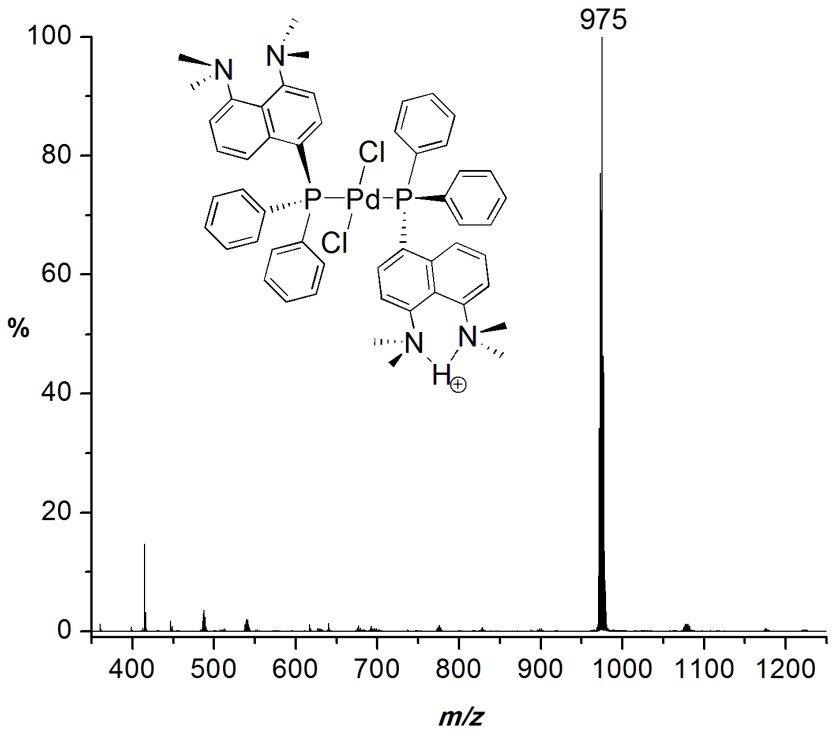

Figure 3.12: ESI(+)-MS of **6** intercepted from a dichloromethane solution of $PdCl_2$(COD) and **5b**. Small peaks are observed at: *m/z* 415 for the oxidized ligand $[O=\mathbf{5b}H]^+$, *m/z* 488 for the doubly-charged complex $[PdCl_2(\mathbf{5b})_2H_2]^{2+}$ and *m/z* 539 and *m/z* 1077 for the singly- and doubly-charged versions of the dimer $Pd_2Cl_2(\mathbf{5b})_2$.

Given the observed success of **5b** as a chargeable ligand on coordination to a metal center, we next employed **5b** in the study of a catalytic reaction. Our goal was to study palladium-catalyzed systems, and to that end we chose a Stille reaction which Santos had previously studied by MS[78] to further test the performance of our chargeable ligand. An acetonitrile solution containing the catalyst $Pd(O_2CCH_3)_2$ and **5b** was examined by MS, and the result was somewhat disappointing (Figure 3.13). While species consistent with the ones reported by Santos were detected, more than one ionization pathway was operative; protonation of **5b** was observed, and many of the palladium-containing species were also oxidized to form radical cations. The latter ionization method involves oxidation of Pd(0) at the tip of the electrospray capillary, and was in fact the method that Santos relied on in his experiments to obtain positive ions. We had hoped that protonation of **5b** would be a much more facile process and would suppress the oxidation of palladium; however this was not the case.

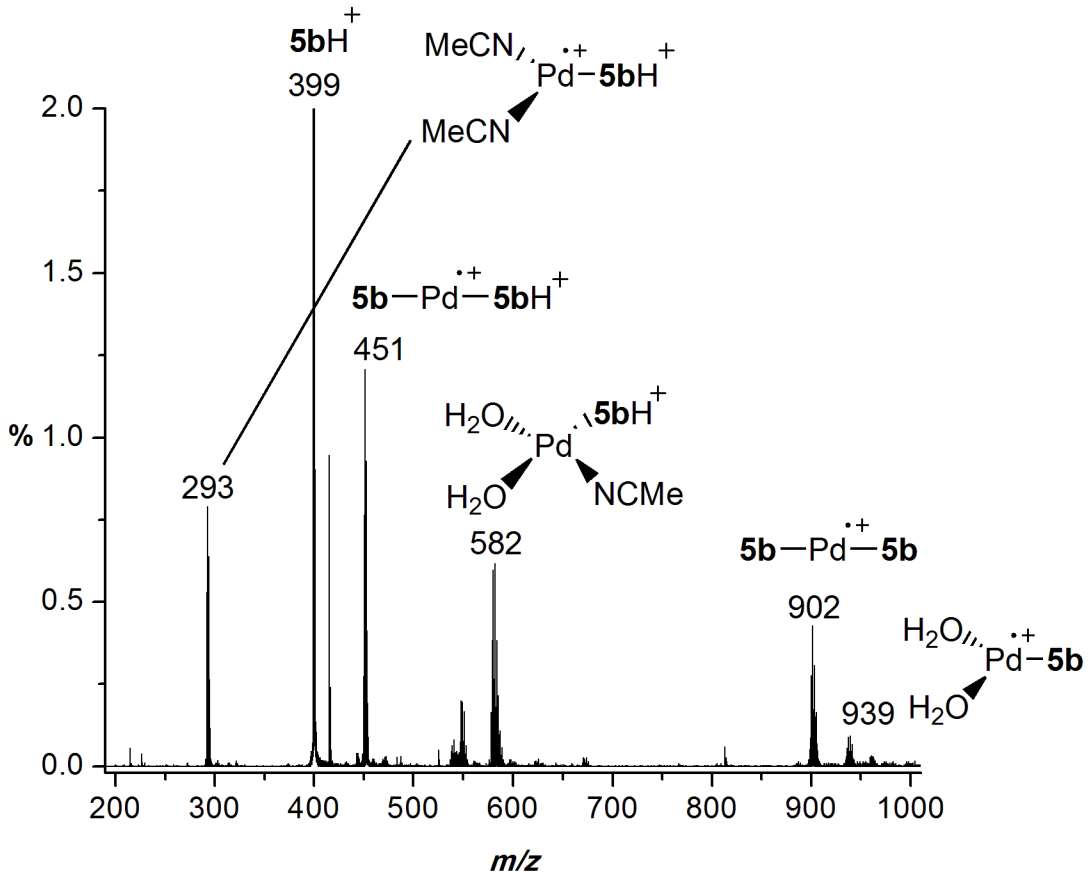

Figure 3.13: ESI(+)-MS of an acetonitrile solution of $Pd(OAc)_2$ and **5b**. Speciation is similar to that observed by Santos.[78]

Further investigation of Stille and Suzuki reactions using **5b** produced spectra containing many peaks that were difficult to assign (an example is given in Figure 3.14). We attributed these peaks to the products of unknown reactivity involving the radical species formed in the electrospray process and we conclude that while **5b** can perform as an ESI tag, it is not suited to the study of systems for which there are viable metal-based ionization pathways.

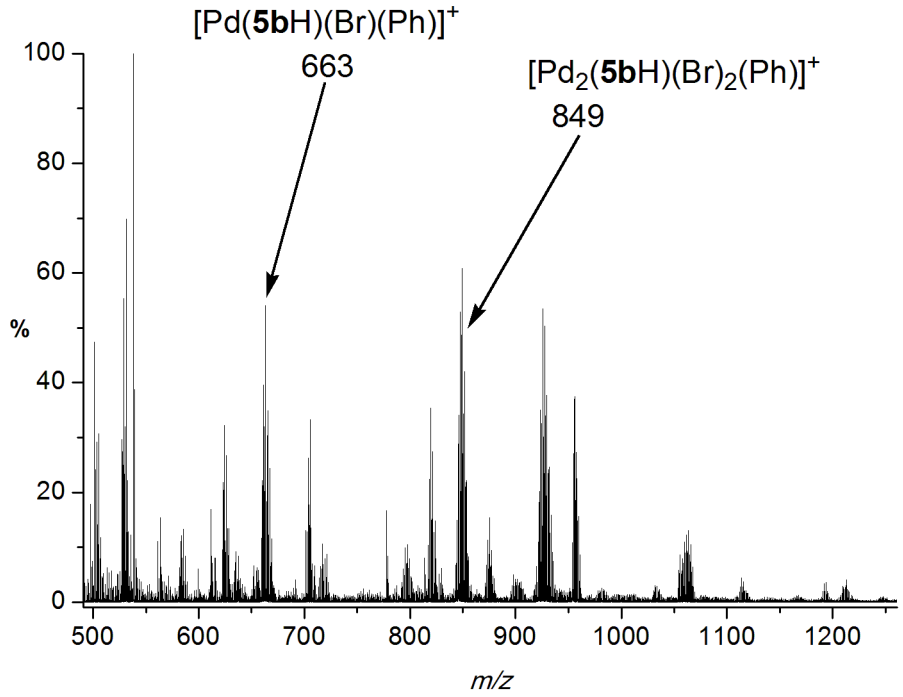

Figure 3.14: ESI(+)-MS of the reaction of bromobenzene with tributylvinyl tin catalyzed by $PdCl_2COD$ and **5b** in 1,2-dichloroethane under N_2 after 1.5 h; 100 °C (experimental procedure adapted from reference 147). Only the identities of the two labelled peaks could be determined despite extensive analysis.

3.2 Charged ESI-active ligands

The difficulty in obtaining straightforward MS data on palladium-catalyzed reactions using the chargeable-type ESI tags led us to search for a permanently-charged ESI-active ligand that would be suited to the study of palladium-catalyzed systems. Permanently-charged ESI tags have the advantage of (1) being less pH dependent than chargeable tags, and (2) having fewer potential avenues for reactivity that may interfere with the system of interest. In our experience the use of a permanently-charged tag generally results in simpler spectra. Ammonium or phosphonium groups are most commonly employed as the charged group (see Section 1.2.3 for examples) and if solubility of the molecule in organic solvents is compromised due to the addition of this polar group, the counter ion may be exchanged to obtain more desirable solubility properties.

3.2.1 Negatively-charged phosphine ligand analogue

We were interested in developing that was both permanently charged and anionic. By operating in the negative ion mode of the mass spectrometer the potential oxidation of palladium is avoided; Pd(0) is easy to oxidized to Pd(II) [148, 149] but difficult to reduce since it is already in the zero-oxidation state. One obvious candidate was triphenylphosphine-*m*-sulfonate (TPPMS, **7**), a *meta*-sulfonated phosphine ligand commonly used as a water-soluble phosphine ligand (Figure 3.15).[150]

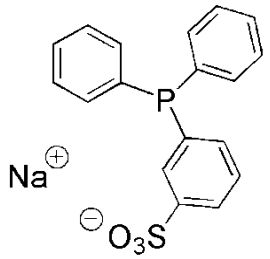

Figure 3.15: Sodium triphenylphosphine *meta*-sulfonate (Na**7**)

The use of Na**7** as a ligand was first reported by Chatt in 1958.[151] Since then it has been used to facilitate biphasic catalytic reactions such as the rhodium-catalyzed hydrogenation and hydroformylation of alkenes,[152, 153] the palladium-catalyzed carbonylation of benzyl chloride,[154] and the single phase aqueous alkylations of various biomolecules and organic substrates catalyzed by palladium.[155] **7** belongs to a family of sulfonated water-soluble phosphines and a number of reviews have been published examining the role of these ligands in catalysis.[156-158]

7 was particularly appealing to us for a number of reasons:

(1) It is a permanently-charged, anionic version of the triphenylphosphine ligand (one of the most commonly used ligands in organometallic/coordination chemistry).

(2) The synthesis of Na**7** is straightforward. The procedure reported by Chatt involving oxidation with oleum and quenching with sodium hydroxide is still widely used,[151] although alternative synthetic methods have also been published.[159, 160] The starting

materials are all commercially available and inexpensive, and the reaction can be performed in air.

(3) **7** is structurally similar to triphenylphosphine, and it has been shown to act effectively as a ligand in a variety of aqueous palladium-catalyzed coupling reactions.[161] The Tolman cone angle of **7** is 151° and triphenylphosphine is 145° indicating that the steric requirements of the two ligands are similar (cone angles for common triaryl phosphine ligands range from 145 – 200°).[150, 162]

In fact, the only property of **7** that did not suit our purposes is the one for which it is most well known; its water solubility. Almost all common metal-catalyzed reactions proceed in organic solvents; therefore we required a ligand that is soluble in organic solvents. To improve the solubility of **7** in organic solvents, we performed a cation exchange reaction to replace the standard sodium cation with the bulky, non-coordinating bis(triphenylphosphine)iminium cation [PPN]. The resulting complex (Figure 3.16), **7**[PPN] is soluble in all common organic solvents.

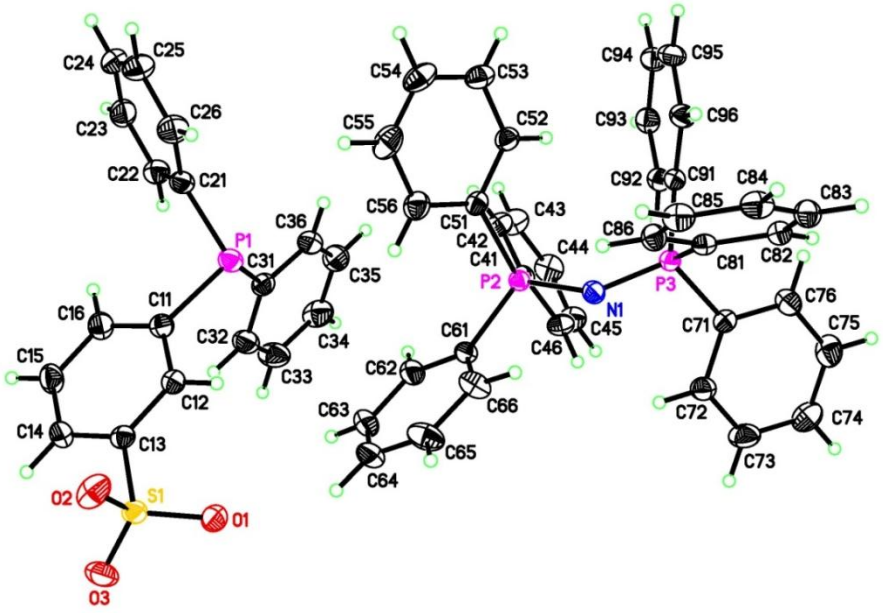

Figure 3.16: Crystal structure of **7**[PPN] obtained by Matthew Henderson.[163]

The use of PPN as a cation imparted our ligand with two other desirable traits:

(1) The non-coordinating nature of the cation disfavours the formation of tightly bound cation-anion complexes (ion pairing) which would be neutral and invisible to MS. The anion remains uncomplexed and as a result it has high surface activity which leads a low detection limit for the ligand and its complexes (<1 μM is enough to obtain a high quality spectrum).

(2) The bulk of the cation makes the positive charge relatively inaccessible; therefore, the formation of aggregates which would complicate the mass spectrum (e.g. 2 anions + 1 cation) is avoided. The mass spectrum of the ligand contains only one peak ($[M]^-$, *m/z* 341).

Preliminary MS tests on a chloroform solution of $PdCl_2COD$ and **7**[PPN] show a signal for the metal complex containing one charged ligand, and demonstrate the ability of **7** to coordinate to palladium (Figure 3.17). There is only one dominant ionization pathway. The presence of a peak for free ligand is common in MS experiments using this tag, but the signal appears in a lower *m/z* region and does not usually cause any interference.

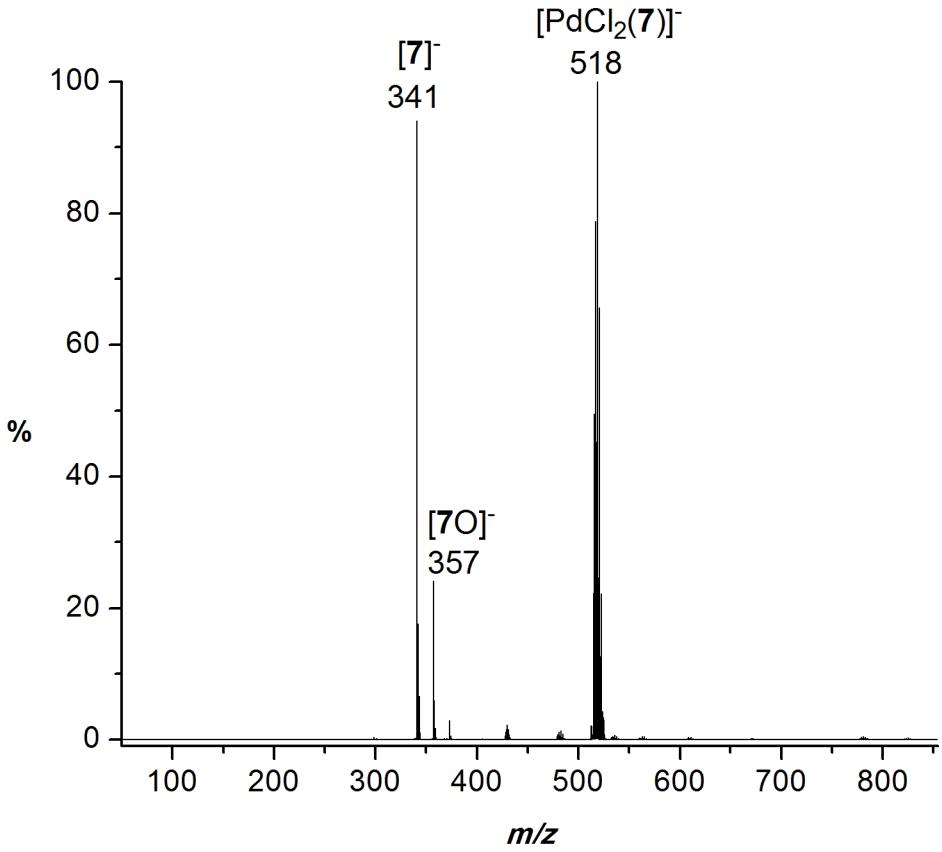

Figure 3.17: ESI(-)-MS of a chloroform solution of $PdCl_2COD$ and **7**[PPN]. Cone voltage = 20 V. Signals are observed for the free ligand (**7**$^-$, *m/z* 341), the oxide of the ligand ([**7**O]$^-$, *m/z* 357) and [$PdCl_2$(**7**)]$^-$ (*m/z* 518).

The behaviour of this ligand when placed under reaction conditions is predictable and well understood; unlike the Proton Sponge®-based ligand **5b**. Examples of this can be found in Chapter 5. In light of these results **7**[PPN] was deemed an appropriate ESI tag for the study of metal-catalyzed, and specifically palladium-catalyzed, reactions.

3.3 Experimental

General information

Dry and degassed solvents were obtained from a solvent purification system. All solvents were HPLC grade. Reagents were purchased from Aldrich and used without further purification

except for Proton Sponge® **(1)**, which was recrystallized from hot methanol before use. Reactions performed under nitrogen were carried out using standard Schlenk techniques. All electrospray mass spectra were collected using a Micromass Q-TOF *micro* instrument. Capillary voltage was set to 2900 V, source and desolvation temperatures were at 80 ºC and 150 ºC, respectively. Samples were infused via syringe pump at 10 μL min^{-1}. NMR spectra were recorded on a Bruker AC-300 spectrometer. Chemical shifts are quoted in ppm using $CDCl_3$ (^1H δ 7.26 ppm) or CD_3CN (^1H δ 1.94 ppm) as references where appropriate. Melting points were recorded on a Gallenkamp Melting Point Apparatus and are uncorrected. IR spectra were recorded using a solution cell in a Perkin Elmer Spectrum 1000 FT-IR spectrometer. X-Ray crystallographic data was collected by Dr. Robert McDonald (University of Alberta) and Dr. Allen Oliver (University of Notre Dame). See Appendices A and B for details.

{1,8-bis(dimethylamino)naphthalene-2-yl}bromide (**2a**)

2a was synthesized according to related literature.[96] A THF solution of Proton Sponge® (10 g in 40 mL) and a THF solution of NBS (8.5 g in 250 mL) were cooled to -78 ºC. The NBS solution was added dropwise to the Proton Sponge® solution with stirring to form a cherry red solution. The mixture was warmed to room temperature and turned an opaque canary yellow. THF was removed by rotary evaporation, and the resulting yellow sludge was vacuum-filtered and washed with portions of cold diethyl ether to give the succinimide byproduct as a light yellow powder and the product as an orange filtrate. The filtrate was reduced by rotary evaporation. Filtration and rotary evaporation were repeated until all succinimide had been removed. The product was further purified by vacuum distillation at 216 ºC to yield the product as bright yellow oil in 63% yield (8.61 g), and its identity was confirmed with comparison to the literature.[96]

1,8-bis(dimethylamino)-2-(4-methoxyphenyl)naphthalene (**3**)

Under a nitrogen atmosphere, **2a** (5.00 g, 0.017 mol) and 4-methoxyphenylboronic acid (2.74 g, 0.018 mol) were dissolved in *n*-propanol (30 mL) with stirring. Distilled water (6 mL), sodium bicarbonate (10 mL, 2 M), palladium(II) acetate (0.034 g, 0.051 mmol), and triphenylphosphine (0.21 g, 0.8 mmol) were added consecutively and the mixture was refluxed overnight. The reaction mixture was cooled to room temperature and quenched by the dropwise

addition of deionized water (21 mL) with stirring in air. The mixture was extracted twice with ethylacetate and the organic layer was washed with sodium bicarbonate (5% w/v, 2×) and brine (2×), and dried with sodium sulfate and activated charcoal (3 g). The mixture was filtered through a 3 cm bed of celite and the filtrate was reduced by rotary evaporation. Hexanes were added to yield the product as a white ppt in 41% yield (2.27 g). ^{1}H NMR (300MHz, $CDCl_3$) δ_H **3**: 7.50-6.97 (m, aromatic protons, 9 H), 3.88 (s, $OC\underline{H}_3$, 3 H), 2.78 (s, $N(C\underline{H}_3)_2$, 6 H), 2.63 (s, $N(C\underline{H}_3)_2$, 6 H). ^{13}C NMR (400MHz, CDCl3) δ_C **3**: 158.3 (C), 137.3 (C), 130.5 (C), 130.2 (C), 125.5 (C), 123.1 (C), 122.5 (C), 113.7 (C), 55.5 ($O\underline{C}H_3$), 45.4 ($N(\underline{C}H_3)_2$), 45.1 ($N(\underline{C}H_3)_2$). ESI-MS (MeOH) *m/z*: 321.1983 ([**3** + H]$^+$, model $C_{21}H_{24}ON_2$ 321.1967). m.p.: 105-107ºC.

1,8-bis(dimethylamino)-2-(4-methoxyphenyl)naphthalene hydrofluoroborate ([**3**H]$^+$[BF_4]$^-$)

3 (0.0020 g, 4.9 µmol) was dissolved in ethanol and tetrafluoroboronic acid (0.004 mL, 48% in water) was added dropwise. Slow evaporation of solvent yielded colorless crystals (98%, 0.0039 g). ^{1}H NMR (300MHz, $CDCl_3$) δ_H [**3**H]$^+$: 19.4 (s, H$^+$, 1 H), 8.00-6.97 (m, aromatic protons, 9 H), 3.79 (s, $OC\underline{H}_3$, 3 H), 3.04 (s, $N(C\underline{H}_3)_2$, 6 H), 2.79 (s, $N(C\underline{H}_3)_2$, 6 H).

pK_a *determination of* ***3****: ^{1}H transprotonation experiments*[164]

Equimolar amounts of [**1**H]$^+$[BF_4]$^-$ (0.0040 g, 0.013 mmol) and **3** (0.0042 g, 0.013 mmol) were dissolved together in dry CD_3CN (0.7 mL), allowed to stand overnight, and a ^{1}H NMR spectrum was recorded. The experiment was repeated four separate times. The average integrations for the coordinated proton of the two protonated species were (CD_3CN, 300 MHz) δ_H: ppm (**3H**$^+$, ∫ 1.00), ppm (**1H**$^+$, ∫ 1.01) (Std. Dev. = 0.04, %RSD = 4). The first pK_a of **3** (CD_3CN) was determined by calculation using the ratio of the integrations of the two peaks and the known pK_a of **1** (18.18 in CH_3CN)[165] Analysis of the equilibrium gave $K_{a3} = K_{a1} / K_{eq}$ where K_{a1} (known) = [**1**][H$^+$]/[**1**·H$^+$] = 1.514 x 10^{18}, K_{a3} = [**3**][H$^+$]/[**3**·H$^+$] and K_{eq} (known) = (∫**3**·H/ ∫**1**·H) = 0.99.[128] K_{a3} =1.514 x 10^{18} / 0.99 = (1.50 ± 0.06) x 10^{18}. pK_a of **3** = 18.2 ± 0.7 in CD_3CN.

*Chromium(**3**) tricarbonyl* (**4**)

Under a nitrogen atmosphere, dry THF (0.13 mL) and dibutylether (2.5 mL) were added to **3** (0.1005 g, 0.314 mmol) and chromium hexacarbonyl (0.0521 g, 0.233 mmol). The mixture was refluxed for 24 hours. The air-sensitive solution was quickly filtered in air and the solvent was

removed by rotary evaporation to yield a yellow oil (28%, 0.030 g). Product was recrystallized under inert atmosphere from a solution of toluene by evaporation. ^{1}H NMR (300MHz, $CDCl_3$) δ_H **4**: 7.47-7.05 (m, aromatic protons, 5 H), 5.74 (d, anisole aromatic protons, 2 H), 5.20 (d, anisole aromatic protons, 2 H), 3.78 (s, OC$\underline{H}_3$, 3 H), 2.74 (s, N(C$\underline{H}_3$)$_2$, 6 H), 2.73 (s, N(C$\underline{H}_3$)$_2$, 6 H). ν_{CO} bands: 1964cm^{-1}, 1890cm^{-1}. ESI-MS (MeOH) *m/z*: 457.1224 ([**4** + H]$^+$, model $C_{24}H_{24}O_4N_2Cr$ 457.1220). m.p.: 167-169 ºC.

{1,8-bis(dimethylamino)naphthalene-4-yl}bromide (**2b**)

A solution of bromine (2.15 mL, 0.042 mol) in carbon tetrachloride (40 mL) was added dropwise over 2.5 h to a stirring solution of Proton Sponge® (10.0 g, 0.047 mol) in dry carbon tetrachloride (60 mL) under inert atmosphere resulting in a dark red solution. Aqueous sodium thiosulfate (1 M, 20 mL) and aqueous sodium hydroxide (20% w/v, 20 mL) were added dropwise with stirring. The yellow brown mixture was filtered to remove the beige salt byproduct which was washed with dichloromethane. The organic layer was collected and reduced to a dark reddish brown oil by rotary evaporation (7.07 g, 52% crude yield). The product was used directly without further purification to synthesize **5b**. ^{1}H NMR (300MHz, $CDCl_3$) δ_H **2b**: 7.80-6.71 (m, aromatic protons, 5 H), 2.81-2.77 (m, 2(N$\underline{Me}_3$), 12 H).

{1,8-bis(dimethylamino) naphthalene-4-yl}diphenylphosphine (**5b**)

Under inert atmosphere, a solution of **2b** (1.5 g, 5.1 mmol) in THF (15 mL) was cooled to -78 °C. n-BuLi (3.3 mL, 1.6 M in hexanes, 5.1 mmol) was added dropwise with stirring. The solution was allowed to stir for 30 minutes resulting in an amber coloured solution. Chloro-diphenylphosphine (1 mL, 5.4 mmol) was added dropwise with vigorous stirring, and stirring was continued at -78 °C for 2 hours to give a bright red-orange solution. The mixture was warmed to room temperature and allowed to settle giving a dark reddish-brown solution and a yellow-brown ppt which was filtered. Orange crystals of **5b** were collected from the filtrate by solvent evaporation (0.76g, 37% yield). ^{1}H NMR (300MHz, $CDCl_3$) δ_H **5b**: 7.98 (m, naphthalene proton, 1 H), 7.27 (m, phenyl protons and one naphthalene proton, 11 H), 6.90 (d, naphthalene proton, 1 H), 6.78 (m, naphthalene proton, 2 H), 2.804 (s, N(C$\underline{H}_3$), 6 H), 2.799 (s, N(C$\underline{H}_3$), 6 H).^{31}P NMR (360MHz, $CDCl_3$) δ_P **5b**: -13.41(s, $\underline{P}Ph_2(C_{10}H_{17}N_2)$), m.p.: 168 -169 ºC.

Bis(triphenylphosphine)iminium 3-diphenylphosphinylbenzenesulphonate (**7**[PPN])

Ammonium 3-diphenylphosphinylbenzenesulphonate was synthesized according to literature procedures.[159] 11.38 g (31.00 mmol) was then dissolved in 100 mL warm deionized water, and bis(triphenylphosphine)iminium chloride (17.34 g, 31.00 mmol) was dissolved in 60 mL dichloromethane. The two solutions were mixed together, stirred vigorously for 5 min and transferred to a separating funnel. 30 mL of water containing ammonium chloride was added, the mixture was shaken and allowed to settle. The lower organic layer was collected, and the majority of the solvent was removed by rotary evaporation. The resulting material was left under vacuum overnight to obtain the product as a white solid 24.21 g, 89% isolated yield). ^{1}H NMR (300 MHz, CD_2Cl_2) δ: 7.14–7.20 (m, 1 H), 7.22–7.32 (m, 10 H), 7.44–7.52 (m, 25 H), 7.62–7.68 (m, 6 H), 7.80–7.86 (m, 2 H). ^{31}P NMR (300 MHz, CD_2Cl_2) δ: - 4.5 (s, $\underline{P}Ph_2C_6H_4SO_3^-$), 21.6 (s, $N(\underline{P}Ph_3)_2^+$).

Chapter 4. Instrument Modifications and Method Development

In the past, the study of air- or moisture- sensitive reaction mixtures using soft ionization MS techniques has been a challenge for us and others.[166-168] It is essential when investigating reactive intermediates at low concentrations that the presence of oxygen and water is kept to an absolute minimum. The most common method currently employed is to sample a reaction using a gas-tight syringe that has been kept rigorously oxygen- and moisture-free (preferably in a glovebox) and then to inject the sample into the MS through a short length of PEEK tubing that has been kept similarly dry and oxygen-free.[167] This method is time consuming and it is practically impossible to exclude all oxygen and water during the process of transferring the sample from the reaction vessel to the mass spectrometer. In some cases, extreme measures have been taken to obtain an air- and moisture-free environment. The Fogg group at the University of Ottawa has integrated a glovebox into the front of a MALDI-MS,[166] field desorption ionization has been modified for aspiration of a liquid sample from a sealed vial (LIFDI – liquid introduction field desorption ionization),[168] and our group has installed a glovebox in-line with a Q-TOF *micro* instrument so that reactions can be performed in the glovebox and injected directly into the MS.[167] However, even if the sample is successfully delivered to the source of an ESI-MS instrument without any exposure, the source itself is under atmospheric pressure and is not free of oxygen and water. In addition, the reaction mixture cannot easily be stirred or heated while it is being injected into the MS via syringe.

We wished to develop methodology that would allow for the continuous introduction of an air- or moisture-sensitive reaction into the MS in real time, and under standard reaction conditions (i.e. with stirring, normal concentrations of all reagents, at any temperature and using any solvent). Initially, we thought that the setup of such a system would simply involve running a length of tubing from a reaction vessel to the source of the MS with a small pump in-line to

continuously deliver the sample. This would allow for simple heating and stirring of the reaction as it was being sampled; a feat that is difficult when using a syringe pump. Unfortunately, we discovered that an in-line pump is impractical for the following reasons: we required a pump capable of delivering liquid at rates between 1 and 50 μL min^{-1}. This excludes all peristaltic pumps since the inner diameter of the tube that would be required is too small for peristaltic pumping. It also excludes all rotary pumps because even the smallest internal pump volumes we could find were on the order of 100 μL. This means that for a pumping rate of 10 μL min^{-1} the reaction mixture spends 10 minutes inside the pump before entering the mass spectrometer. Another possibility was to use a small HPLC-type pump; however, these pumps are made of stainless steel and designed to deal with pure solvents. Addition of reactive sample mixtures would likely ruin the pump (a Teflon interior would be more suitable). With no other pump options available we turned to the development of a straightforward sample introduction system that would allow for the continuous introduction of air- or moisture-sensitive reactions into the mass spectrometer.

4.1 Pressurized sample infusion (PSI)

Pressurized sample infusion is a simple and convenient way to analyze air- or moisture-sensitive samples by ESI-MS.[169] It can also be used to monitor reactions continuously in real time. In the simplest terms it is a cannula transfer from a Schlenk flask into at mass spectrometer through a length of small ID PEEK tubing. All required materials for a PSI system are common to synthetic organometallic or mass spectrometry labs: a Schlenk flask, rubber septum, rubber hose, a short length of PEEK tubing (~0.5 m), a PEEK chromatography fitting (nut and ferrule) and a source of pressurized and regulated inert gas (usually N_2). The Schlenk flask is positioned as close as is practical to the ESI-MS source and connected to a source of pressurized inert gas via a short length of rubber tubing. One end of a piece of PEEK capillary tubing is then inserted through a punctured rubber septum (which is wired to the flask to ensure it does not pop off during pressurization) into the Schlenk flask, while the other end is connected to the electrospray inlet (see Figure 4.1, left). Here we show a Schlenk flask that has been modified to include a condenser so that reaction temperatures up to reflux may be accommodated; however, an

unmodified Schlenk flask will suffice and even standard glassware with ground glass joints will work if care is taken to avoid gas leakage (Figure 4.1, right). A slight overpressure (0.5 - 5 psi) is applied to the contents of the Schlenk flask to facilitate continuous introduction of the sample into the mass spectrometer. It is important that a regulator capable of accurately measuring these small pressures is used since over-pressurizing the flask is dangerous. The flask may be equipt with a stir bar and placed in a temperature-controlled bath to allow for stirring and temperature control throughout the reaction. The sample solution must be completely homogeneous to avoid blockage of the PEEK tubing. If dilution of the sample solution is required, this may be accomplished on-line by incorporating a tee in the PEEK tubing immediately outside the flask as shown in Figure 4.1 (right). Up to a 100:1 dilution can be obtained in this fashion with careful adjustment of pressure and solvent flow rate. Dilution with large volumes of room temperature or cold solvent can also effectively quench the reaction.

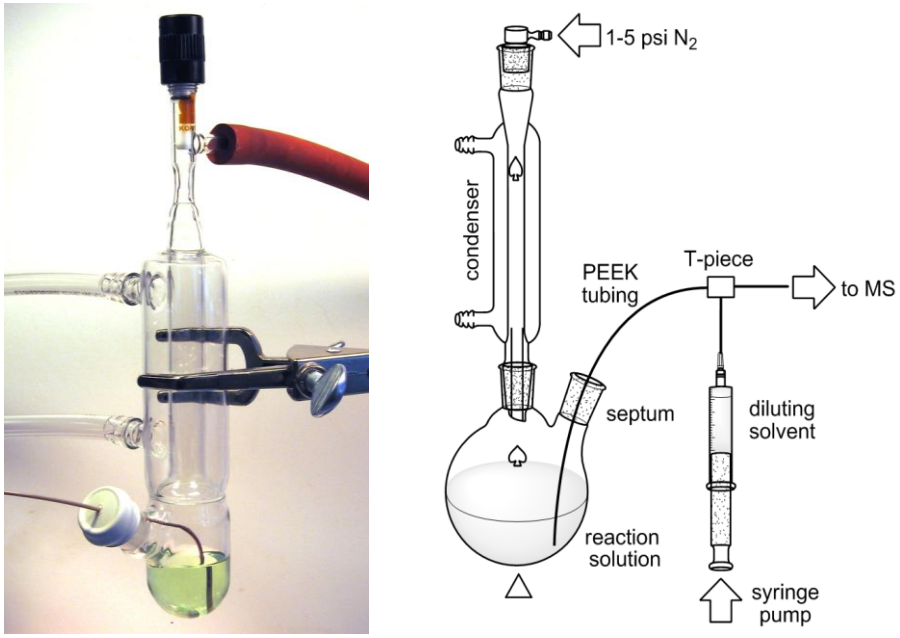

Figure 4.1: (left) Pressurized sample infusion setup. (right) Schematic of a pressurized sample infusion setup using standard glassware and with on-line dilution.

During a typical ESI-MS experiment the sample is introduced into the source of the MS via syringe pump at a rate between 1 – 50 μL min^{-1}. We usually operate at the lower end of this range. The Hagen-Poiseuille equation predicts that the flow rate exiting the tubing should be related to the relative pressure applied to the flask in the following manner:

$$\Delta P = \frac{128 \mu L Q}{\pi d^4} \quad (3)$$

ΔP is the pressure drop, μ is the dynamic viscosity, L is length of tube, Q is the volumetric flow rate and d is the inner diameter of the tube. Rearranging to predict a flow rate from a given overpressure, for water (μ = 0.001 Pa·s), 1 psi (6900 Pa) of pressure applied to a tube of length 0.5 m and diameter 127 μm should generate a flow rate of $(6900 \times 3.14 \times \{1.27 \times 10^{-4}\}^4)/(128 \times 0.001 \times 0.5) = 8.8 \times 10^{-11}$ m^3 s^{-1} $= 8.8 \times 10^{-2}$ μL s^{-1} $= 5.3$ μL min^{-1}. This value is ideal for our purposes and we set out to confirm that the Hagen-Poiseuille equation would hold under our experimental conditions.

A series of flow rate measurements at different pressures were taken for a variety of solvents and using a range of PEEK tubing lengths to determine the pressure required to obtain a given flow rate in this range. The solvents investigated were those commonly used by us for ESI-MS experiments: water, acetonitrile, a 50:50 water:acetonitrile mixture, methanol and dichloromethane. 45 cm is the minimum required PEEK tubing length for our laboratory set up and PEEK tube lengths of 45, 50, 55 and 60 cm were tested. PEEK tubing with an inner diameter of 0.005” (127 μm) (internal volume = ~ 12 μL / meter) was used in all cases. These measurements were performed by students enrolled in the University of Victoria undergraduate class Chem361 during the spring of 2010 and 2011 as part of a teaching lab designed around the use of this sampling method (see Appendix C) Each student was assigned a solvent and PEEK tubing length combination for which they measured flow rates at pressures between 0.5 psi and 3 psi. The mass of solvent forced through a length of PEEK tubing over time was recorded using the experimental setup shown in Figure 4.2 and each flow rate was measured a minimum of ten times. Each student collected enough data to generate one of the lines in a plot like the one shown in Figure 4.3.

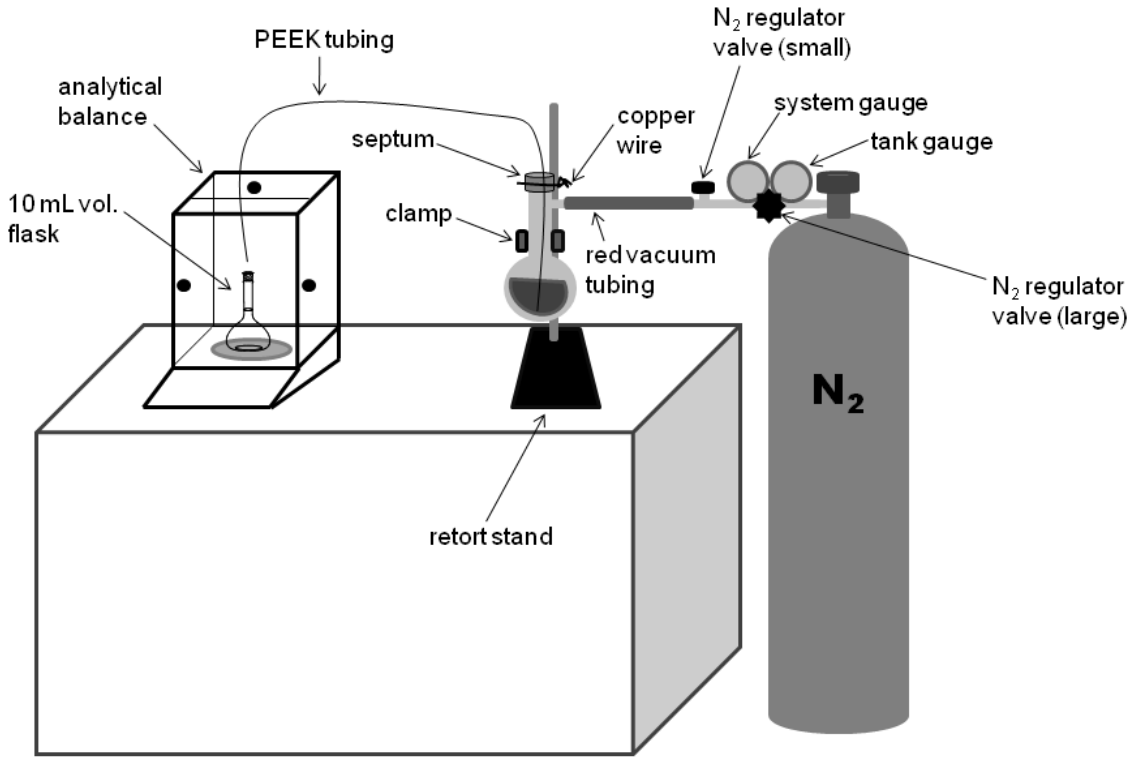

Figure 4.2: Schematic of the experimental setup for flow rate determinations used by Chem361 students. The Schlenk flask is pressurized and the mass of solvent dropping from the tip of the PEEK tubing is recorded with time using an analytical balance and a stopwatch.

The effect of tube length on flow rate over the experimental range did not follow any trend, however the effect of solvent type on flow rate was found to be related qualitatively to the viscosity of the solvent. The flow rates of solvent through a given PEEK tube length at a given pressure from highest to lowest are acetonitrile (0.36 cP, 20 °C), dichloromethane (0.44 cP, 20 °C), methanol (0.59 cP, 20 °C), 50:50 acetonitrile:water, and water (1.0 cP, 20 °C) (Figure 4.3).[170] As expected the least viscous solvents have the highest flow rate at a given pressure and tube length. Vertical error bars are included in Figure 4.3, but they are almost too small to be seen, indicating high precision in the flow rate measurements. This high precision is evident in the plots of mass vs. time used to determine flow rate (Figure 4.4 is a representative sample of this data). Some slight deviations from linearity are observed in Figure 4.3 and this can be attributed to the precision with which the pressure was set for each experiment. Error in the pressure readings was approximately ± 0.1 psi.

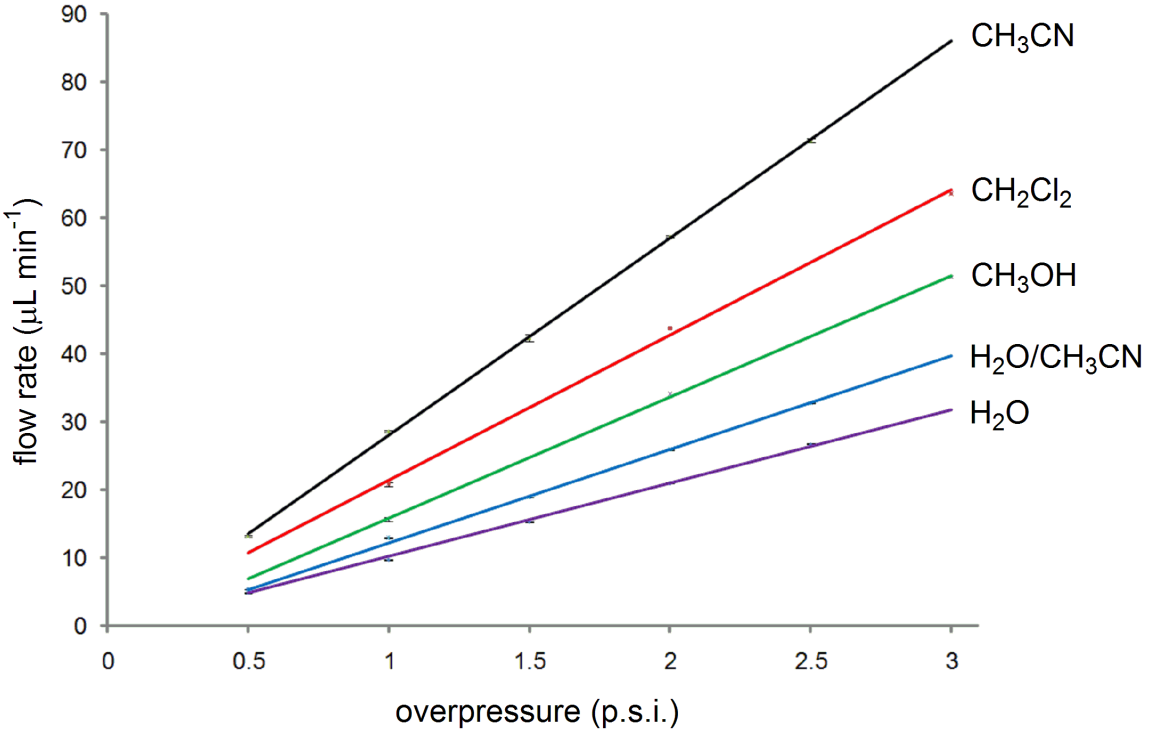

Figure 4.3: Determination of the relationship between the pressure applied to a PSI system and the resulting flow rate for a variety of common solvents when a 60 cm length of PEEK tubing is used. Vertical error bars included.

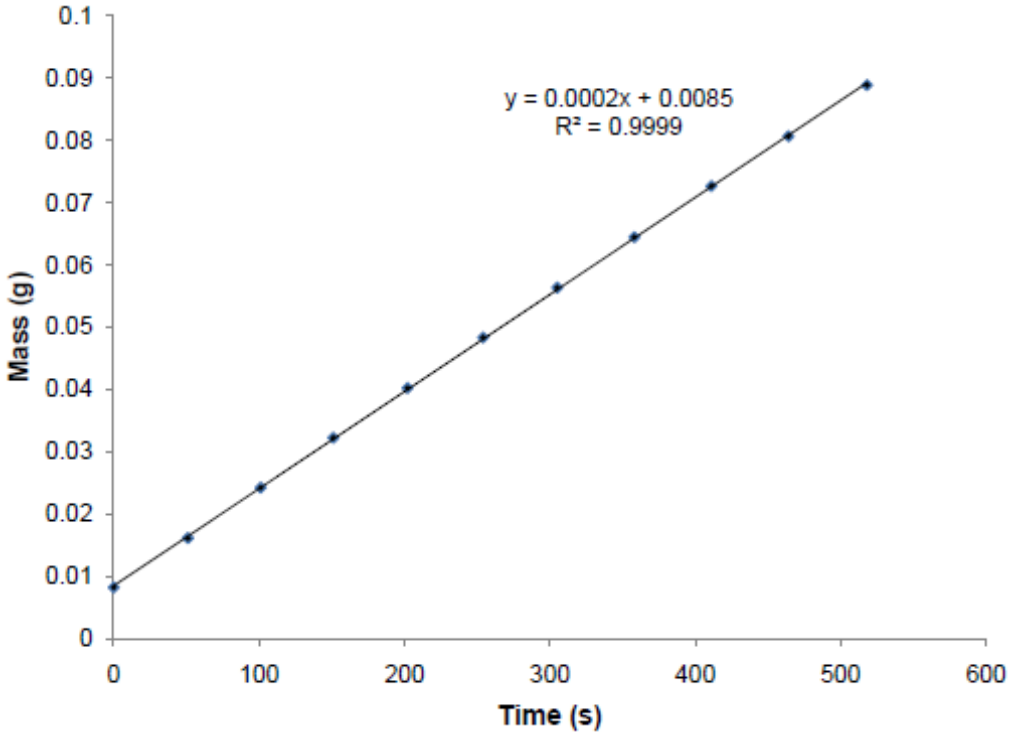

Figure 4.4: Determination of the flow rate of methanol through a 45 cm length of PEEK tubing at an overpressure of 0.5 psi. Data collected by Chem361 student Manuel Ma. This data represents one point on a graph like the one shown in Figure 4.3.

All of the data collected can be summarized by plotting the actual flow rate at a given combination of solvent, pressure and tubing length against the calculated value (derived from the Hagen-Poiseuille equation) (Figure 4.5).

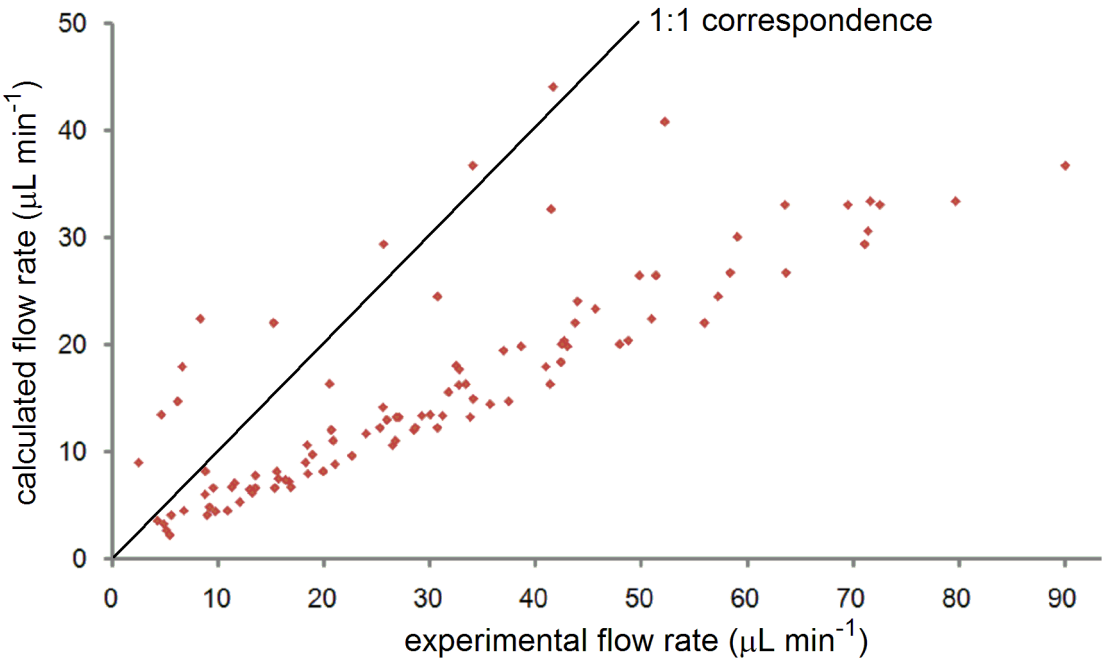

Figure 4.5: Experimental flow rates (red dots) plotted against theoretical flow rates calculated using the Hagen-Poiseuille equation. The solid black line indicates a 1:1 correspondence. The 100 data points include flow rates calculated using five different solvents, four different tube lengths and five different values of overpressure (see Appendix C for data used to generate this plot).

It is clear that under our conditions the Hagen-Poiseuille equation generally underestimates the flow rate by a factor of approximately 2 for a given pressure regardless of the choice of solvent. There are a number of outliers from the general experimental trend, and these are likely due to variations in the inner diameters of specific pieces of tubing. The manufacturer's listed tolerance for 1/16" outer diameter 0.005" ID PEEK tubing is ± 0.001" (i.e. ± 20% error). Any discrepancy in the tube diameter is magnified by a power of four in the Hagen-Poiseuille equation so a 20% greater diameter than listed is enough to account for the observed outliers. Because of this variation, if precise flow rates are required it is recommended that the flow rate for a given length of tubing be measured initially at one pressure. From there, a corrected version of the Hagen-Poiseuille equation (using the experimentally-calculated diameter of the tubing) can be used to determine expected flow rates for other solvents and pressures. The corrected version of the equation simplifies to $Q = k\Delta P/\mu$, where k combines the experimental correction with $\pi d^4/128L$ which is a constant for a given piece of tubing. In reality, ESI-MS is capable of dealing

with a wide range of flow rates and in most cases the variations caused by differing tube diameters will not significantly affect the data obtained during PSI experiments.

A copper-free Sonogashira reaction involving a charged substrate (Scheme 4.1) was monitored over time using PSI-ESI-MS to determine if reliable real-time kinetic data could be obtained using this sample introduction method.

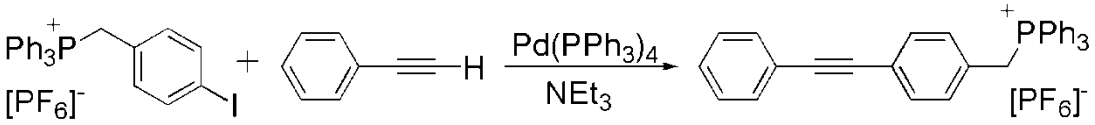

Scheme 4.1: Copper-free Sonogashira reaction between $[PPh_3CH_2ArI]^+$ PF_6^- and phenylacetylene using tetrakistriphenylphosphine as the catalyst and triethylamine as the base.

The reaction being monitored by ESI-MS was periodically sampled for NMR and and UV-Vis analysis, and using each of these techniques a trace was generated for the appearance of product. This experiment required three experimenters in order to simultaneously collect data from all three techniques and was performed by Zohrab Ahmadi and Cara Manning from the McIndoe group and myself. A comparison of the resulting traces is shown in Figure 4.6.

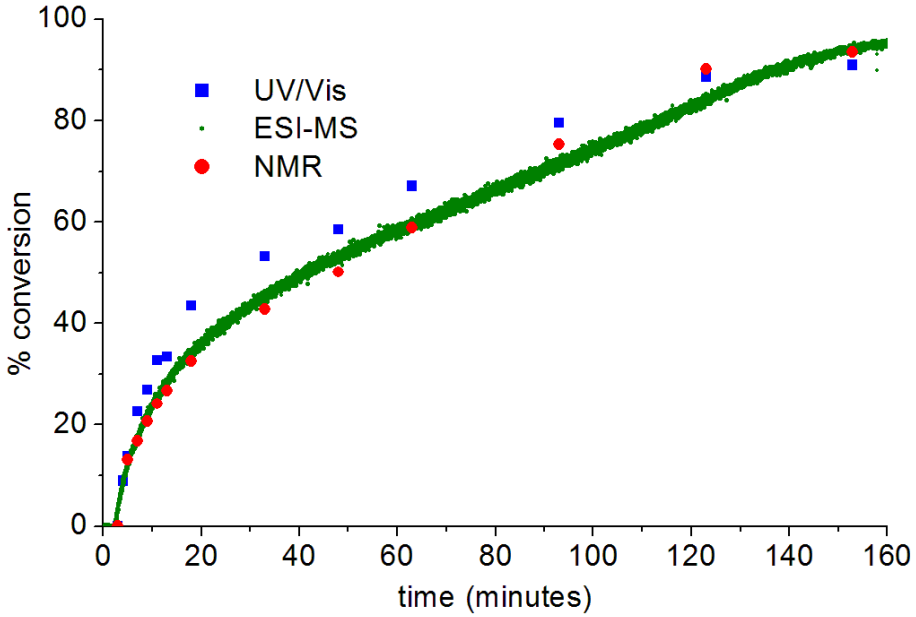

Figure 4.6: Appearance of $[PPh_3CH_2ArC_2Ar]^+$ PF_6^- as tracked by UV/Vis, ESI-MS and NMR.

For ESI-MS, trace data was collected every 1.1 seconds as the reaction mixture was sprayed continuously into the MS (over 9500 points in total); however, for the NMR and UV/Vis traces periodic sampling followed by work-up was required to obtain each data point. Consequently the number of data points for theses traces is drastically lower. The traces overlay well indicating that our sampling method is reliable.

4.2 An air- and moisture-free source

Despite running air- or moisture-sensitive samples directly from a glovebox into the mass spectrometer we still observed evidence of trace amounts of oxygen or water in the spectra of highly reactive samples. Since the source of an ESI-MS is designed to operate at atmospheric pressure and is not gas-tight, we hypothesized that if a very slight negative pressure existed in the source it could cause water and oxygen from the surrounding atmosphere to be drawn into the source where it could react with our sample. To test this theory a U-tube filled with water was connected to a port in the source housing. When the instrument was operating under standard conditions (cone gas = 100 L/h, desolvation gas = 100 L/h) we observed the water shift in the U-tube towards the side connected to the source. This indicates that a slight negative pressure does in fact exist within the source housing. A positive pressure was obtained when the combined gas flow from the cone gas and desolvation gas was set at or above 600 L/h; however, this is not a realistic solution to the problem since at these parameters the intensity of the analyte signal is low and fragmentation of fragile species is likely. A negative pressure in the source means that air is constantly being introduced into the instrument and this makes accurate analysis of highly air- or moisture-sensitive samples impossible. To address the problem, we designed a source housing which allows the inlet of the instrument to operate under a slight positive pressure of nitrogen (argon must not be used due to its low ionization energy and the possibility of sparks in the ESI source).

The standard housing for the source was replaced with one made from Plexiglas®, into which inlets were inserted for the introduction of gases and a pressure gauge was installed (Figure 4.7).

Under standard operating conditions, the gauge indicates that the pressure in the source is approximately -0.5 to -1 in. H_2O. By running additional nitrogen in through the source-housing inlet we can increase the pressure in the source without interfering with the sample spray. Typically an overpressure of 1 in. H_2O is used for analysis (an overpressure of 4 in. H_2O is used for purging the source beforehand). A valve was inserted into the exhaust line for the source so that the exhaust can be throttled or completely closed. This allows us to attain a positive pressure in the source without wasting excess nitrogen to maintain the positive pressure.

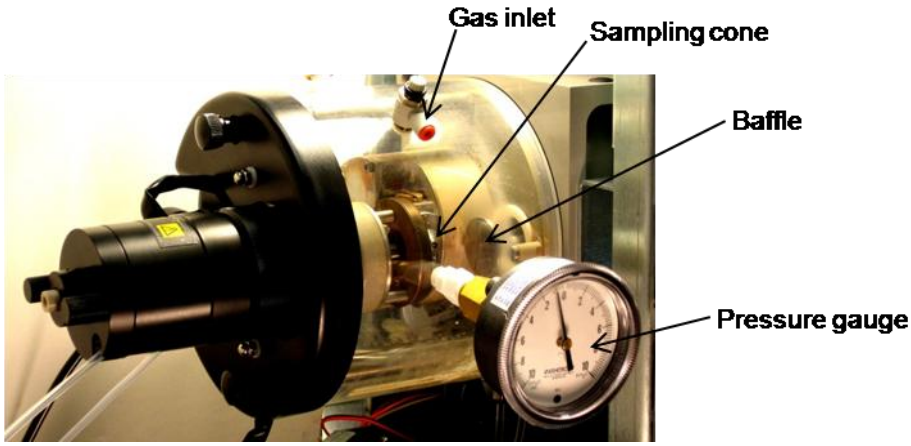

Figure 4.7: The modified source housing with gas inlet and pressure gauge.

To assess the effectiveness of these modifications a fluorobenzene solution containing $[Pd(PPh_3)_n(\mathbf{7})]^-$ (n = 1 - 3) was injected directly into the MS (from the adjacent glovebox) after the source had been purged with nitrogen for an hour. The source was then opened up to the air and a second spectrum was recorded. After purging with N_2 the major species was expected to be unoxidized $[Pd(PPh_3)_n(\mathbf{7})]^-$ (n = 1 or 2). After the source was opened to oxygen, we expected that the palladium complex would react with oxygen[171] to give $[PdO_2(PPh_3)(\mathbf{7})]^-$ as the major species. However, when precautions were taken to ensure the sample solution was completely oxygen free and the chromatography fittings used were flushed thoroughly with nitrogen the dominant species both before *and after* purging the source with nitrogen were the unoxidized $[Pd(PPh_3)_n(\mathbf{7})]^-$ (n = 1 or 2). This suggests that any reaction with oxygen in the source was not fast enough to significantly alter the results.

To confirm these findings, a second experiment was performed by Tyler Trefz (unpublished results) in which a highly air- and moisture-sensitive solution of MAO (methylaluminoxane) and tetrabutylammonium chloride in fluorobenzene was run both before and after purging the source with nitrogen. Again the solution was run directly from an adjacent glovebox into the source of the MS. While the spectrum for this highly reactive solution is complicated, the effect of source pressurization is obvious. Figure 4.8 (left) shows the spectrum acquired before source pressurization and Figure 4.8 (right) shows the spectrum acquired after purging with nitrogen. The major peaks in Figure 4.8 (right) (*m/z* 1261, *m/z* 1541, *m/z* 1811 and *m/z* 2115) correspond to various oligomers of MAO containing coordinated trimethylaluminum. The major peaks in the spectrum when the source is *not* purged with nitrogen (Figure 4.8, left) correspond to the same oligomers, but where one or two methyl groups have been replaced by OH groups due to reactivity with trace water vapour in the source. The resulting peaks are shifted by 2 or 4 Daltons respectively (*m/z* 1263, *m/z* 1543, *m/z* 1815 and *m/z* 2119). Starting with an unpressurized source, 20 minutes of purging with nitrogen was required to obtain the spectrum observed in Figure 4.8 on the right. The clear difference in these two spectra demonstrates the importance of source pressurization when the composition of highly air- or moisture-sensitive samples is being investigated.

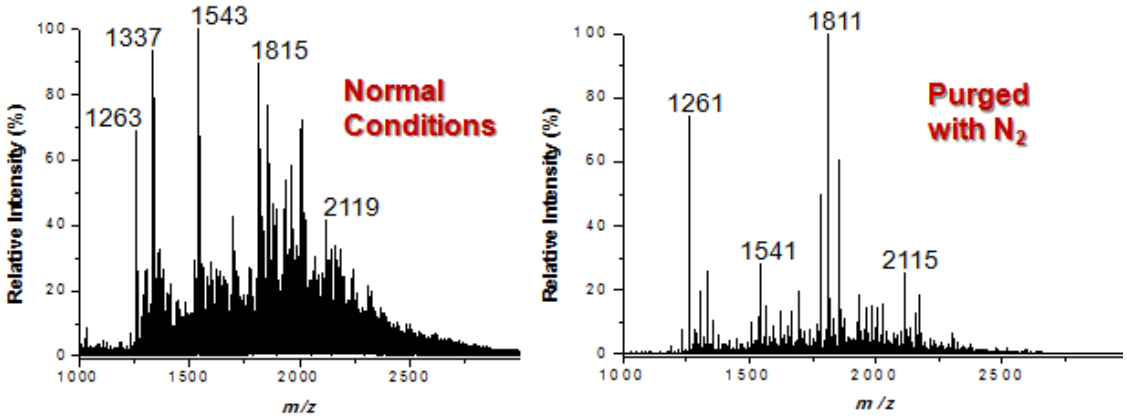

Figure 4.8: (left) MS spectrum of a fluorobenzene solution of MAO and terabutylammonium chloride under normal source conditions. (right) MS spectrum of a fluorobenzene solution of MAO and terabutylammonium chloride after purging the source with N_2 for 20 min.

Step-by-step instructions for how to set the source to operate under a positive pressure are provided in Appendix D.

4.3 In-source "dilution"

In many cases, samples are too concentrated to be submitted directly for ESI-MS analysis (concentrations less than 10^{-6} M are desirable). It is especially important that the concentration of the sample does not exceed the linear response range of the instrument if quantitative measurements or even relative comparisons between peaks will be performed. The standard method to address this concentration issue is to dilute the sample either on- or off-line before analysis, but for moisture-sensitive solutions this is not always a viable option. Even dry solvents contain trace amounts of water, and dilution with relatively large volumes of solvent may result in the complete decomposition of important, low-concentration reactive intermediates.

There is another possible location in which dilution can take place: in the source of the instrument. A "gas-phase dilution" can be performed by limiting the number of ions that proceed past the source into the reduced-pressure portion of the mass spectrometer. We accomplished this by hijacking a valve normally used to isolate the MS proper from the source during source cleaning. For normal operation this valve is left completely open and for cleaning it is completely closed; however, it can easily be adjusted to hold positions anywhere on a continuum between these two extremes. Taking advantage of this, we measured a rough relationship between signal intensity (number of ions reaching the detector) and "openness" of the isolation valve (Figure 4.9).

This relationship may be used to estimate the required position of the isolation valve in order to achieve appropriate signal intensity. Fine adjustments should be done on a case-by-case basis, and the exposed portion of the valve should be wiped clean before returning it to the open position at the end of the experiment.

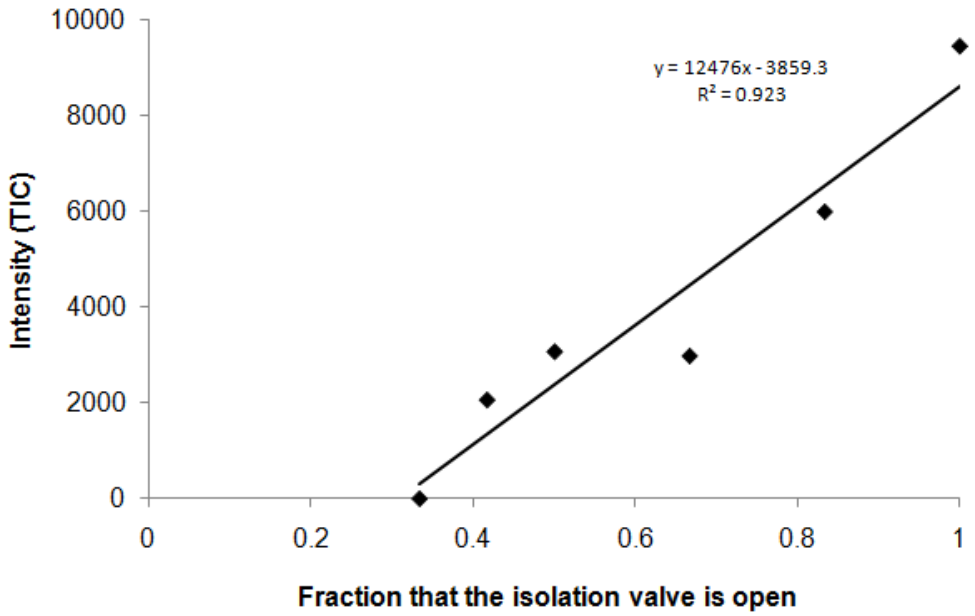

Figure 4.9: Determination of the relationship between overall MS signal intensity and the fraction that the isolation valve is left open.

A reduced signal may also be achieved by moving the ESI probe away from the entrance to the mass spectrometer, but there is one caveat: for a given set of experiments the position of the capillary tip at the end of the probe must remain constant because the intensity of each ion does not respond in the same way when the capillary is moved. Figure 4.10 illustrates this. There are two axes along which the ESI probe can be moved: towards or away from the baffle, and towards or away from the sampling cone (see Figure 4.7). Figure 4.10 below shows what happens to the intensity of two different ions ($(PPh_3)_2N^+$ and PPh_3Me^+) and the intensity of all ions being detected (TIC – total ion current) as the ESI probe is moved along each axis. The most important feature of this chromatogram occurs between 4.5 and 6.5 minutes during which the ESI probe is moved away from the baffle. Although the TIC and the intensity of the PPh_3Me^+ ion increase, the intensity of the $(PPh_3)_2N^+$ decreases. This implies that if the relative position of the ESI probe is not noted and held constant, inconsistent results may be obtained with respect to the relative signal intensities of different ions. Therefore, it is imperative that the position of the probe remain constant during experiments in which the relative intensities of different ions will be compared.

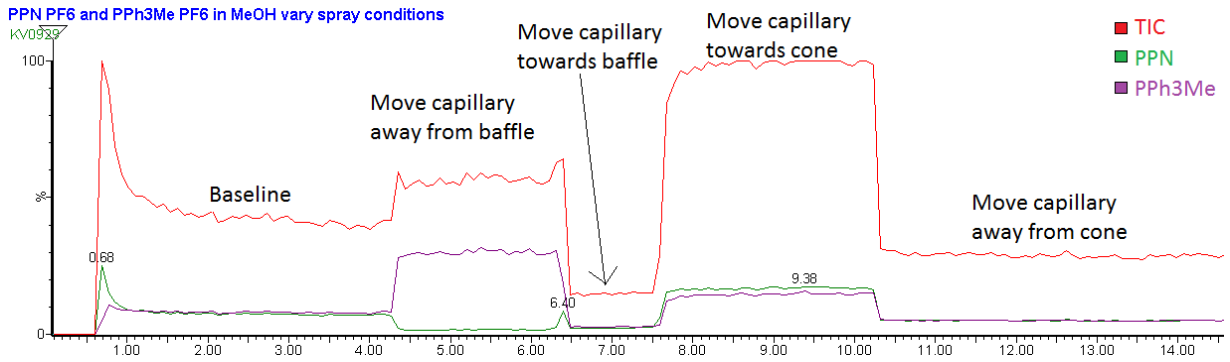

Figure 4.10: Experimental data demonstrating the effect of capillary (or ESI probe) position on various ions with respect to the positions of the sampling cone and baffle in the ESI source. y-axis: relative signal intensity, x-axis: time (min).

4.4 Experimental

General information

Reactions were performed under an inert atmosphere of N_2 using standard glovebox or Schlenk procedures. Except for triphenylphosphine (Alfa Aesar), triethylamine (ACP, Montreal, Quebec) and tetrakistriphenylphosphine palladium (Pressure Chemical Co.) chemicals were obtained from Aldrich and used without further purification. Solvents were HPLC grade and purified on an MBraun solvent purification system. Gases were obtained from Airgas (Calgary, Canada).

Mass spectrometry

All mass spectra were collected on a Micromass Q-TOF micro mass spectrometer using pneumatically assisted electrospray ionization. Capillary voltage: 2900 V. Cone voltage: 10 V. Extraction voltage: 0.5 V. Source temperature: 80 °C. Desolvation temperature: 150 °C. Cone gas flow: 100 L/h. Desolvation gas flow: 100 L/h. Collision voltage: 2 V. MCP voltage: 2700 V.

Flow rate determination experiments

Each student was assigned a tube length (45, 50, 55, 60 cm) and a solvent (water, acetonitrile, 50:50 water:acetonitrile, methanol, dichloromethane). Approximately 10 mL of the assigned solvent was placed into a Schlenk flask and the setup shown in Figure 4.2 was reproduced with

the PEEK tubing being forced through a pierced rubber septum. The pressure in the flask was adjusted to 0.5 or 1 psi. Once solvent began dropping into the collection flask a time and mass reading were recorded for each new drop. If the drops were falling too fast to record a reading for every drop, a reasonable time interval was selected and mass measurements were taken at each interval. At least ten readings were taken. The process was repeated at four more flask pressures in increments of 0.5 psi. Raw data was collected from all students and manipulated using Microsoft Excel.

Copper-free Sonogashira reaction monitored by ESI-MS, NMR and UV-Vis

Using PSI, a solution of $IArCH_2PPh_3PF_6$ (20 mL, 0.5 mM in methanol) was monitored by ESI-MS. To this solution phenylacetylene (1.3 μL, 12 μmol) and base (triethylamine or 1,8-diazabicyclo[5.4.0]undec-7-ene (DBU), 0.1 mmol) were added. 6% $Pd(PPh_3)_4$ (2 mL, 17 μM stock catalyst in THF) was added by syringe through the septum to initiate the reaction. The palladium tetrakis(triphenylphosphine) stock solution was stored in an inert atmosphere glovebox at -32 °C between uses. Overpressure in the flask was held at 2.5 psi throughout the reaction and the temperature was held at reflux throughout. The reaction mixture was diluted online en route to the MS with methanol at 10-20 μL min^{-1}. The diluted solution was split and flow rate to the mass spectrometer was approximately 0.5 μL min^{-1}. The flask was sampled periodically for UV/Vis and NMR analysis. **UV/Vis**: Samples of the reaction mixture were removed periodically via syringe (0.1 mL, one sample was taken before addition of catalyst), diluted 10× in methanol and analyzed by UV/Vis. **NMR**: Samples of the reaction mixture were removed periodically via syringe (1 mL, the initial sample was taken before addition of catalyst), sealed in glass vials and immediately frozen in liquid N_2. Solvent was removed by rotary evaporation and the remaining mixture was diluted with $CDCl_3$ and analyzed via ^1H NMR (300 MHz). The relative integrations of product and substrate peaks were used to determine the reaction progress.

ArC*H*$_2$PPh$_3^+$: substrate δ: 4.70 (d, 2H, $^2J_{HP}$ = 14 Hz); product δ: 4.76 (d, 2H, $^2J_{HP}$ = 14 Hz). **Ar protons *meta* to $CH_2PPh_3^+$:** substrate δ: 6.70 (dd, 2H, $^3J_{HH}$ = 8 Hz, $^4J_{HP}$ = 2 Hz). The signals for the corresponding protons on the product appeared at δ 6.93 (dd, 2H, $^3J_{HH}$ = 8 Hz, $^4J_{HP}$ = 2 Hz), but were not used for quantitative analysis because they were obscured by contaminants.

Source pressurization experiments

The MS source was purged with N_2 for 1 h and then kept at a positive pressure of 1 in. H_2O. The PEEK tubing connecting the MS source to a syringe inside the glovebox was also purged with N_2. In a glovebox, palladium tetrakis(triphenylphosphine) (3 mg, 2.6 μmol) and $[PPh_2C_6H_4SO_3]^-$ $[PPh_3NPPh_3]^+$ (1 mg, 1.1 μmol) were dissolved in fluorobenzene (10 mL, distilled over P_2O_5). The solution was then injected via syringe into the MS (10 μL min^{-1}) and a spectrum was acquired. The source was then opened to air and the solution was re-run while a second spectrum was acquired.

Isolation valve experiments

Palladium tetrakis(triphenylphosphine) (3 mg, 2.6 μmol) and **7**[PPN] (1 mg, 1.1 μmol) were dissolved in dichloromethane (10 mL). The solution was then injected via syringe into the MS (10 μL min^{-1}) and a spectrum was acquired with the isolation valve fully open, $1/6^{th}$, $2/6^{th}$, $3/6^{th}$, $7/12^{th}$, and $4/6^{th}$ closed.

Capillary position experiments

$[MePPh_3]^+[PF_6]^-$ (0.8 mg, 2 μmol) and $[PPN]^+[PF_6]^-$ (0.7 mg, 1 μmol) were dissolved in methanol (20 mL) and then diluted with methanol by a factor of 400. The diluted solution was placed in a Schlenk flask that was fitted with a septum. The flask was placed next to the ESI source and connected to it via a short length of PEEK tubing. The flask was pressurized to ~1 psi with N_2, data collection was initiated, and the PEEK tubing was submerged in the solution. The capillary was moved as described in Figure 4.10.

Chapter 5. Investigating the Mechanism of the Copper-Free Sonogashira Reaction

Portions of this chapter have been previously published, and are reproduced in part by permission of the Royal Society of Chemistry from "Direct observation of key intermediates by negative-ion electrospray ionisation mass spectrometry in palladium-catalysed cross-coupling" Krista L. Vikse, Matthew A. Henderson, Allen G. Oliver and J. Scott McIndoe, *Chem. Commun*., 2010, **46**, 7412-7414.

Portions of this chapter have been previously published, and are reproduced in part with permission from "Pressurized sample infusion for the continuous analysis of air- and moisture-sensitive reactions using electrospray ionization mass spectrometry" Krista L. Vikse, Michael P. Woods and J. Scott McIndoe, *Organometallics*, 2010, 29(23), 6615-18. Copyright ©2010 American Chemical Society.

With the suite of tools and methods described in Chapters 2 - 4 in hand, we were prepared to investigate a catalytic system. We chose the copper-free Sonogashira reaction as a test case because:

(1) Despite numerous efforts to study the copper-free Sonogashira reaction by conventional methods, the mechanism of the reaction is not well understood.
(2) The reaction employs phosphine ligands for which we have a charged analog.
(3) The reaction is homogeneous which allows direct sampling for MS analysis.
(4) The copper-free reaction has fewer reagents and is likely to be less complicated than the copper-containing version.

A brief introduction to the reaction and what is known of its mechanism is provided below.

5.1 Introduction

The palladium-catalyzed C-C bond-forming reaction between a terminal alkyne and an aryl or vinyl halide was reported independently in 1975 by Heck[172] and Cassar.[173] Both alkynylation procedures involved the use of a phosphine-containing catalyst, a base, and temperatures

between 40 °C and 100 °C. Just after these procedures were published, Sonogashira reported that addition of copper iodide as a co-catalyst allows the reaction to proceed at room temperature, and with improved yields in most cases (Scheme 5.1).[174]

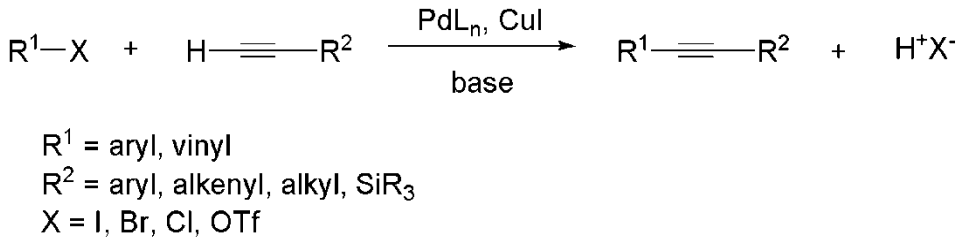

Scheme 5.1: The Sonogashira reaction.

This reaction has become the most commonly used tool for preparation of aryl and vinyl alkynes and is heavily used in the synthesis of natural products and pharmaceuticals;[175] however, recently there has been a shift away from using a copper co-catalyst. The reasons for this are twofold: (1) the copper additive is environmentally unfriendly and difficult to recover from the reaction, and (2) homo-coupling of the alkyne can become a significant side reaction.[176]

The Heck alkynylation reaction (commonly known as the copper-free Sonogashira reaction) addresses these concerns. It requires the use of a large excess of base (usually a secondary or tertiary amine) in place of copper to effect the reaction. The exact mechanism for the reaction is not well understood; however, it is presumed to occur in a fashion similar to other palladium-catalyzed cross-coupling reactions (Scheme 5.2). The general steps are: oxidative addition of an aryl or vinyl halide to an unsaturated palladium(0) catalyst (step 1), coordination of the acetylide to palladium (transmetallation) (steps 2 and 3), and reductive elimination of the product and regeneration of the catalyst (step 4).

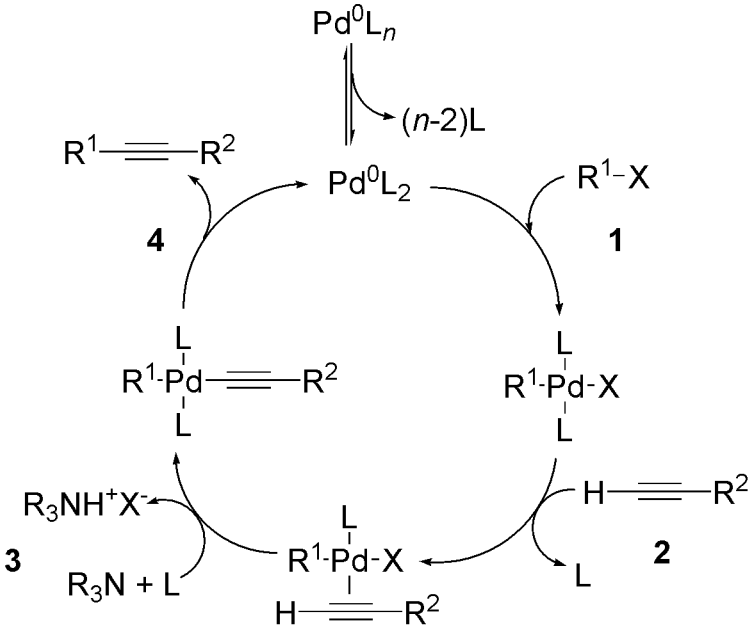

Scheme 5.2: A proposed mechanism for the copper-free Sonogashira reaction.[175] L = phosphine; X = halide; R^1 = aryl or vinyl; R^2 = aryl, alkenyl, alkyl or silyl; NR_3 = amine.

Recently there have been a number of efforts made to unravel the outstanding mechanistic details, but in some cases conflicting results have only raised more questions. A short summary of especially relevant works is provided here. For further discussion on the mechanism of the Sonogashira and the copper-free Sonogashira reactions the reader is directed to a recent comprehensive review by Chinchilla and Nájera.[175]

Amatore and Jutand, who have been principle contributors in this area, suggest that in addition to and superseding the canonical Pd-catalyzed cross-coupling mechanism shown above (Figure 1), an anionic mechanism may be in effect.[177] Electrochemical and NMR techniques were used to identify anionic tricoordinate Pd(0) and pentacoordinate Pd(II) species in which the anion bound to palladium was an acetate (from a $Pd(O_2C_2H_3)_2$ pre-catalyst) or halide ion (from R^1-X or a $PdCl_2$ pre-catalyst). These species dominate when there are "free" (not ion-paired) anions in solution, and they can have a strong effect on the kinetics of oxidative addition and the reactivity of Pd(II) species with the alkyne reactant or other nucleophiles in general.

A study published in 2004 using amperometry monitored the oxidation of Pd(0) during a Sonogashira reaction and demonstrated that the terminal alkyne can play multiple roles in

determining reaction efficiency.[178] Aside from coordinating with palladium in the transmetallation step, the alkyne can also coordinate to the $Pd(0)L_2$ active catalyst thus producing a species that is non-reactive, or only slowly reactive towards oxidative addition. In cases where transmetallation is the rate-determining step lowering the rate of oxidative addition improves the overall efficiency of the reaction. However, when oxidative addition is rate-determining (such as when $X = Cl^-$ or Br^-), alkyne coordination to the active catalyst is detrimental.

Transmetallation follows the oxidative addition step and is the least understood step in the cycle. The species bearing both carbon fragments that will reductively eliminate to form product is traditionally called the 'transmetallated intermediate' because in most palladium-catalyzed cross-coupling reactions the second carbon fragment is transferred from another metal onto palladium (for example in the Stille reaction it is tin, in the Kumada reaction it is magnesium, and in the Sonogashira reaction it is copper). Although there is no transmetallation reagent in the copper-free Sonogashira coupling the nomenclature is still used.

The difficulty in understanding the mechanism of the transmetallation step in this reaction stems from the fact that, in almost all cases, the base employed in the reaction is not strong enough to deprotonate the alkyne in solution. So how is σ-coordination of the terminal alkyne to palladium achieved? Two possibilities have been presented. There is a general consensus that first there must be coordination of the alkyne to the palladium in an η^2-fashion. From there the reaction could proceed by carbopalladation and base-assisted β-hydride elimination[172, 179] or deprotonation of the alkyne by base followed by reductive elimination.[180]

Through NMR studies Amatore et al. identified both the *trans*- and *cis*- product of carbopalladation when reacting $EtO_2C\text{-}C{\equiv}CH$ with *trans*-$PhPdI(PPh_3)_2$ and thus argued for a carbopalladation mechanism (Scheme 5.3, A). The carbopalladation was regeospecific with the favoured product having -$PdI(PPh_3)_2$ on the more hindered carbon of the alkyne and -Ph on the less hindered one. The *trans*-product was favoured over the *cis*-product in a ratio of 64:36.[179] A later paper published by Ljungdahl et al.[180] cast doubt on a carbopalladation mechanism by showing that hydride elimination to expel the product did not occur under typical reaction conditions. They argued in favour of a rate-determining step that involves deprotonation of the

alkyne coordinated to palladium and proposed two possible deprotonation pathways. The first was an anionic pathway (Scheme 5.3, B1) in which the neutral complex $Pd^{II}(PPh_3)(R^1)(X)(\eta^2\text{-}HC{\equiv}CR_2)$ is deprotonated to give an anionic palladium intermediate. The second was a cationic pathway (Scheme 5.3, B2) in which the same neutral complex undergoes ligand exchange (replacing the halide with a neutral amine ligand) to form a cationic complex. The cationic complex is then deprotonated by an external base to form a neutral intermediate. A Hammett correlation study suggested that for electron-rich alkynes pathway B2 is favoured and for electron-poor alkynes pathway B1 is favoured.

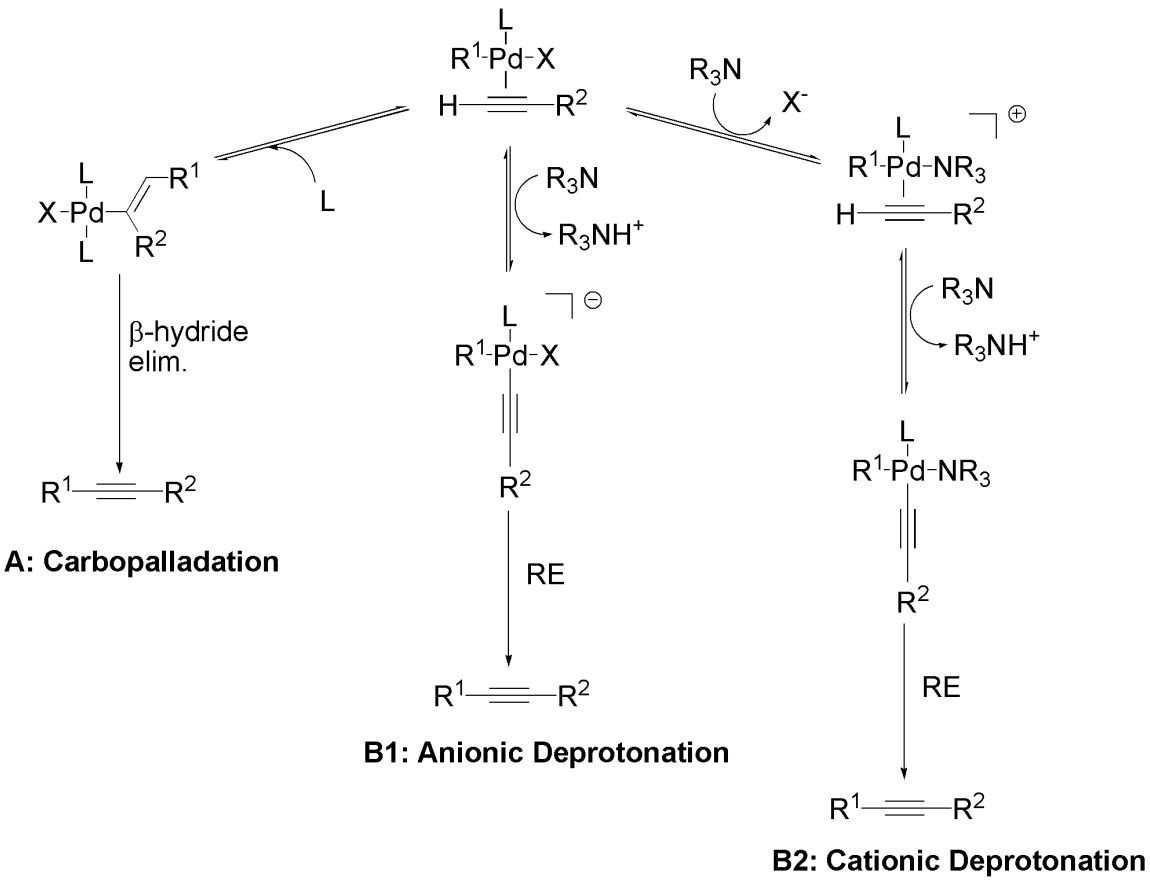

Scheme 5.3: Proposed mechanisms for activation of a terminal alkyne in the copper-free Sonogashira reaction. L = phosphine; X = halide; R^1 = aryl or vinyl; R^2 = aryl, alkenyl, alkyl or silyl; NR_3 = amine.

Amine bases have also been shown to participate in other parts of the catalytic cycle. Secondary amines can compete with terminal alkynes for coordination to $Pd^{II}L_2(R^1)(X)$.[181, 182] When L = PPh_3, substitution of L for alkyne is the dominant pathway but when L = $AsPh_3$, substitution of L for amine is more favourable. The authors suggest that this may be the

underlying reason for why reactions with $AsPh_3$ as the ligand are less efficient. An equilibrium has also been shown to exist at the beginning of the catalytic cycle where an amine takes the place of a phosphine ligand to give $Pd^0(PPh_3)$(amine). $Pd^0(PPh_3)$(amine) may then be the true active catalyst when amines are used, and indeed Jutand et al. found that in the presence of amines the oxidative addition of iodobenzene to Pd(0) was faster.[181]

Finally, a theoretical study was recently published in which the effects of phosphine ligands on reductive elimination were investigated.[183] There has been some question as to whether reductive elimination occurs from a four-coordinate palladium intermediate or whether ligand dissociation to a T-shaped, three-coordinate species occurs before reductive elimination. Triphenylphosphine demonstrated good reactivity in both pathways indicating that both pathways may be operating to some extent or that other factors may influence which pathway dominates.

It is clear from recent literature that there is still much work to be done. The mechanism by which the terminal alkyne is installed on palladium is unknown, and even the exact details of final product formation are under scrutiny. We have learned that it is important to consider the potential effects of all species present in the reaction vessel; for example, coordination of alkyne, amine or halide to the catalyst in place of the classical phosphine or arsine ligands at any stage in the cycle can lead to inactive or highly active palladium species that must be considered. In addition, since most of the techniques used to study these processes under normal reaction conditions lack the ability to provide detailed structural information on the proposed catalytic intermediates the identities of these intermediates discussed above have only been inferred. With this background in mind we began investigating the various processes and species involved in the copper-free Sonogashira reaction using ESI-MS.

5.2 The catalyst

Initially we focused on the catalyst. The classically proposed active catalyst for the copper-free Sonogashira reaction, and in fact for most palladium-catalyzed carbon-carbon bond-forming reactions,[184, 185] is the unsaturated bis(phosphine)palladium complex $Pd^0(PPh_3)_2$. While this

Pd(0) species has been generally accepted as the active catalyst, to our knowledge it has never been directly observed under standard reaction conditions -though other $Pd(PR_3)_2$ species have been, particularly where the phosphine is bulky, e.g. $Pd(P^tBu_3)_2$. To this end a dichloromethane solution of equimolar amounts of $Pd(PPh_3)_4$ and [**7**][PPN] was prepared and analyzed by ESI(-)-MS. Preparation of the solution and injection into the MS was performed in a glovebox connected directly to the MS via a short length of nitrogen-purged PEEK tubing to avoid reaction with oxygen. The resulting spectrum is shown in Figure 5.1. The proposed active catalyst is directly observed at *m/z* 709.0, where one of the labile triphenylphosphine ligands has been replaced by the charged phosphine ligand **7**. The solution is composed mostly of the precatalyst bearing three phosphine ligands (*m/z* 971.1) and the fully coordinated palladium species with four phosphine ligands is not observed. This is consistent with the expected behaviour of palladium tetrakis(triphenylphosphine) in solution.[186]

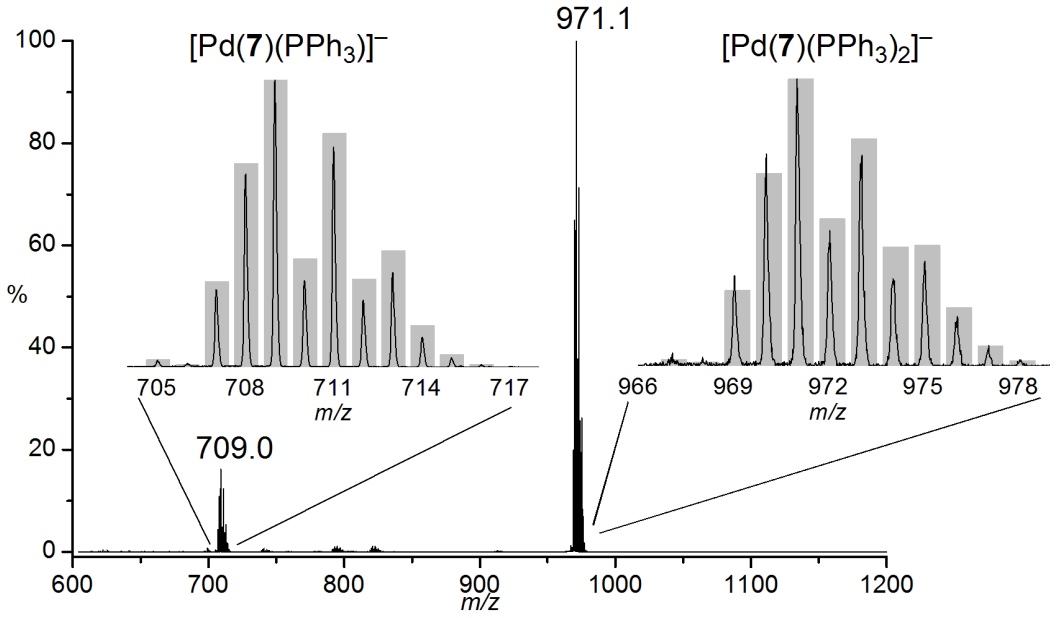

Figure 5.1: ESI(-)-MS of a dichloromethane solution of equimolar amounts of $Pd(PPh_3)_4$ and [**7**][PPN]. Cone voltage = 10 V. Insets: black lines = experimental signals, grey bars = calculated isotope patterns.

If the solution is analyzed again after it is allowed to age, a new spectrum is obtained which contains peaks corresponding to association of oxygen (*m/z* 741), chlorine (*m/z* 780) and dichloromethane (*m/z* 795) to the active catalyst (Figure 5.2). An MS/MS experiment, performed

on the peak corresponding to $[Pd(\mathbf{7})(PPh_3) + CH_2Cl_2]^-$, reveals that the complex fragments by loss of triphenylphosphine. Loss of dichloromethane does not occur (Figure 5.3). This strongly suggests that oxidative addition (OA) of one of the carbon-chlorine bonds in dichloromethane has occurred to give the signal at *m/z* 795 and the signal is not the result of simple association of CH_2Cl_2 to the metal complex.

Oxidative addition of dichloromethane to the catalyst was a surprising result since it is known to be a relatively difficult reaction,[187] so the experiment was repeated using deuterated dichloromethane to validate our assignment of the signal. The isotope pattern match for the signals in both experiments is excellent (Figure 5.2) and confirms our assignment. This type of reactivity is known for $Pd(PCy_3)_2$ and $(P^tBu_2H)_2$ with dichloromethane.[188, 189] The observed association with oxygen at *m/z* 471.1 is also known,[171] and the MS/MS experiment that was performed on this species shows fragmentation to regenerate the active catalyst at low collision voltages (~5 V) which suggests that the coordination of oxygen is a reversible process. Oxidative addition of dichloromethane and coordination of trace amounts of oxygen to $Pd(PPh_3)_2$ are both excellent indications of the high reactivity of this unsaturated Pd(0) species.

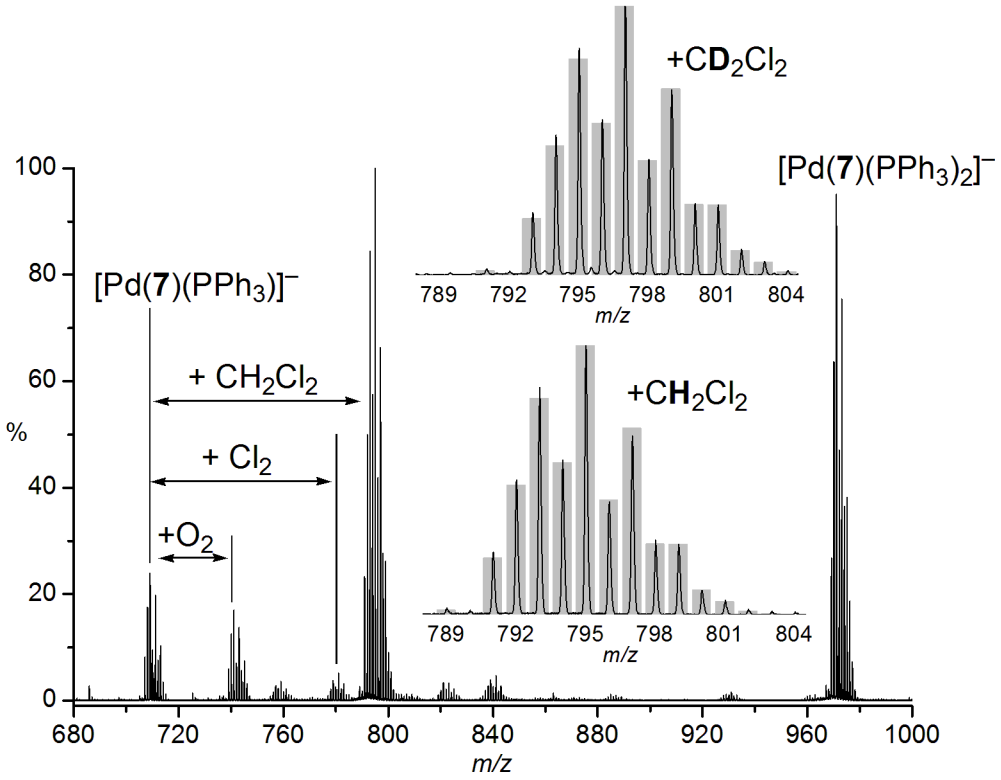

Figure 5.2: ESI(-)-MS of an aged solution of $Pd(PPh_3)_4$ + [**7**][PPN] in dichloromethane. The inset shows the isotope pattern match for $[Pd(\mathbf{7})(PPh_3) + CH_2Cl_2]^-$ and $[Pd(\mathbf{7})(PPh_3) + CD_2Cl_2]^-$ (black line = experimental, grey bars = calculated).

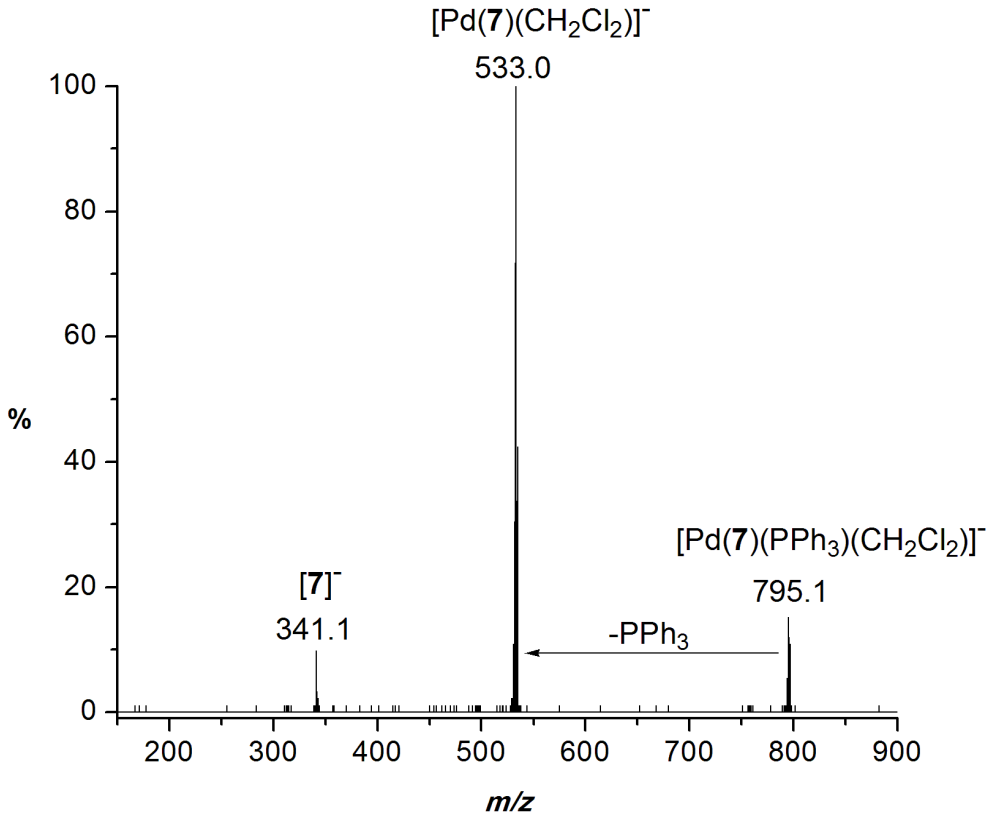

Figure 5.3: ESI(-)-MS/MS of $[Pd(\mathbf{7})(PPh_3)(CH_2Cl_2)]^-$ (*m/z* 795.1). Fragmentation occurs via loss of triphenylphosphine not loss of dichloromethane indicating that dichloromethane has oxidatively added to palladium and the species is most accurately represented as $[Pd(\mathbf{7})(PPh_3)(CH_2Cl)(Cl)]^-$.

To further define the oxidative addition of CH_2Cl_2 by palladium, the process was monitored over time by PSI-ESI-MS in refluxing dichloromethane (40 °C) and doped with the charged ligand [**7**][PPN] (Figure 5.4). Disappearance of $[Pd^0(\mathbf{7})(PPh_3)_n]^-$ (n = 1, 2) occurred as a first-order process with a half life of 10.7 minutes and the major product was $[Pd^{II}(\mathbf{7})(PPh_3)_n(Cl)(CH_2Cl)]^-$ (n = 0, 1). $[Pd(PPh_3)(\mathbf{7}) + (CHCl)]^-$ and $[Pd^{II}(\mathbf{7})(PPh_3) + Cl_2]^-$ were observed as byproducts and their formation appears to be related since the intensities of their signals change in the same way throughout the reaction. The Pd(0) species disappears faster than the Pd(II) appears; perhaps because the Pd(II) species are decomposing further. There is evidence for this at reaction times greater than 40 min as the trace for $[Pd^{II}(\mathbf{7})(PPh_3)(Cl)(CH_2Cl)]^-$ begins to drop off. No new palladium-containing species are observed so any products of this further decomposition must be neutral.

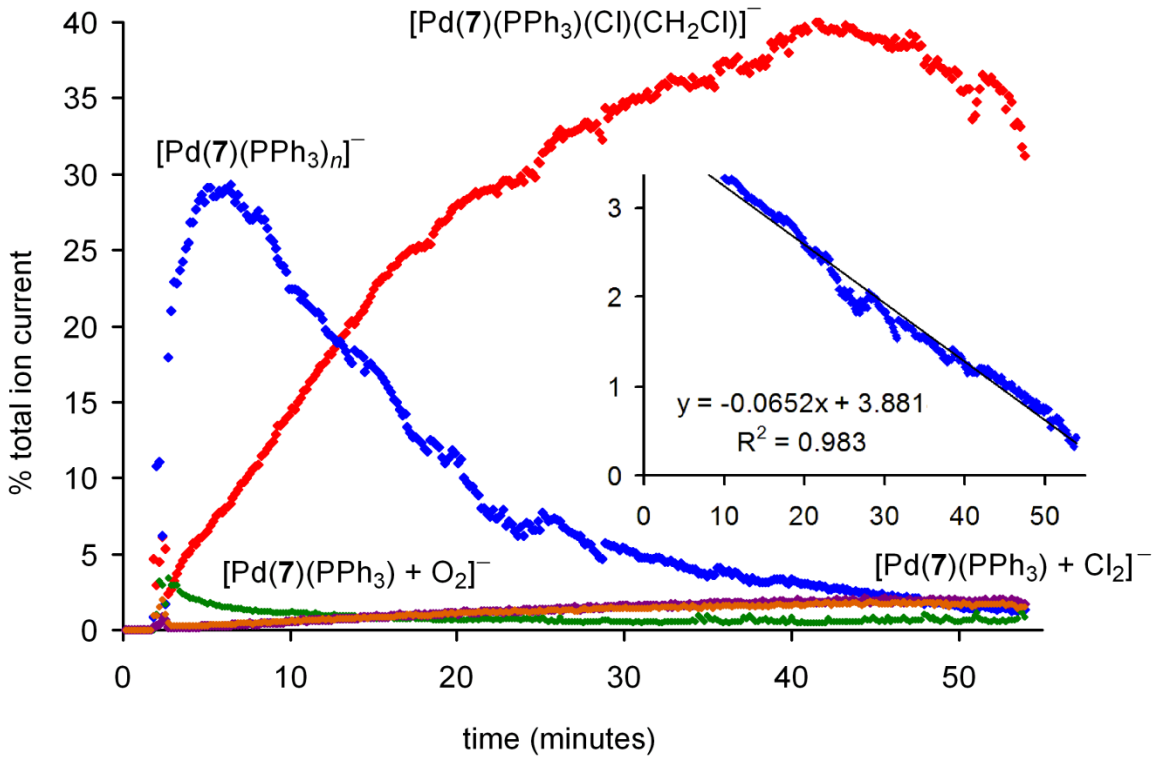

Figure 5.4: ESI(-)-MS intensities of palladium-containing signals as a percentage of the total ion current (*m/z* 400 -1500) for a solution of $Pd(PPh_3)_4$ and [**7**][PPN] in CH_2Cl_2 at 40 °C. $[Pd^0(\mathbf{7})(PPh_3)_n]^-$ is shown in blue and $[Pd^{II}(\mathbf{7})(PPh_3)(Cl)(CH_2Cl)]^-$ is shown in red. Small amounts of $[Pd(\mathbf{7})(PPh_3) + (CHCl)]^-$ (orange), $[Pd^{II}(\mathbf{7})(PPh_3) + Cl_2]^-$ (violet), and $[Pd^{II}(\mathbf{7})(PPh_3)(O)_2]^-$ (green) are also observed. Inset: plot of $\ln([Pd^0(\mathbf{7})(PPh_3)_n]^-)$ vs. *t*.

A calculation-based study has recently been published proposing that the true active catalyst for palladium-catalyzed carbon-carbon bond-forming reactions is in fact $Pd(PPh_3)$ and not the more traditionally invoked $Pd(PPh_3)_2$.[190] With a charged version of the catalyst in hand we decided to investigate the difference in reactivity between $Pd(PPh_3)$ and $Pd(PPh_3)_2$ in the gas phase. As stated earlier, only signals corresponding to $[Pd(\mathbf{7})(PPh_3)]^-$ and $[Pd(\mathbf{7})(PPh_3)_2]^-$ were observed by ESI-MS using our standard source parameters; however, $[Pd(\mathbf{7})]^-$ can easily be generated in the gas phase by increasing the energy that is imparted to the ions as they are sprayed into the MS. The parameter that controls this is the cone voltage and by increasing it to 35 V (from 10 V) a spectrum is obtained that includes both species of interest (Figure 5.5). Palladium bearing a single charged phosphine ligand appears at *m/z* 446.9 alongside the

bisphosphine complex at *m/z* 709.0. The other signals observed correspond to ions that do not contain palladium.

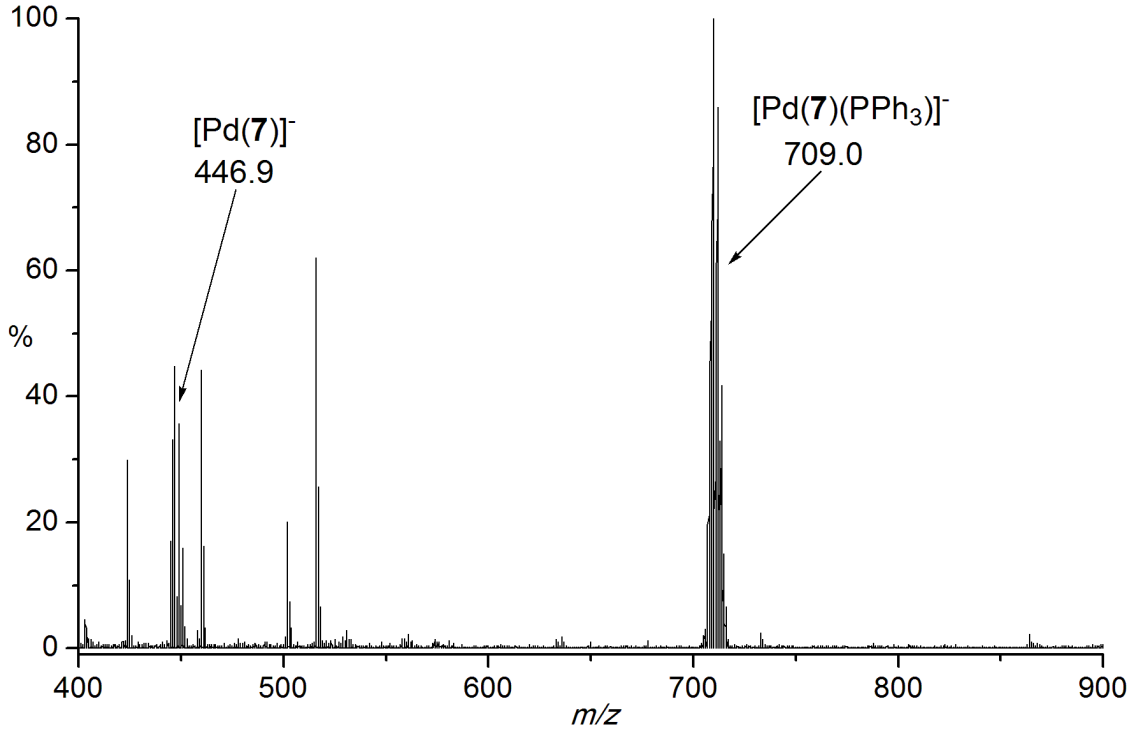

Figure 5.5: ESI(-)-MS of $Pd(PPh_3)_4$ and [**7**][PPN] in fluorobenzene. Cone voltage = 35 V.

To test the reactivity of these species, iodomethane was introduced as a gas into the source of the mass spectrometer while a solution of the catalyst in fluorobenzene was simultaneously being injected. The spectrum from the resulting in-source ion/molecule reactions is shown below (Figure 5.6). Two major new palladium-containing species are observed; the first at *m/z* 588.8 corresponds to oxidative addition of iodomethane to $[Pd(\mathbf{7})]^-$. MS/MS of this peak shows that the species initially fragments by loss of *m/z* 200. This is consistent with loss of PPh_2Me due to rearrangement of groups on palladium and phosphine leaving $[Pd(I)(C_6H_4SO_3)]^-$ (*m/z* 389) behind. These types of rearrangements are known to occur for palladium catalysts with phosphine ligands through a reductive elimination/oxidative addition mechanism involving the formation of phosphonium ion intermediates (Scheme 5.4).[191, 192]

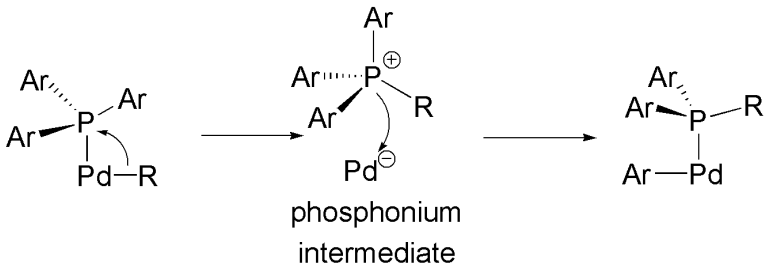

Scheme 5.4: Reorganization of a phosphine ligand on palladium via a reductive elimination/oxidative addition reaction mechanism.

The observed reorganization of the phosphine ligand, and the lack of a fragmentation pathway for loss of CH_3I provide strong evidence that oxidative addition of iodomethane to palladium has occurred, not simply weak association of iodomethane.

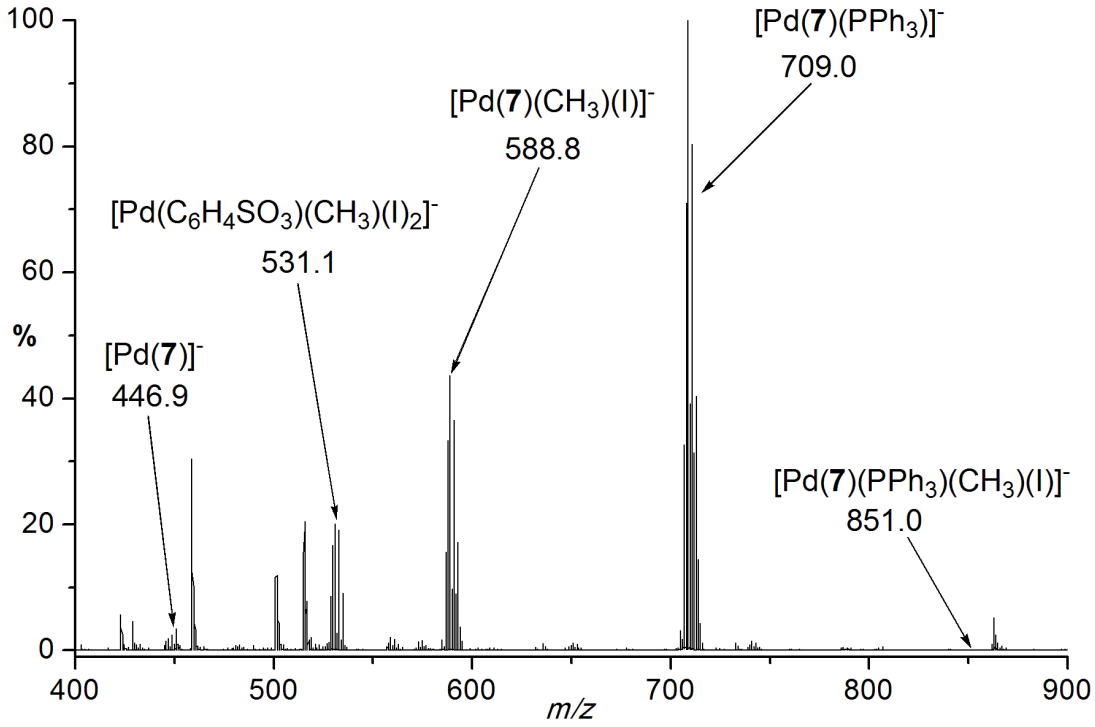

Figure 5.6: ESI(-)-MS of $Pd(PPh_3)_4$ and [**7**][PPN] in fluorobenzene. Iodomethane was introduced into the source as a reagent in a stream of N_2 gas. Cone voltage = 35 V.

The other new palladium-containing species at *m/z* 531.1 is consistent with $[Pd(I)_2(CH_3)(C_6H_4SO_3)]^-$; a byproduct of the reactivity in the source (MS/MS of this signal

shows fragments for loss of ICH_3 (142 Da) and Pd (106 Da). Somewhat surprisingly there is no signal that corresponds to oxidative addition of iodomethane to the bisphosphine complex $[Pd(\mathbf{7})(PPh_3)]^-$; it would appear at *m/z* 851.0. While more than 90% of $[Pd(\mathbf{7})]^-$ is observed to react, less than 0.1% of $[Pd(\mathbf{7})(PPh_3)]^-$ does the same, indicating that the monophosphine complex is more than 10,000 times more reactive towards oxidative addition!

It is possible that oxidative addition of iodomethane to $[Pd(\mathbf{7})(PPh_3)]^-$ does in fact occur, but that loss of PPh_3 happens immediately after the oxidative addition so only $[Pd(\mathbf{7})(I)(Me)]^-$ is observed in the spectrum. However, a qualitative look at the spectrum after addition of iodomethane shows $[Pd(\mathbf{7})(PPh_3)]^-$ is still the dominant peak whereas the signal for $[Pd(\mathbf{7})]^-$ has almost completely disappeared suggesting that $[Pd(\mathbf{7})(PPh_3)]^-$ is not being transformed into something else. These results are consistent with the results from the theoretical paper which states that oxidative addition is more likely to occur to a palladium center bearing only one phosphine ligand. The reaction was repeated using iodoethane and iodobutane as reagent gases, but no oxidative addition was observed in these cases (probably due to a lack of volatility of these reagents: b.p. 72 °C and 130 °C vs. 42 °C for MeI).

After examining solution- and gas-phase reactivity of palladium tetrakis(triphenylphosphine), we moved on to systematically investigating the mechanism of the copper-free Sonogashira reaction by adding the required reagents one at a time and examining the effect that each one had on the reaction mixture. Various types of MS experiments were employed and the following is a detailed description of those studies.

5.3 Oxidative addition

Upon addition of an aryliodide, specifically iodotoluene, to a dichloromethane solution containing catalytic amounts of $Pd(PPh_3)_4$ and [**7**][PPN] at room temperature, all peaks corresponding to Pd(0) species were immediately replaced by one dominant palladium-containing signal at *m/z* 927.1. This signal corresponds to the palladium catalyst which has undergone oxidative addition: $[Pd(PPh_3)(\mathbf{7})(C_6H_4Me)(I)]^-$ (Figure 5.7). Similar species were

observed when a series of *para*-substituted aryl iodides were tested (*p*-IC_6H_4R. R = CH_3, H, OCH_3, NH_2, NO_2, CN, F, CF_3, and $COCH_3$). When subjected to CID these complexes decompose exclusively via loss of [**7**]$^-$ or triphenylphosphine, consistent with oxidative addition of the aryl iodide to palladium.

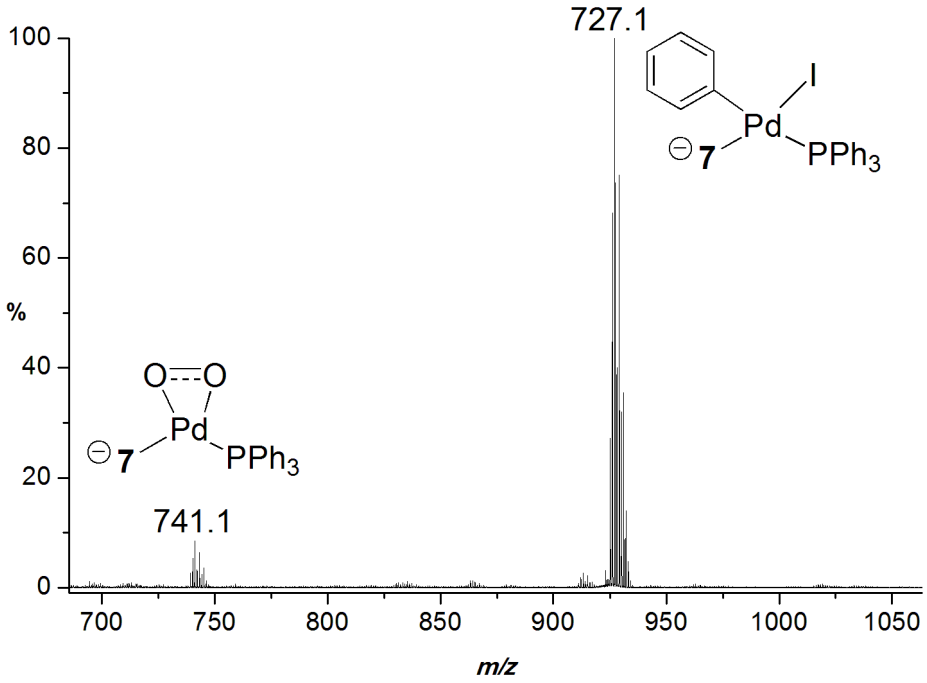

Figure 5.7: ESI(-)-MS of PhI, $Pd(PPh_3)_4$ and [**7**][PPN] in dichloromethane.

Figure 5.8 shows the oxidative addition reaction with iodotoluene over time as monitored by PSI-MS. The summed intensity of the signals corresponding to Pd(0)-type species (blue) and the intensity of the signal representing the oxidative addition intermediate (red) are both plotted with respect to time. Addition of iodotoluene occurred at approximately 15.6 minutes and oxidative addition was almost instantaneous. This high reactivity is expected since aryl iodides are known to undergo oxidative addition to palladium very rapidly.[193] The presence of a signal for free iodide (*m/z* 126.9) after addition of iodotoluene provides further evidence of oxidative addition.

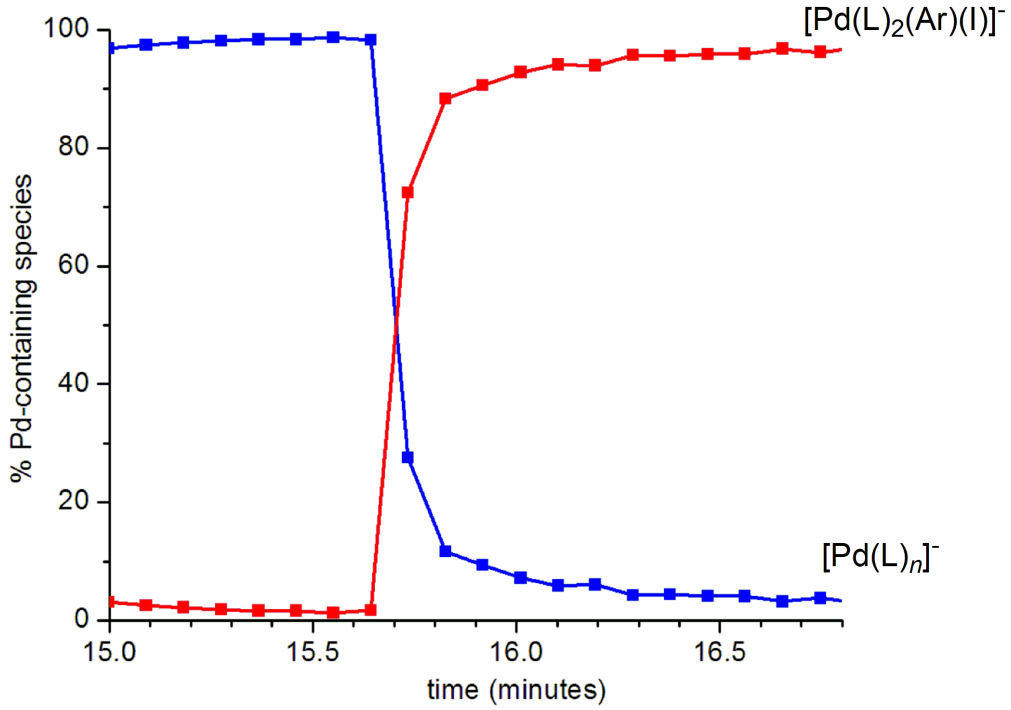

Figure 5.8: Oxidative addition of iodotoluene to palladium as monitored over time by PSI-MS. L = PPh_3 or 7 (n = 2, 3), Ar = C_6H_4Me.

We looked for evidence of anionic intermediates of the type proposed by Amatore and Jutand (tricoordinate $[Pd^0L_2I]^-$ or pentacoordinate $[Pd^{II}L_2(Ar)(I)_2]^-$ where L = triphenylphosphine) but none were observed when the charged tag **7** was present, or when no charged tag was employed. In fact, in the absence of a charged tag no palladium-containing species were observed at all (Figure 5.15), demonstrating the necessity of a charged tag for these experiments.

5.4 Coordination of alkyne

Addition of a terminal alkyne (phenylacetylene) to the aforementioned solution containing catalyst and aryl iodide resulted in the formation of a new set of peaks centered at *m/z* 887.1. This signal corresponds to the palladium complex in which both carbon fragments that eventually join to form the product are σ-bound to palladium: $[Pd(PPh_3)(\mathbf{7})(Ph)(C_2Ph)]^-$ (Figure 5.11).

The most commonly proposed mechanism for coordination of the terminal acetylene to palladium involves initial η^2-coordination of the terminal alkyne through the triple bond, which makes the terminal proton more acidic and allows for deprotonation by amine to give the σ-bound acetylide. This initial coordination of the alkyne is theoretically required since the pK_a values for most of the bases employed in this reaction indicate that they are not strong enough to deprotonate phenylacetylene directly (e.g. the pK_a of phenylacetylene is 28.8 in DMSO at 25 °C[194] and the pK_a of triethylamine is 9.0 at 25 °C in DMSO[195]). When we investigated a solution of $Pd(PPh_3)_4$ + [**7**][PPN] + PhI + PhC_2H in CH_2Cl_2, no evidence of any species in which phenylacetylene is bound to palladium in an η^2-fashion could be observed. We hypothesized that these types of species may be too fragile to survive the ESI process.

To test whether the formation of η^2-acetylene adducts could be observed in the gas phase a dichloromethane solution containing the catalyst, charged ligand and phenyl iodide was subjected to analysis. The collision cell of the MS was saturated with acetylene, and in two separate experiments the peaks corresponding to $[Pd(\mathbf{7})(PPh_3)(Ph)(I)]^-$ and $[Pd(\mathbf{7})(Ph)(I)]^-$ were isolated in the quadrupole and allowed to undergo ion/molecule reactions with acetylene in the collision cell. The resulting ions were separated by the TOF analyzer and detected.

No acetylene was observed to coordinate to $[Pd(\mathbf{7})(PPh_3)(Ph)(I)]^-$; however, for the species with one less phosphine ligand, $[Pd(\mathbf{7})(Ph)(I)]^-$, three new signals were observed after reaction with acetylene. A small peak at *m/z* 677.1 corresponds to the acetylene adduct $[Pd(\mathbf{7})(Ph)(I)(HC_2H)]^-$ (Figure 5.9). The two other new peaks present in the spectrum are a result of acetone and PH_3 coordinating to $[Pd(\mathbf{7})(Ph)(I)]^-$ (*m/z* 709.2 and 685.1 respectively). Acetylene gas is dissolved in acetone when stored in pressurized tanks and it is always contaminated with small amounts of PH_3 gas.[196] We were unable to obtain a source of acetylene gas that did not contain these components. From the spectrum below it appears that acetone is a much better ligand for this palladium complex than acetylene.

The gas-phase reaction of acetylene with $[Pd(\mathbf{7})(Ph)(I)]^-$ was performed using very low collision voltages (1 V). Above a collision voltage of 2 V the peak representing acetylene coordination disappeared. This confirmed that acetylene coordination to $[Pd(\mathbf{7})(Ph)(I)]^-$ is indeed

a very fragile one, and if it occurs in solution the ESI process is energetic enough to cause alkyne dissociation.

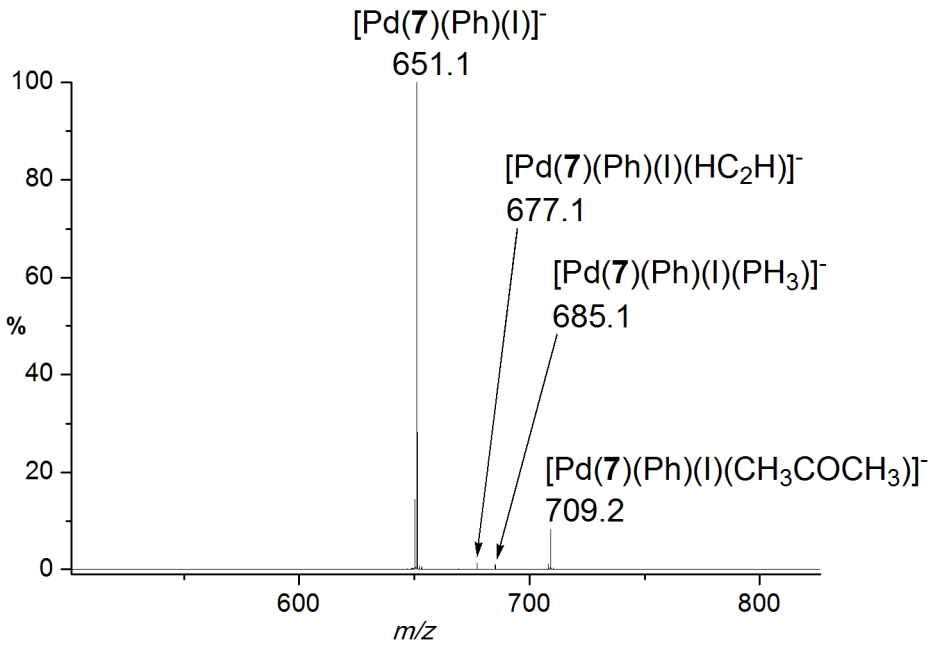

Figure 5.9: ESI(-)-MS/MS of the signal at *m/z* 651.1 with an acetylene-saturated collision cell and low collision voltage (1 V).

We also analyzed a dichloromethane solution of just catalyst, charged ligand and acetylene to test for acetylene adducts in the absence of iodobenzene and we did in fact observe coordination of phenylacetylene. The signal at *m/z* 811.2 represents $[Pd(\mathbf{7})(PPh_3)(HC_2Ph)]^-$ (Figure 5.10). The MS/MS experiment on *m/z* 811.2 showed complete fragmentation to the active catalyst $[Pd(\mathbf{7})(PPh_3)]^-$ (*m/z* 709.0) even at very low collision voltages confirming that acetylene coordination is very weak.

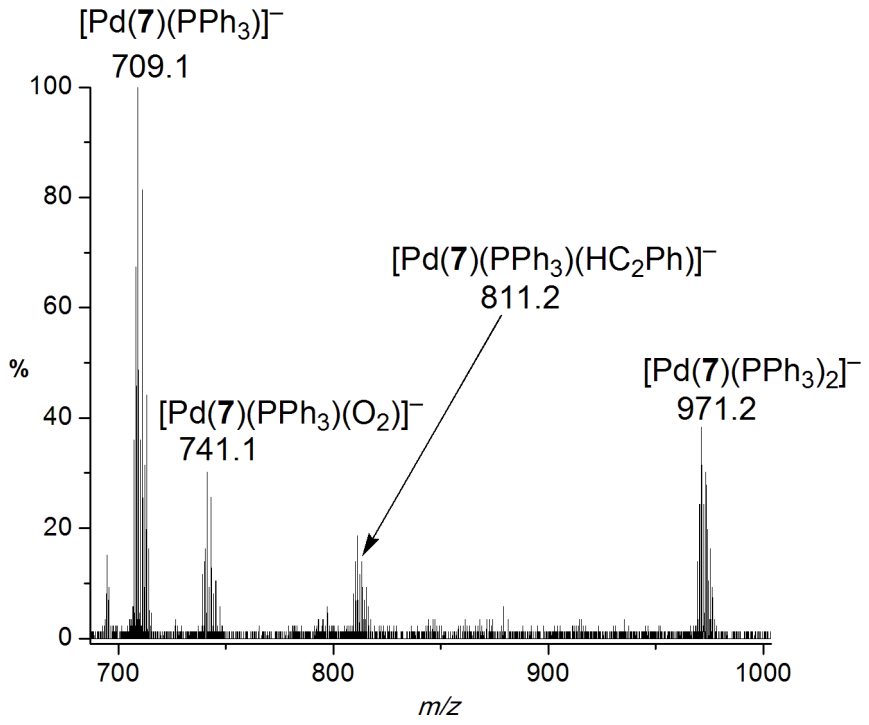

Figure 5.10: ESI(-)-MS of a dichloromethane solution containing $Pd(PPh_3)_4$, [**7**][PPN], and PhC_2H. The signal at *m/z* 811.2 corresponds to phenylacetylene coordinating in an η^2-fashion to $[Pd(\mathbf{7})(PPh_3)]^-$.

We expected the transmetallated intermediate (TM) that we observed at *m/z* 887.1 (Figure 5.11) to be much more robust since the phenylacetylene has already been deprotonated and is sigma-bound to palladium, and we found this was the case. MS/MS of the signal at *m/z* 887.1 fragments via loss of one of the phosphine ligands and not loss of the acetylene unit. Surprisingly this transmetallated species is observed not only when base is present, but also in the absence of any added base. This observation is in conflict with the proposed mechanisms **B1** and **B2** in Scheme 5.3 which require the presence of base to deprotonate the terminal acetylene; however it does not exclude the possibility that a carbopalladation mechanism (Scheme 5.3 **A**) is active.

5.5 The role of base

Standard reaction conditions for the copper-free Sonogashira reaction call for a large excess of base, and often the reaction is done in neat base. When we added one equivalent or a ten-fold

excess of a tertiary amine (triethylamine) to a dichloromethane solution of $Pd(PPh_3)_4$, [**7**][PPN], PhI and PhC_2H, we observed speciation similar to that when no base was added (Figure 5.11).

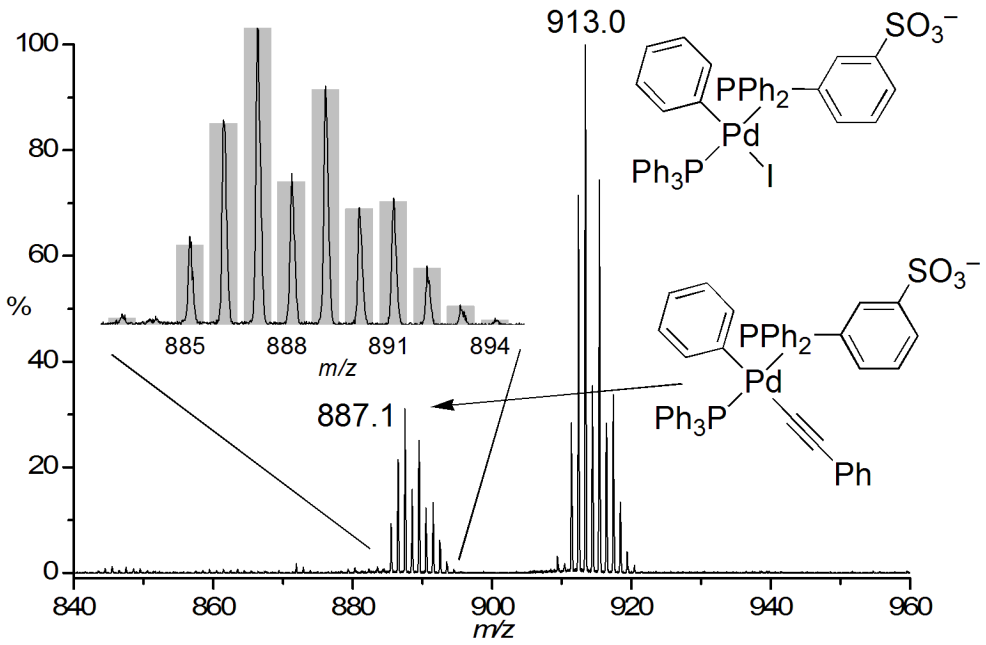

Figure 5.11: ESI(-)-MS of a solution containing PhC_2H, NEt_3, PhI, $Pd(PPh_3)_4$ and [7][PPN] in dichloromethane showing TM (*m/z* 887.1) and OA (*m/z* 913.0) species. An identical spectrum is obtained in the absence of NEt_3.

In the case of triethylamine we did not observe any base-containing palladium species. Even when base is added to a dichloromethane solution of just the catalyst and the charged ligand no amine adducts were observed (Figure 5.12).

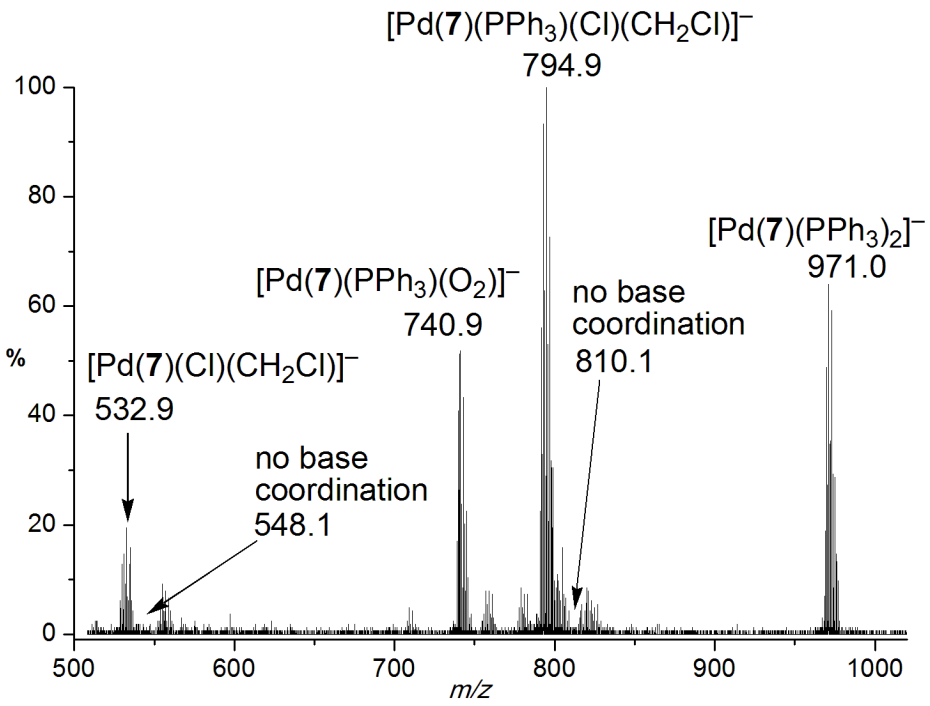

Figure 5.12: ESI(-)-MS of a dichloromethane solution of $Pd(PPh_3)_4$, [**7**][PPN], and NEt_3. No peak is observed at *m/z* 810.1 or *m/z* 548.1 where the signals for base coordination to $[Pd(\mathbf{7})(PPh_3)]^-$ and $[Pd(\mathbf{7})]^-$ would appear respectively.

Despite seeing no evidence of triethylamine coordinating to palladium it was apparent that the base did have a significant role: a signal for the protonated base was observed in the positive-ion mode (*m/z* 102.1), and negatively-charged adducts of the form $[2I^- + HNEt_3^+]^-$ (*m/z* 356.0) were observed in the negative-ion mode (Figure 5.15). Later we also found evidence to indicate that the base has a direct effect on the rate of the reaction (See Chapter 6).

We then tested two secondary amine bases that are used commonly in the copper-free Sonogashira reaction (morpholine and piperidine) and compared them to the results we obtained using triethylamine. The reactivity with secondary amines showed markedly different speciation: signals corresponding to amine-palladium adducts were observed along with η^2-coordination of the terminal alkyne. Our assignment of these signals as $[Pd(\mathbf{7})(amine)(Ph)(I)(HC_2Ph)]^-$ (amine = HNC_5H_{10} or HNC_4H_8O) was confirmed by MS/MS studies (Figure 5.13 and Figure 5.14). CID resulted in facile loss of PhC_2H (Col V = 5 V) followed by loss of the secondary amine. No loss of benzene is observed (78 Da) which led us to rule out the presence of the six-coordinate Pd(IV)

species [Pd(**7**)(amine)(Ph)(I)(H)(C_2Ph)]$^-$ that would also have a mass-to-charge ratio of 838 in the case of piperidine (and 840 in the case of morpholine).

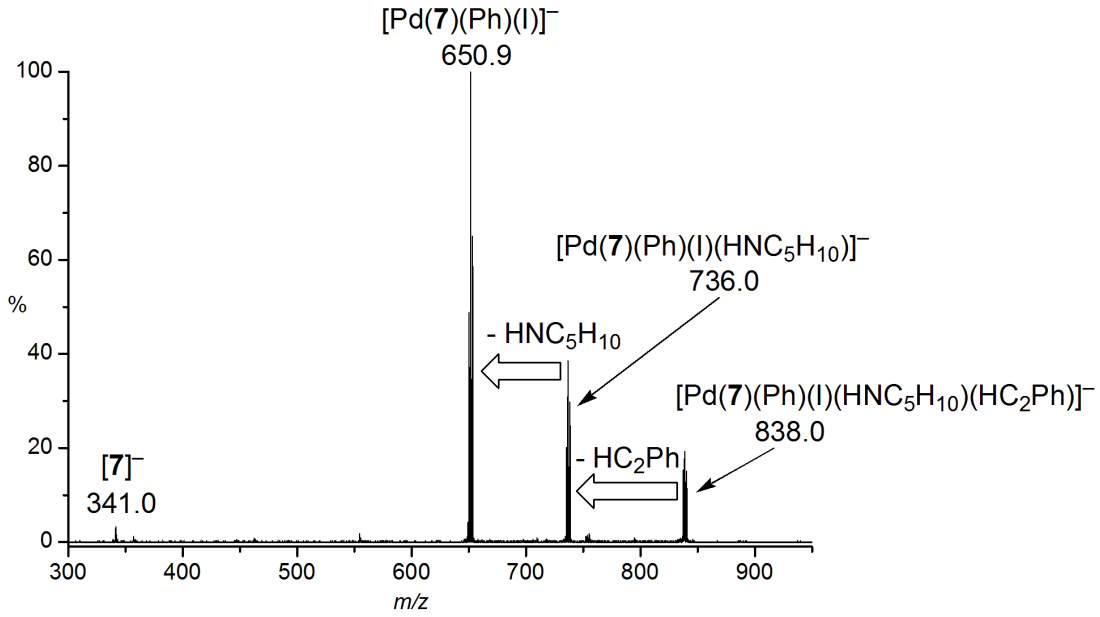

Figure 5.13: ESI(-)-MS/MS of the signal at *m/z* 838.0. Collision voltage = 5 V. Fragmentation pathways for loss of phenylacetylene and loss of piperidine are observed.

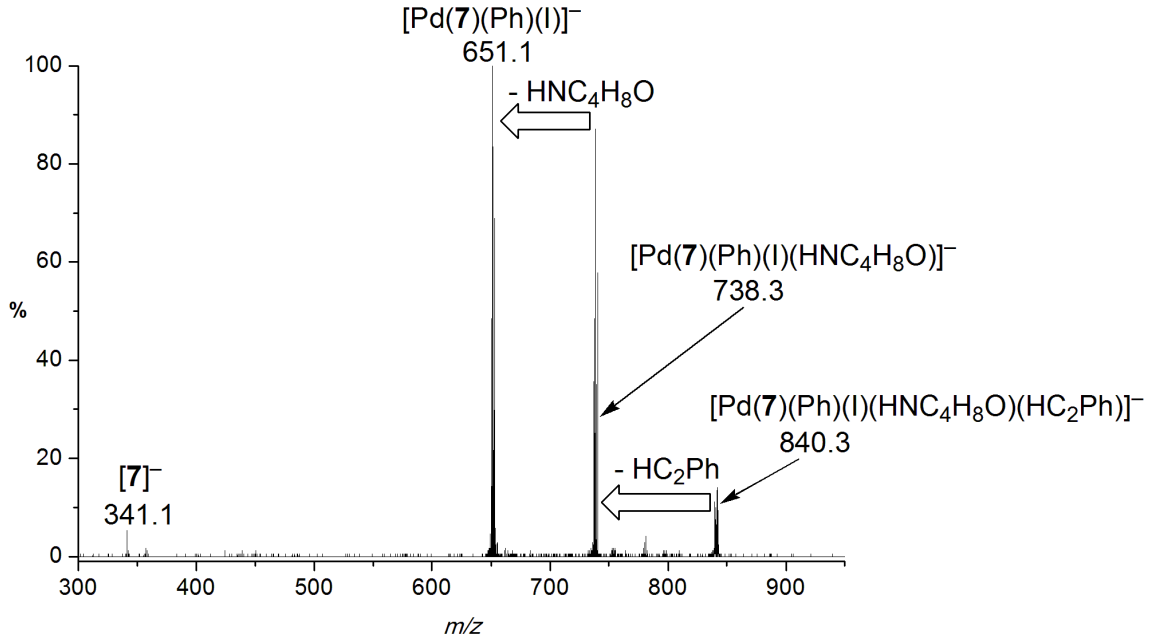

Figure 5.14: ESI(-)-MS/MS of the signal at *m/z* 840.3. Collision voltage = 5 V. Fragmentation pathways for loss of phenylacetylene and loss of morpholine are observed.

We searched for evidence of a fragmentation process that would indicate that the piperidine-containing complex at *m/z* 838.0 could undergo deprotonation of the terminal alkyne in the gas phase (which might manifest as fragmentation of *m/z* 838.0 by loss of protonated amine) but we saw no evidence for one. In retrospect this is not surprising since in the gas phase the deprotonation step would require separation of the cationic protonated amine from the dianion $[Pd^{II}(\mathbf{7})(Ph)(I)(C_2Ph)]^{2-}$ which is highly energetically unfavourable. A more likely fragmentation pathway that might be observed if the phenylacetylene is deprotonated in the complex would be loss of the neutral ion pair $[H_2NC_5H_{10}]^+[I]^-$ (or $[H_2NC_4H_8O]^+[I]^-$ for morpholine) to leave $[Pd(\mathbf{7})(Ph)(C_2Ph)]^-$. This was also not observed.

All of these results make us confident that the ion which gives rise to the peak at *m/z* 838.0 is correctly represented as $[Pd(\mathbf{7})(amine)(Ph)(I)(HC_2Ph)]^-$. Ions of this type that are coordinated to both an amine and acetylene have been previously proposed[172, 180, 197] but not directly observed until now.

Finally, as a control experiment the reaction in dichloromethane was performed without the charged ligand (**7**). The ESI(-)-MS spectrum shows only iodide and halide adducts with protonated base. No palladium-containing species that might indicate the activity of an anionic mechanism were detected (Figure 5.15).

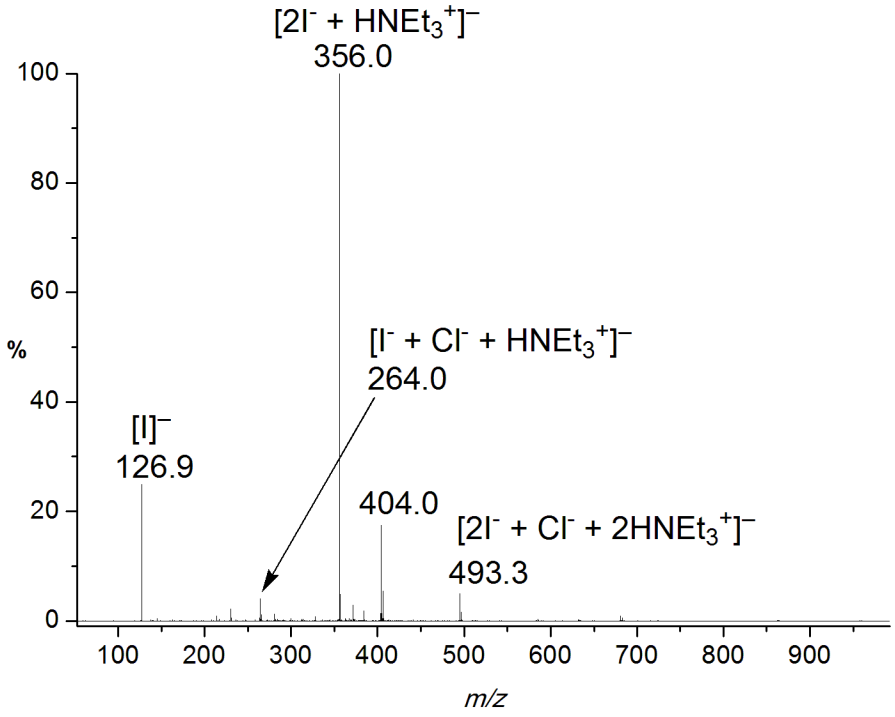

Figure 5.15: ESI(-)-MS of a solution of dichloromethane containing $Pd(PPh_3)_4$ + PhI + PhC_2H + NEt_3 (no charged ligand). Signals are seen for adducts of protonated triethylamine plus iodide and/or chlorine, but no anionic palladium-containing species are observed.

5.6 Reductive elimination

We can directly probe the process of reductive elimination (RE) in the gas phase by performing MS/MS and EDESI experiments on the transmetallated species $PdL_2R^1R^2$. To do this, a dichloromethane solution of $Pd(PPh_3)_4$, [**7**][PPN], PhI, PhC_2H and NEt_3 was injected into the MS at room temperature and the quadrupole was set to isolate $[Pd(PPh_3)(\mathbf{7})(Ph)(C_2Ph)]^-$ (*m/z* 887.1). An MS/MS experiment was performed at a moderate collision voltage of 15 V (Figure 5.16) and reductive elimination from the palladium complex was clearly observed as loss of

178.1 Da (PhC_2Ph) from the reacting ion to give a signal at *m/z* 709.0. Fragmentation peaks were also seen for loss of triphenylphosphine (*m/z* 625.0), loss of both phosphine and diphenylacetylene (*m/z* 446.9) and loss of $[\mathbf{7}]^-$ (*m/z* 341.0).

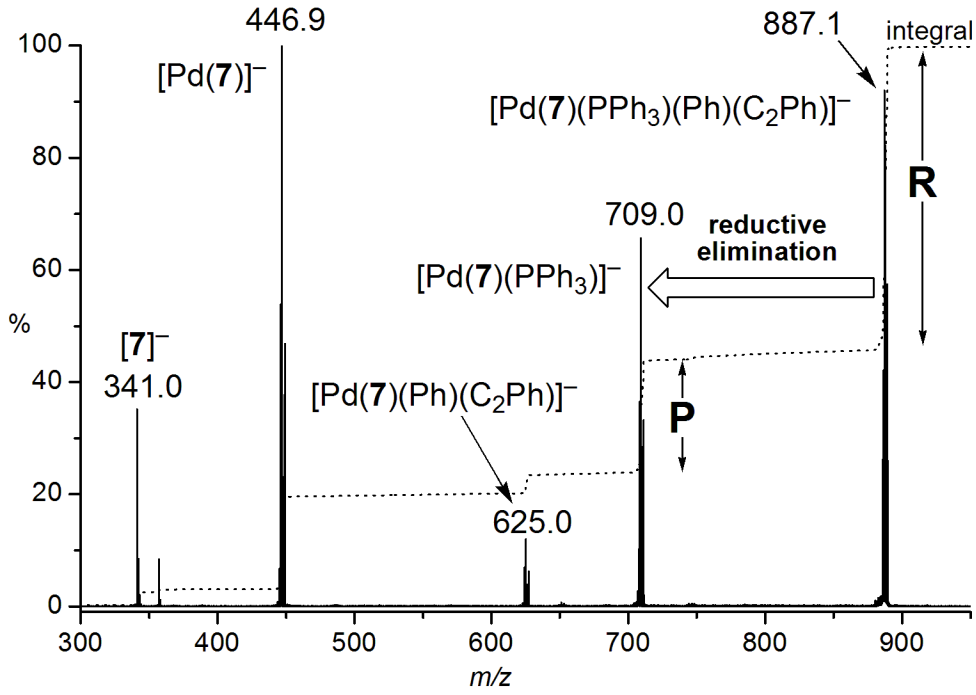

Figure 5.16: ESI(-)-MS/MS of $[Pd(\mathbf{7})(PPh_3)(Ph)(C_2Ph)]^-$, showing reductive elimination to $[Pd(\mathbf{7})(PPh_3)]^-$, at a collision voltage of 15 V. The area under each signal has been integrated to assess the extent of reactivity.

An EDESI experiment was also performed in which the transmetallated intermediate, $[Pd(\mathbf{7})(PPh_3)(Ph)(C_2Ph)]^-$, was isolated in the collision cell and the collision voltage was increased systematically from 0 to 20 V over the course of 40 minutes (Figure 5.17). From this experiment it was clear that loss of the diphenylacetylene product was the lowest energy process (Col V = 5 V) followed closely by loss of triphenylphosphine (Col V = 6 V).

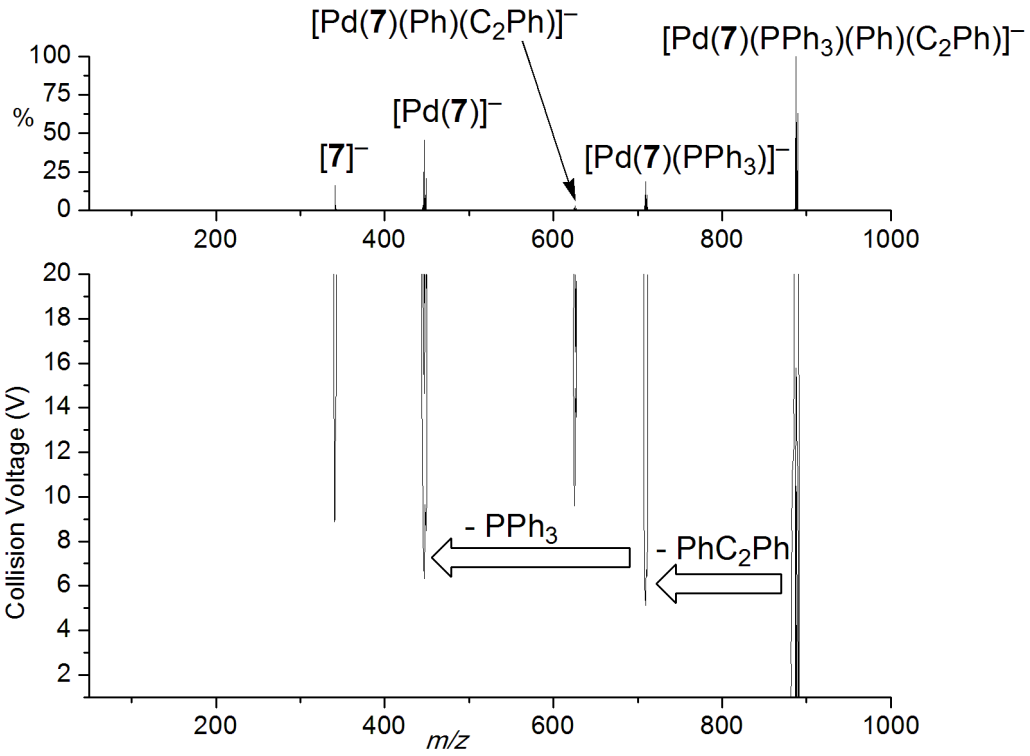

Figure 5.17: EDESI(-) of *m/z* 887.1, the transmetallated intermediate. Loss of diphenylacetylene (-178.1 Da) is followed closely by loss of triphenylphosphine (- 262.0 Da). Dwell time at each collision voltage: 120 seconds.

Finally, the energy required for RE of a variety of different [Pd(**7**)(PPh_3)(C_6H_4X)(C_2Ph)]$^-$ complexes (X = NH_2, OMe, Me, H, F, COMe, CF_3, CN, NO_2) was measured. While measurement of these relative energies is difficult (or impossible) using solution-phase techniques due to the transient nature of the transmetallated intermediate, we can access this information easily in the gas phase by gathering CID data for the reductive elimination of each species under identical conditions (collision voltage = 15 V, collision cell pressure = 2.05 ± 0.05 × 10^{-5} mbar) (Scheme 5.5). ESI(-)-MS/MS plots for [Pd(**7**)(PPh_3)(C_6H_4X)(C_2Ph)]$^-$ where X = NH_2, OMe, Me, H, F, COMe, CF_3, CN, and NO_2 are provided in Appendix E.

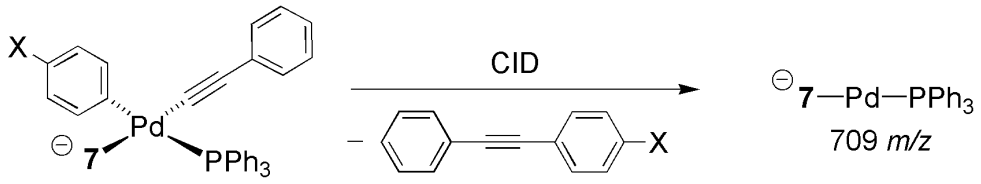

Scheme 5.5: Reductive elimination by CID. X = NH_2, OMe, Me, H, F, COMe, CF_3, CN, NO_2.

We noted that the energy required for reductive elimination from these complexes was related to the electronic nature of the *para*-substituted aryl group. The observed trend was quantified by taking the log of the ratio of the integral of the product (P) ion $[Pd(\mathbf{7})(PPh_3)]^-$ to the reacting (R) ion $[Pd(\mathbf{7})(PPh_3)(C_6H_4X)(C_2Ph)]^-$ and plotting it against the Hammett σ_p parameter for each *para*-substituent tested. In this way a Hammett plot was generated using ESI(-)-MS/MS data (Figure 5.18).

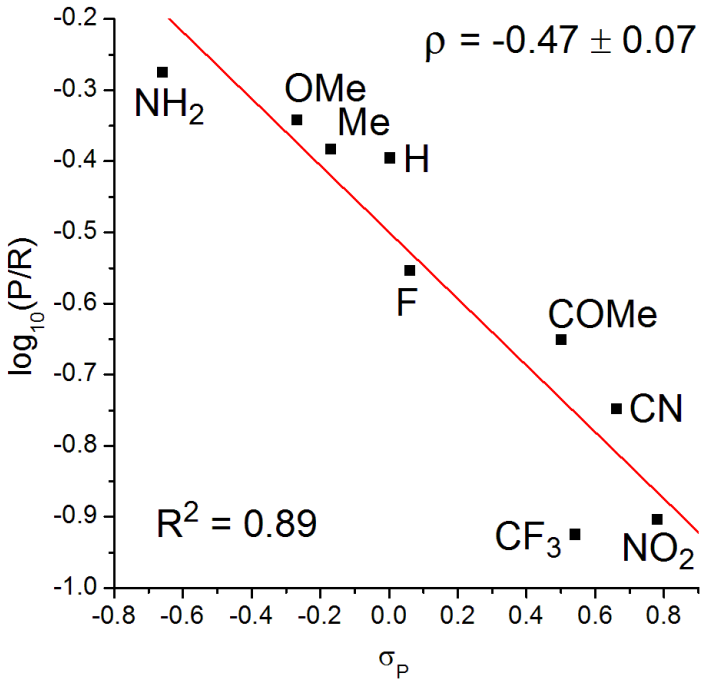

Figure 5.18: Plot of $\log_{10}(P/R)$ vs. Hammett σ_p parameter for a variety of *para*-substituted aryl iodides.

The negative slope of the plot ($\rho = -0.5$) indicates that reductive elimination is more favourable for aryl groups with electron-donating substituents in the *para*-position. This is consistent with results documented in the literature for bi-aryl platinum complexes [198, 199] and with theoretical

studies.[200] It also makes sense qualitatively: reductive elimination requires the reduction of palladium from Pd(II) to Pd(0) therefore RE is more facile for aryl groups which can donate more electron density to palladium.

A summary of all the peak height data obtained in the CID experiments of the various TM species is presented in Figure 5.19. The four observed product ions are shown and each differently coloured bar represents a different *para*-substituent. The bar to the far left in each set represents the most electron-donating substituent (NH_2), the bar to the far right represents the most electron-withdrawing (NO_2), and the remainder are plotted in order of their Hammett σ_p parameter. From this presentation of the data it is clear that while the energy required for RE is influenced by the different para-substituted aryl groups, the energy required for phosphine dissociation does not follow an obvious trend.

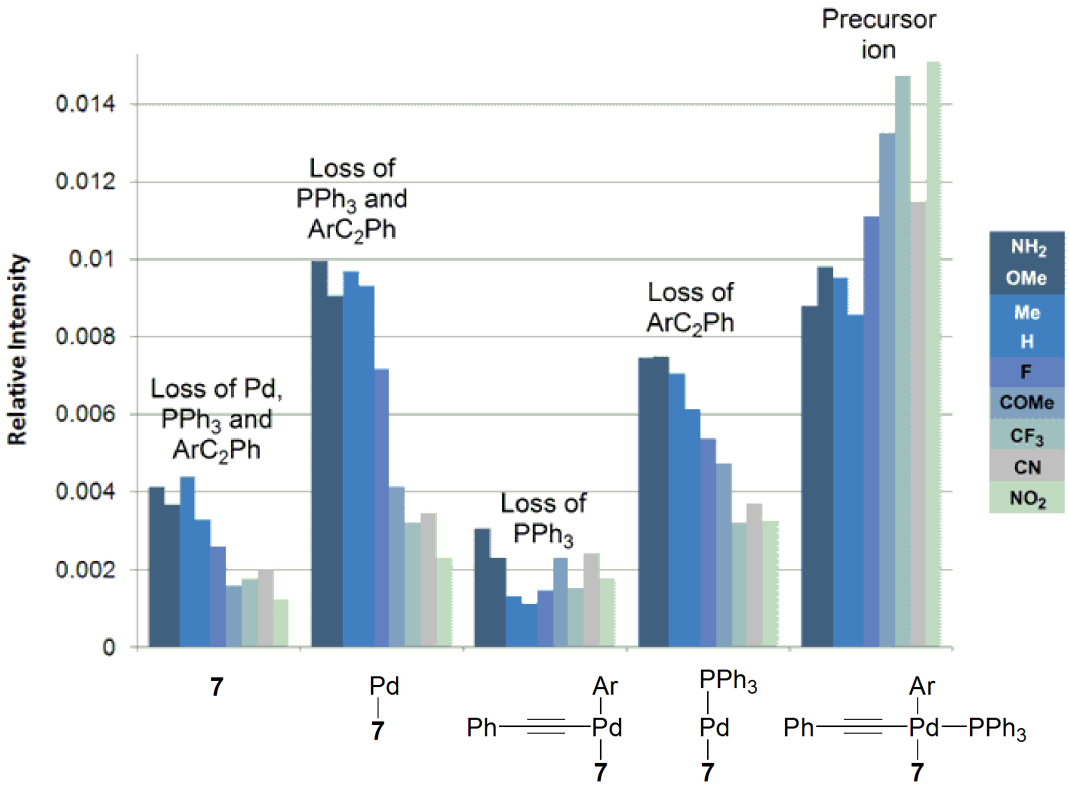

Figure 5.19: Summary of all negative-ion ESI-MS/MS plots of $[Pd(\mathbf{7})(PPh_3)(C_6H_4X)(C_2Ph)]^-$, showing the precursor ion and the four product ions, at a collision voltage of 15 V (X = NH_2, OMe, Me, H, F, COMe, CF_3, CN, NO_2).

It is important to note that the resolution of all EDESI data collected in the collision cell on our instrument is limited to plus or minus 0.5 V. This is due to a software limitation. Although it seems as if the computer software we use to control MS parameters (MassLynx) will accept fractional voltage increments, in reality it only allows the collision voltage to be stepped up or down in 1 V increments. This was demonstrated by monitoring a product ion from the fragmentation of $[\mathbf{7}]^-$ in the collision cell over time as the collision voltage was adjusted in 0.1 V increments (Figure 5.20). It is clear from the appearance of this plot that the energy imparted to the reacting ion only changes after every ten 0.1 V increments; hence, this method cannot distinguish between processes which occur within a 1 V window in the collision cell.

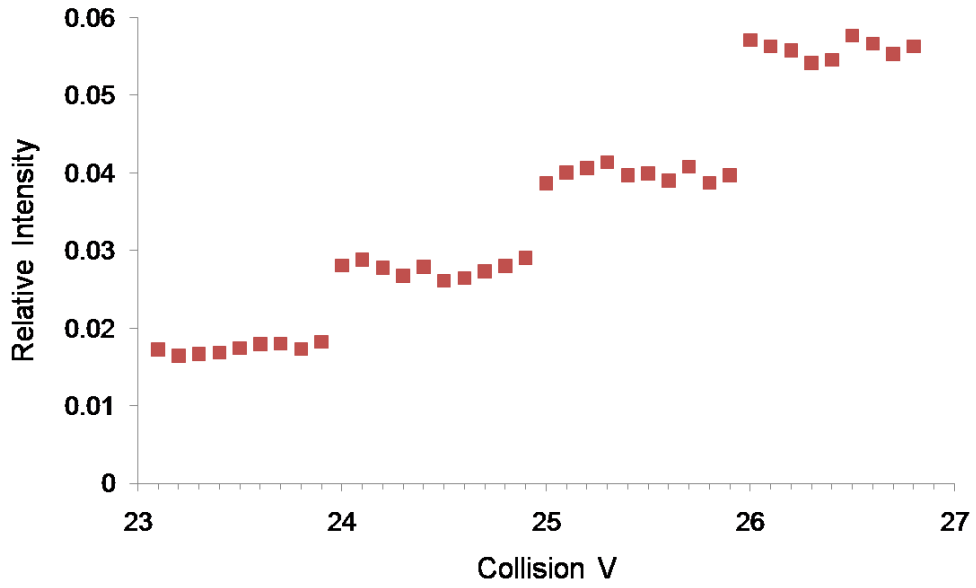

Figure 5.20: Appearance of the fragmentation product $[\mathbf{7} - C_6H_5]^-$ (*m/z* 264) during CID of $[\mathbf{7}]^-$ (*m/z* 341.0) when collision voltage is increased in 0.1 V increments.

5.7 Conclusions

Using the information gathered, we propose a possible catalytic cycle for the palladium-catalyzed copper-free Sonogashira cross-coupling reaction (Scheme 5.6).

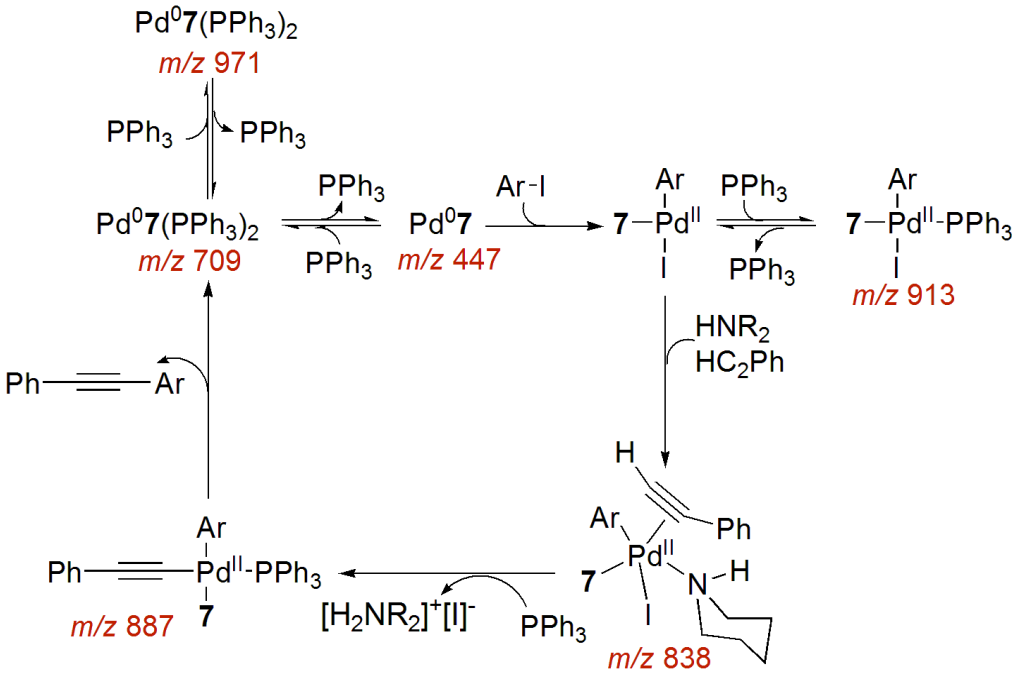

Scheme 5.6: A proposed catalytic cycle for the copper-free Sonogashira cross-coupling reaction based on species observed by ESI(-)-MS. Mass-to-charge values are given for species observed directly by ESI(-)-MS when ArI = iodobenzene and HNR_2 = piperidine. Note: when tertiary amine NEt_3 is used, no base coordination to palladium is observed and intermolecular deprotonation likely occurs.

In solution the palladium catalyst exists primarily as Pd^0L_3 and Pd^0L_2 with transient Pd^0L acting primarily as the active catalyst (L = phosphine). Oxidative addition occurs rapidly on addition of aryl iodide, and under the conditions we employed no anionic species are involved. Terminal alkynes were observed to coordinate weakly to palladium in an η^2-fashion and secondary amines were also seen to act as ligands for palladium. In the presence of base the terminal alkyne is deprotonated to give a so-called transmetallated intermediate, and in the absence of base the same intermediate can also form (potentially via a carbopalladation mechanism). Reductive elimination occurs from the transmetallated intermediate and the ease with which it occurs can be influenced electronically by placing different substituents in the *para*-position of the aryl iodide. More electron-donating substituents favour reductive elimination.

As we have shown using the copper-free Sonogashira cross-coupling reaction: characterization of the pre- and active catalyst is straightforward; the reactivity of each proposed catalytically

active species can be examined; the role of additives such as base can be investigated; highly reactive intermediates can be isolated in the gas phase; and data on elementary reaction steps in the catalytic cycle can be collected. The combined use of a charged ligand, PSI-MS and gas-phase reactivity studies is a rapid and facile way of gaining mechanistic insights into palladium-catalyzed reactions. Furthermore, these methods can be easily used to study other types of organometallic catalytic reactions, and organocatalytic or stoichiometric reactions.

5.8 Experimental

Mass spectrometry

All mass spectra and gas-phase experiments were performed on a Micromass Q-TOF *micro* hybrid quadrupole/time-of-flight mass spectrometer in negative-ion mode using pneumatically-assisted electrospray ionization.Capillary Voltage: 2900 V. Cone Voltage: 10 V (unless othewise stated). Extraction Voltage: 0.5 V. Source Temperature: 30 °C for dichloromethane, 85 °C for fluorobenzene. Desolvation Temperature: 60 °C for dichloromethane, 160 °C for fluorobenzene. Cone Gas Flow: 100 L/h. Desolvation Gas Flow: 200 L/h. Collision Voltage: 2 V (for MS experiments). Collision Voltage: 15 V (for MS/MS experiments unless otherwise stated). Low and High Mass Resolution: 10.0 (for MS/MS experiments). MCP Voltage: 2700 V.

Solutions were run in dichloromethane or fluorobenzene and introduced to the mass spectrometer by a syringe pump or by PSI at a rate of 10 - 20 μL min^{-1}. MS/MS experiments were conducted with argon in the collision cell. The appropriate peak was mass selected (usually with a broad enough window to accommodate the full isotope pattern, *i.e.* ~8 Da) and the selected ion fragmented at the stated voltage(s) in the argon-filled collision cell. All mass spectra were collected for a sufficiently long period to obtain a signal-to-noise ratio of at least 20:1; this ranged from a few seconds for ordinary mass spectra to 10 minutes for some of the MS/MS and EDESI experiments.

General experimental details

Solvents were dried and degassed by purging with nitrogen using an MBraun solvent purification system. [**7**][PPN] was synthesized according to the procedure outlined in Chapter 3

(experimental section). All other chemicals were obtained from Aldrich and used without further purification. In a glovebox, palladium tetrakistriphenylphosphine (0.006 g, 5 μmol) and **1** (0.004g, 5 μmol) were dissolved in 5 mL dichloromethane. The catalyst solution was then mixed with iodobenzene or the appropriate *para*-substituted phenyl iodide (0.4 mmol), and phenylacetylene (0.044 mL, 0.4 mmol) was added. Finally, either triethylamine (0.055 mL, 0.4 mmol or 0.55 mL, 4 mmol), piperidine (0.040 mL, 0.4 mmol), or morpholine (0.035 mL, 0.4 mmol) was added. The amounts correspond to a 1.25% catalyst loading (and 1.25% loading of the charged ligand). The reaction mixture was injected into the MS by syringe pump or PSI. In some cases the reaction mixture was sampled for MS analysis as (or immediately after) each reagent was added to the solution.

Gas-phase reductive elimination experiments

Dichloromethane solutions of $Pd(PPh_3)_4$, [**7**][PPN], PhC_2H, NEt_3, and one of the selected *para*-substituted aryl iodides XC_6H_4I (X = NH_2, OMe, Me, H, F, COMe, CF_3, CN, NO_2) were prepared and allowed to mix for ten minutes, they were then injected via syringe pump into the MS. The complexes $[Pd(\mathbf{7})(PPh_3)(C_6H_4X)(C_2Ph)]^-$ were isolated using the first quadrupole mass analyzer. EDESI experiments were performed in which the collision voltage was increased from 0 – 20 V at 2 minute intervals. MS/MS experiments were performed at a collision voltage of 15 V and the integral of the reacting ion peak and the product ion peaks were taken. A center-of-mass correction was made in each case[201] to account for the amount of energy available to effect dissociation given the mass of the reacting ion (variable) and the mass of the argon collision gas (40 Da). $E_{COM} = E_{LAB} \times (m_{Ar}/m_{Ar} + m_{ion}))$.

Online monitoring of oxidative addition of palladium tetrakis(triphenylphosphine) by dichloromethane or iodotoluene by PSI-MS

$Pd(PPh_3)_4$ and [**7**][PPN] were added to a Schlenk flask, under nitrogen (1 psi), that was fitted with a condenser and septum. The flask was placed next to the ESI source and connected to a pressurized nitrogen tank. A length of PEEK tubing (ID = 127 μm) was inserted through the septum and the other end was connected to the MS via a standard chromatography fitting. The Schlenk flask was heated to 40 °C in an oil bath, MS acquisition was initiated, and dichloromethane (10 mL) was injected via syringe through the septum into the Schlenk flask.

The reaction was stirred and the PEEK tubing tip was immediately lowered into the solution. Spectra were collected every 5 seconds for 1 hour. In the case of the oxidative addition of iodotoluene, the same procedure was carried out but the reaction mixture was left at room temperature and iodotoluene was injected after addition of CH_2Cl_2. Spectra were collected every 10 seconds.

Chapter 6. Future Directions: Online Reaction Monitoring

Portions of this chapter are reproduced in part with permission from "Powerful insight into catalytic mechanisms through simultaneous monitoring of reactant, products and intermediates" Krista L. Vikse, Zohrab Ahmadi, Cara C. Manning, David A. Harrington and J. Scott McIndoe, *Angew. Chem., Int. Ed.,* published online 14 JUN 2011, DOI: 10.1002/anie.201102630.

The future of this project lies in using charged tags and PSI-MS to collect continuous kinetic data from *reactants, products and intermediates* for reactions that are not well understood. The following is a description of our first foray into this area and it demonstrates that the type of data we obtain can be instrumental in understanding the details of catalytic processes. The project is ongoing and has been taken up by graduate student Zohrab Ahmadi in our research group. The experimental data for this work was collected by him and Cara Manning (a BSc student employed in our lab). My contribution included: initial training of Zohrab and Cara, experimental design, data analysis informed by extensive literature research, refinement of the proposed catalytic mechanism and drafting of the manuscript for the paper in collaboration with Dr. Scott McIndoe.

6.1 Preliminary results and discussion

Once again we focused on the copper-free Sonogashira (Heck alkynylation) reaction. With a clear picture of the *types* of palladium-containing species present in solution, we became interested in the behaviour of those species over time with respect the overall progress of the reaction. To ensure that this behaviour was in fact related to product formation, we 'tagged' one of the reactants instead of the phosphine ligand (Scheme 6.1). In this way, we could observe the charged reactant, the product, and any intermediates containing the charged reactant by ESI-MS.

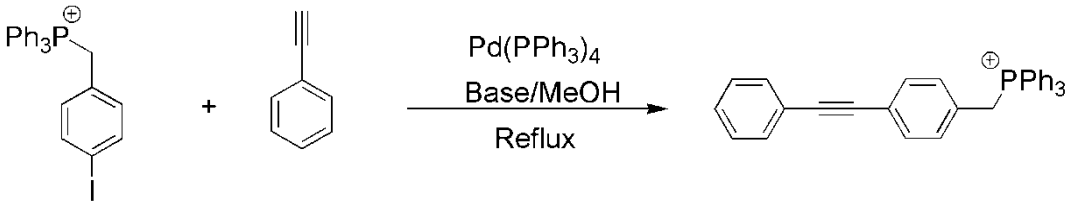

Scheme 6.1: Copper-free Sonogashira reaction with a charged aryl iodide as an ESI(+) handle.

The charged tag we used is an aryl iodide that has been functionalized with a phosphonium hexafluorophosphate salt, $[p\text{-}IC_6H_4CH_2PPh_3]^+[PF_6]^-$. The tag allows us to obtain very low detection limits due to its high surface activity, and its non-coordinating counter-ion (which reduces ion-pairing). The bulky nature of the charged group ensures that the ionization efficiency is largely insensitive to the remaining structure of the ion, so the intensity of the various ions track very closely to their real concentrations. Figure 6.1 shows the relative responses of the charged reactant and product from ESI(+)-MS as they were mixed together in different known ratios and analyzed. There is a clear linear relationship between MS intensity and concentration for these ions. This predictable instrument response gave us confidence that the MS intensity data for ions in this reaction could be related to concentration in solution.

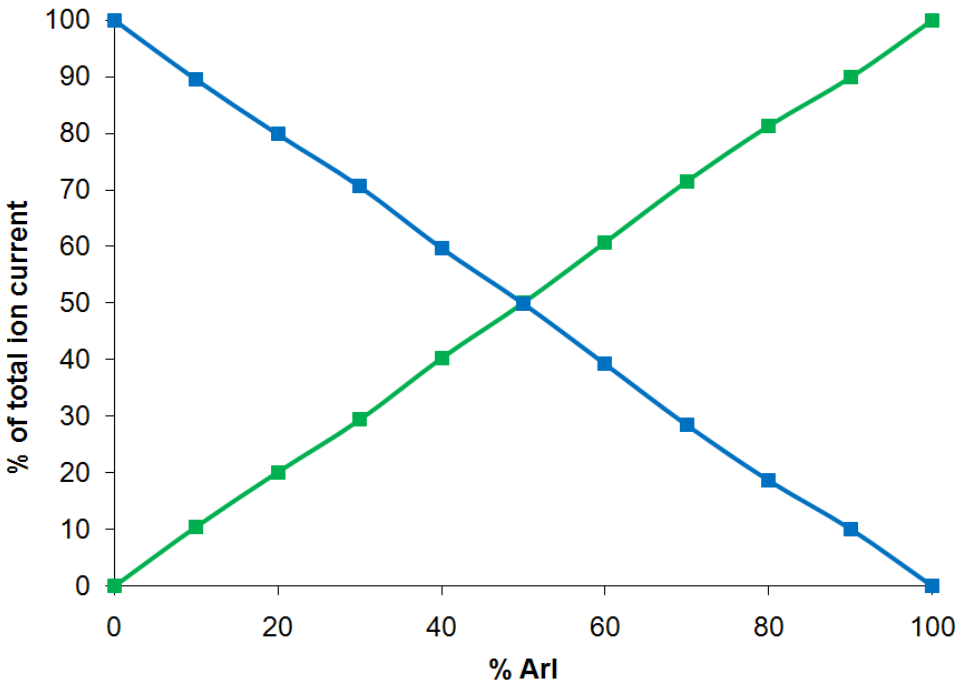

Figure 6.1: Relative intensity of starting material $[IC_6H_4CH_2PPh_3]^+$ (green) and product $[Ph(C_2)C_6H_4CH_2PPh_3]^+$ (blue) as a function of mixture composition showing the linear relationship between intensity and concentration.

Data was collected by PSI-MS in the positive-ion mode, and as discussed in Chapter 4 the traces obtained by this method agree well with data collected by ^{1}H NMR and UV/VIS for the same reaction (Figure 4.6). An example of the data collected over the course of a typical reaction is provided below (Figure 6.2).

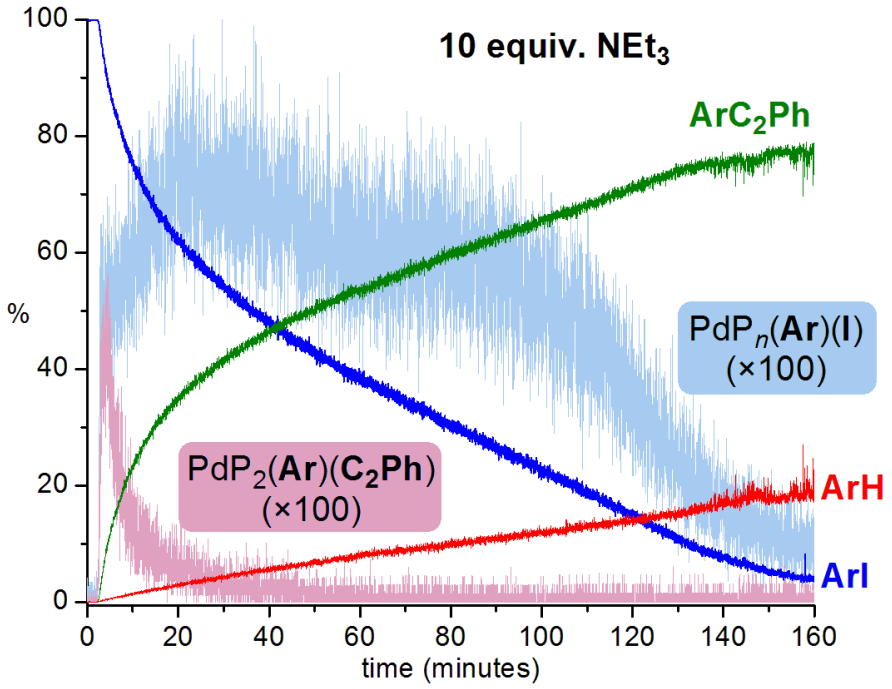

Figure 6.2: ESI(+)-MS over time for the intensity of all key species bearing the charged tag $[C_6H_4CH_2PPh_3]^+$ (Ar = $[C_6H_4CH_2PPh_3]^+$; P = PPh_3). The intensities of the palladium-containing intermediates have been multiplied by 100.

The relative intensities of all major tagged species are depicted: substrate (ArI, *m/z* 479.1), product (ArC_2Ph, *m/z* 453.2), byproduct (ArH, *m/z* 353.2), and under 100× magnification the oxidative addition (OA) and transmetallated (TM) intermediates $PdP_n(Ar)(I)$ (*m/z* 1109.4) and $PdP_2(Ar)(C_2Ph)$ (*m/z* 1083.4) where Ar = $[C_6H_4CH_2PPh_3]^+$, *n* = 1 or 2. There are over 9500 data points represented in this plot each representing a full mass spectrum. Figure 6.3 is an example of a single spectrum from this experiment.

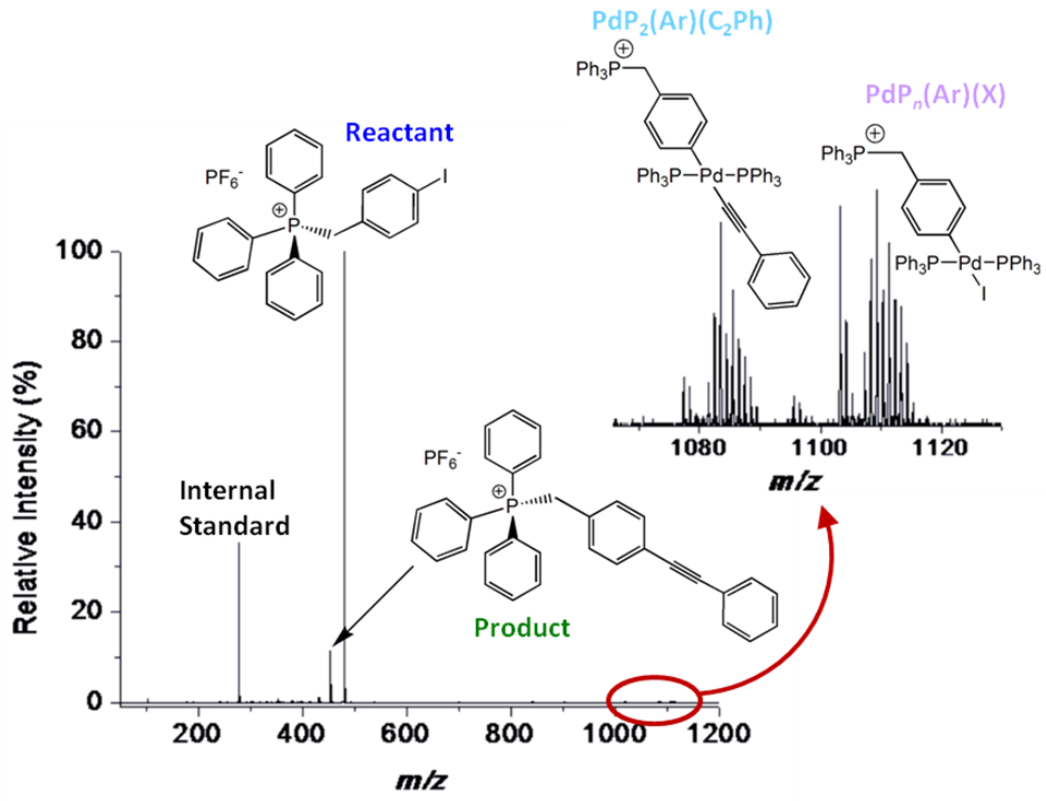

Figure 6.3: A single spectrum from the experiment shown in Figure 6.2. Product and reactant are observed at *m/z* 453 and 479 respectively. The Pd-containing intermediates (*m/z* 1083 and 1109) are lost in the baseline and require 100 fold magnification to become easily observed (inset); however, note that the signal-to-noise of these peaks is still more than satisfactory. The internal standard is $[PPh_3Me]^+[PF_6]^-$ (*m/z* 277).

Figure 6.2 shows a distinct change in the reaction rate between 20 and 40 minutes where it appears as if an initial fast process was replaced by a much slower zero-order process. The rate of formation of byproduct was unaffected by this mechanistic changeover and remains zero order throughout. Initially we hypothesized that the rate change might be related to the previously proposed "anionic mechanism" described by Jutand.[177] Specifically, the initial fast rate may be due to catalysis occurring at the more traditionally proposed Pd(0)L_2-type species, whereas the slower process may correspond to catalysis occurring at anionic species of the type $[PdL_2I]^-$. As I^- is produced in the reaction, the slower anionic mechanism would begin to dominate just as we observe. However, despite our best efforts we did not observe any evidence for the proposed anionic species (see section 5.3 and Figure 5.15).

Upon closer examination of the behaviour of the intermediates during the changeover (Figure 6.2) another cause for the rate change in the reaction became apparent (refer to Scheme 6.2). The change in rate corresponds to the disappearance of the TM intermediate and the increase of the OA intermediate signal to a maximum (the intermediate then levels off and remains roughly constant for the rest of the reaction). In the initial fast reaction we see a build up of the TM intermediate so reductive elimination (RE) must be the rate-determining step. The TM intermediate then disappears and the relatively high steady state concentration of the OA intermediate suggests that, for this second portion of the reaction, the "transmetallation" process is rate-determining.

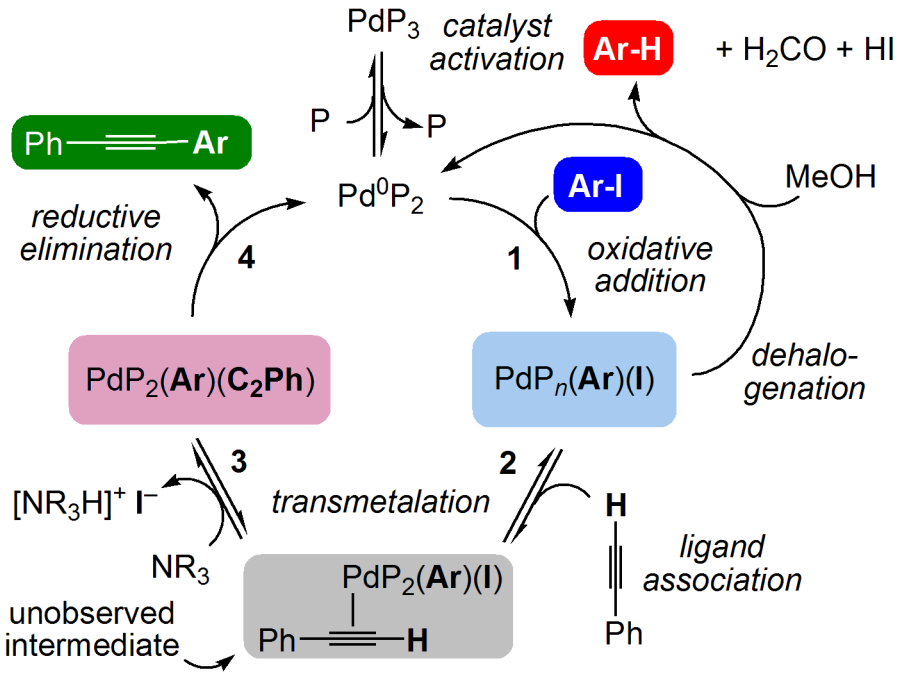

Scheme 6.2: Proposed catalytic cycle for the copper-free Sonogashira reaction. Only species containing $[C_6H_4CH_2PPh_3]^+$ (Ar) are visible by ESI(+)-MS. The intermediate in the grey box was not observed in these experiments, but we have previously observed similar species.[163]

For the transmetallation process to slow down and become rate-determining, either step **2** or **3** must slow down. We hypothesized that build up of either H^+ or I^- over time at step **3** could slow

the reaction by driving step **3** backwards. To test whether build up of I^- was responsible for the observed rate change $[NEt_4]^+[I]^-$ was added as a source of iodide to the reaction in a 1:1 ratio with catalyst. The iodide had no effect on the progress of the reaction and the reaction profile remained unchanged. To test whether build up of protons was responsible for the observed rate change, the acid $[NEt_3H]^+[I]^-$ was added in a 1:1 ratio with catalyst and the change in reaction profile was very telling (Figure 6.4).

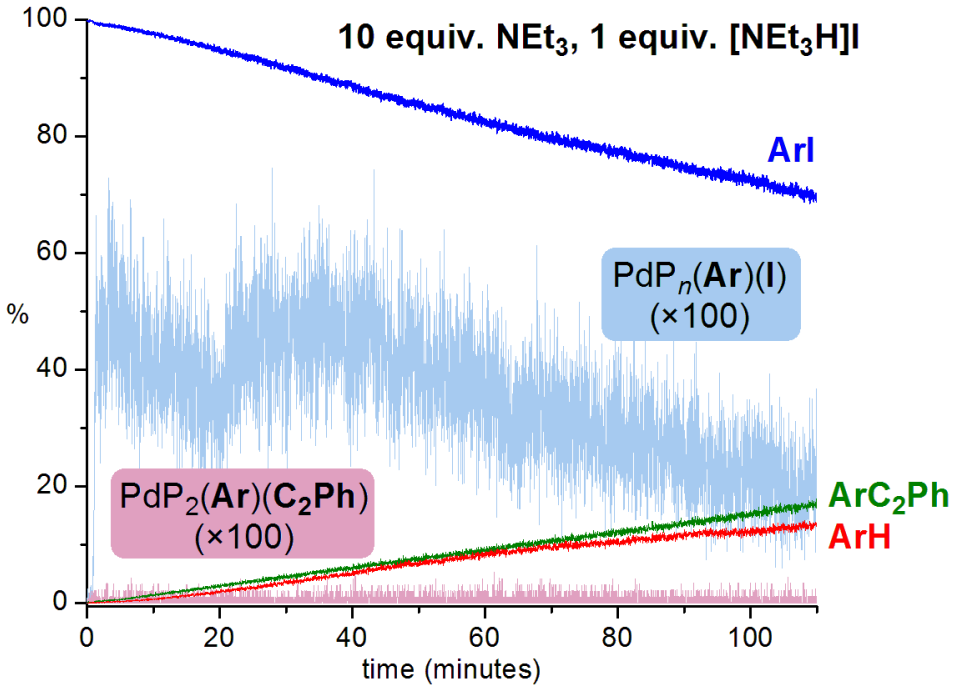

Figure 6.4: ESI(+)-MS over time for the intensity of all key species bearing the charged tag $[C_6H_4CH_2PPh_3]^+$ (Ar = $[C_6H_4CH_2PPh_3]^+$; P = PPh_3), where 1 equivalent of $[NEt_3H]^+[I]^-$ was added to the reaction. The intensities of the palladium-containing intermediates have been multiplied by 100.

The addition of protons completely shuts down the initial fast reaction which proceeds under zero-order kinetics throughout. The TM intermediate is almost non-existent and the concentration of the OA intermediate is roughly steady state. The overall slow rate of reaction means that the hydrodehalogenation side reaction is competitive with the desired reaction. That the side reaction is unaffected by addition of acid indicates that the RDS for formation of the byproduct does not involve protonation/deprotonation.

For practical applications, a system in which the initial fast rate of reaction is preserved is desirable, and given that the presence of protons slows the reaction, a stronger base should more effectively sequester the proton and allow the reaction to continue operating in the faster regime. The reaction was repeated with DBU (1,8-diazabicyclo[5.4.0]undec-7-ene) as base (pK_a of 13.9 (estimated)[202] compared to 9.0 for NEt_3[195] in DMSO) and the faster first-order process is maintained for the entire reaction (Figure 6.5). The reaction is complete within 90 minutes, the yield is higher and the product cleaner because the dehalogenation side reaction cannot compete as effectively with the desired coupling reaction.

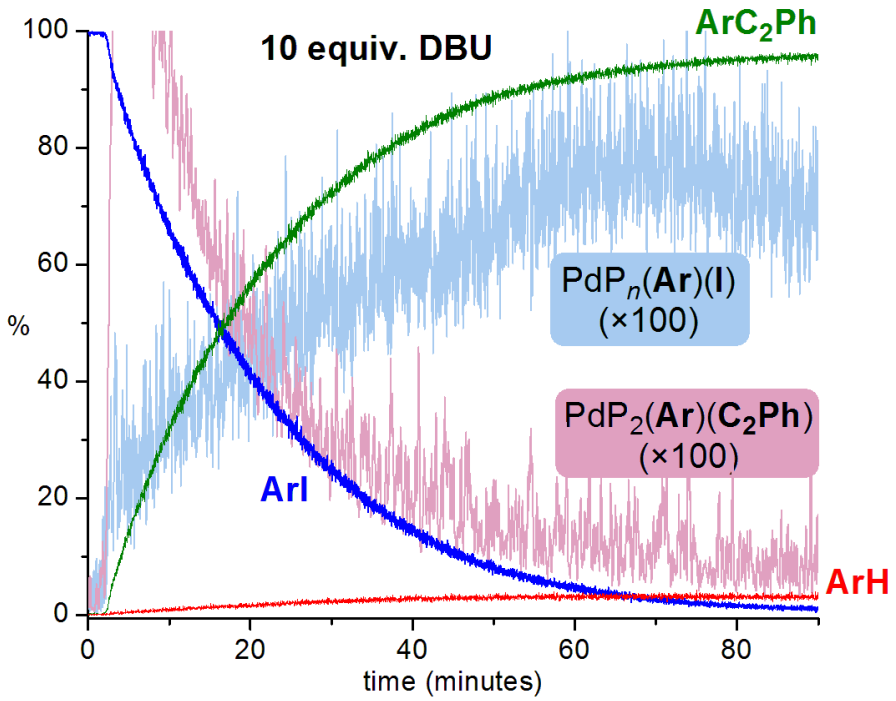

Figure 6.5: ESI(+)-MS over time for the intensity of all key species bearing the charged tag $[C_6H_4CH_2PPh_3]^+$ (Ar = $[C_6H_4CH_2PPh_3]^+$; P = PPh_3), where DBU was used in place of NEt_3. The intensities of the palladium-containing intermediates have been multiplied by 100.

The amount of TM intermediate is higher in this reaction and the reductive elimination step remains rate-determining for longer presumably because the stronger base slows the reverse reaction (protonation) at step **3**.

Figure 6.6 allows for a direct comparison of the formation of product under the three different reaction conditions. It shows the effect of adding acid or using a stronger base, and it highlights the importance of understanding reaction mechanisms so that we can rationally tune reaction conditions and develop more efficient processes.

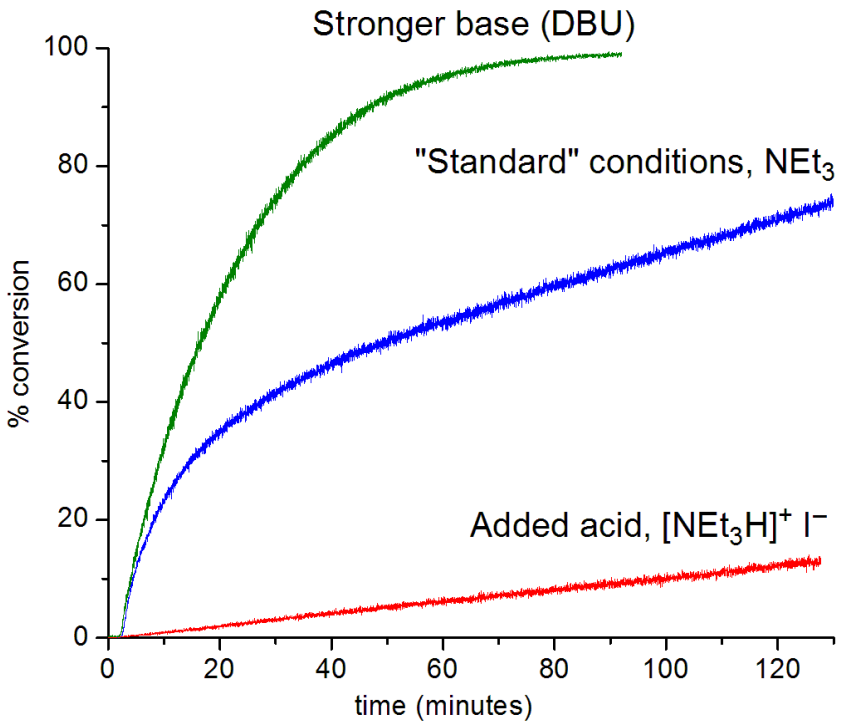

Figure 6.6: ESI(+)-MS over time for the intensity of $[PhC_2C_6H_4CH_2PPh_3]^+$ when using different bases and added acid (all other experimental conditions kept constant).

The exact nature of the "deprotonation" or "transmetallation" step is still not known and while simple deprotonation of an η^2-bound terminal acetylene by base seems to be the most popular explanation, we observe different catalyst speciation depending on whether a secondary or tertiary amine is employed (see section 5.5). Furthermore, a carbopalladation mechanism cannot be ruled out under our reaction conditions. In fact, we have some evidence that suggests that this process can be active: when no base is added the reaction still proceeds (Figure 6.7). The reaction is slow and does not go to completion (~50%) but nevertheless product is formed without the addition of base. Carbopalladation is the only proposed mechanism which can account for this.

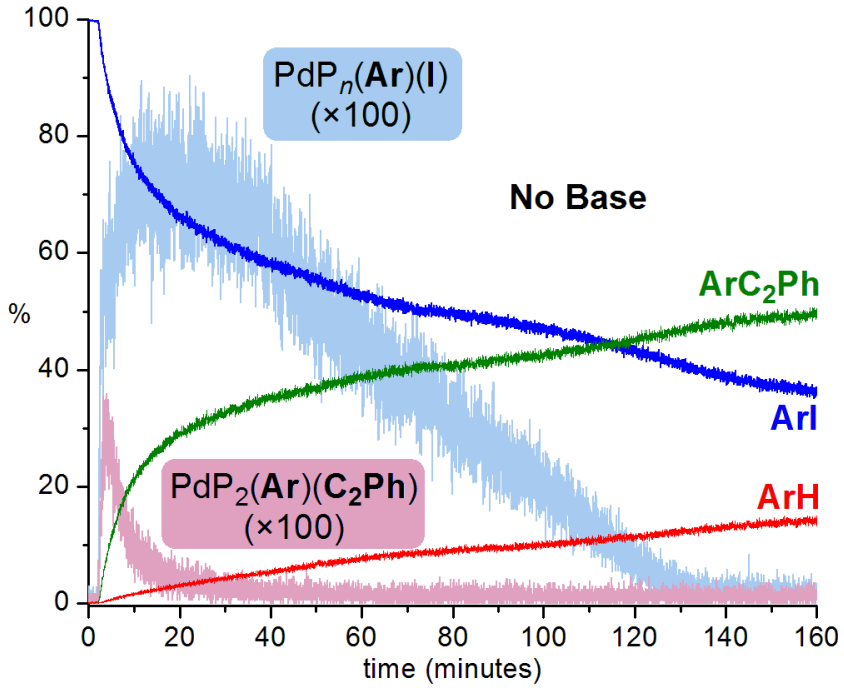

Figure 6.7: ESI(+)-MS over time for the intensity of all key species bearing the charged tag $[C_6H_4CH_2PPh_3]^+$ (Ar = $[C_6H_4CH_2PPh_3]^+$; P = PPh_3), where the reaction was run without base. The intensities of the palladium-containing intermediates have been multiplied by 100.

It is clear from these initial results that even a qualitative picture of the behaviour of reactants, products and intermediates during a reaction is extremely valuable and can very simply provide insight into the reaction mechanism. We are working now to rigorously quantify our data and further expand the generality of this approach.

6.2 Future work

Work is ongoing to develop new additions to our library of charged ligands and substrates for use as ESI tags, and the current focus is more heavily on the design of charged substrates since they allow for the observation of all species of interest simultaneously. We are also in the preliminary stages of applying numerical modelling to our systems in order to simulate reactions of interest and complement our experimental findings. Initial results in this area have been very promising.

The methodology described in this dissertation can be applied to a seemingly endless number of systems. Currently members of the McIndoe group are using it to investigate the copper-containing version of the Sonogashira reaction, the dehydrocoupling of silanes catalyzed by Wilkinson's catalyst, and the phosphine-catalyzed conjugate addition of alcohols to α,β-unsaturated alkynic acid esters. In the immediate future we will investigate other palladium-catalyzed coupling reactions which are not yet fully understood, and subsequently we will turn our attentions to other metal-catalyzed and organo-catalyzed reactions with the end goal of developing more effective catalysts and reaction conditions.

6.3 Experimental

Note: All experimental work for this chapter was performed by graduate student Zohrab Ahmadi in the McIndoe Group.

General information

All syntheses and catalytic reactions were performed under an inert atmosphere of N_2 using standard glovebox or Schlenk procedures. Except for triphenylphosphine (Alfa Aesar), triethylamine (ACP, Montreal, Quebec) and tetrakistriphenylphosphine palladium (Pressure Chemical Co.) chemicals were obtained from Aldrich and used without further purification. Solvents were HPLC grade and purified on an MBraun solvent purification system. Gases were obtained from Airgas (Calgary, Canada). $[Et_3NH]I$ was prepared by a literature method.[203]

Synthesis of $[4\text{-}IC_6H_4(CH_2)PPh_3][PF_6]$

Triphenylphosphine (0.7 g, 2.7 mmol) and 4-iodobenzyl bromide (0.76 g, 2.6 mmol) were added to toluene (10 mL). The reaction was stirred at room temperature for 16 h. The white precipitate was filtered and washed with toluene to remove extra PPh_3 and provide the product $[4\text{-}IC_6H_4CH_2PPh_3]Br$ (yield: 1.1 g, 77%) (m.p. = 248 °C uncorrected). Salt metathesis with $Na[PF_6]$ (0.67 g, 4 mmol) gave $[4\text{-}IC_6H_4CH_2PPh_3][PF_6]$ (yield: 1.1 g, 85%) after stirring for 1 h in methanol (5 mL). ^1H NMR (300 MHz, $CDCl_3$) δ: 4.53, (d, 2H, J = 14 Hz), 6.7 (dd, 2H, J = 2,

8 Hz) δ: 7.57-7.45 (m, 8H), 7.66 (td, 6H, J = 3.5, 8 Hz), 7.80 (td, 3H, J = 2, 7 Hz). ^{31}P NMR (300 MHz, $CDCl_3$) δ: 23.60(s).

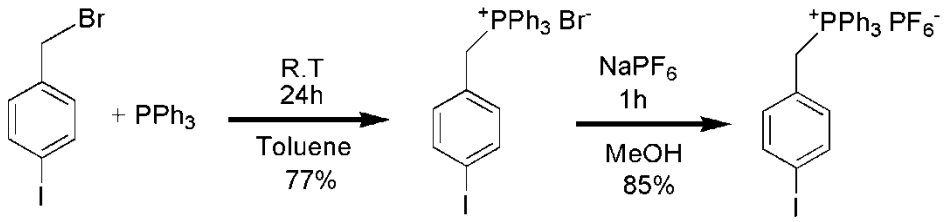

Synthesis of [$MePPh_3$][PF_6]

Triphenylphosphine (2 g, 7.6 mmol) and iodomethane (0.48 mL, 7.6 mmol) were dissolved in toluene (5 mL). After 5 h white precipitate was collected and washed with toluene then dried in vacuo (yield: 2.5 g, 83%). Salt metathesis was carried out by adding [$MePPh_3$]I (2.5 g, 6.3 mmol) and Na[PF_6] (2 g, 12 mmol) to MeOH (5 mL) and stirring for 1 h. Solvent was removed by rotary evaporation and the resulting product was washed with water to remove extra Na[PF_6] (yield: 2.3 g, 87%).

Mass spectrometry

All mass spectra were collected on a Micromass Q-TOF *micro* mass spectrometer in positive-ion mode using pneumatically-assisted electrospray ionization. Capillary voltage: 2900 V. Cone voltage: 10 V. Extraction voltage: 0.5 V. Source temperature: 80 °C. Desolvation temperature: 150 °C. Cone gas flow: 100 L/h. Desolvation gas flow: 200 L/h. Collision voltage: 2 V (for MS experiments). Collision voltage: 15-25 V (for MS/MS experiments). Low and high mass resolution: 10.0. MCP voltage: 2700 V.

General experimental details

Using PSI, a solution of [$I(C_6H_4)CH_2PPh_3$][PF_6] (20 mL, 0.5 mM in methanol) was monitored by ESI(+)-MS. To this solution phenylacetylene (1.3 µL, 12 µmol) and base (triethylamine or 1,8-diazabicyclo[5.4.0]undec-7-ene (DBU), 0.1 mmol) were added. 6% $Pd(PPh_3)_4$ (2 mL, 17 µM stock catalyst in THF) was added by syringe through the septum to initiate the reaction. The palladium tetrakis(triphenylphosphine) stock solution was stored in an inert atmosphere glovebox at -32 °C between uses. Overpressure in the flask was held at 2.5 psi throughout the

reaction and the temperature was held at reflux throughout. The reaction mixture was diluted online en route to the MS with methanol at 10-20 μL min^{-1}. The diluted solution was split and flow rate to the mass spectrometer was about 0.5 μL min^{-1}. Data was processed by normalizing the abundance of each species to the total ion current attributable to species containing Ar.

Chapter 7. Conclusions

In Chapter 2 a number of barriers were described that inhibit the application of ESI-MS to the study of catalytic organometallic reactions. First, only species that are already charged in solution are visible by ESI-MS. Second, air- and moisture-sensitive solutions are difficult to handle. Third, quantification of ESI-MS data is not straightforward and fourth, sampling rate is limited. This dissertation has presented solutions to each of these setbacks by employing a combination of rationally designed ESI tags and the use of a new sample introduction method dubbed “pressurized sample infusion mass spectrometry” (PSI-MS).

The first and third barriers (above) have been addressed by the use of ESI-active charged ligands or substrates. The synthesis of a number of novel ESI tags was described in Chapter 3. These tags allow otherwise neutral and invisible molecules to be observed by ESI-MS. A permanently-charged cationic or anionic moiety placed in a position that is remote from the portion of the substrate or ligand that interacts with the metal is best, because they possess the most predictable behaviour and cause the least perturbation of the reaction. A bulky, non-coordinating counter ion and a large, relatively greasy charged group ensure that any molecule bearing the charged tag is efficiently transferred into the gas phase. We have also shown that in the resulting mass spectra species bearing the same charged tag are represented as a function of their concentration in solution relative to each other. This ensures straightforward quantification of tagged species in the reaction mixture.

The second and fourth barriers can be overcome by using PSI-MS which was introduced in Chapter 4. PSI-MS greatly simplifies the handling of air- and moisture- sensitive solutions by maintaining them in a Schlenk flask environment and transferring them cannula-style directly into the mass spectrometer in a continuous, regulated flow. The continuous nature of sample introduction means that sampling time is reduced almost to zero and pseudo real-time data can be collected.

In addition to addressing the four major problems outlined above, we have also demonstrated that our approach can be successfully employed to (1) obtain information on the identity and reactivity of catalytically active species in a reaction mixture and (2) gather rich kinetic data relating to the products, reactants *and* intermediates in a catalytic reaction; all in a single experiment. This was established in Chapters 5 and 6 using the copper-free Sonogashira reaction as a test case. The kinetic data we obtain can be quantitative and initial tests indicate that the mechanism we propose for the copper-free Sonogashira cross-coupling reaction can be accurately modelled using numerical methods.

The methodology described herein provides organometallic chemists with an inexpensive and easy-to-implement method for monitoring reactions continuously, with stirring, in any solvent and at any temperature. PSI can also be used for routine MS analysis of air- or moisture-sensitive molecules; a task that has been non-trivial in the past. The experimental setup can detect low-concentration, highly reactive organometallic compounds, and simultaneously provide reliable data for the more abundant and stable, charged reactants and products. By making use of both charged substrates and charged ligands to visualize the reaction, and by employing both the positive- and negative-ion modes of ESI-MS we can obtain a comprehensive view of the processes that occur during a catalytic reaction; all of this in real-time and under standard reaction conditions. We anticipate that this methodology will become a valuable tool for chemists investigating the detailed mechanisms of catalytic and stoichiometric homogeneous reactions.

References

1. Grayson, M. A., *Measuring Mass: From Positive Rays to Proteins*. Chemical Heritage Press: Philadelphia, 2002.

2. Thomson, J. J., *Proceedings of the Royal Society of London. Series A* **1913,** *89* (607), 1-20.

3. Dempster, A. J., *Phys. Rev.* **1918,** *11* (4), 316.

4. Dempster, A. J., *Philos. Mag. (1798-1977)* **1916,** *31*, 438-43.

5. Traeger, J. C., Electron Ionization (EI): Principles and Instrumentation. In *The Encyclopedia of Mass Spectrometry*, Gross, M. L.; Caprioli, R. M., Eds. Elsevier Ltd.: Amsterdam, 2007; Vol. 6, p 119.

6. Munson, M. S. B.; Field, F. H., *J. Am. Chem. Soc.* **1966,** *88* (12), 2621-30.

7. Yamashita, M.; Fenn, J. B., *J. Phys. Chem.* **1984,** *88* (20), 4451-9.

8. Fenn, J. B.; Mann, M.; Meng, C. K.; Wong, S. F.; Whitehouse, C. M., *Science* **1989,** *246* (4926), 64-71.

9. Tanaka, K.; Waki, H.; Ido, Y.; Akita, S.; Yoshida, Y.; Yohida, T., *Rapid Commun. Mass Spectrom.* **1988,** *2* (8), 151-3.

10. Dole, M.; Mack, L. L.; Hines, R. L.; Mobley, R. C.; Ferguson, L. D.; Alice, M. B., *J. Chem. Phys.* **1968,** *49* (5), 2240-9.

11. Zenobi, R.; Knochenmuss, R., *Mass Spectrom. Rev.* **1999,** *17* (5), 337-366.

12. Hillenkamp, F.; Karas, M., *Int. J. Mass Spectrom.* **2000,** *200* (1-3), 71-77.

13. Dawson, P. H., *Quadrupole Mass Spectrometry and its Applications*. Elsevier: Amsterdam, 1976. Republished in 1997.

14. Paul, W.; Steinwedel, H., *Z. Naturforsch.* **1953,** *8a*, 448-50.

15. Stephens, W. E., *Phys. Rev.* **1946,** *69*, 691.

16. Paul, W.; Reinhard, H. P.; Zahn, O., *Z. Phys.* **1958,** *152*, 143-82.

17. Comisarow, M. B.; Marshall, A. G., *Chem. Phys. Lett.* **1974,** *25* (2), 282-3.

18. Futrell, J. H.; Miller, C. D., *Rev. Sci. Instrum.* **1966,** *37* (11), 1521-6.

19. de Hoffmann, E.; Stroobant, V.; Eds. Analysis of Biomolecules. In *Mass Spectrometry: Principles and Applications, Third Edition*, John Wiley & Sons, Ltd.: 2007; pp 305-388.

20. De la Mora, J. F.; Van Berkel, G. J.; Enke, C. G.; Cole, R. B.; Martinez-Sanchez, M.; Fenn, J. B., *J. Mass Spectrom.* **2000,** *35* (8), 939-952.

21. Eberlin, M. N., *Eur. J. Mass Spectrom.* **2007,** *13* (1), 19-28.

22. Siu, K. W. M.; Guevremont, R.; Le Blanc, J. C. Y.; Gardner, G. J.; Berman, S. S., *J. Chromatogr. A* **1991,** *554* (1-2), 27-38.

23. Canty, A. J.; Traill, P. R.; Colton, R.; Thomas, I. M., *Inorg. Chim. Acta* **1993,** *210* (1), 91-7.

24. Bonchio, M.; Licini, G.; Modena, G.; Bortolini, O.; Moro, S.; Nugent, W. A., *J. Am. Chem. Soc.* **1999,** *121* (26), 6258-6268.

25. Li, Z.; Tang, Z. H.; Hu, X. X.; Xia, C. G., *Chem. Eur. J.* **2005,** *11* (4), 1210-1216.

26. Gilbert, B. C.; Lindsay Smith, J. R.; Mairata i Payeras, A.; Oakes, J.; Pons i Prats, R., *J. Mol. Cat. A: Chem.* **2004,** *219* (2), 265-272.

27. Chen, H.; Tagore, R.; Olack, G.; Vrettos, J. S.; Weng, T. C.; Penner-Hahn, J.; Crabtree, R. H.; Brudvig, G. W., *Inorg. Chem.* **2007,** *46* (1), 34-43.

28. Dyson, P. J.; Russell, K.; Welton, T., *Inorg. Chem. Commun.* **2001,** *4* (10), 571-573.

29. Pelagatti, P.; Carcelli, M.; Calbiani, F.; Cassi, C.; Elviri, L.; Pelizzi, C.; Rizzotti, U.; Rogolino, D., *Organometallics* **2005,** *24* (24), 5836-5844.

30. Daguenet, C.; Scopelliti, R.; Dyson, P. J., *Organometallics* **2004,** *23* (21), 4849-4857.

31. Vicent, C.; Viciano, M.; Mas-Marza, E.; Sanau, M.; Peris, E., *Organometallics* **2006,** *25* (15), 3713-3720.

32. Wilson, S. R.; Wu, Y., *Organometallics* **1993,** *12* (4), 1478-80.

33. Raminelli, C.; Prechtl, M. H. G.; Santos, L. S.; Eberlin, M. N.; Comasseto, J. V., *Organometallics* **2004,** *23* (16), 3990-3996.

34. Chevrin, C.; Le Bras, J.; Henin, F.; Muzart, J.; Pla-Quintana, A.; Roglans, A.; Pleixats, R., *Organometallics* **2004,** *23* (20), 4796-4799.

35. Masllorens, J.; Gonzalez, I.; Roglans, A., *Eur. J. Org. Chem.* **2007,** (1), 158-166.

36. Sabino, A. A.; Machado, A. H. L.; Correia, C. R. D.; Eberlin, M. N., *Angew. Chem. Int. Ed.* **2004,** *43* (19), 2514-2518.

37. Enquist, P. A.; Nilsson, P.; Sjoberg, P.; Larhed, M., *J. Org. Chem.* **2006,** *71* (23), 8779-8786.

38. Svennebring, A.; Sjoberg, P. J. R.; Larhed, M.; Nilsson, P., *Tetrahedron* **2008,** *64* (8), 1808-1812.

39. Chevrin, C.; Le Bras, J.; Roglans, A.; Harakat, D.; Muzart, J., *New J. Chem.* **2007,** *31* (1), 121-126.

40. Markert, C.; Neuburger, M.; Kulicke, K.; Meuwly, M.; Pfaltz, A., *Angew. Chem. Int. Ed. Engl.* **2007,** *46* (31), 5892-5.

41. Roglans, A.; Pla-Quintana, A., Palladium intermediates in solution. In *Reactive Intermediates: MS Investigations in Solution*, Santos, L. S., Ed. Wiley-VCH Verlag GmbH & Co. KGaA: 2010; pp 229-275.

42. O'Hair, R. A. J., Gas phase ligand fragmentation to unmask reactive metallic species. In *Reactive Intermediates: MS Investigations in Solution*, Santos, L. S., Ed. Wiley-VCH Verlag GmbH & Co. KGaA: 2010; pp 199-227.

43. McIndoe, J. S., Mass spectrometry in organmetallic chemistry. In *Spectroscopic Properties of Inorganic and Organometallic Compounds*, Yarwood, J.; Douthwaite, R.; Duckett, S., Eds. Royal Society of Chemistry: 2010; Vol. 41, pp 288-308.

44. Bonchio, M.; Bortolini, O.; Conte, V.; Primon, S., *J. Chem. Soc., Perkin Trans. 2* **2001,** (5), 763-765.

45. Bonchio, M.; Licini, G.; Modena, G.; Moro, S.; Bortolini, O.; Traldi, P.; Nugent, W., *Chem. Commun.* **1997,** (9), 869-870.

46. Bortolini, O.; Carraro, M.; Conte, V.; Moro, S., *Eur. J. Inorg. Chem.* **2003,** (1), 42-46.

47. Gilbert, B. C.; Kamp, N. W. J.; Lindsay Smith, J. R.; Oakes, J., *J. Chem. Soc., Perkin Trans. 2* **1998,** (9), 1841-1844.

48. Gilbert, B. C.; Lindsay Smith, J. R.; Newton, M. S.; Oakes, J.; Pons i Prats, R., *Org. Biomol. Chem.* **2003,** *1* (9), 1568-1577.

49. Kim, C.; Chen, K.; Kim, J.; Que, L., Jr., *J. Am. Chem. Soc.* **1997,** *119* (25), 5964-5965.

50. Feichtinger, D.; Plattner, D. A., *Angew. Chem., Int. Ed. Engl.* **1997,** *36* (16), 1718-1719.

51. Oyman, Z. O.; Ming, W.; Van der Linde, R., *Appl. Catal., A* **2007,** *316* (2), 191-196.

52. Dubois, L.; Caspar, R.; Jacquamet, L.; Petit, P. E.; Charlot, M. F.; Baffert, C.; Collomb, M. N.; Deronzier, A.; Latour, J. M., *Inorg. Chem.* **2003,** *42* (16), 4817-4827.

53. Dubois, L.; Xiang, D. F.; Tan, X. S.; Latour, J. M., *Eur. J. Inorg. Chem.* **2005,** (8), 1565-1571.

54. Lessa, J. A.; Horn, A.; Bull, E. S.; Rocha, M. R.; Benassi, M.; Catharino, R. R.; Eberlin, M. N.; Casellato, A.; Noble, C. J.; Hanson, G. R.; Schenk, G.; Silva, G. C.; Antunes, O. A. C.; Fernandes, C., *Inorg. Chem.* **2009,** *48* (10), 4569-4579.

55. Yin, C. X.; Finke, R. G., *J. Am. Chem. Soc.* **2005,** *127* (25), 9003-9013.

56. Fujii, A.; Hagiwara, E.; Sodeoka, M., *J. Am. Chem. Soc.* **1999,** *121* (23), 5450-5458.

57. Gao, Y. H.; Yang, L.; Zhou, W.; Xu, L. W.; Xia, C. G., *Appl. Organomet. Chem.* **2009,** *23* (3), 114-118.

58. Kikukawa, K.; Matsuda, T., *Chem. Lett.* **1977,** (2), 159-62.

59. Stefani, H. A.; Pena, J. M.; Gueogjian, K.; Petragnani, N.; Vaz, B. G.; Eberlin, M. N., *Tetrahedron Lett.* **2009,** *50* (40), 5589-5595.

60. Nunes, C. M.; Monteiro, A. L., *J. Braz. Chem. Soc.* **2007,** *18* (7), 1443-1447.

61. Zawartka, W.; Gniewek, A.; Trzeciak, A. M.; Ziolkowski, J. J.; Pernak, J., *J. Mol. Catal. A: Chem.* **2009,** *304* (1-2), 8-15.

62. Tromp, M.; Sietsma, J. R. A.; Bokhoven, S. A. v.; Strijdonck, G. P. F. v.; Haaren, R. J. v.; Eerden, A. M. J. v. d.; Leewen, P. W. N. M. v.; Koningsberger, D. C., *Chem. Commun.* **2003**, 128-129.

63. Adlhart, C.; Chen, P., *Helv. Chim. Acta* **2003,** *86* (4), 941-949.

64. Kim, Y. M.; Chen, P., *Int. J. Mass Spectrom.* **1999,** *185/186/187*, 871-881.

65. Hinderling, C.; Adlhart, C.; Chen, P., *Angew. Chem. Int. Ed.* **1998,** *37* (19), 2685-2689.

66. Feichtinger, D.; Plattner, D. A.; Chen, P., *J. Am. Chem. Soc.* **1998,** *120* (28), 7125-7126.

67. Chen, P., *Angew. Chem. Int. Ed.* **2003,** *42* (25), 2832-2847.

68. Hinderling, C.; Plattner, D. A.; Chen, P., *Angew. Chem. Int. Ed. Engl.* **1997,** *36* (3), 243-244.

69. Hinderling, C.; Feichtinger, D.; Plattner, D. A.; Chen, P., *J. Am. Chem. Soc.* **1997,** *119* (44), 10793-10804.

70. Henderson, W.; Evans, C., *Inorg. Chim. Acta* **1999,** *294* (2), 183-192.

71. Bonchio, M.; Licini, G.; Modena, G.; Moro, S.; Bortolini, O.; Traldi, P.; Nugent, W., *Chem. Commun.* **1997,** (9), 869-870.

72. Brown, J. M.; Hii, K. K., *Angew. Chem. Int. Ed. Engl.* **1996,** *35* (6), 657-9.

73. Ripa, L.; Hallberg, A., *J. Org. Chem.* **1996,** *61* (20), 7147-7155.

74. Aramendia, M. A.; Lafont, F.; Moreno-Manas, M.; Pleixats, R.; Roglans, A., *J. Org. Chem.* **1999,** *64* (10), 3592-3594.

75. Anna Pla-Quintana, A. R., *Arkivoc* **2005,** (ix), 51-62.

76. Fernandes, T. d. A.; Gontijo, V. B.; Eberlin, M. N.; da Silva, A. J. M.; Costa, P. R. R., *J. Org. Chem.* **2010,** *75* (21), 7085-7091.

77. Buarque, C. D.; Pinho, V. D.; Vaz, B. G.; Eberlin, M. N.; da Silva, A. J. M.; Costa, P. R. R., *J. Organomet. Chem.* **2010,** *695* (18), 2062-2067.

78. Santos, L. S.; Rosso, G. B.; Pilli, R. A.; Eberlin, M. N., *J. Org. Chem.* **2007,** *72* (15), 5809-5812.

79. Zhou, J.; Tang, W.; Guo, Y.; Ding, Y., *Chin. J. Chem.* **2009,** *27* (9), 1733-1740.

80. Thiery, E.; Chevrin, C.; Le, B. J.; Harakat, D.; Muzart, J., *J. Org. Chem.* **2007,** *72* (5), 1859-1862.

81. Guo, H.; Qian, R.; Liao, Y.; Ma, S.; Guo, Y., *J. Am. Chem. Soc.* **2005,** *127* (37), 13060-13064.

82. Kenny, J. A.; Wills, M.; Versluis, K.; Heck, A. J. R.; Walsgrove, T., *Chem. Commun.* **2000,** (1), 99-100.

83. Noyori, R.; Hashiguchi, S., *Acc. Chem. Res.* **1997,** *30* (2), 97-102.

84. Aliprantis, A. O.; Canary, J. W., *J. Am. Chem. Soc.* **1994,** *116* (15), 6985-6.

85. Colton, R.; Traeger, J. C., *Inorg. Chim. Acta* **1992,** *201* (2), 153-5.

86. Ahmed, I.; Bond, A. M.; Colton, R.; Jurcevic, M.; Traeger, J. C.; Walter, J. N., *J. Organomet. Chem.* **1993,** *447* (1), 59-65.

87. Bryce, D. J. F.; Dyson, P. J.; Nicholson, B. K.; Parker, D. G., *Polyhedron* **1998,** *17* (17), 2899-2905.

88. Decker, C.; Henderson, W.; Nicholson, B. K., *J. Chem. Soc., Dalton Trans.* **1999,** (19), 3507-3513.

89. Adlhart, C.; Hinderling, C.; Baumann, H.; Chen, P., *J. Am. Chem. Soc.* **2000,** *122* (34), 8204-8214.

90. Chen, P., *Angew. Chem. Int. Ed.* **2003,** *42* (25), 2832-2847.

91. Wang, H.; Metzger, J. O., *Organometallics* **2008,** *27* (12), 2761-2766.

92. Kirkland, T. A.; Lynn, D. M.; Grubbs, R. H., *J. Org. Chem.* **1998,** *63* (26), 9904-9909.

93. Mohr, B.; Lynn, D. M.; Grubbs, R. H., *Organometallics* **1996,** *15* (20), 4317-4325.

94. Beierlein, C. H.; Breit, B.; Paz, S. R. A.; Plattner, D. A., *Organometallics* **2010,** *29* (11), 2521-2532.

95. Schade, M. A.; Fleckenstein, J. E.; Knochel, P.; Koszinowski, K., *J. Org. Chem.* **2010,** *75* (20), 6848-6857.

96. Farrer, N. J.; McDonald, R.; McIndoe, J. S., *Dalton Trans.* **2006,** (38), 4570-4579.

97. Chisholm, D. M.; Oliver, A. G.; McIndoe, J. S., *Dalton Trans.* **2010,** *39* (2), 364-373.

98. Jackson, S. M.; Chisholm, D. M.; McIndoe, J. S.; Rosenberg, L., *Eur. J. Inorg. Chem.* **2011,** *2011* (3), 327-330.

99. Crawford, E.; Lohr, T.; Leitao, E. M.; Kwok, S.; McIndoe, J. S., *Dalton Trans.* **2009,** (42), 9110-9112.

100. Takahashi, H.; Hayakawa, T.; Ueda, M., *Chem. Lett.* **2000,** (6), 684-685.

101. Santos, L. S., *J. Org. Chem.* **2008**, 235-253.

102. Santos, L. S., On-line monitoring reactions by electrospray ionization mass spectrometry. In *Reactive Intermediates: MS Investigations in Solution*, Santos, L. S., Ed. Wiley-VCH Verlag GmbH & Co. KGaA: 2010; pp 133-198.

103. Santos, L. S.; Knaack, L.; Metzger, J. O., *Int. J. Mass Spectrom.* **2005,** *246* (1-3), 84-104.

104. Griep-Raming, J.; Meyer, S.; Bruhn, T.; Metzger, J. O., *Angew. Chem., Int. Ed.* **2002,** *41* (15), 2738-2742.

105. Wilson, D. J.; Konermann, L., *Anal. Chem.* **2003,** *75* (23), 6408-6414.

106. Modestov, A. D.; Gun, J.; Savotine, I.; Lev, O., *J. Electroanal. Chem.* **2004,** *565* (1), 7-19.

107. Arakawa, R.; Lu, J.; Yoshimura, A.; Nozaki, K.; Ohno, T.; Doe, H.; Matsuo, T., *Inorg. Chem.* **1995,** *34* (15), 3874-8.

108. Brum, J.; Dell'Orco, P., *Rapid Commun. Mass Spectrom.* **1998,** *12* (11), 741-745.

109. Ding, W.; Johnson, K. A.; Amster, I. J.; Kutal, C., *Inorg. Chem.* **2001,** *40* (27), 6865-6866.

110. Dell'Orco, P.; Brum, J.; Matsuoka, R.; Badlani, M.; Muske, K., *Anal. Chem.* **1999,** *71* (22), 5165-5170.

111. Santos, V. G.; Regiani, T. s.; Dias, F. F. G.; Romao, W.; Jara, J. L. P.; Klitzke, C. c. F.; Coelho, F.; Eberlin, M. N., *Anal. Chem. 83* (4), 1375-1380.

112. Henderson, W., *Mass Spectrometry of Inorganic and Organometallic Compounds*. John Wiley & Sons Publishers: 2005. Section 3.9.

113. Schneider, B. B.; Chen, D. D. Y., *Anal. Chem.* **2000,** *72* (4), 791-799.

114. Iribarne, J. V.; Thomson, B. A., *J. Chem. Phys.* **1976,** *64* (6), 2287-94.

115. McQuinn, K.; Hof, F.; McIndoe, J. S., *Chem. Commun.* **2007,** (40), 4099-4101.

116. de Hoffmann, E.; Stroobant, V.; Eds., Electrospray. In *Mass Spectrometry: Principles and Applications, Third Edition*, John Wiley & Sons, Ltd.: 2007; pp 43-55.

117. Di Marco Valerio, B.; Bombi, G. G., *Mass Spectrom. Rev.* **2006,** *25* (3), 347-79.

118. Manisali, I.; Chen, D. D. Y.; Schneider, B. B., *Trends Anal. Chem.* **2006,** *25* (3), 243-256.

119. de Hoffmann, E.; Stroobant, V.; Eds., Quadrupole Analysers. In *Mass Spectrometry: Principles and Applications, Third Edition*, John Wiley & Sons, Ltd.: 2007; pp 88-100.

120. Henderson, W.; McIndoe, J. S., Orthogonal TOF. In *Mass Spectrometry of Inorganic and Organometallic Compounds*, John Wiley & Sons Ltd.: West Sussex, 2005; p 38.

121. Dyson, P. J.; Johnson, B. F. G.; McIndoe, J. S.; Langridge-Smith, P. R. R., Energy-Dependent Electrospray Ionisation Mass Spectrometry: Applications in Transition Metal Carbonyl Chemistry. John Wiley & Sons, Ltd.: 2000; Vol. 14, pp 311-313.

122. Plattner, D. A., *Int. J. Mass Spectrom.* **2001,** *207* (3), 125-144.

123. Henderson, M.; Kwok, S.; McIndoe, J., *J. Am. Soc. Mass Spectrom.* **2009,** *20* (4), 658-666.

124. de Hoffmann, E.; Stroobant, V., Mass Spectrometry: Principles and Applications. 3rd ed.; John Wiley & Sons, Ltd: 2007.

125. Chisholm, D. M.; Scott McIndoe, J., *Dalton Trans.* **2008,** (30), 3933-3945.

126. Alder, R. W.; Bowman, P. S.; Steele, W. R. S.; Winterman, D. R., *Chem. Commun.* **1968,** (13), 723-4.

127. Alder, R. W., *Chem. Rev.* **1989,** *89* (5), 1215-23.

128. Llamas-Saiz, A. L.; Foces-Foces, C.; Elguero, J., *J. Mol. Struct.* **1994,** *328*, 297-323.

129. Nagasawa, K., Related Organocatalysts (1): A Proton Sponge. In *Superbases for Organic Synthesis*, Ishikawa, T., Ed. John Wiley & Sons, Ltd: 2009; pp 251-271.

130. Pozharskii, A. F.; Ozeryanskii, V. A. In *Proton Sponges*, John Wiley & Sons Ltd.: 2007; pp 931-1139.

131. Staab, H. A.; Saupe, T., *Angew. Chem.* **1988,** *100* (7), 895-909.

132. Howard, S. T., *J. Am. Chem. Soc.* **2000,** *122* (34), 8238-8244.

133. Pozharskii, A. F.; Degtyarev, A. V.; Ryabtsova, O. V.; Ozeryanskii, V. A.; Kletskii, M. E.; Starikova, Z. A.; Sobczyk, L.; Filarowski, A., *J. Org. Chem.* **2007,** *72* (8), 3006-3019.

134. Pampaloni, G., *Coord. Chem. Rev.* **2010,** *254* (5-6), 402-419.

135. Rigby, J. H.; Kondratenko, M. A., Arene Complexes as Catalysts. In *Transition Metal Arene pi-Complexes in Organic Synthesis and Catalysts*, Springer Berlin/Heidelberg: 2004; Vol. 7, pp 181-204.

136. Alder, R. W.; Eastment, P.; Hext, N. M.; Moss, R. E.; Orpen, A. G.; White, J. M., *J. Chem. Soc., Chem. Commun.* **1988,** (23), 1528-30.

137. Mahaffy, C. A. L.; Pauson, P. L.; Rausch, M. D.; Lee, W., *(η6 -Arene) Tricarbonylchromium Complexes*. John Wiley & Sons, Inc.: 2007; p 154-158.

138. Carter, O. L.; McPhail, A. T.; Sim, G. A., *J. Chem. Soc. A: Inorg., Phys., Theor.* **1966**, 822-838.

139. Alamiry, M. A. H.; Brennan, P.; Long, C.; Pryce, M. T., *J. Organomet. Chem.* **2008,** *693* (17), 2907-2914.

140. McGrady, J. E.; Dyson, P. J., *J. Organomet. Chem.* **2000,** *607* (1-2), 203-207.

141. Gilow, H. M.; Burton, D. E., *J. Org. Chem.* **1981,** *46* (11), 2221-5.

142. Hibbert, F.; Emsley, J., *Adv. Phys. Org. Chem.* **1990,** *26*, 255-79.

143. Charmant, J. P. H.; Lloyd-Jones, G. C.; Peakman, T. M.; Woodward, R. L., *Eur. J. Org. Chem.* **1999,** (10), 2501-2510.

144. Berthelot, J.; Guette, C.; Essayegh, M.; Desbene, P. L.; Basselier, J. J., *Synth. Commun.* **1986,** *16* (13), 1641-5.

145. Vistorobskii, N. V.; Pozharskii, A. F., *Zh. Org. Khim.* **1989,** *25* (10), 2154-61.

146. Farrer, N. J. Synthesis of Electrospray-Active Phosphine Ligands and their Complexes. PhD Dissertation. University of Cambridge, 2007.

147. Kosugi, M.; Sasazawa, K.; Shimizu, Y.; Migita, T., *Chem. Lett.* **1977,** (3), 301-2.

148. Amatore, C.; Jutand, A.; M'Barki, M. A., *Organometallics* **1992,** *11* (9), 3009-3013.

149. Amatore, C.; Jutand, A.; Medeiros, M. J.; Mottier, L., *J. Electroanal. Chem.* **1997,** *422* (1-2), 125-132.

150. Stelzer, O.; Rossenbach, S.; Hoff, D., Catalysts for an Aqueous Catalysis: Section 3.2. In *Aqueous-Phase Organometallic Catalysis*, Boy Cornils, W. A. H., Ed. Wiley-VCH Verlag GmbH & Co. KGaA: 2005; pp 100-197.

151. Ahrland, S.; Chatt, J.; Davies, N. R.; Williams, A. A., *J. Chem. Soc.* **1958**, 276-88.

152. Borowski, A. F.; Cole-Hamilton, D. J.; Wilkinson, G., *Nouv. J. Chim.* **1978,** *2* (2), 137-44.

153. Andriollo, A.; Bolívar, A.; López, F. A.; Páez, D. E., *Inorg. Chim. Acta* **1995,** *238* (1-2), 187-192.

154. Okano, T.; Uchida, I.; Nakagaki, T.; Konishi, H.; Kiji, J., *J. Mol. Catal.* **1989,** *54* (1), 65-71.

155. Casalnuovo, A. L.; Calabrese, J. C., *J. Am. Chem. Soc.* **1990,** *112* (11), 4324-30.

156. Joó, F.; Tóth, Z., *J. Mol. Catal.* **1980,** *8* (4), 369-383.

157. Barton, M.; Atwood, J. D., *J. Coord. Chem.* **1991,** *24* (1), 43 - 67.

158. Herrmann, W. A.; Kohlpaintner, C. W., *Angew. Chem. Int. Ed. Engl.* **1993,** *32* (11), 1524-1544.

159. Barton, M. R.; Yuegang, Z.; Atwood, J. D., *J. Coord. Chem.* **2002,** *55*, 969-983.

160. Gulyas, H.; Bacsik, Z.; Szollosy, A.; Bakos, J., *Advanced Synthesis & Catalysis* **2006,** *348*, 1306-1310.

161. Darensbourg, D. J.; Ortiz, C. G., in *Catalysts for an Aqueous Catalysis* Wiley-VCH Verlag GmbH & Co. KGaA: 2005; p 70-99.

162. Tolman, C. A., *Chem. Rev.* **1977,** *77* (3), 313-348.

163. Vikse, K. L.; Henderson, M. A.; Oliver, A. G.; McIndoe, J. S., *Chem. Commun.* **2010,** *46* (39), 7412-7414.

164. Saupe, T.; Krieger, C.; Staab, H. A., *Angew. Chem.* **1986,** *98* (5), 460-462.

165. Raab, V.; Kipke, J.; Gschwind, R. M.; Sundermeyer, J., *Chem. Eur. J.* **2002,** *8*, 1682-1693.

166. Eelman, M. D.; Blacquiere, J. M.; Moriarty, M. M.; Fogg, D. E., *Angew. Chem. Int. Ed.* **2008,** *47* (2), 303-306.

167. Lubben, A. T.; McIndoe, J. S.; Weller, A. S., *Organometallics* **2008,** *27* (13), 3303-3306.

168. Linden, H. B., *Eur. J. Mass Spectrom.* **2004,** *10*, 459-468.

169. Vikse, K. L.; Woods, M. P.; McIndoe, J. S., *Organometallics* **2010,** *29* (23), 6615-6618.

170. Knovel Critical Tables (2nd Edition). Knovel: 2008. (http://www.knovel.com)

171. Nyman, C. J.; Wymore, C. E.; Wilkinson, G., *J. Chem. Soc. A* **1968,** (3), 561-3.

172. Dieck, H. A.; Heck, F. R., *J. Organomet. Chem.* **1975,** *93* (2), 259-263.

173. Cassar, L., *J. Organomet. Chem.* **1975,** *93* (2), 253-257.

174. Sonogashira, K.; Tohda, Y.; Hagihara, N., *Tetrahedron Lett.* **1975,** *16* (50), 4467-4470.

175. Chinchilla, R.; Najera, C., *Chem. Rev.* **2007,** *107* (3), 874-922.

176. Siemsen, P.; Livingston, R. C.; Diederich, F., *Angew. Chem. Int. Ed. Engl.* **2000,** *39*, 2632-2657.

177. Amatore, C.; Jutand, A., *Acc. Chem. Res.* **2000,** *33* (5), 314-321.

178. Amatore, C.; Bensalem, S.; Ghalem, S.; Jutand, A.; Medjour, Y., *Eur. J. Org. Chem.* **2004**, 366-371.

179. Amatore, C.; Bensalem, S.; Ghalem, S.; Jutand, A., *J. Organomet. Chem.* **2004,** *689* (24), 4642-4646.

180. Ljungdahl, T.; Bennur, T.; Dallas, A.; Emtenaes, H.; Maartensson, J., *Organometallics* **2008,** *27* (11), 2490-2498.

181. Tougerti, A.; Negri, S.; Jutand, A., *Chem. Eur. J.* **2007,** *13* (2), 666-676.

182. Jutand, A.; Négri, S.; Principaud, A., *Eur. J. Inorg. Chem.* **2005,** *2005* (4), 631-635.

183. Ananikov, V. P.; Musaev, D. G.; Morokuma, K., *Eur. J. Inorg. Chem.* **2007,** *2007*, 5390-5399.

184. Stambuli, J. P.; Incarvito, C. D.; Buehl, M.; Hartwig, J. F., *J. Am. Chem. Soc.* **2004,** *126* (4), 1184-1194.

185. Barder, T. E.; Walker, S. D.; Martinelli, J. R.; Buchwald, S. L., *J. Am. Chem. Soc.* **2005,** *127* (13), 4685-4696.

186. Fischer, E. O.; Werner, H., *Chem. Ber.* **1962,** *95*, 703-8.

187. Ghilardi, C. A.; Midollini, S.; Moneti, S.; Orlandini, A.; Ramirez, J. A., *J. Chem. Soc., Chem. Commun.* **1989,** (5), 304-6.

188. Huser, M.; Youinou, M. T.; Osborn, J. A., *Angew. Chem.* **1989,** *101* (10), 1427-1430.

189. Leoni, P., *Organometallics* **1993,** *12* (7), 2432-4.

190. Ahlquist, M. r.; Fristrup, P.; Tanner, D.; Norrby, P. O., *Organometallics* **2006,** *25* (8), 2066-2073.

191. Kwong, F. Y.; Chan, K. S., *Chem. Commun.* **2000,** (12), 1069-1070.

192. Macgregor, S. A., *Chem. Soc. Rev.* **2007,** *36* (1), 67-76.

193. Fitton, P.; Rick, E. A., *J. Organomet. Chem.* **1971,** *28* (2), 287-291.

194. Bordwell, F. G.; Drucker, G. E.; Andersen, N. H.; Denniston, A. D., *J. Am. Chem. Soc.* **1986,** *108* (23), 7310-13.

195. Kolthoff, I. M.; Chantooni, M. K., Jr.; Bhowmik, S., *J. Am. Chem. Soc.* **1968,** *90* (1), 23-8.

196. Long, G. L.; Boss, C. B., *Anal. Chem.* **1981,** *53* (14), 2363-2365.

197. Soheili, A.; Albaneze-Walker, J.; Murry, J. A.; Dormer, P. G.; Hughes, D. L., *Org. Lett.* **2003,** *5* (22), 4191-4194.

198. Shekhar, S.; Hartwig, J. F., *J. Am. Chem. Soc.* **2004,** *126* (40), 13016-13027.

199. Hartwig, J. F., *Inorg. Chem.* **2007,** *46* (6), 1936-1947.

200. Low, J. J.; Goddard, W. A., *J. Am. Chem. Soc.* **1986,** *108* (20), 6115-28.

201. Williams, J. P.; Smith, D. C.; Green, B. N.; Marsden, B. D.; Jennings, K. R.; Roberts, L. M.; Scrivens, J. H., *Biophys. J.* **2006,** *90* (9), 3246-3254.

202. Lepore, S. D.; Khoram, A.; Bromfield, D. C.; Cohn, P.; Jairaj, V.; Silvestri, M. A., *J. Org. Chem.* **2005,** *70* (18), 7443-7446.

203. Chen, J. G.; Suryanarayanan, V.; Lee, K. M.; Ho, K. C., *Sol. Energ. Mat. Sol. C.* **2007,** *91* (15-16), 1432-1437.

Appendix A: Crystallographic details for 1,8-bis(dimethylamino)-2-(4-methoxyphenyl)naphthalene (3)

Solved by Dr. Robert MacDonald, University of Alberta

Table 1. Crystallographic Experimental Details for **3**

A. Crystal Data	
formula	$C_{21}H_{24}N_2O$
formula weight	320.42
crystal dimensions (mm)	0.48 x 0.47 x 0.31
crystal system	monoclinic
space group	$P2_1/c$ (No. 14)
unit cell parameters[a]	
a (Å)	9.3443 (6)
b (Å)	20.9023 (13)
c (Å)	9.7917 (6)
β (deg)	112.4583 (8)
V (Å^3)	1767.44 (19)
Z	4
ρ_{calcd} (g cm^{-3})	1.204
μ (mm^{-1})	0.074
B. Data Collection and Refinement Conditions	
diffractometer	Bruker PLATFORM/SMART 1000 CCD[b]
radiation (λ [Å])	graphite-monochromated Mo Kα (0.71073)
temperature (°C)	–80
scan type	ω scans (0.3°) (15 s exposures)
data collection 2θ limit (deg)	52.76
total data collected	13946 ($-11 \le h \le 11$, $-26 \le k \le 26$, $-12 \le l \le 12$)
independent reflections	3613 (R_{int} = 0.0153)
number of observed reflections (*NO*)	3165 [$F_o^2 \ge 2\sigma(F_o^2)$]
structure solution method	direct methods (*SHELXS–86*[c])
refinement method	full-matrix least-squares on F^2 (*SHELXL–93*[d])
absorption correction method	multi-scan (*SADABS*)
range of transmission factors	0.9773–0.9652
data/restraints/parameters	3613 [$F_o^2 \ge -3\sigma(F_o^2)$] / 0 / 221
goodness-of-fit (S)[e]	1.032 [$F_o^2 \ge -3\sigma(F_o^2)$]
final R indices[f]	
R_1 [$F_o^2 \ge 2\sigma(F_o^2)$]	0.0364
wR_2 [$F_o^2 \ge -3\sigma(F_o^2)$]	0.1059
largest difference peak and hole	0.208 and –0.137 e Å^{-3}

[a]Obtained from least-squares refinement of 6300 reflections with $4.72° < 2\theta < 52.68°$.

[b]Programs for diffractometer operation, data collection, data reduction and absorption correction were those supplied by Bruker.

[c]Sheldrick, G. M. *Acta Crystallogr.* **1990**, *A46*, 467–473.

[d]Sheldrick, G. M. *SHELXL-93*. Program for crystal structure determination. University of Göttingen, Germany, 1993.

[e]$S = [\Sigma w(F_o^2 - F_c^2)^2/(n - p)]^{1/2}$ (n = number of data; p = number of parameters varied; $w = [\sigma^2(F_o^2) + (0.0549P)^2 + 0.3566P]^{-1}$ where $P = [\text{Max}(F_o^2, 0) + 2F_c^2]/3$).

[f]$R1 = \Sigma||F_o| - |F_c||/\Sigma|F_o|$; $wR2 = [\Sigma w(F_o^2 - F_c^2)^2/\Sigma w(F_o^4)]^{1/2}$.

Table 2. Atomic Coordinates and Equivalent Isotropic Displacement Parameters

Atom	*x*	*y*	*z*	U_{eq}, Å^2
O	0.49743(10)	-0.19108(4)	0.29424(10)	0.0464(2)*
N1	0.15999(11)	0.07747(5)	0.28003(11)	0.0380(2)*
N2	0.01932(12)	0.18758(5)	0.33252(12)	0.0399(2)*
C1	0.30975(14)	0.05674(7)	0.38501(16)	0.0504(3)*
C2	0.16268(16)	0.11639(7)	0.15933(15)	0.0483(3)*
C3	0.12173(16)	0.17131(7)	0.48249(15)	0.0512(3)*
C4	0.00357(18)	0.25659(6)	0.3140(2)	0.0599(4)*
C11	0.02209(12)	0.04578(5)	0.26564(11)	0.0315(2)*
C12	0.01415(13)	-0.02074(5)	0.26050(12)	0.0342(2)*
C13	-0.12647(14)	-0.05222(6)	0.24009(14)	0.0418(3)*
C14	-0.25858(14)	-0.01876(6)	0.21510(15)	0.0432(3)*
C15	-0.25696(13)	0.04876(6)	0.21897(13)	0.0366(3)*
C16	-0.39810(14)	0.08195(7)	0.18837(14)	0.0439(3)*
C17	-0.39950(14)	0.14661(7)	0.19549(15)	0.0459(3)*
C18	-0.26002(14)	0.18085(6)	0.24121(14)	0.0421(3)*
C19	-0.11826(13)	0.15120(5)	0.27560(12)	0.0346(2)*
C20	-0.11361(12)	0.08261(5)	0.25417(11)	0.0322(2)*
C21	0.14640(13)	-0.06258(5)	0.26732(12)	0.0342(2)*
C22	0.19921(13)	-0.06546(5)	0.15283(13)	0.0370(3)*
C23	0.31639(13)	-0.10752(6)	0.15679(13)	0.0383(3)*
C24	0.38268(12)	-0.14720(5)	0.27836(13)	0.0365(3)*
C25	0.33236(13)	-0.14444(6)	0.39459(13)	0.0395(3)*
C26	0.21532(14)	-0.10301(5)	0.38854(13)	0.0382(3)*
C27	0.54344(16)	-0.19962(7)	0.17311(17)	0.0514(3)*

Anisotropically-refined atoms are marked with an asterisk (*). The form of the anisotropic displacement parameter is: $\exp[-2\pi^2(h^2a^{*2}U_{11} + k^2b^{*2}U_{22} + l^2c^{*2}U_{33} + 2klb^*c^*U_{23} + 2hla^*c^*U_{13} + 2hka^*b^*U_{12})]$.

Table 3. Selected Interatomic Distances (Å)

Atom1	Atom2	Distance	Atom1	Atom2	Distance
O	C24	1.3739(13)	C14	C15	1.4117(17)
O	C27	1.4188(17)	C15	C16	1.4172(16)
N1	C1	1.4504(16)	C15	C20	1.4357(15)
N1	C2	1.4430(16)	C16	C17	1.3537(19)
N1	C11	1.4071(13)	C17	C18	1.4019(18)
N2	C3	1.4540(17)	C18	C19	1.3825(16)
N2	C4	1.4543(16)	C19	C20	1.4521(16)
N2	C19	1.4122(15)	C21	C22	1.3880(16)
C11	C12	1.3923(16)	C21	C26	1.3978(16)
C11	C20	1.4505(15)	C22	C23	1.3933(16)
C12	C13	1.4138(15)	C23	C24	1.3875(17)
C12	C21	1.4945(15)	C24	C25	1.3887(17)
C13	C14	1.3573(17)	C25	C26	1.3785(17)

Table 4. Selected Interatomic Angles (deg)

Atom1	Atom2	Atom3	Angle	Atom1	Atom2	Atom3	Angle
C24	O	C27	117.51(10)	C16	C17	C18	120.00(11)
C1	N1	C2	115.78(10)	C17	C18	C19	122.44(12)
C1	N1	C11	121.94(10)	N2	C19	C18	119.86(10)
C2	N1	C11	119.02(10)	N2	C19	C20	121.04(9)
C3	N2	C4	110.75(11)	C18	C19	C20	119.09(10)
C3	N2	C19	114.92(10)	C11	C20	C15	117.71(10)
C4	N2	C19	116.83(10)	C11	C20	C19	125.90(10)
N1	C11	C12	120.51(10)	C15	C20	C19	116.40(10)
N1	C11	C20	119.87(10)	C12	C21	C22	122.16(10)
C12	C11	C20	119.62(9)	C12	C21	C26	119.78(10)
C11	C12	C13	120.25(10)	C22	C21	C26	117.97(10)
C11	C12	C21	123.44(10)	C21	C22	C23	121.54(10)
C13	C12	C21	116.23(10)	C22	C23	C24	119.32(11)
C12	C13	C14	121.18(11)	O	C24	C23	124.71(11)
C13	C14	C15	120.71(11)	O	C24	C25	115.39(10)
C14	C15	C16	118.96(11)	C23	C24	C25	119.89(10)
C14	C15	C20	119.91(10)	C24	C25	C26	120.16(11)
C16	C15	C20	121.14(11)	C21	C26	C25	121.13(11)
C15	C16	C17	120.29(11)				

Table 5. Torsional Angles (deg)

Atom1	Atom2	Atom3	Atom4	Angle	Atom1	Atom2	Atom3	Atom4	Angle
C27	O	C24	C23	-4.77(16)	C13	C14	C15	C20	-1.96(18)
C27	O	C24	C25	174.71(10)	C14	C15	C16	C17	178.06(12)
C1	N1	C11	C12	-44.92(16)	C20	C15	C16	C17	-1.66(18)
C1	N1	C11	C20	135.87(11)	C14	C15	C20	C11	7.92(15)
C2	N1	C11	C12	113.84(12)	C14	C15	C20	C19	-171.88(10)
C2	N1	C11	C20	-65.37(14)	C16	C15	C20	C11	-172.36(10)
C3	N2	C19	C18	115.67(12)	C16	C15	C20	C19	7.84(15)
C3	N2	C19	C20	-63.49(14)	C15	C16	C17	C18	-3.55(19)
C4	N2	C19	C18	-16.62(17)	C16	C17	C18	C19	2.19(19)
C4	N2	C19	C20	164.21(11)	C17	C18	C19	N2	-174.85(11)
N1	C11	C12	C13	-177.46(10)	C17	C18	C19	C20	4.34(17)
N1	C11	C12	C21	-0.93(16)	N2	C19	C20	C11	-9.63(16)
C20	C11	C12	C13	1.75(16)	N2	C19	C20	C15	170.15(10)
C20	C11	C12	C21	178.29(10)	C18	C19	C20	C11	171.20(10)
N1	C11	C20	C15	171.44(10)	C18	C19	C20	C15	-9.02(15)
N1	C11	C20	C19	-8.78(16)	C12	C21	C22	C23	-176.05(10)
C12	C11	C20	C15	-7.78(15)	C26	C21	C22	C23	0.50(17)
C12	C11	C20	C19	172.00(10)	C12	C21	C26	C25	176.75(10)
C11	C12	C13	C14	4.53(18)	C22	C21	C26	C25	0.12(17)
C21	C12	C13	C14	-172.25(11)	C21	C22	C23	C24	-0.42(17)
C11	C12	C21	C22	-69.17(15)	C22	C23	C24	O	179.19(10)
C11	C12	C21	C26	114.34(12)	C22	C23	C24	C25	-0.27(17)
C13	C12	C21	C22	107.50(13)	O	C24	C25	C26	-178.63(10)
C13	C12	C21	C26	-68.99(14)	C23	C24	C25	C26	0.88(17)
C12	C13	C14	C15	-4.43(19)	C24	C25	C26	C21	-0.81(17)
C13	C14	C15	C16	178.32(11)					

Table 6. Anisotropic Displacement Parameters (U_{ij}, Å^2)

Atom	U_{11}	U_{22}	U_{33}	U_{23}	U_{13}	U_{12}
O	0.0388(5)	0.0469(5)	0.0507(5)	0.0029(4)	0.0141(4)	0.0095(4)
N1	0.0293(5)	0.0405(5)	0.0454(6)	-0.0007(4)	0.0158(4)	-0.0030(4)
N2	0.0394(5)	0.0353(5)	0.0463(6)	-0.0010(4)	0.0180(4)	-0.0016(4)
C1	0.0309(6)	0.0536(8)	0.0603(8)	-0.0117(6)	0.0102(6)	-0.0034(5)
C2	0.0474(7)	0.0538(7)	0.0536(8)	-0.0029(6)	0.0303(6)	-0.0128(6)
C3	0.0489(7)	0.0574(8)	0.0442(7)	-0.0119(6)	0.0145(6)	-0.0036(6)
C4	0.0546(8)	0.0394(7)	0.0914(12)	0.0005(7)	0.0343(8)	-0.0027(6)
C11	0.0292(5)	0.0388(6)	0.0275(5)	0.0000(4)	0.0120(4)	-0.0025(4)
C12	0.0350(6)	0.0384(6)	0.0311(5)	0.0010(4)	0.0148(4)	-0.0006(4)
C13	0.0438(7)	0.0370(6)	0.0490(7)	0.0008(5)	0.0227(6)	-0.0051(5)
C14	0.0363(6)	0.0457(7)	0.0526(7)	-0.0024(5)	0.0226(6)	-0.0101(5)
C15	0.0329(6)	0.0460(6)	0.0348(6)	0.0004(5)	0.0173(5)	-0.0025(5)
C16	0.0319(6)	0.0580(8)	0.0463(7)	-0.0007(6)	0.0200(5)	-0.0025(5)
C17	0.0350(6)	0.0580(8)	0.0488(7)	0.0034(6)	0.0206(5)	0.0095(5)
C18	0.0438(6)	0.0432(6)	0.0438(7)	0.0025(5)	0.0220(5)	0.0067(5)
C19	0.0360(6)	0.0397(6)	0.0322(5)	0.0024(4)	0.0176(4)	0.0010(4)
C20	0.0317(5)	0.0396(6)	0.0276(5)	0.0012(4)	0.0138(4)	-0.0005(4)
C21	0.0347(5)	0.0326(5)	0.0351(6)	-0.0012(4)	0.0129(5)	-0.0029(4)
C22	0.0381(6)	0.0383(6)	0.0335(6)	0.0034(5)	0.0126(5)	0.0027(5)
C23	0.0380(6)	0.0422(6)	0.0361(6)	-0.0010(5)	0.0157(5)	0.0001(5)
C24	0.0297(5)	0.0345(6)	0.0410(6)	-0.0024(5)	0.0085(4)	-0.0016(4)
C25	0.0397(6)	0.0386(6)	0.0354(6)	0.0052(5)	0.0089(5)	-0.0002(5)

C26	0.0422(6)	0.0395(6)	0.0340(6)	0.0008(5)	0.0160(5)	-0.0032(5)
C27	0.0478(7)	0.0462(7)	0.0630(8)	-0.0018(6)	0.0243(6)	0.0079(6)

The form of the anisotropic displacement parameter is:
$\exp[-2\pi^2(h^2a^{*2}U_{11} + k^2b^{*2}U_{22} + l^2c^{*2}U_{33} + 2klb^*c^*U_{23} + 2hla^*c^*U_{13} + 2hka^*b^*U_{12})]$

Table 7. Derived Atomic Coordinates and Displacement Parameters for Hydrogen Atoms

Atom	*x*	*y*	*z*	U_{eq}, Å^2
H1A	0.2959	0.0327	0.4650	0.060
H1B	0.3751	0.0942	0.4261	0.060
H1C	0.3595	0.0293	0.3348	0.060
H2A	0.2068	0.0917	0.0998	0.058
H2B	0.2262	0.1545	0.1987	0.058
H2C	0.0569	0.1294	0.0975	0.058
H3A	0.0878	0.1937	0.5528	0.061
H3B	0.2278	0.1843	0.4987	0.061
H3C	0.1186	0.1250	0.4971	0.061
H4A	-0.0595	0.2666	0.2106	0.072
H4B	0.1063	0.2759	0.3412	0.072
H4C	-0.0467	0.2737	0.3776	0.072
H13	-0.1285	-0.0976	0.2439	0.050
H14	-0.3531	-0.0410	0.1948	0.052
H16	-0.4921	0.0587	0.1627	0.053
H17	-0.4950	0.1688	0.1695	0.055
H18	-0.2630	0.2261	0.2489	0.050
H22	0.1544	-0.0381	0.0698	0.044
H23	0.3506	-0.1090	0.0771	0.046
H25	0.3787	-0.1712	0.4785	0.047
H26	0.1809	-0.1019	0.4681	0.046
H27A	0.6269	-0.2313	0.1991	0.062
H27B	0.5803	-0.1588	0.1496	0.062
H27C	0.4549	-0.2146	0.0870	0.062

Appendix B: Crystallographic details for chromium(3)tricarbonyl (4)

Solved by Dr. Allen G. Oliver, University of Notre Dame

DISCUSSION

The complex crystallizes as yellow rod-like crystals. There are four molecules of the complex in the uinit cell of the primitive, centrosymmetric, monoclinic space group $P2_1/n$.

The chromium is coordinated in a three-legged stool fashion by the phenyl ring of a phenoxy group and three carbonyl ligands. The phenoxy group is part of a 1,8 (dimethylamino), 2-phenoxy naphthalene ligand. (formally: 2-(4-methoxyphenyl)-N^1,N^1,N^8,N^8-tetramethylnaphthalene-1,8-diamine).

The crystal was found to be twinned

CRYSTAL SUMMARY

Crystal data for $C_{24}H_{24}CrN_2O_4$; M_r = 456.45; Monoclinic; space group $P2_1/n$; *a* = 9.383(4) Å; *b* = 7.425(3) Å; *c* = 31.562(14) Å; α = 90°; β = 94.852(9)°; γ = 90°; V = 2191.1(16) $Å^3$; Z = 4; T = 150(2) K; λ(Mo-Kα) = 0.71073 Å; μ(Mo-Kα) = 0.555 mm^{-1}; d_{calc} = 1.384g.cm^{-3}; 3458 reflections collected; 3458 unique (R_{int} = 0.0000); giving R_1 = 0.0498, wR_2 = 0.1187 for 2733 data with [I>2σ(I)] and R_1 = 0.0727, wR_2 = 0.1308 for all 3458 data. Residual electron density (e^-.$Å^{-3}$) max/min: 0.235/-0.362.

An arbitrary sphere of data were collected on a yellow rod-like crystal, having approximate dimensions of 0.37 × 0.07 × 0.06 mm, on a Bruker APEX-II diffractometer using a combination of ω- and φ-scans of 0.3°. Data were corrected for absorption and polarization effects and analyzed for space group determination. The structure was solved by direct methods and expanded routinely. The model was refined by full-matrix least-squares analysis of F^2 against all reflections. All non-hydrogen atoms were refined with anisotropic thermal displacement parameters. Unless otherwise noted, hydrogen

atoms were included in calculated positions. Thermal parameters for the hydrogens were tied to the isotropic thermal parameter of the atom to which they are bonded (1.5 × for methyl, 1.2 × for all others).

Table 1. Crystal data and structure refinement for **4**.

Identification code	jsm006
Empirical formula	$C_{24}H_{24}CrN_2O_4$
Formula weight	456.45
Temperature	150(2) K
Wavelength	0.71073 Å
Crystal system	Monoclinic
Space group	$P2_1/n$
Unit cell dimensions	a = 9.383(4) Å α = 90°
	b = 7.425(3) Å β = 94.852(9)°
	c = 31.562(14) Å γ = 90°
Volume	2191.1(16) $Å^3$
Z	4
Density (calculated)	1.384 $g.cm^{-3}$
Absorption coefficient (μ)	0.555 mm^{-1}
F(000)	952
Crystal size	0.37 × 0.07 × 0.06 mm^3
θ range for data collection	2.22 to 25.48°
Index ranges	$-11 \le h \le 11, 0 \le k \le 8, 0 \le l \le 37$
Reflections collected	3458
Independent reflections	3458 [R_{int} = 0.0000]
Completeness to θ = 25.48°	84.6 %
Absorption correction	Semi-empirical from equivalents
Max. and min. transmission	0.9675 and 0.8210
Refinement method	Full-matrix least-squares on F^2
Data / restraints / parameters	3458 / 0 / 286
Goodness-of-fit on F^2	0.930
Final R indices [I>2σ(I)]	R_1 = 0.0498, wR_2 = 0.1187
R indices (all data)	R_1 = 0.0727, wR_2 = 0.1308
Largest diff. peak and hole	0.235 and -0.362 $e^-.Å^{-3}$

Table 2. Atomic coordinates and equivalent isotropic displacement parameters ($Å^2$) for **4**. U(eq) is defined as one third of the trace of the orthogonalized U_{ij} tensor.

	x	y	z	U(eq)
Cr(1)	0.87009(7)	0.74005(10)	0.07671(2)	0.032(1)
O(1)	1.0467(4)	0.7707(5)	0.16016(11)	0.053(1)
O(2)	1.0086(4)	0.3886(5)	0.05823(13)	0.058(1)
O(3)	1.1072(4)	0.9282(5)	0.03626(11)	0.047(1)
O(4)	0.6562(3)	0.4646(5)	0.01851(10)	0.043(1)
N(1)	0.4671(4)	1.0211(5)	0.14430(11)	0.031(1)
N(2)	0.3429(4)	1.3015(5)	0.18744(13)	0.037(1)
C(1)	0.9791(5)	0.7577(7)	0.12808(16)	0.038(1)
C(2)	0.9568(5)	0.5255(7)	0.06583(16)	0.040(1)
C(3)	1.0148(5)	0.8576(7)	0.05179(15)	0.037(1)
C(11)	0.6965(4)	0.9276(6)	0.09451(14)	0.030(1)
C(12)	0.7140(5)	0.9415(7)	0.05056(15)	0.034(1)
C(13)	0.7029(5)	0.7897(7)	0.02362(15)	0.038(1)
C(14)	0.6734(5)	0.6208(6)	0.04064(15)	0.033(1)
C(15)	0.6623(5)	0.6014(6)	0.08475(14)	0.031(1)
C(16)	0.6756(4)	0.7531(6)	0.11141(13)	0.029(1)
C(17)	0.6833(6)	0.4705(9)	-0.02570(18)	0.059(2)
C(21)	0.7038(5)	1.0883(5)	0.12273(14)	0.030(1)
C(22)	0.5901(5)	1.1310(5)	0.14687(13)	0.025(1)
C(23)	0.6021(5)	1.2809(5)	0.17588(13)	0.028(1)
C(24)	0.4882(5)	1.3472(6)	0.19966(14)	0.036(1)
C(25)	0.5216(7)	1.4600(7)	0.23351(17)	0.051(2)
C(26)	0.6616(8)	1.5267(8)	0.2426(2)	0.067(2)
C(27)	0.7649(6)	1.4906(6)	0.21657(19)	0.050(2)
C(28)	0.7392(5)	1.3669(6)	0.18288(17)	0.036(1)
C(29)	0.8481(5)	1.3227(6)	0.15764(18)	0.041(1)
C(30)	0.8313(5)	1.1906(6)	0.12749(16)	0.038(1)
C(31)	0.3872(5)	0.9767(7)	0.10457(16)	0.045(1)
C(32)	0.4263(5)	0.9271(6)	0.18112(16)	0.039(1)
C(33)	0.2922(5)	1.3647(7)	0.14524(17)	0.044(1)
C(34)	0.2392(6)	1.3344(7)	0.21837(18)	0.056(2)
H(12A)	0.7501	1.0572	0.0393	0.041
H(13A)	0.7303	0.7992	-0.0062	0.046
H(15A)	0.6626	0.4782	0.0976	0.037
H(16A)	0.6840	0.7359	0.1429	0.035
H(17A)	0.6671	0.3510	-0.0384	0.089
H(17B)	0.7826	0.5070	-0.0282	0.089
H(17C)	0.6186	0.5576	-0.0406	0.089
H(25A)	0.4490	1.4939	0.2512	0.061
H(26A)	0.6834	1.5978	0.2673	0.080
H(27A)	0.8552	1.5487	0.2210	0.060

H(29A)	0.9364	1.3857	0.1614	0.050
H(30A)	0.9057	1.1673	0.1096	0.046
H(31A)	0.4196	1.0527	0.0819	0.067
H(31B)	0.2851	0.9975	0.1071	0.067
H(31C)	0.4027	0.8498	0.0978	0.067
H(32A)	0.4855	0.9684	0.2063	0.059
H(32B)	0.4402	0.7974	0.1774	0.059
H(32C)	0.3254	0.9511	0.1848	0.059
H(33A)	0.3661	1.3439	0.1256	0.066
H(33B)	0.2711	1.4938	0.1464	0.066
H(33C)	0.2051	1.2991	0.1353	0.066
H(34A)	0.2723	1.2779	0.2455	0.083
H(34B)	0.1466	1.2830	0.2080	0.083
H(34C)	0.2288	1.4644	0.2225	0.083

Table 3. Anisotropic displacement parameters ($Å^2$) for **4**. The anisotropic displacement factor exponent takes the form: $-2\pi^2[h^2a^{*2}U_{11} + ... + 2hka^*b^*U_{12}]$

	U_{11}	U_{22}	U_{33}	U_{23}	U_{13}	U_{12}
Cr(1)	0.0251(3)	0.0377(4)	0.0325(4)	0.0021(4)	0.0063(3)	0.0037(4)
O(1)	0.0435(19)	0.070(3)	0.044(2)	0.007(2)	-0.0077(18)	0.002(2)
O(2)	0.056(2)	0.046(2)	0.076(3)	0.002(2)	0.035(2)	0.0130(19)
O(3)	0.0292(19)	0.069(2)	0.042(2)	0.0151(19)	0.0056(16)	-0.0046(17)
O(4)	0.0356(18)	0.053(2)	0.042(2)	-0.0197(17)	0.0064(17)	0.0023(16)
N(1)	0.028(2)	0.037(2)	0.028(2)	-0.0126(17)	-0.0013(17)	-0.0030(17)
N(2)	0.043(2)	0.038(2)	0.031(2)	0.0023(18)	0.010(2)	0.0073(18)
C(1)	0.031(2)	0.042(3)	0.041(3)	0.010(3)	0.010(2)	0.000(2)
C(2)	0.030(3)	0.045(3)	0.047(3)	0.004(2)	0.012(2)	0.005(2)
C(3)	0.030(3)	0.048(3)	0.034(3)	0.000(2)	-0.003(2)	0.009(2)
C(11)	0.022(2)	0.036(2)	0.031(3)	0.001(2)	0.0013(19)	0.0034(19)
C(12)	0.027(2)	0.045(3)	0.031(3)	0.008(2)	0.000(2)	-0.002(2)
C(13)	0.031(2)	0.060(3)	0.024(2)	-0.004(2)	0.004(2)	0.007(2)
C(14)	0.021(2)	0.045(3)	0.034(3)	-0.006(2)	0.008(2)	0.010(2)
C(15)	0.021(2)	0.036(2)	0.034(3)	-0.003(2)	0.000(2)	0.0057(19)
C(16)	0.024(2)	0.031(2)	0.032(2)	-0.001(2)	0.0054(18)	0.006(2)
C(17)	0.040(3)	0.093(5)	0.045(4)	-0.026(3)	0.014(3)	-0.008(3)
C(21)	0.029(2)	0.027(2)	0.033(3)	0.0099(19)	0.005(2)	0.0059(18)
C(22)	0.029(2)	0.024(2)	0.022(2)	0.0032(18)	-0.0006(18)	-0.0018(18)
C(23)	0.036(2)	0.021(2)	0.027(2)	0.0050(18)	-0.0067(18)	0.0006(18)
C(24)	0.053(3)	0.029(2)	0.024(3)	0.003(2)	-0.003(2)	0.011(2)
C(25)	0.074(4)	0.038(3)	0.039(3)	-0.012(2)	-0.008(3)	0.016(3)
C(26)	0.102(5)	0.038(3)	0.053(4)	-0.020(3)	-0.036(4)	0.010(3)
C(27)	0.056(3)	0.025(3)	0.064(4)	0.004(3)	-0.026(3)	-0.004(2)
C(28)	0.042(3)	0.016(2)	0.048(3)	0.007(2)	-0.017(2)	0.0011(19)
C(29)	0.037(3)	0.025(2)	0.060(4)	0.011(3)	-0.009(3)	-0.008(2)
C(30)	0.030(2)	0.030(2)	0.056(3)	0.013(2)	0.007(2)	-0.0017(19)
C(31)	0.026(2)	0.060(3)	0.046(3)	-0.021(3)	-0.010(2)	0.006(2)
C(32)	0.035(3)	0.033(2)	0.053(3)	0.003(2)	0.015(2)	-0.005(2)
C(33)	0.037(3)	0.046(3)	0.050(4)	0.000(3)	0.004(2)	0.011(2)
C(34)	0.064(4)	0.048(3)	0.058(4)	0.002(3)	0.028(3)	0.018(3)

Table 4. Bond lengths [Å] for **4**.

atom-atom	distance	atom-atom	distance
Cr(1)-C(2)	1.834(5)	Cr(1)-C(3)	1.845(5)
Cr(1)-C(1)	1.847(5)	Cr(1)-C(12)	2.204(5)
Cr(1)-C(16)	2.209(4)	Cr(1)-C(13)	2.227(5)
Cr(1)-C(15)	2.238(5)	Cr(1)-C(11)	2.250(4)
Cr(1)-C(14)	2.265(5)	O(1)-C(1)	1.152(6)
O(2)-C(2)	1.161(6)	O(3)-C(3)	1.157(6)
O(4)-C(14)	1.356(5)	O(4)-C(17)	1.440(6)
N(1)-C(22)	1.410(5)	N(1)-C(32)	1.435(6)
N(1)-C(31)	1.444(6)	N(2)-C(24)	1.426(6)
N(2)-C(33)	1.454(6)	N(2)-C(34)	1.456(6)
C(11)-C(12)	1.414(6)	C(11)-C(16)	1.421(6)
C(11)-C(21)	1.487(6)	C(12)-C(13)	1.410(7)
C(13)-C(14)	1.401(7)	C(14)-C(15)	1.412(6)
C(15)-C(16)	1.405(6)	C(21)-C(22)	1.399(6)
C(21)-C(30)	1.415(6)	C(22)-C(23)	1.440(6)
C(23)-C(28)	1.436(6)	C(23)-C(24)	1.443(7)
C(24)-C(25)	1.373(7)	C(25)-C(26)	1.410(9)
C(26)-C(27)	1.349(9)	C(27)-C(28)	1.411(7)
C(28)-C(29)	1.388(7)	C(29)-C(30)	1.366(7)

Table 5. Bond angles [°] for **4**.

atom-atom-atom	angle	atom-atom-atom	angle
C(2)-Cr(1)-C(3)	88.7(2)	C(2)-Cr(1)-C(1)	90.3(2)
C(3)-Cr(1)-C(1)	88.1(2)	C(2)-Cr(1)-C(12)	144.1(2)
C(3)-Cr(1)-C(12)	90.5(2)	C(1)-Cr(1)-C(12)	125.6(2)
C(2)-Cr(1)-C(16)	121.96(19)	C(3)-Cr(1)-C(16)	149.25(19)
C(1)-Cr(1)-C(16)	88.91(17)	C(12)-Cr(1)-C(16)	66.74(17)
C(2)-Cr(1)-C(13)	107.4(2)	C(3)-Cr(1)-C(13)	95.63(19)
C(1)-Cr(1)-C(13)	162.03(19)	C(12)-Cr(1)-C(13)	37.11(17)
C(16)-Cr(1)-C(13)	78.86(17)	C(2)-Cr(1)-C(15)	91.50(19)
C(3)-Cr(1)-C(15)	160.99(19)	C(1)-Cr(1)-C(15)	110.86(18)
C(12)-Cr(1)-C(15)	78.30(17)	C(16)-Cr(1)-C(15)	36.84(16)
C(13)-Cr(1)-C(15)	66.21(17)	C(2)-Cr(1)-C(11)	157.86(19)
C(3)-Cr(1)-C(11)	112.83(19)	C(1)-Cr(1)-C(11)	95.48(19)
C(12)-Cr(1)-C(11)	37.01(16)	C(16)-Cr(1)-C(11)	37.16(16)
C(13)-Cr(1)-C(11)	66.84(17)	C(15)-Cr(1)-C(11)	66.46(16)
C(2)-Cr(1)-C(14)	85.5(2)	C(3)-Cr(1)-C(14)	124.64(19)
C(1)-Cr(1)-C(14)	146.73(19)	C(12)-Cr(1)-C(14)	65.78(18)
C(16)-Cr(1)-C(14)	66.05(16)	C(13)-Cr(1)-C(14)	36.33(17)
C(15)-Cr(1)-C(14)	36.55(16)	C(11)-Cr(1)-C(14)	77.95(16)
C(14)-O(4)-C(17)	116.7(4)	C(22)-N(1)-C(32)	120.5(4)
C(22)-N(1)-C(31)	123.0(4)	C(32)-N(1)-C(31)	116.0(4)
C(24)-N(2)-C(33)	113.7(4)	C(24)-N(2)-C(34)	117.2(4)
C(33)-N(2)-C(34)	112.0(4)	O(1)-C(1)-Cr(1)	179.3(5)
O(2)-C(2)-Cr(1)	178.2(5)	O(3)-C(3)-Cr(1)	178.7(4)
C(12)-C(11)-C(16)	117.7(4)	C(12)-C(11)-C(21)	121.7(4)
C(16)-C(11)-C(21)	120.5(4)	C(12)-C(11)-Cr(1)	69.7(3)
C(16)-C(11)-Cr(1)	69.8(2)	C(21)-C(11)-Cr(1)	130.4(3)
C(13)-C(12)-C(11)	121.6(4)	C(13)-C(12)-Cr(1)	72.3(3)
C(11)-C(12)-Cr(1)	73.3(3)	C(14)-C(13)-C(12)	119.4(4)
C(14)-C(13)-Cr(1)	73.3(3)	C(12)-C(13)-Cr(1)	70.6(3)
O(4)-C(14)-C(13)	125.9(4)	O(4)-C(14)-C(15)	113.9(4)
C(13)-C(14)-C(15)	120.2(4)	O(4)-C(14)-Cr(1)	130.5(3)
C(13)-C(14)-Cr(1)	70.3(3)	C(15)-C(14)-Cr(1)	70.7(3)
C(16)-C(15)-C(14)	119.9(4)	C(16)-C(15)-Cr(1)	70.4(2)
C(14)-C(15)-Cr(1)	72.8(3)	C(15)-C(16)-C(11)	120.9(4)
C(15)-C(16)-Cr(1)	72.7(2)	C(11)-C(16)-Cr(1)	73.0(2)
C(22)-C(21)-C(30)	119.8(4)	C(22)-C(21)-C(11)	120.6(4)
C(30)-C(21)-C(11)	119.3(4)	C(21)-C(22)-N(1)	119.7(4)
C(21)-C(22)-C(23)	120.0(4)	N(1)-C(22)-C(23)	120.3(4)
C(28)-C(23)-C(22)	117.5(4)	C(28)-C(23)-C(24)	117.5(4)
C(22)-C(23)-C(24)	124.9(4)	C(25)-C(24)-N(2)	120.4(5)
C(25)-C(24)-C(23)	118.8(5)	N(2)-C(24)-C(23)	120.8(4)
C(24)-C(25)-C(26)	121.3(6)	C(27)-C(26)-C(25)	120.8(5)

C(26)-C(27)-C(28)	120.1(5)	C(29)-C(28)-C(27)	119.9(5)
C(29)-C(28)-C(23)	120.0(4)	C(27)-C(28)-C(23)	120.0(5)
C(30)-C(29)-C(28)	121.5(5)	C(29)-C(30)-C(21)	120.4(5)

Appendix C: Chem361 MS experiment and raw data

** Experiment developed and written by Krista Vikse, Nichole Taylor, Jen Pape and Scott McIndoe*

Experiment MS: Determination of Flow Rates for a Novel MS Sampling Method

Learning Outcomes:

- Collect and interpret mass spectra
- Contribute to a research project: describe the overall goal of the project and why your contribution is important

Purpose:

Mass spectrometry as a technique for the detection and study of organic molecules has been in use since the 1940s. However it is only in the last decade or so that inorganic chemists have taken an interest in using this technique to study metal-catalyzed reactions. The most common method currently used for studying these systems is to periodically sample a reaction vessel (quenching is sometimes performed to halt the reaction) and then to collect a mass spectrum. This method has two major drawbacks:

First, it is difficult to sample air- or moisture-sensitive samples without exposing them to air and moisture.

Second, the reaction is not monitored continuously. The maximum sampling rate is about one mass spectrum every 5 minutes (this is due to the time it takes to sample the reaction vessel, and prepare the sample for injection into the mass spectrometer – the actual time required to collect a spectrum is on the order of a few seconds).

To address these problems a new method of sampling reactions for analysis by mass spectrometry has been proposed by the McIndoe group at UVic. The method allows continuous sampling directly from a reaction vessel with effectively no exposure to air or moisture.

To determine the usefulness of this technique, the range of accessible sampling rates or flow rates must be defined. Flow rates are expected to depend on a number of different variables. Your job is to determine the accessible flow rates (along with applicable errors) for your assigned set of variables.

Mass Spectrometry

Mass spectrometry (MS) is a sophisticated instrumental technique that produces, separates, and detects gas-phase ions. During Part 2 of this experiment, you will be using the Q-TOF *micro* mass spectrometer in the McIndoe research lab.

Mass spectrometry detects ions based on their mass-to-charge ratio (*m/z*). In most cases when using MS, the analytes are neutral and need to be ionized. Therefore an important part of a MS instrument is the ionization source. Several different types of ionization methods are available (see Table 1).

Table 1. Comparison of some common MS Ionization Methods[1]

Ionization Method	Typical Analytes	Sample Introduction	Method Highlights
Electron Impact (EI)	Relatively small and volatile	GC or liquid-solid probe	Hard method. Libraries of data available for searching.
Chemical Ionization (CI)	Relatively small and volatile	GC or liquid-solid probe	Soft method. Quasimolecular ion peak $[M + H]^+$
Electrospray (ESI)	Peptides, proteins, nonvolatile, charged species	Liquid chromatography or direct injection	Very soft method. Analytes must be pre-charged in solution, or be easily protonated.
Matrix-Assisted Laser Desorption (MALDI)	Peptides, proteins, nucleotides	Sample in solid matrix	Very soft method, very high mass range

Please note that “hard” ionization methods, as opposed to “soft” methods, result in a greater degree of fragmentation of the analyte.

The Q-TOF *micro* MS is equipped with an electrospray ionization (ESI) source. This is a soft ionization technique, good for thermally fragile analytes, or analyses in which little or no fragmentation of the analytes is desirable. It is also good for cases like the one you will be investigating, where the analytes are already charged, or ionic.

Electrospray ionization involves creating an aerosol of charged microdroplets in a strong electric field. The analyte, dissolved in a polar solvent, is pumped through a heated, charged capillary and emerges in the form of a Taylor cone (See Fig.1 below) . A spray of fine droplets is produced (nebulization) and solvent begins evaporating from the droplets causing an increase in charge

density within the droplet. This eventually leads to ion evaporation and/or Coulombic explosions to provide gas-phase ions. The gas-phase ions are then drawn into the mass analyzer.

After leaving the ionization source, the gas-phase ions will travel through a hexupole ion guide, a quadrupole mass analyzer and a time-of-flight (TOF) mass analyzer.

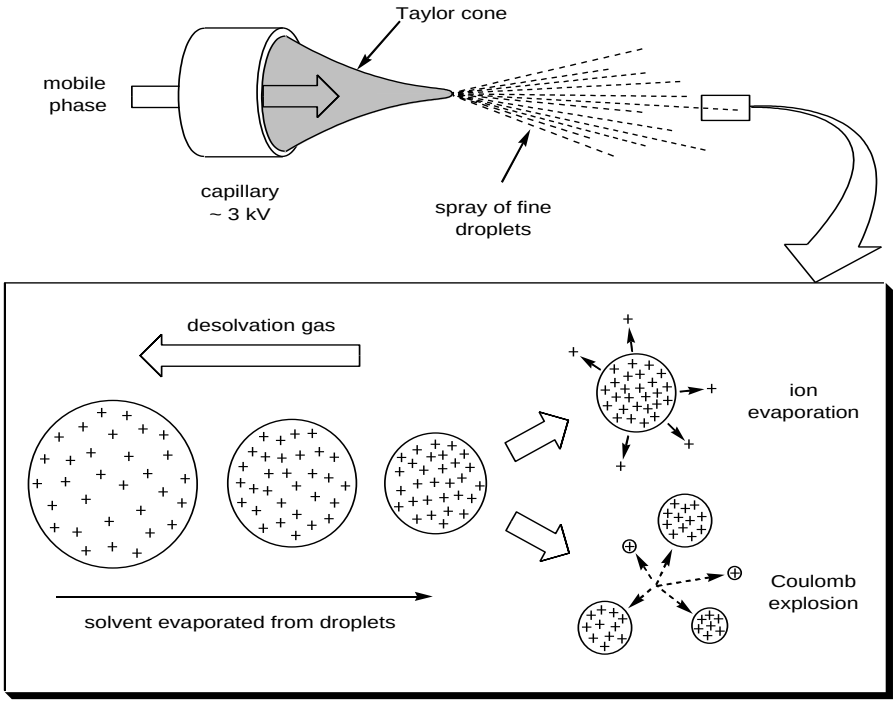

Figure 1: The electrospray process.
(From Henderson, W., & McIndoe, J. S. Mass Spectrometry of Inorganic and Organometallic Compounds. West Sussex: John Wiley & Sons Ltd. 2005[2] – reproduced with permission of the author.)

The hexupole ion guide focuses the beam of ions into the quadrupole mass analyzer. For the analysis you will be performing, the quadrupole simply acts as an ion guide, but it is capable of much more. When used in MS/MS mode, the quadrupole screens the ions to only let those with a specific mass-to-charge ratio pass through to the detector. It does this by varying the applied voltage and polarity of charge along its four parallel metal rods. These rods have both a DC voltage applied as well as an oscillating radio frequency voltage. By varying these applied voltages, only ions that resonate along the field will have a stable path through to the detector. Otherwise they will be deflected out of the field, collide with the electrodes, and be lost. A scan can be conducted by varying voltages very quickly to filter through ions of many different masses.

The second mass analyzer (a time-of-flight or TOF analyzer) works by accelerating all ions through accelerator plates with a large applied voltage. They then enter the flight tube with a constant kinetic energy. You might remember kinetic energy is related to mass (think back to high school physics… KE = ½ mv^2). Therefore ions with different masses will have different velocities. Detection is based on the time it takes for the ion to reach the detector.

For further information on the various components of the mass spectrometer instrumentation, please consult the references.[1,2,3,4]

Procedure:

This lab will be divided into two parts.

Part 1 – In the Chem361 lab, you will be experimenting with different conditions and measuring resulting flow rates, which will be used later for Part 2.

Part 2 – In the McIndoe research lab, you will be performing an experiment on the mass spectrometer using the optimal conditions that you found in Part 1.

Part 1 – Measuring Flow Rates

You will have been assigned a set of conditions for testing earlier in the semester. Obtain your assigned solvent, tube length and Schlenk flask. Add approximately 10 mL of your solvent to the flask. Stopper the flask with the septum and complete the experimental setup (see Figure 2).

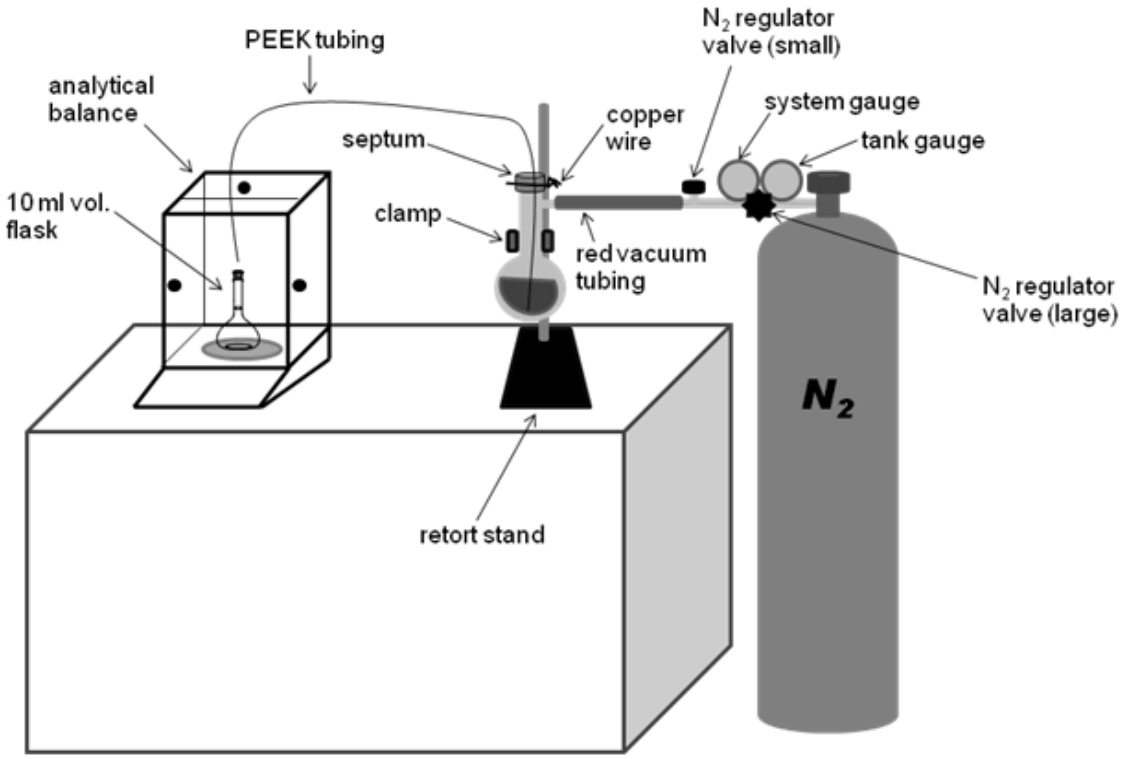

Figure 2: Experiment Setup

Pierce the top of the septum with a needle to allow insertion of the PEEK tubing.

Check with your instructor that everything is set up properly before proceeding.

Once your setup has been approved:

1) Disconnect the red vacuum tubing from the Schlenk flask and close the stopcock on the Schlenk tube.

2) Ensure all regulator valves are fully closed, and then open the nitrogen at the tank.

3) Use the large black regulator knob to adjust the second regulator gauge until it reads 0.5 psi.

4) Reconnect the red vacuum tubing and open the final small black regulator valve. Open the Schlenk tube stopcock.

5) **Slowly** readjust the large black regulator knob until the pressure reads 0.5 psi again. Once it hits this targeted pressure, decrease the pressure (back out the diaphragm) on the regulator.

You might notice that the pressure reading does not actually change. This is fine. It is because you are dealing with an essentially closed system, so the pressure inside will stay constant. If you do not decrease the pressure on the regulator, pressure will build and you will not have a constant pressure for your run. Keep an eye on the pressure throughout the run. It will probably not change, but if it should decrease, you might need a new septum. Change the septum and try again.

6) Wait until solvent begins dripping into the volumetric flask (this may take a while, but no longer than 5 minutes).

You are now ready to begin recording data. Tare the balance and start the stopwatch when the first new droplet drops into the volumetric flask. Record the new mass at time zero. Continue recording the time (in seconds) and mass every time another droplet drops. If the drops are falling too fast to record a reading at every drop, simply record mass and time at reasonable time intervals. Take *at least* ten readings. Repeat this process at 1, 1.5, 2, and 2.5 psi. **DO NOT EXCEED 5 PSI!!! Exceeding this pressure can result in breaking the regulator and the Schlenk tube exploding!**

Data Manipulation:

(to be done before Part 2 - the analysis day, but *to be submitted with your final report*)

For each different pressure used, plot mass of solvent measured vs. time.

Use these graphs to get a flow rate corresponding to each pressure setting.

Plot flow rate vs. pressure (include error bars – for information on what error to use for the error bars, see the course web page).

Using this graph, determine the pressure required to get a flow rate of 20 µL min^{-1} for your system, and to get a flow rate of 60 µL min^{-1}. You will use a pressure within this range on analysis day.

Part 2 - Analysis Day

On analysis day, come to the mass spectrometry lab (SCI B213). Bring your notebook, a pen and the pressures that you have calculated to give you flow rates of 20 µL min^{-1} and 60 µL min^{-1}. You will be assigned two solutions (each will contain one compound of interest dissolved in your assigned solvent). When the two solutions are mixed interactions will occur that can be monitored by mass spectrometry. The instrument you will be using to monitor the reaction will be a Q-TOF *micro* mass spectrometer, equipped with a quadrupole mass filter and a time of

flight (TOF) detector. Equipment will be provided for you to set up your experiment in the same way as you did in Part 1 of the experiment.

Add 5 mL of your first assigned solution to the Schlenk tube. Rinse the mass spectrometer with some of your assigned solvent using the syringe and PEEK tubing provided. Set up the equipment as you did for Part 1 of the experiment, BUT instead of collecting the solvent in a volumetric flask, the PEEK tubing will be connected to the mass spectrometer using a ferrule and fingertight union.

Set the pressure for the system and wait for a signal to appear on the computer screen.

The mass spectrometer software (MassLynx) will be open for you and the 'tune page' should be what you see (if in doubt, check with your TA). On this 'tune page' enter the appropriate settings according to Table 2, provided below. Hit 'Enter' after each entry.

	Water	Acetonitrile	Methanol	ACN/Water mix	Dichloromethane
Capillary Voltage	2900 V				
Cone Voltage	20 V				
Extraction Voltage	0.5 V				
Source Temp.	100 °C	80 °C	65 °C	100 °C	40 °C
Desolvation Temp.	250 °C	150 °C	120 °C	200 °C	100 °C
Cone Gas Flow	100 L/hr				
Desolvation Gas Flow	100 L/hr				

Table 2: Tune page parameters.

Once you observe an acceptable signal (see Fig. 3 for example) in the tune page window (check with the TA), you may begin acquiring.

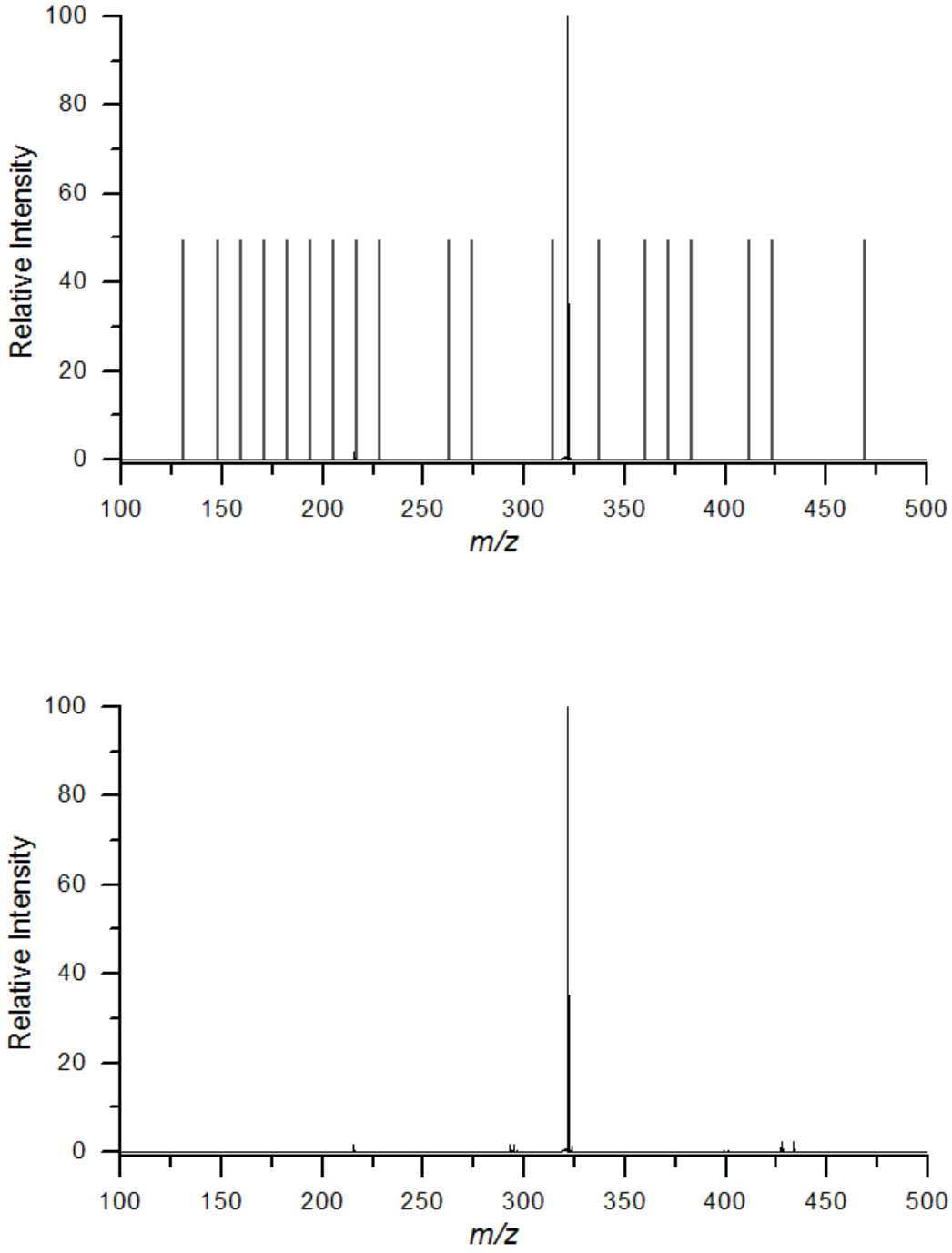

Figure 3: A poor quality spectrum (top). A high quality spectrum (bottom).

To acquire, click on the ‘Acquire’ button in the bottom left corner of the tune page window.

Give the experiment a file name, and enter any comments you think are necessary.

Set function to TOF MS.

Set data format to ‘continuum’.

Set the start mass to 50 and the end mass to 2000.

Set scan time to 1 second and interscan time to 0.1 seconds.

Set run duration to 20 min.

Click ‘start acquisition’

From the MassLynx main window click on ‘spectrum’ and ‘chromatogram’ and in each of the windows that appear click the clock button to display your data in real-time.

After everything is set up, inject 5 mL of your second assigned solution into the Schlenk flask via the septum. Observe any changes in the chromatogram and spectrum windows. Continue acquiring data for 30 seconds after the spectrum stops changing (or for 5 minutes if no changes are observed).

When you stop seeing changes, you can stop the acquisition. To stop acquiring, click on the button with a picture of a hand at the top of the screen.

Print the chromatogram window.

In the chromatogram window, right click and drag your cursor across the data collected in the last 30 seconds. This will give you a summed mass spectrum in the spectrum window. Print this as well.

Turn the gas off at the cylinder then at the regulator and safely disconnect your Schlenk flask from the red tubing.

Disconnect the PEEK tubing from the mass spectrometer.

Rinse the capillary with your assigned solvent using the syringe and PEEK tubing provided until the tune page displays a spectrum that is only background noise. This could take several minutes.

Discussion:

For Part 1:

Discuss the results from your graphs (both the mass versus time graphs, and the flow rate versus pressure graphs). Were there any outliers, or deviations from trends? Discuss.

Compare your data against the others in your group. How does flow rate change between the different variables you each tried? Does this agree with what you would expect to see? Why or why not?

Compare your results with the results from your assigned group. Are the flow rates that you each obtained for a given pressure (pick one) statistically different? Is this the result you expected? Why/ why not?

How precise are the flow rates that you determined? Would you recommend your results for publication?

No experiment is completely free of errors. Please discuss your observed errors in this experiment, or errors you suspect may have occurred but are not possible to observe. What effect(s) would these errors have on your final reported results?

For Part 2:

In many analysis methods, a signal for the solvent is present (eg. GC, NMR, etc). Why don't you see a peak for the solvent in your mass spectrum?

What changes (if any) did you observe in the mass spectrum and chromatogram after addition of the second solution? Can you explain these changes? (Or the lack of any changes?)

From the list provided on the course web page, and your collected mass spec data, can you identify the species in your reaction mixture?

References:

1. Christian, G. D. Analytical Chemistry, 6th Ed. Hoboken: John Wiley & Sons. 2004.
2. Henderson, W., & McIndoe, J. S. Mass Spectrometry of Inorganic and Organometallic Compounds. West Sussex: John Wiley & Sons Ltd. 2005
3. Harris, D. C. Quantitative Chemical Analysis, 7th Ed. New York: W. H. Freeman and Co. 2007.
4. Skoog, Holler, & Nieman. Principles of Instrumental Analysis. 5th Ed. Toronto: Thomson Learning, Inc. 1998

Raw Data:

The above experiment was performed by Chem361 students in the Spring semesters of 2010 and 2011. The raw data that was collected is provided below. Data collected in 2010 was used to refine the experimental setup and data collection procedures, and is not presented here. Data collected in 2011 was used quantitatively and is listed below.

Water 50 cm															
0.5 PSI			1 PSI			1.5 PSI			2 PSI			2.5 PSI			
time (s)	mass (g)	vol (mL)	time (s)	mass (g)	vol (mL)	time (s)	mass (g)	vol (mL)	time (s)	mass (g)	vol (mL)	time (s)	mass (g)	vol (mL)	
0	0		0	0		0	0		0	0		0	0		
287	0.0269		123	0.0268		83	0.0266		60	0.0267		45	0.0265		
571	0.0529		268	0.0536		166	0.0529		122	0.0532		91	0.0527		
869	0.0794		405	0.0803		251	0.0789		181	0.0793		139	0.0793		
1165	0.1057		532	0.107		336	0.1055		241	0.106		185	0.1053		
1481	0.1322		657	0.1335		421	0.1322		300	0.1325		232	0.1317		
1831	0.1589		789	0.1601		509	0.1581		361	0.1591		280	0.1581		
2135	0.1853		922	0.1867		595	0.1846		421	0.1854		326	0.1847		
2473	0.2117		1063	0.2133		684	0.2112		481	0.2118		373	0.2107		
2820	0.2384		1209	0.2399		772	0.2376		541	0.2384		420	0.2374		
	Flowrate:	8.44E-05		Flowrate:	0.0002		Flowrate:	0.000307		Flowrate:	0.000441		Flowrate:	0.000563	

Water 55 cm															
1 PSI			1.5 PSI			2 PSI			2.5 PSI			3 PSI			
time (s)	mass (g)	vol (mL)	time (s)	mass (g)	vol (mL)	time (s)	mass (g)	vol (mL)	time (s)	mass (g)	vol (mL)	time (s)	mass (g)	vol (mL)	
0	0.0022		0	0.026		0	0.0266		0.0269	0		0	0.0267		
134	0.0212		90	0.0529		64	0.0531		0.0532	59		25	0.0533		
170	0.0295		183	0.0791		133	0.0795		0.0796	110		71	0.0798		
220	0.0347		273	0.104		202	0.106		0.1061	167		119	0.106		
247	0.0412		372	0.1313		276	0.1324		0.1325	227		159	0.1326		
262	0.043		462	0.1574		340	0.159		0.159	277		200	0.159		
275	0.0449		531	0.1773		410	0.1853		0.1855	333		253	0.1855		
384	0.0611		645	0.2063		480	0.2121		0.2119	390		296	0.219		
460	0.0739		743	0.2329		559	0.2384		0.2383	447		391	0.2648		
522	0.0799		787	0.2451		634	0.2648		0.2649	504		437	0.2911		
	Flowrate:	0.000152		Flowrate:	0.000277		Flowrate:	0.000377		Flowrate:	0.000474		Flowrate:	0.000595	

Water 60 cm															
.5 PSI			1 PSI			1.5 PSI			2 PSI			2.5 PSI			
time (s)	mass (g)	vol (mL)	time (s)	mass (g)	vol (mL)	time (s)	mass (g)	vol (mL)	time (s)	mass (g)	vol (mL)	time (s)	mass (g)	vol (mL)	
0	0.0269		0	0.0266		0	0.0266		0	0.0264		0	0.0263		
301	0.053		160	0.0525		99	0.0525		73	0.0526		59	0.0525		
586	0.0787		316	0.0783		200	0.0783		146	0.0785		115	0.0787		
860	0.1048		480	0.105		306	0.105		220	0.1047		174	0.1047		
1143	0.1306		640	0.1308		403	0.1308		295	0.1309		233	0.1308		
1435	0.1562		797	0.157		509	0.157		369	0.1571		292	0.1571		
1720	0.1817		960	0.1828		612	0.1828		444	0.1834		351	0.183		
2021	0.2078		1122	0.2088		713	0.2088		522	0.2094		410	0.2093		
2309	0.2338		1289	0.2347		810	0.2347		596	0.2355		469	0.2354		
2617	0.2596		1450	0.261		917	0.261		670	0.2615		527	0.2615		
	Flowrate:	8.94141E-05		Flowrate:	0.000162		Flowrate:	0.000255		Flowrate:	0.00035		Flowrate:	0.000445	

CH2Cl2 45 cm

3 PSI			1 PSI			1.5 PSI			2 PSI			2.5 PSI		
time (s)	mass (g)	vol (mL)	time (s)	mass (g)	vol (mL)	time (s)	mass (g)	vol (mL)	time (s)	mass (g)	vol (mL)	time (s)	mass (g)	vol (mL)
0	0.0104	0.00784	0	0.0067	0.005051	0	0.0113	0.008518	0	0.0115	0.008669	0	0.0117	0.00882
11	0.0206	0.015528	24	0.015	0.011307	28	0.0196	0.014775	21	0.0223	0.01681	15	0.0228	0.017187
22	0.0309	0.023293	71	0.02	0.015076	57	0.0284	0.021408	40	0.0335	0.025253	30	0.0342	0.02578
33	0.0412	0.031057	117	0.0286	0.021559	86	0.0372	0.028042	60	0.0444	0.033469	45	0.0452	0.034072
45	0.0513	0.03867	163	0.0336	0.025328	114	0.0463	0.034901	80	0.0557	0.041987	60	0.0563	0.042439
56	0.0614	0.046284	208	0.0413	0.031132	142	0.0555	0.041836	99	0.0665	0.050128	75	0.0678	0.051108
67	0.0718	0.054123	255	0.0466	0.035127	169	0.0649	0.048922	119	0.0777	0.058571	90	0.0791	0.059626
77	0.0817	0.061586	301	0.0522	0.039349	198	0.0744	0.056083	138	0.089	0.067089	105	0.0901	0.067918
89	0.092	0.06935	348	0.0558	0.042062	224	0.0841	0.063395	158	0.1002	0.075531	120	0.1012	0.076285
99	0.1023	0.077114	395	0.064	0.048244	252	0.094	0.070858	177	0.1109	0.083597	134	0.1126	0.084879
121	0.1228	0.092567	443	0.0703	0.052993	278	0.1039	0.078321	196	0.1221	0.09204	149	0.1238	0.093321
134	0.1327	0.10003	491	0.0764	0.057591	306	0.1136	0.085632			0	164	0.1351	0.101839
	Flowrate:	0.000694		Flowrate:	0.000102		Flowrate:	0.000253		Flowrate:	0.000427		Flowrate:	0.000567

CH2Cl2 50 cm

0.5 PSI			1 PSI			1.5 PSI			2 PSI			2.5 PSI		
time (s)	mass (g)	vol (mL)	time (s)	mass (g)	vol (mL)	time (s)	mass (g)	vol (mL)	time (s)	mass (g)	vol (mL)	time (s)	mass (g)	vol (mL)
0	0.0099	0.007463	0	0.0102	0.007689	0	0.0092	0.006935	0	0.0092	0.006935	0	0.0091	0.00686
32	0.0195	0.014699	16	0.0172	0.012965	36	0.0348	0.026232	26	0.0346	0.026082	25	0.0437	0.032941
68	0.0288	0.02171	31	0.0255	0.019222	68	0.0638	0.048093	57	0.0586	0.044173	52	0.078	0.058797
92	0.0381	0.02872	43	0.0334	0.025177	103	0.0915	0.068973	81	0.0834	0.062867	74	0.1137	0.085708
123	0.048	0.036183	58	0.0403	0.030378	143	0.121	0.091211	103	0.108	0.081411	105	0.1502	0.113222
154	0.0578	0.04357	72	0.0475	0.035806	180	0.1522	0.114729	130	0.1338	0.100859	133	0.1982	0.149404
186	0.0671	0.05058	85	0.0553	0.041686	215	0.1836	0.138399	155	0.1638	0.123474	164	0.267	0.201266
219	0.0766	0.057742	100	0.0635	0.047867	252	0.2153	0.162295	177	0.1875	0.141339	184	0.2866	0.216041
250	0.0859	0.064752	112	0.0727	0.054802	290	0.2478	0.186793	203	0.2135	0.160938	214	0.3268	0.246344
281	0.095	0.071612	126	0.0806	0.060757	323	0.2794	0.210614	232	0.2418	0.18227	234	0.3688	0.278004
311	0.1043	0.078622	138	0.0852	0.064224	361	0.3096	0.233379	250	0.271	0.204282	262	0.4105	0.309438
340	0.1137	0.085708	151	0.0942	0.071009	395	0.3399	0.256219	276	0.301	0.226896	285	0.4526	0.341173
371	0.1231	0.092794	162	0.1012	0.076285	427	0.3703	0.279135	301	0.3325	0.250641	312	0.4952	0.373285
405	0.131	0.098749	178	0.1102	0.08307	462	0.4012	0.302427	327	0.364	0.274386	340	0.5492	0.413991
440	0.1394	0.105081	187	0.1185	0.089326	501	0.4324	0.325946	353	0.396	0.298507	366	0.5922	0.446404
471	0.1486	0.112016	201	0.1268	0.095583		Flowrate:	0.000643		Flowrate:	0.00083		Flowrate:	0.001209
	Flowrate:	0.000224	215	0.1353	0.10199									
			228	0.1422	0.107191									
			238	0.1507	0.113599									
			251	0.1607	0.121137									
				Flowrate:	0.000451									

CH2Cl2 50 cm

0.5 PSI			1.1 PSI			1.5 PSI			2.1 PSI			2.6 PSI		
time (s)	mass (g)	vol (mL)	time (s)	mass (g)	vol (mL)	time (s)	mass (g)	vol (mL)	time (s)	mass (g)	vol (mL)	time (s)	mass (g)	vol (mL)
0	0.0123	0.009272	0	0.0124	0.009347	0	0.0112	0.008443	0	0.0111	0.008367	0	0.0107	0.008066
51	0.0232	0.017488	21	0.0241	0.018167	13	0.0224	0.016885	9	0.022	0.016584	7	0.0214	0.016131
100	0.0337	0.025403	41	0.0359	0.027062	26	0.0334	0.025177	19	0.033	0.024876	14	0.0323	0.024348
153	0.0446	0.03362	60	0.048	0.036183	38	0.0445	0.033544	29	0.044	0.033167	21	0.0431	0.032489
208	0.0558	0.042062	81	0.0598	0.045078	50	0.0557	0.041987	38	0.055	0.041459	28	0.0539	0.04063
263	0.0667	0.050279	101	0.0718	0.054123	61	0.0668	0.050354	48	0.066	0.049751	35	0.0645	0.048621
316	0.0787	0.059325	121	0.0836	0.063018	73	0.0778	0.058646	58	0.0767	0.057817	42	0.0754	0.056837
367	0.0895	0.067466	141	0.0956	0.072064	84	0.0888	0.066938	67	0.0887	0.066863	49	0.0861	0.064903
419	0.1002	0.075531	161	0.1074	0.080959	95	0.0998	0.07523	77	0.0988	0.074476	56	0.0967	0.072893
470	0.1112	0.083823	181	0.1194	0.090005	106	0.1108	0.083522	87	0.1096	0.082617	63	0.1076	0.08111
522	0.1217	0.091738	201	0.1312	0.098899	117	0.1218	0.091814	96	0.1205	0.090834	70	0.1183	0.089175
	Flowrate:	0.000158		Flowrate:	0.000447		Flowrate:	0.000716		Flowrate:	0.000856		Flowrate:	0.001159

CH2Cl2 55 cm

0.5 PSI			1 PSI			1.5 PSI			2 PSI			2.5 PSI		
time (s)	mass (g)	vol (mL)	time (s)	mass (g)	vol (mL)	time (s)	mass (g)	vol (mL)	time (s)	mass (g)	vol (mL)	time (s)	mass (g)	vol (mL)
0	0.0091	0.00686	0	0.0124	0.009347203	0	0.0119	0.00897	0	0.0117	0.00882	0	0.0116	0.008744
33	0.0205	0.015453	30	0.0237	0.017865219	20	0.0234	0.017639	15	0.023	0.017338	10	0.023	0.017338
79	0.0286	0.021559	55	0.0353	0.026609377	35	0.0351	0.026459	25	0.0347	0.026157	15	0.0347	0.026157
113	0.0356	0.026836	80	0.0469	0.035353535	50	0.0466	0.035127	35	0.0463	0.034901	25	0.0462	0.034826
160	0.0425	0.032037	105	0.0586	0.044173074	65	0.0587	0.044248	50	0.058	0.043721	35	0.0578	0.04357
195	0.051	0.038444	132	0.0701	0.052841851	85	0.0701	0.052842	60	0.0695	0.05239	45	0.0691	0.052088
235	0.058	0.043721	155	0.0817	0.061586009	105	0.0814	0.06136	70	0.081	0.061058	50	0.0808	0.060908
273	0.0648	0.048847	180	0.0933	0.070330167	115	0.0933	0.07033	85	0.0926	0.069803	60	0.0921	0.069426
312	0.0717	0.054048	205	0.1047	0.078923564	130	0.1047	0.078924	95	0.1044	0.078697	70	0.1036	0.078094
350	0.0792	0.059701	230	0.1162	0.087592341	145	0.1162	0.087592	110	0.1158	0.087291	80	0.1152	0.086839
	Flowrate:	0.000145		Flowrate:	0.000344432		Flowrate:	0.000541		Flowrate:	0.000732		Flowrate:	0.000984

CH2Cl2 55 cm

0.6 PSI			1.1 PSI			1.6 PSI			2.1 PSI			2.4 PSI		
time (s)	mass (g)	vol (mL)	time (s)	mass (g)	vol (mL)	time (s)	mass (g)	vol (mL)	time (s)	mass (g)	vol (mL)	time (s)	mass (g)	vol (mL)
0	0	0	0	0	0	0	0	0	0	0	0	0	0	0
48	0.0068	0.005126	66	0.0091	0.006859641	62	0.0106	0.00799	42	0.0101	0.007613	33	0.01	0.007538
98	0.0109	0.008216	129	0.016	0.012060908	185	0.0291	0.021936	84	0.02	0.015076	66	0.0194	0.014624
148	0.0171	0.01289	190	0.0249	0.018769787	246	0.0379	0.028569	127	0.029	0.02186	99	0.0287	0.021634
199	0.0237	0.017865	251	0.0329	0.024800241	307	0.0478	0.036032	174	0.0383	0.028871	132	0.0384	0.028946
249	0.0323	0.024348	317	0.0412	0.031056837	371	0.0572	0.043118	215	0.0483	0.036409	164	0.048	0.036183
301	0.0388	0.029248	382	0.0501	0.037765717	432	0.0668	0.050354	257	0.0584	0.044022	197	0.0577	0.043495
351	0.0474	0.03573	514	0.0655	0.04937434	493	0.0754	0.056837	302	0.0681	0.051334	231	0.067	0.050505
402	0.0547	0.041233	579	0.0744	0.05608322	555	0.0842	0.063471	341	0.0776	0.058495	263	0.0765	0.057666
453	0.063	0.04749	649	0.0819	0.061736771	617	0.0944	0.071159	383	0.0872	0.065732	295	0.0857	0.064601
504	0.0701	0.052842	711	0.0894	0.067390321	681	0.104	0.078396	424	0.097	0.073119	327	0.0955	0.071989
561	0.0734	0.055329	807	0.0958	0.072214684	744	0.1131	0.085256	466	0.1066	0.080356	360	0.1056	0.079602
612	0.085	0.064074		Flowrate:	9.23236E-05		Flowrate:	0.000114	508	0.1159	0.087366	393	0.1151	0.086763
666	0.0928	0.069953								Flowrate:	0.000172	425	0.1243	0.093698
720	0.1007	0.075908										458	0.1348	0.101613
	Flowrate:	0.000106											Flowrate:	0.000221

CH2Cl2 60 cm

1.1 PSI			2 PSI			3 PSI			2 PSI			2.5 PSI		
time (s)	mass (g)	vol (mL)	time (s)	mass (g)	vol (mL)	time (s)	mass (g)	vol (mL)	time (s)	mass (g)	vol (mL)	time (s)	mass (g)	vol (mL)
0	0	0	0	0	0	0	0	0						
24	0.0108	0.008141	13	0.0122	0.009196	9	0.0119	0.00897						
46	0.0215	0.016207	24	0.0233	0.017564	17	0.0234	0.017639						
68	0.0321	0.024197	36	0.0347	0.026157	25	0.0352	0.026534						
92	0.043	0.032414	48	0.0404	0.030454	33	0.0469	0.035354						
115	0.0538	0.040555	60	0.058	0.043721	42	0.0586	0.044173						
139	0.0648	0.048847	72	0.0697	0.05254	50	0.0701	0.052842						
163	0.0756	0.056988	84	0.0812	0.061209	58	0.082	0.061812						
188	0.0864	0.065129	97	0.093	0.070104	67	0.0936	0.070556						
210	0.0973	0.073345	109	0.1044	0.078697	75	0.1052	0.0793						
234	0.1085	0.081788	121	0.116	0.087442	83	0.117	0.088195						
258	0.1194	0.090005	133	0.1278	0.096336	91	0.1286	0.09694						
282	0.1304	0.098296	145	0.1394	0.105081	101	0.1402	0.105684						
306	0.1413	0.106513	157	0.1509	0.113749	108	0.1518	0.114428						
331	0.1525	0.114956	169	0.1627	0.122644	116	0.1634	0.123172						
355	0.1635	0.123247	181	0.1743	0.131389	125	0.1751	0.131992						
	Flowrate:	0.000347		Flowrate:	0.000728		Flowrate:	0.001059						

CH3CN 55 cm

0.5 PSI			1 PSI			1.5 PSI			2 PSI			2.5 PSI		
time (s)	mass (g)	vol (mL)	time (s)	mass (g)	vol (mL)	time (s)	mass (g)	vol (mL)	time (s)	mass (g)	vol (mL)	time (s)	mass (g)	vol (mL)
45	0.0106	0.013486	24	0.0103	0.013104	16	0.0101	0.01285	12	0.0103	0.013104	9	0.0103	0.013104
91	0.021	0.026718	48	0.0204	0.025954	31	0.0204	0.025954	24	0.0207	0.026336	19	0.0203	0.025827
136	0.0316	0.040204	73	0.0307	0.039059	48	0.0306	0.038931	36	0.031	0.03944	28	0.0306	0.038931
183	0.0422	0.05369	97	0.0409	0.052036	64	0.0408	0.051908	48	0.0412	0.052417	38	0.0408	0.051908
229	0.0527	0.067048	122	0.0511	0.065013	79	0.051	0.064885	61	0.0516	0.065649	48	0.051	0.064885
277	0.0633	0.080534	147	0.0612	0.077863	96	0.0611	0.077735	73	0.0618	0.078626	58	0.0612	0.077863
325	0.0738	0.093893	172	0.0716	0.091094	112	0.0713	0.090712	85	0.0722	0.091858	67	0.0714	0.09084
373	0.0843	0.107252	196	0.082	0.104326	128	0.0815	0.10369	98	0.0825	0.104962	77	0.0816	0.103817
422	0.0949	0.120738	248	0.1026	0.130534	145	0.0919	0.116921	111	0.0929	0.118193	87	0.0919	0.116921
471	0.1053	0.133969	274	0.113	0.143766	161	0.102	0.129771	123	0.1033	0.131425	97	0.1023	0.130153
520	0.1159	0.147455	300	0.1232	0.156743	178	0.1122	0.142748	135	0.1136	0.144529	107	0.1124	0.143003
570	0.1264	0.160814	325	0.1338	0.170229	194	0.1225	0.155852	148	0.1239	0.157634	117	0.1226	0.15598
	Flowrate:	0.000281	352	0.1442	0.183461	211	0.1327	0.16883	160	0.1342	0.170738	126	0.1328	0.168957
				Flowrate:	0.000519		Flowrate:	0.000799		Flowrate:	0.001061		Flowrate:	0.001328

CH3CN 55 cm

0.5 PSI			1 PSI			1.5 PSI			2 PSI			2.4 PSI		
time (s)	mass (g)	vol (mL)	time (s)	mass (g)	vol (mL)	time (s)	mass (g)	vol (mL)	time (s)	mass (g)	vol (mL)	time (s)	mass (g)	vol (mL)
0	0.0119	0.01514	0	0.0115	0.014631	0	0.0114	0.014504	0	0.0112	0.014249	0	0.0117	0.014885
77	0.0236	0.030025	32	0.0228	0.029008	20	0.0223	0.028372	15	0.0223	0.028372	11	0.0234	0.029771
153	0.035	0.044529	59	0.0342	0.043511	40	0.0338	0.043003	30	0.035	0.044529	23	0.035	0.044529
230	0.0468	0.059542	89	0.0456	0.058015	60	0.045	0.057252	47	0.0472	0.060051	36	0.0467	0.059415
308	0.0583	0.074173	119	0.0572	0.072774	80	0.0562	0.071501	63	0.0596	0.075827	48	0.0585	0.074427
386	0.07	0.089059	149	0.0685	0.08715	100	0.0676	0.086005	79	0.0721	0.09173	61	0.0702	0.089313
465	0.0816	0.103817	180	0.0803	0.102163	121	0.079	0.100509	95	0.0845	0.107506	73	0.0818	0.104071
546	0.0931	0.118448	210	0.0919	0.116921	141	0.0904	0.115013	111	0.0969	0.123282	86	0.0934	0.11883
627	0.1046	0.133079	241	0.1036	0.131807	162	0.1013	0.12888	128	0.1092	0.138931	99	0.1052	0.133842
711	0.1163	0.147964	272	0.1155	0.146947	183	0.1137	0.144656	144	0.1219	0.155089	111	0.1168	0.148601
	Flowrate:	0.000187	303	0.1272	0.161832	204	0.1243	0.158142	162	0.1341	0.170611	123	0.1286	0.163613
			334	0.139	0.176845		Flowrate:	0.000707	176	0.1463	0.186132	136	0.1402	0.178372
				Flowrate:	0.000487					Flowrate:	0.000973		Flowrate:	0.001194

CH3CN 60 cm

0.5 PSI			1 PSI			1.5 PSI			2 PSI			2.5 PSI		
time (s)	mass (g)	vol (mL)	time (s)	mass (g)	vol (mL)	time (s)	mass (g)	vol (mL)	time (s)	mass (g)	vol (mL)	time (s)	mass (g)	vol (mL)
0	0.0104	0.013232	0	0.0108	0.01374	0	0.0108	0.01374	0	0.0106	0.013486	0	0.0107	0.013613
57	0.021	0.026718	32	0.0215	0.027354	20	0.0214	0.027226	14	0.0213	0.027099	12	0.0212	0.026972
118	0.0311	0.039567	56	0.0322	0.040967	38	0.0321	0.04084	28	0.0318	0.040458	23	0.0319	0.040585
191	0.0412	0.052417	83	0.043	0.054707	57	0.0428	0.054453	42	0.0424	0.053944	34	0.0424	0.053944
256	0.0515	0.065522	113	0.0539	0.068575	76	0.0534	0.067939	56	0.0532	0.067684	45	0.0533	0.067812
322	0.0622	0.079135	144	0.0645	0.082061	106	0.0642	0.081679	70	0.0638	0.08117	57	0.0638	0.08117
385	0.0729	0.092748	171	0.075	0.09542	116	0.0748	0.095165	85	0.0744	0.094656	68	0.0744	0.094656
442	0.0839	0.106743	201	0.086	0.109415	134	0.0854	0.108651	100	0.0851	0.10827	79	0.0851	0.10827
500	0.0944	0.120102	229	0.0966	0.122901	155	0.0962	0.122392	113	0.0958	0.121883	91	0.0958	0.121883
556	0.1052	0.133842	254	0.1073	0.136514	174	0.1069	0.136005	127	0.1065	0.135496	103	0.1062	0.135115
616	0.1161	0.14771	288	0.118	0.150127	192	0.1175	0.149491	142	0.1171	0.148982	114	0.1169	0.148728
676	0.1267	0.161196	316	0.1288	0.163868	211	0.1283	0.163232	156	0.1277	0.162468	125	0.1277	0.162468
733	0.1376	0.175064		Flowrate:	0.000476		Flowrate:	0.000706		Flowrate:	0.000954		Flowrate:	0.00119
	Flowrate:	0.000219												

MeOH 45 cm

0.5 PSI			1 PSI			1.5 PSI			2 PSI			2.5 PSI		
time (s)	mass (g)	vol (mL)	time (s)	mass (g)	vol (mL)	time (s)	mass (g)	vol (mL)	time (s)	mass (g)	vol (mL)	time (s)	mass (g)	vol (mL)
0	0.0082	0.010356	0	0.0081	0.01023	0	0.0082	0.010356	0	0.008	0.010104	0	0.008	0.010104
51	0.0161	0.020333	25	0.0161	0.020333	16	0.0163	0.020586	12	0.0161	0.020333	9	0.0161	0.020333
101	0.0242	0.030563	50	0.0244	0.030816	32	0.0243	0.03069	24	0.0242	0.030563	19	0.0241	0.030437
151	0.0322	0.040667	75	0.0324	0.040919	48	0.0324	0.040919	36	0.0325	0.041046	28	0.0322	0.040667
202	0.0402	0.05077	100	0.0407	0.051402	66	0.0405	0.051149	48	0.0404	0.051023	37	0.0403	0.050897
254	0.0483	0.061	125	0.0487	0.061505	82	0.0487	0.061505	60	0.0486	0.061379	46	0.0484	0.061127
305	0.0563	0.071104	150	0.0568	0.071735	98	0.0568	0.071735	72	0.0567	0.071609	56	0.0564	0.07123
358	0.0644	0.081334	175	0.065	0.082091	115	0.065	0.082091	84	0.0648	0.081839	65	0.0645	0.08146
411	0.0726	0.09169	200	0.0731	0.092321	132	0.0731	0.092321	96	0.0729	0.092069	74	0.0726	0.09169
464	0.0806	0.101793	226	0.0813	0.102677	148	0.0811	0.102425	107	0.0809	0.102172	83	0.0806	0.101793
518	0.0888	0.11215	251	0.0893	0.112781	165	0.0893	0.112781	119	0.089	0.112402	92	0.0887	0.112023
	Flowrate:	0.000197		Flowrate:	0.000409		Flowrate:	0.00062		Flowrate:	0.000858	102	0.0968	0.122253
													Flowrate:	0.001104

MeOH 45 cm

0.5 PSI			1 PSI			1.5 PSI			2 PSI			2.5 PSI		
time (s)	mass (g)	vol (mL)	time (s)	mass (g)	vol (mL)	time (s)	mass (g)	vol (mL)	time (s)	mass (g)	vol (mL)	time (s)	mass (g)	vol (mL)
0	0.0093	0.011745	0	0.0091	0.011493	0	0.0091	0.011493	32	0.0451	0.056959	26	0.045	0.056833
62	0.0183	0.023112	16	0.018	0.022733	10	0.0181	0.022859	64	0.0542	0.068452	69	0.0721	0.091058
125	0.0273	0.034478	33	0.0272	0.034352	22	0.0271	0.034226	73	0.0631	0.079692	76	0.0812	0.102551
188	0.0363	0.045845	73	0.036	0.045466	32	0.0361	0.045592	80	0.0722	0.091185	82	0.0901	0.113791
251	0.0453	0.057211	89	0.0451	0.056959	67	0.0451	0.056959						
316	0.0544	0.068704	130	0.0543	0.068578	78	0.0542	0.068452						
380	0.0634	0.080071	147	0.0633	0.079944	89	0.0633	0.079944						
445	0.0726	0.09169	187	0.0723	0.091311	124	0.0723	0.091311						
510	0.0815	0.10293	204	0.0814	0.102804	135	0.0813	0.102677						
575	0.0907	0.114549	245	0.0902	0.113918	146	0.0903	0.114044						
	Flowrate:	0.000179		Flowrate:	0.00041		Flowrate:	0.000642		Flowrate:	0.000647		Flowrate:	0.000955

MeOH 50 cm

0.5 PSI			1 PSI			1.6 PSI			2.1 PSI			2.5 PSI		
time (s)	mass (g)	vol (mL)	time (s)	mass (g)	vol (mL)	time (s)	mass (g)	vol (mL)	time (s)	mass (g)	vol (mL)	time (s)	mass (g)	vol (mL)
0	0.3822	0.482698	0	0.0148	0.018691589	0	0.0973	0.122884567	0	0.1999	0.252463	0	0.2949	0.372443
61	0.3907	0.493433	230	0.023	0.029047739	133	0.1058	0.133619601	96	0.2084	0.263198	77	0.3037	0.383556
122	0.3995	0.504547	469	0.0316	0.039909068	269	0.1144	0.14448093	194	0.2171	0.274185	156	0.3122	0.394291
182	0.4081	0.515408	711	0.0397	0.050138924	406	0.1228	0.155089669	292	0.2259	0.285299	232	0.3212	0.405658
243	0.4169	0.526522	963	0.0479	0.060495075	547	0.1314	0.165950998	391	0.2343	0.295908	312	0.3297	0.416393
304	0.4255	0.537383	1219	0.0563	0.071103814	685	0.14	0.176812326	491	0.243	0.306896	392	0.3386	0.427633
364	0.4344	0.548623	1481	0.0644	0.08133367	829	0.1485	0.18754736	592	0.2519	0.318136	473	0.3472	0.438495
426	0.4432	0.559737	1751	0.0725	0.091563526	975	0.157	0.198282395	696	0.2607	0.32925	555	0.3561	0.449735
488	0.4517	0.570472	2033	0.0808	0.102045971	1122	0.1656	0.209143723	799	0.2692	0.339985	638	0.3647	0.460596
550	0.4606	0.581713	2316	0.0889	0.112275827	1272	0.1741	0.219878757	904	0.2778	0.350846	720	0.3734	0.471584
	Flowrate:	0.00018		Flowrate:	4.03753E-05		Flowrate:	7.62951E-05		Flowrate:	0.000109		Flowrate:	0.000138

MeOH 50 cm

0.5 PSI			1 PSI			1.5 PSI			2 PSI			2.5 PSI		
time (s)	mass (g)	vol (mL)	time (s)	mass (g)	vol (mL)	time (s)	mass (g)	vol (mL)	time (s)	mass (g)	vol (mL)	time (s)	mass (g)	vol (mL)
87	0.0096	0.012124	35	0.0092	0.011619096	24	0.0092	0.011619096	16	0.0092	0.011619	13	0.0092	0.011619
176	0.019	0.023996	72	0.0185	0.023364486	47	0.0186	0.023490781	33	0.0185	0.023364	27	0.0186	0.023491
268	0.0283	0.035741	109	0.028	0.035362465	70	0.0279	0.035236171	50	0.0276	0.034857	41	0.0278	0.03511
362	0.0377	0.047613	146	0.037	0.046728972	94	0.037	0.046728972	67	0.0369	0.046603	54	0.037	0.046729
461	0.047	0.059358	184	0.0465	0.058726951	117	0.0466	0.058853246	83	0.0459	0.057969	68	0.0463	0.058474
564	0.0563	0.071104	222	0.0555	0.070093458	141	0.0559	0.070598636	100	0.0554	0.069967	82	0.0555	0.070093
673	0.0659	0.083228	260	0.065	0.082091437	164	0.0648	0.081838848	118	0.0645	0.08146	96	0.0648	0.081839
788	0.0752	0.094973	299	0.0743	0.093836827	188	0.0748	0.0944683	135	0.0738	0.093205	109	0.0738	0.093205
910	0.0844	0.106593	339	0.0837	0.105708512	211	0.0835	0.105455923	152	0.0829	0.104698	123	0.0828	0.104572
1041	0.0938	0.118464	379	0.0929	0.117327608	234	0.0927	0.117075019	169	0.0922	0.116444	137	0.092	0.116191
	Flowrate:	0.000112	420	0.1025	0.129451882	258	0.1019	0.128694115	186	0.1014	0.128063	150	0.1017	0.128442
			462	0.1115	0.140818388	281	0.1112	0.140439505	204	0.1105	0.139555	164	0.1109	0.140061
				Flowrate:	0.000303667		Flowrate:	0.000500139		Flowrate:	0.000682		Flowrate:	0.000849

MeOH 55 cm

0.5 PSI			1.1 PSI			1.6 PSI			2.1 PSI			2.5 PSI		
time (s)	mass (g)	vol (mL)	time (s)	mass (g)	vol (mL)	time (s)	mass (g)	vol (mL)	time (s)	mass (g)	vol (mL)	time (s)	mass (g)	vol (mL)
0	0.008	0.010103562	0	0.0095	0.011998	0	0.0094	0.011872	0	0.0094	0.011872	0	0.0093	0.011745
69	0.017	0.021470068	35	0.0188	0.023743	23	0.0188	0.023743	17	0.0187	0.023617	14	0.0188	0.023743
143	0.0254	0.032078808	69	0.0283	0.035741	46	0.0281	0.035489	34	0.0281	0.035489	29	0.0283	0.035741
300	0.0473	0.059737307	105	0.0378	0.047739	70	0.0375	0.04736	50	0.0374	0.047234	44	0.0377	0.047613
383	0.0564	0.071230109	141	0.0473	0.059737	93	0.0469	0.059232	67	0.0468	0.059106	58	0.047	0.059358
465	0.0668	0.084364739	176	0.0567	0.071609	116	0.0562	0.070978	85	0.0561	0.070851	72	0.0564	0.07123
550	0.0759	0.09585754	213	0.0662	0.083607	139	0.0656	0.082849	102	0.0655	0.082723	87	0.0657	0.082975
639	0.0857	0.108234403	249	0.0757	0.095605	162	0.075	0.094721	120	0.0748	0.094468	102	0.075	0.094721
727	0.0954	0.120484971	286	0.0851	0.107477	186	0.0845	0.106719	136	0.0841	0.106214	116	0.0845	0.106719
816	0.1052	0.132861834	323	0.0947	0.119601	209	0.0939	0.118591	154	0.0935	0.118085	131	0.0937	0.118338
909	0.1139	0.143849457	359	0.1042	0.131599	232	0.1033	0.130462	171	0.1029	0.129957	145	0.103	0.130083
			397	0.1136	0.143471	255	0.1126	0.142208	188	0.1122	0.141702	160	0.1123	0.141829
						278	0.1221	0.154206						
	Flowrate:	0.000148452		Flowrate:	0.000331		Flowrate:	0.000511		Flowrate:	0.000689		Flowrate:	0.000812

MeOH 55 cm

0.5 PSI			1 PSI			1.5 PSI			2 PSI			2.5 PSI		
time (s)	mass (g)	vol (mL)	time (s)	mass (g)	vol (mL)	time (s)	mass (g)	vol (mL)	time (s)	mass (g)	vol (mL)	time (s)	mass (g)	vol (mL)
0	0.0078	0.009850972	0	0.0084	0.010609	0	0.0085	0.010735	0	0.0086	0.010861	0	0.0085	0.010735
110	0.0162	0.020459712	38	0.017	0.02147	25	0.0172	0.021723	19	0.0172	0.021723	15	0.0171	0.021596
229	0.0248	0.031321041	77	0.0255	0.032205	49	0.0257	0.032458	39	0.0257	0.032458	30	0.0256	0.032331
380	0.0336	0.042434958	119	0.0342	0.043193	74	0.0342	0.043193	58	0.0342	0.043193	45	0.0342	0.043193
553	0.0426	0.053801465	161	0.0428	0.054054	99	0.0427	0.053928	77	0.0427	0.053928	61	0.0426	0.053801
687	0.0514	0.064915383	203	0.0515	0.065042	124	0.0513	0.064789	96	0.0513	0.064789	76	0.0511	0.064536
817	0.0603	0.076155595	245	0.06	0.075777	149	0.0599	0.07565	116	0.0598	0.075524	91	0.0595	0.075145
924	0.0688	0.086890629	289	0.0685	0.086512	176	0.068	0.08588	135	0.0683	0.086259	106	0.0682	0.086133
1000	0.0776	0.098004547	332	0.0772	0.097499	202	0.0769	0.09712	155	0.0767	0.096868	121	0.0767	0.096868
1083	0.0866	0.109371053	375	0.086	0.108613	228	0.0855	0.107982	174	0.0854	0.107856	136	0.0854	0.107856
1179	0.0952	0.120232382	417	0.0944	0.119222	256	0.094	0.118717	193	0.0938	0.118464	152	0.0939	0.118591
1292	0.1041	0.131472594	458	0.103	0.130083	282	0.1027	0.129704	213	0.1024	0.129326	166	0.1023	0.129199
	Flowrate:	9.17761E-05		Flowrate:	0.000258		Flowrate:	0.000421		Flowrate:	0.000556		Flowrate:	0.000711

MeOH 60 cm

1 PSI			2 PSI			3 PSI			2 PSI			2.5 PSI		
time (s)	mass (g)	vol (mL)	time (s)	mass (g)	vol (mL)	time (s)	mass (g)	vol (mL)	time (s)	mass (g)	vol (mL)	time (s)	mass (g)	vol (mL)
0	0.0085	0.010735	0	0.0084	0.010609	0	0.0083	0.010482						
40	0.0164	0.020712	19	0.0167	0.021091	12	0.0166	0.020965						
79	0.0247	0.031195	37	0.0251	0.0317	25	0.0248	0.031321						
120	0.0332	0.04193	57	0.0334	0.042182	37	0.0332	0.04193						
159	0.0416	0.052539	75	0.0418	0.052791	49	0.0414	0.052286						
201	0.05	0.063147	93	0.05	0.063147	61	0.0499	0.063021						
240	0.0583	0.07363	110	0.0584	0.073756	74	0.0584	0.073756						
283	0.0669	0.084491	130	0.0667	0.084238	86	0.0667	0.084238						
323	0.0753	0.0951	149	0.0752	0.094973	99	0.0749	0.094595						
364	0.0836	0.105582	168	0.0836	0.105582	110	0.0833	0.105203						
405	0.0917	0.115812	186	0.0919	0.116065	123	0.0916	0.115686						
	Flowrate:	0.000261		Flowrate:	0.000568	136	0.0999	0.126168						
						148	0.1083	0.136777						
							Flowrate:	0.000854						

MeOH 60 cm

1 PSI			2 PSI			3 PSI			2 PSI			2.5 PSI		
time (s)	mass (g)	vol (mL)	time (s)	mass (g)	vol (mL)	time (s)	mass (g)	vol (mL)	time (s)	mass (g)	vol (mL)	time (s)	mass (g)	vol (mL)
38	0.0092	0.011619	15	0.0094	0.011872	12	0.0093	0.011745						
77	0.0185	0.023364	36	0.0187	0.023617	25	0.0187	0.023617						
116	0.0276	0.034857	53	0.0281	0.035489	39	0.0279	0.035236						
155	0.0368	0.046476	75	0.0374	0.047234	52	0.0373	0.047108						
193	0.0461	0.058222	91	0.0468	0.059106	65	0.0466	0.058853						
232	0.0553	0.069841	109	0.0563	0.071104	79	0.0559	0.070599						
271	0.0645	0.08146	132	0.0657	0.082975	89	0.0652	0.082344						
309	0.0737	0.093079	148	0.0751	0.094847	102	0.0746	0.094216						
349	0.083	0.104824	168	0.0845	0.106719	116	0.0839	0.105961						
387	0.0922	0.116444	188	0.0939	0.118591	128	0.0932	0.117706						
427	0.1015	0.128189	206	0.103	0.130083	140	0.103	0.130083						
	Flowrate:	0.0003		Flowrate:	0.000622		Flowrate:	0.000922						

CH3CN/Water 50 cm

1 PSI			1.5 PSI			2 PSI			2.5 PSI			3 PSI		
time (s)	mass (g)	vol (mL)	time (s)	mass (g)	vol (mL)	time (s)	mass (g)	vol (mL)	time (s)	mass (g)	vol (mL)	time (s)	mass (g)	vol (mL)
0	0.0109	0.012961	0	0.0116	0.013793	0	0.011	0.01308	0	0.0116	0.013793	0	0.0116	0.013793
55	0.0217	0.025803	35	0.0231	0.027467	26	0.0228	0.027111	25	0.023	0.027348	18	0.0231	0.027467
114	0.0329	0.03912	69	0.0345	0.041023	55	0.0342	0.040666	45	0.0348	0.041379	37	0.0346	0.041141
172	0.0442	0.052556	105	0.0463	0.055054	78	0.0456	0.054221	67	0.0463	0.055054	54	0.0462	0.054935
232	0.0555	0.065993	139	0.0578	0.068728	104	0.0572	0.068014	91	0.0578	0.068728	74	0.0577	0.068609
292	0.0667	0.07931	175	0.0692	0.082283	128	0.0687	0.081688	113	0.0695	0.08264	90	0.0693	0.082402
352	0.0782	0.092985	206	0.0809	0.096195	156	0.0801	0.095244	134	0.0809	0.096195	109	0.0808	0.096076
414	0.0896	0.10654	241	0.0923	0.10975	181	0.0914	0.10868	157	0.0926	0.110107	129	0.0924	0.109869
476	0.1012	0.120333	275	0.1038	0.123424	207	0.1031	0.122592	181	0.1041	0.123781	145	0.1039	0.123543
541	0.113	0.134364	311	0.1156	0.137455	234	0.1147	0.136385	201	0.1156	0.137455	161	0.1156	0.137455
	Flowrate:	0.000224		Flowrate:	0.000399		Flowrate:	0.000529		Flowrate:	0.000616		Flowrate:	0.00076

CH3CN/Water 55 cm

0.5 PSI			1 PSI			1.5 PSI			2 PSI			2.5 PSI		
time (s)	mass (g)	vol (mL)	time (s)	mass (g)	vol (mL)	time (s)	mass (g)	vol (mL)	time (s)	mass (g)	vol (mL)	time (s)	mass (g)	vol (mL)
0	0.011	0.01308	0	0.0115	0.013674	0	0.0113	0.013436	0	0.0111	0.013199	0	0.0113	0.013436
171	0.0214	0.025446	68	0.0229	0.027229	43	0.0226	0.026873	31	0.022	0.026159	24	0.0227	0.026992
349	0.0321	0.038169	136	0.0341	0.040547	87	0.0341	0.040547	62	0.0338	0.04019	49	0.0334	0.039715
528	0.0433	0.051486	205	0.0451	0.053627	130	0.0453	0.053864	94	0.045	0.053508	74	0.0453	0.053864
710	0.0545	0.064804	274	0.0566	0.067301	174	0.0567	0.06742	125	0.0562	0.066825	98	0.0566	0.067301
895	0.0655	0.077883	344	0.0679	0.080737	218	0.0679	0.080737	157	0.0676	0.08038	123	0.0679	0.080737
1087	0.077	0.091558	414	0.079	0.093936	262	0.0791	0.094055	188	0.079	0.093936	148	0.0791	0.094055
1281	0.0882	0.104875	485	0.0904	0.107491	306	0.0905	0.10761	220	0.0903	0.107372	172	0.0905	0.10761
1480	0.0994	0.118193	555	0.1016	0.120809	350	0.1018	0.121046	252	0.1015	0.12069	197	0.1018	0.121046
1683	0.1109	0.131867	626	0.1129	0.134245	394	0.1131	0.134483	284	0.1128	0.134126	222	0.1132	0.134602
1888	0.1222	0.145303	698	0.1241	0.147562	439	0.1244	0.147919	316	0.1241	0.147562	246	0.1244	0.147919
	Flowrate:	7.03E-05		Flowrate:	0.000192		Flowrate:	0.000306		Flowrate:	0.000426		Flowrate:	0.000546

Appendix D: Source pressurization instructions

1) With the mass spectrometer in standby mode, replace the regular glass source housing with the plastic housing that has been modified with a pressure gauge. Be sure to reconnect everything.

2) Attach the nitrogen line to the plastic housing via one of the available ports. (The nitrogen line you're looking for is connected to the pressure meter built into the desk. 'Gas 1')

3) Set the cone gas and desolvation gas to normal operating values, then throttle the source exhaust using the grey knob on the front of the instrument and increase the external nitrogen flow into the source (using the black 'Gas 1' knob) until the pressure gauge reads +4 in. H_2O.

4) Flush the source in this manner for at least 20 min.

5) Re-adjust the external nitrogen flow so that the pressure gauge reads a positive pressure of 1 in. H_2O.

6) You are now ready to run your sample. If you still see evidence of the presence of oxygen, return to flushing the source with N_2.

7) After you've finished running your sample, there are two states in which the source can be left:

i) Turn the external nitrogen off, return the source exhaust to fully open using the grey knob, turn the instrument to standby and replace the regular source housing,

ii) OR, Increase the pressure back to 4 in. H_2O then completely close the source exhaust using the grey knob. This will maintain the oxygen-free atmosphere overnight if you have more experiments to perform the next day. To close the source exhaust you will have to simultaneously reduce the flow of nitrogen so that too much of an over pressure is not generated.*****Note: if you create too much of an overpressure you will break the pressure valve!***** Once the exhaust is closed adjust the nitrogen flow so that just a slight overpressure is maintained.

Appendix E: ESI(-)-MS/MS plots for gas-phase reductive elimination experiments

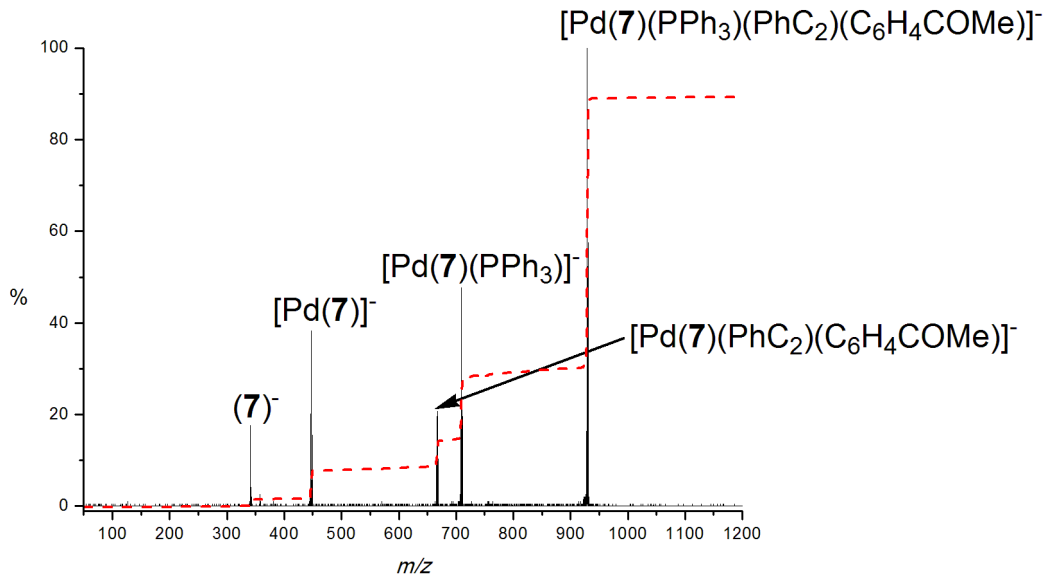

Figure E1: Negative-ion ESI-MS/MS of $[Pd(\mathbf{7})(PPh_3)(C_6H_4COMe)(C_2Ph)]^-$, showing reductive elimination to $[Pd(\mathbf{7})(PPh_3)]^-$, at a collision voltage of 15 V.

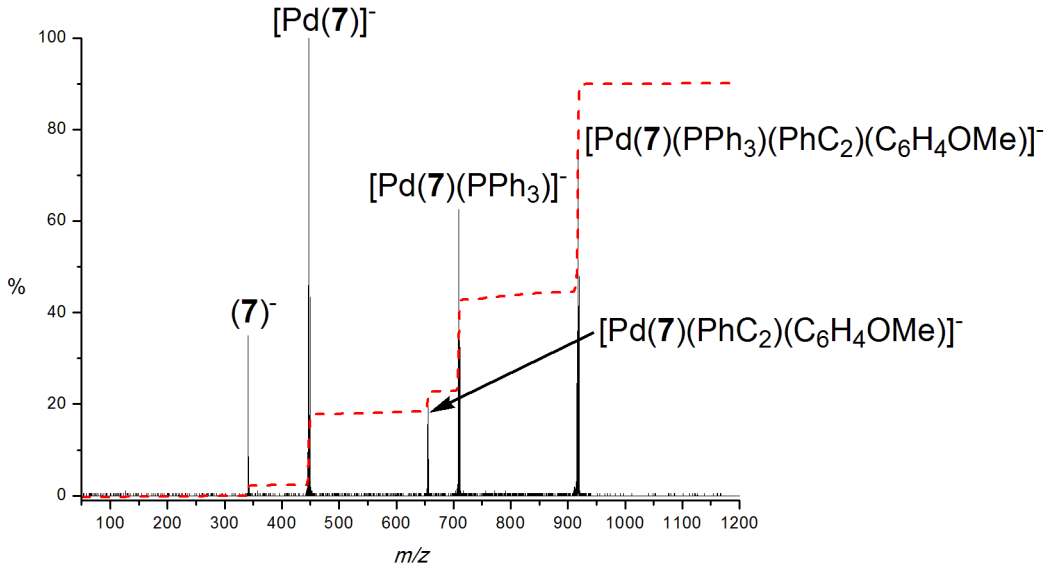

Figure E2: Negative-ion ESI-MS/MS of $[Pd(\mathbf{7})(PPh_3)(C_6H_4OMe)(C_2Ph)]^-$, showing reductive elimination to $[Pd(\mathbf{7})(PPh_3)]^-$, at a collision voltage of 15 V.

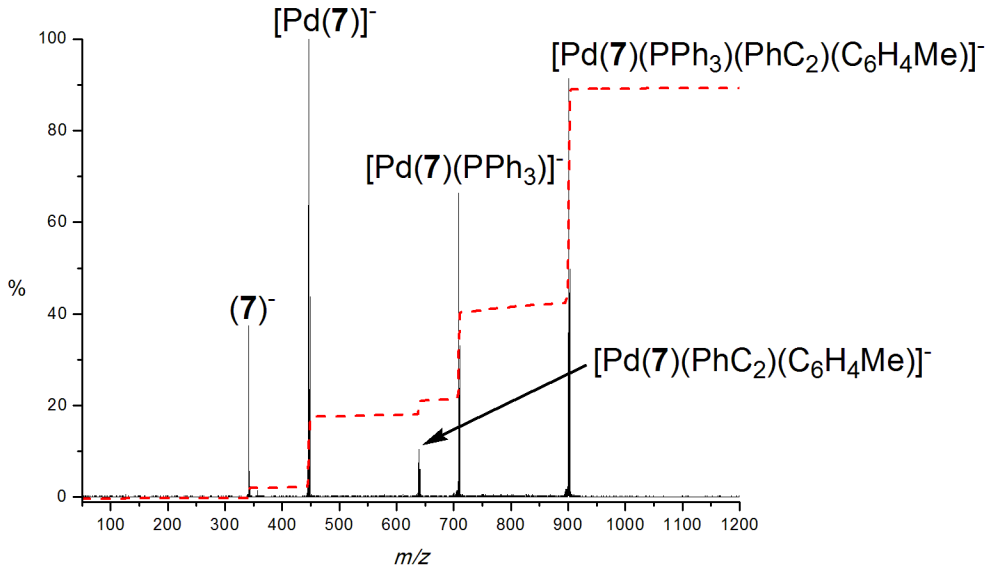

Figure E3: Negative-ion ESI-MS/MS of [Pd(**7**)(PPh_3)(C_6H_4Me)(C_2Ph)]$^-$, showing reductive elimination to [Pd(**7**)(PPh_3)]$^-$, at a collision voltage of 15 V.

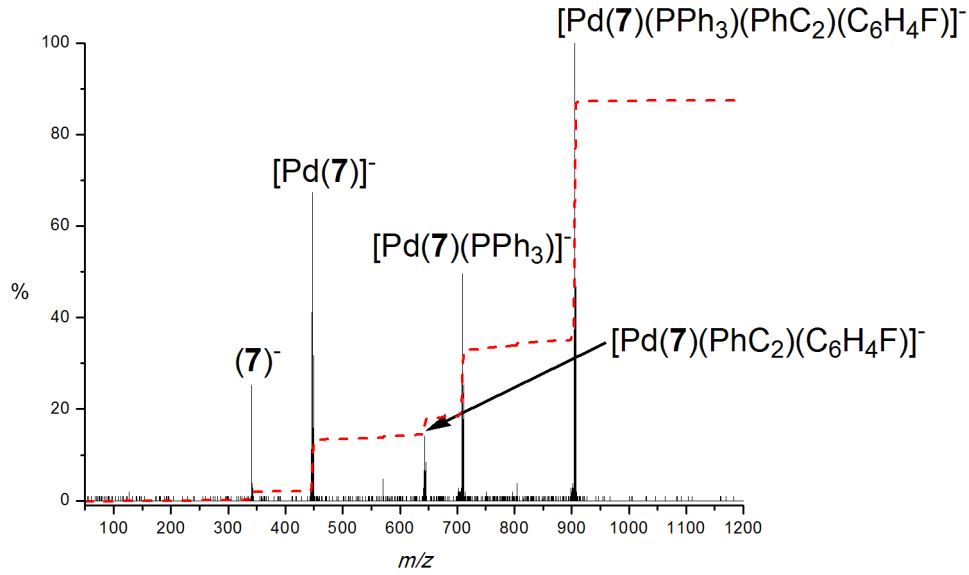

Figure E4: Negative-ion ESI-MS/MS of [Pd(**7**)(PPh_3)(C_6H_4F)(C_2Ph)]$^-$, showing reductive elimination to [Pd(**7**)(PPh_3)]$^-$, at a collision voltage of 15 V.

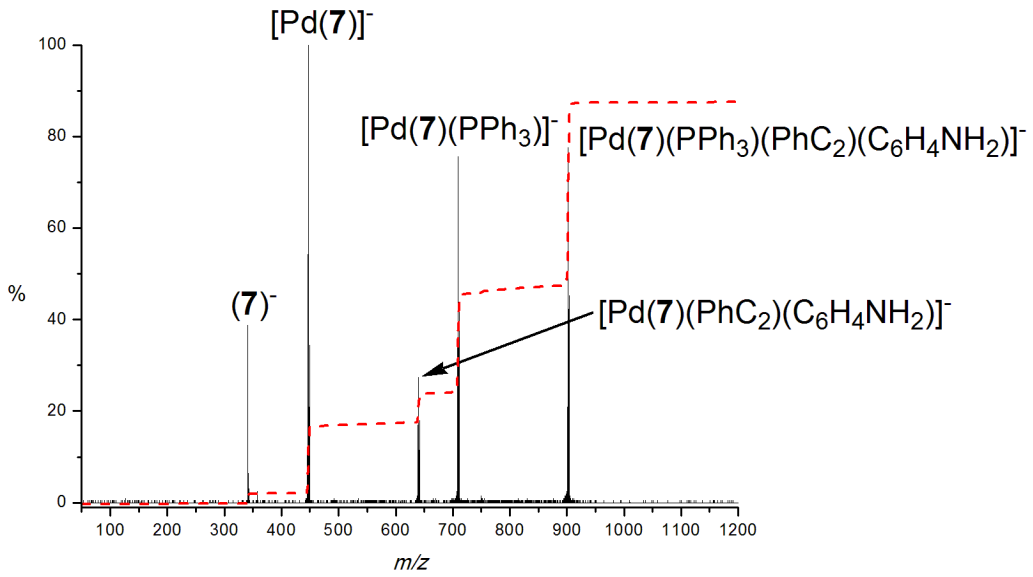

Figure E5: Negative-ion ESI-MS/MS of [Pd(**7**)(PPh_3)($C_6H_4NH_2$)(C_2Ph)]$^-$, showing reductive elimination to [Pd(**7**)(PPh_3)]$^-$, at a collision voltage of 15 V.

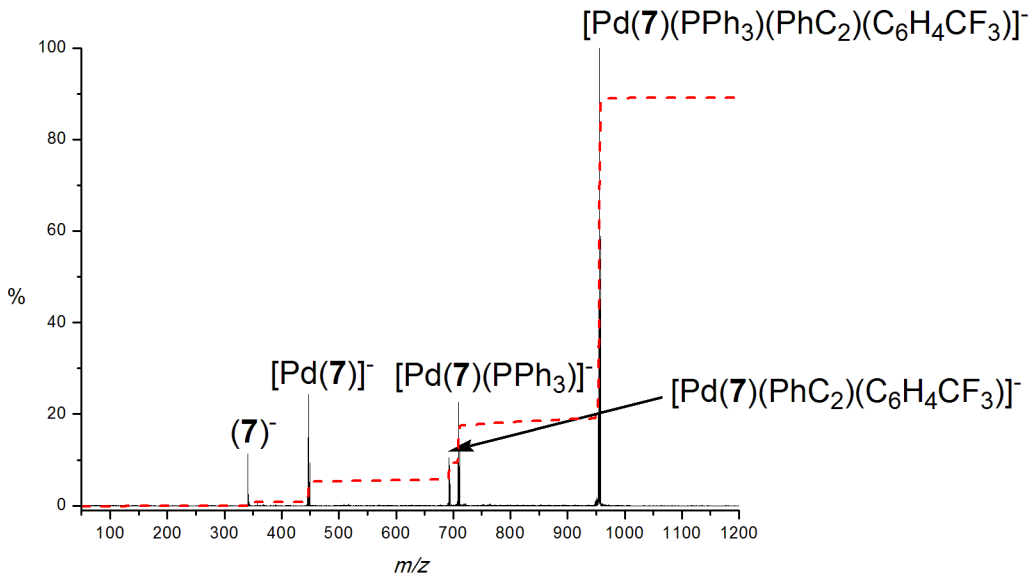

Figure E6: Negative-ion ESI-MS/MS of [Pd(**7**)(PPh_3)($C_6H_4CF_3$)(C_2Ph)]$^-$, showing reductive elimination to [Pd(**7**)(PPh_3)]$^-$, at a collision voltage of 15 V.

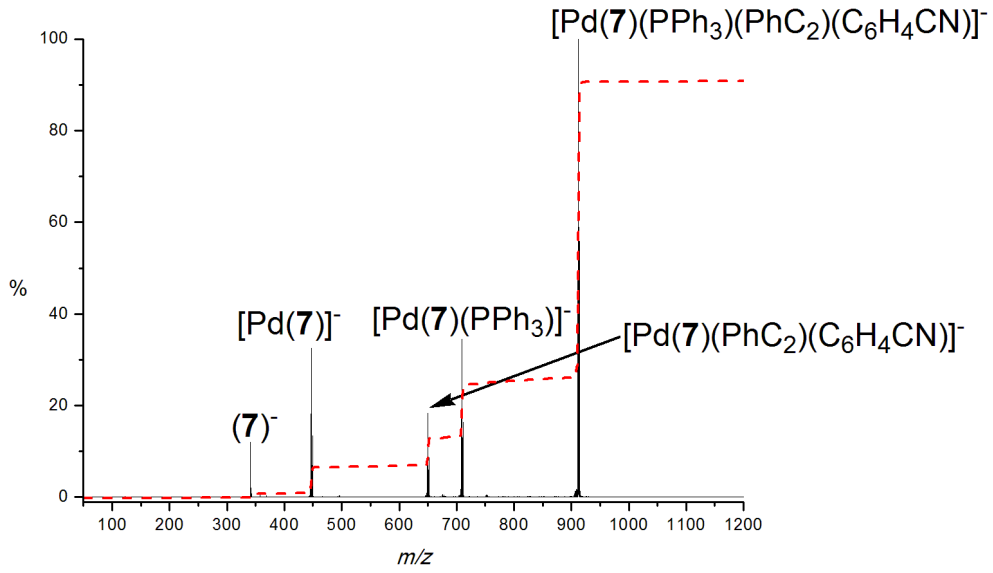

Figure E7: Negative-ion ESI-MS/MS of $[Pd(\mathbf{7})(PPh_3)(C_6H_4CN)(C_2Ph)]^-$, showing reductive elimination to $[Pd(\mathbf{7})(PPh_3)]^-$, at a collision voltage of 15 V.

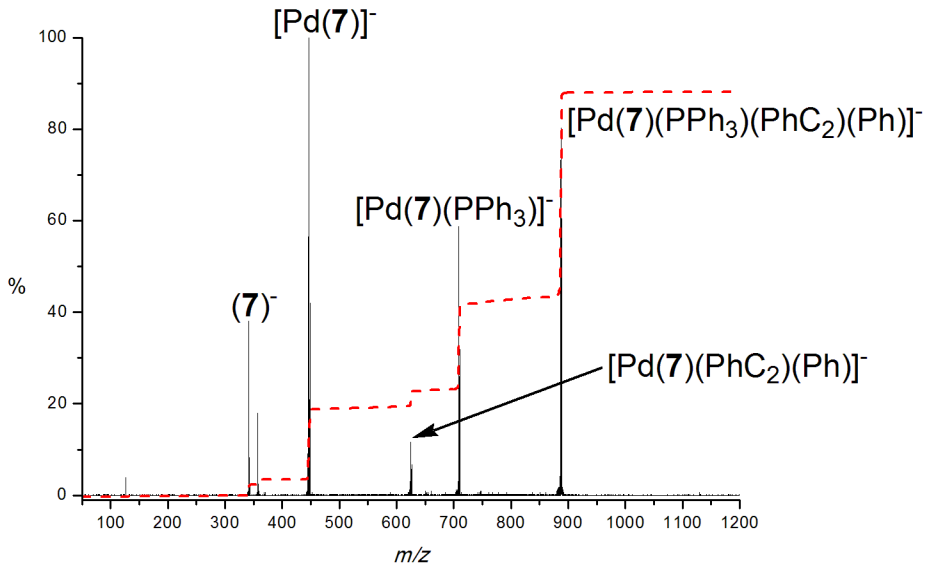

Figure E8: Negative-ion ESI-MS/MS of $[Pd(\mathbf{7})(PPh_3)(C_6H_5)(C_2Ph)]^-$, showing reductive elimination to $[Pd(\mathbf{7})(PPh_3)]^-$, at a collision voltage of 15 V.

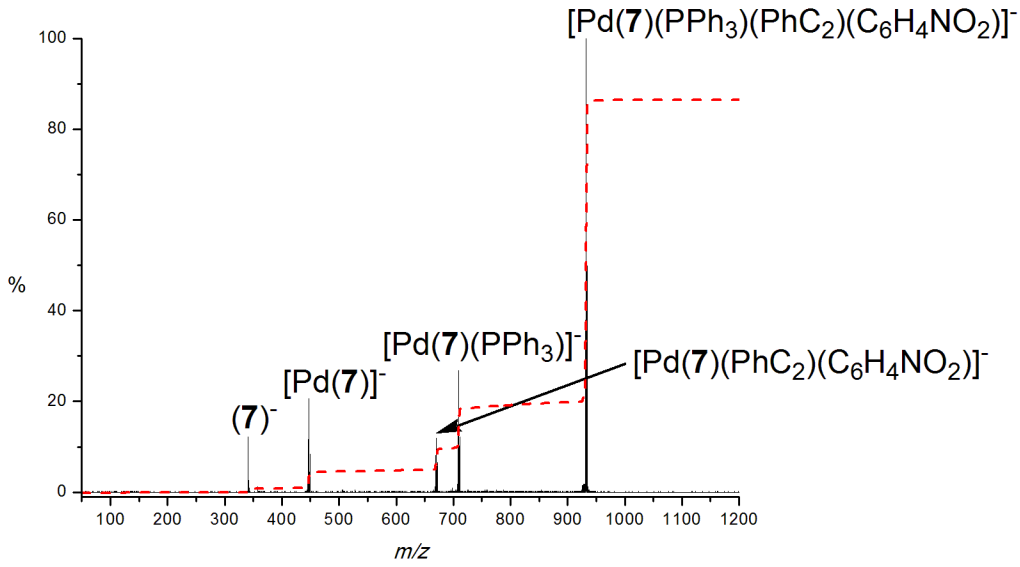

Figure E9: Negative-ion ESI-MS/MS of $[Pd(\mathbf{7})(PPh_3)(C_6H_4NO_2)(C_2Ph)]^-$, showing reductive elimination to $[Pd(\mathbf{7})(PPh_3)]^-$, at a collision voltage of 15 V.